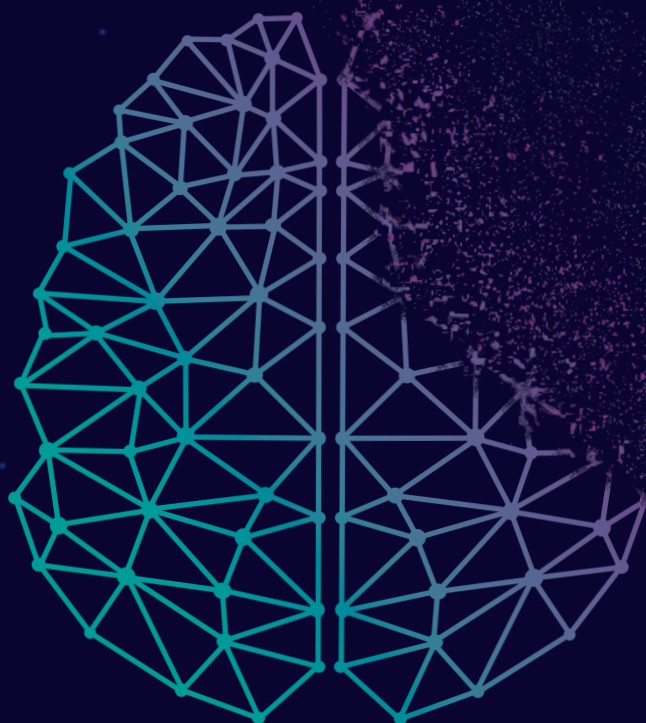# Clearance of toxic amyloids related to neurodegeneration by the human disaggregase machinery

Aitor Franco Budia

Doctoral Thesis
Leioa, 2020

Doctoral Thesis

Clearance of toxic amyloids related to neurodegeneration by the human disaggregase machinery

Aitor Franco Budia

Supervisors:

Prof. Arturo Muga Villate

Prof. Adelina Prado Ruiz

Leioa, 2020

TABLE OF CONTENTS

ACKNOWLEDGEMENTS

LIST OF FIGURES

LIST OF TABLES

LIST OF ABBREVIATIONS

Aβ	Amyloid-β
AAA+	ATPases associated with various cellular activities
Ab	Antibody
AD	Alzheimer's disease
AEP	Asparagine endopeptidase
AFM	Atomic force microscopy
ALPs	Autophagy-lysosome pathways
ALS	Amyotrophic lateral sclerosis
ANS	1-anilino-8-naphthalene sulfonate
ATP	Adenosine triphosphate
CBD	Corticobasal degeneration
CD	Circular Dichroism
CF	Correction factor
CJD	Creutzfelds-Jacobs disease
CP	Core particle of the proteasome
cryo-EM	Cryo-electron microscopy
CTE	Chronic traumatic encephalopathy
CtsB	Cathepsin B
CtsD	Cathepsin D
CtsL	Cathepsin L
DLB	Dementia with Lewy bodies
DLS	Dynamic Light Scattering
DMEM	Dulbecco's modified Eagle's medium
E. coli	*Escherichia coli*
EM	Electron microscopy

FBS	Fetal Bovine Serum
FRET	Fluorescence resonance energy transfer
FTDP-17	Frontotemporal dementia with Parkinsonism linked to chromosome 17
FT-IR	Fourier Transform Infrared
G6P	Glucose-6-phosphate
G6PDH	Glucose-6-phosphate dehydrogenase
GdnHCl	Guanidine hydrochloride
HD	Huntington's disease
Hsp	Heat shock protein
Htt	Huntingtin
IAPP	Islet Amyloid Polypeptide
IPTG	Isopropyl β-D-1-thiogalactopyranoside
JDPs	J-domain proteins
LBs	Lewy bodies
LNs	Lewy neurites
MAPs	Microtubule-associated proteins
MMP	Matrix metalloprotease
MS	Mass spectroscopy
MSA	Multiple system atrophy
MTBD	Microtubule-binding domain
MTS	3-(4,5-dimethylthiazol-2-yl)-5-(3-carboxymethoxyphenyl)-2-(4-sulfophenyl)-2H-tetrazolium
MTs	Microtubules
NAC	Non-amyloid β component
NBD	Nucleotide-binding domain
NDs	Neurodegenerative diseases

NEF	Nucleotide exchange factor
PAGE	Polyacrylamide gel electrophoresis
PCR	Polymerase Chain Reaction
PD	Parkinson's disease
PEP	Phosphoenolpyruvate
PES	Phenazine ethosulfate
PiD	Pick´s disease
PMCA	Protein misfolding cyclic amplification
PN	Proteostasis network
PTMs	Post-translational modifications
RP	Regulatory particle of the proteasome
SBD	Substrate-binding domain
SDS	Sodium dodecyl sulfate
sHsps	Small heat shock proteins
SOD1	Superoxide dismutase 1
TDP-43	TAR DNA binding protein
TEM	Transmission Electron Microscopy
TFE	2,2,2-trifluoroethanol
ThT	Thioflavin T
UBQLN2	Ubiquilin 2
UPS	Ubiquitin-proteasome system
UV	Ultraviolet
α-syn	α-synuclein

CHAPTER

1

INTRODUCTION

1.1. NEURODEGENERATION AND AMYLOIDS

1.1.1. Neurodegenerative diseases

Neurodegenerative diseases (NDs) are a group of neurological disorders characterized by the progressive degeneration of the structure and function of the central and peripheral nervous system. Some of the most common NDs are Alzheimer's disease (AD), Parkinson's disease (PD), amyotrophic lateral sclerosis (ALS), Huntington's disease (HD) and prion diseases such as Creutzfelds-Jacobs disease (CJD). Clinical presentation (signs or symptoms) of these diseases is variable, including memory and cognitive impairments, speaking and breathing problems or motor function disability. Albeit cardiovascular diseases and cancer are the prevailing causes of mortality, NDs are increasingly positioning as leading causes of global deaths. Certainly, with the accelerated aging of the population and considering that NDs are strongly age-related, they have been forecast to be a major global health problem in the upcoming years. Despite this situation, the current number of treatments available only manage the symptoms or attempt to halt the progression of the disease. Therefore, there is an urgent need for understanding the basic molecular mechanisms associated with such diseases, which could lead to new therapies.

1.1.2. Aggregate deposition in neurodegeneration

NDs have a multifactorial etiology, likely resulting from an intricate relationship between genetic and environmental factors affecting fundamental cellular processes. A histopathological hallmark of most NDs include the deposition of

aggregated proteins called amyloids into extracellular or intracellular inclusions. Which protein is conformationally altered, as well as the anatomical brain regions and cell types affected, differ depending on the disease (**Figure 1.1**). For instance, AD is characterized by the deposition of two distinct types of aggregates in the temporal and parietal lobes of the brain: extracellular plaques composed of amyloid-β (Aβ) peptides (cleavage products of the transmembrane protein APP), and intracellular neurofibrillary tangles composed of tau proteins. In PD, aggregates of the protein α-synuclein (α-syn) accumulate inside dopaminergic neurons of the *substantia nigra pars compacta*. Deposits of superoxide dismutase 1 (SOD1), TAR DNA binding protein (TDP-43), RNA-binding protein FUS, huntingtin (Htt) or PrP prion protein have been identified in different NDs (**Figure 1.1**).
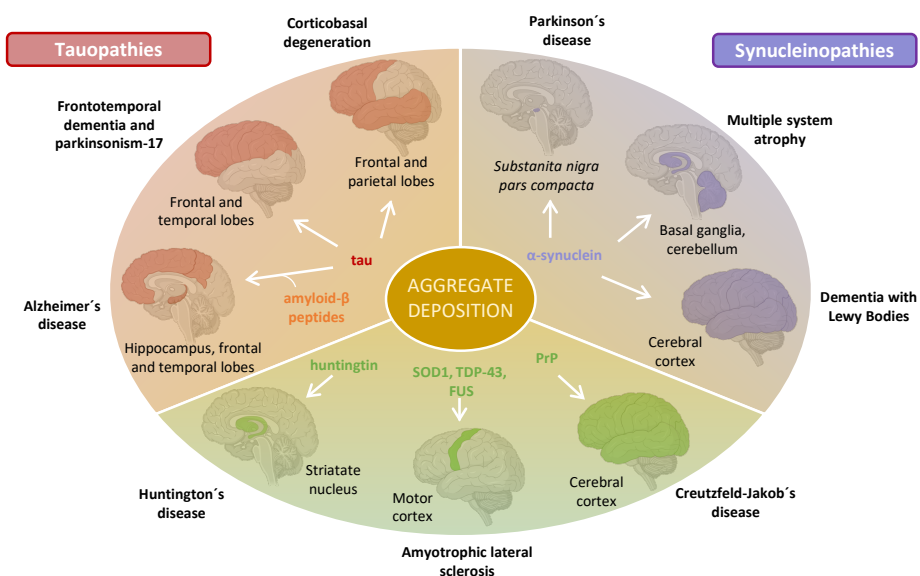
Figure 1.1. Protein aggregate deposition disorders affecting the nervous system. A multiplicity of proteins have been found forming aggregate deposits in the brain of patients with NDs. Depending on the disease, the amyloidogenic protein that form such deposits and their brain location vary. Aggregates of the same protein can be found in different locations resulting in different disorders, as is the case of tau and α-syn. NDs involving the aggregation of tau or α-syn are referred to as tauopathies and synucleopathies, respectively. This figure illustrates the main brain locations of amyloid deposits of each protein, which may fluctuate with the progression of the disease or among patients.

Aggregate deposition in more than 80% of ND cases is sporadic/idiopathic and has a relatively late age of onset. Disease-causing mutations involving the sequences of the proteins undergoing amyloid aggregation have also been documented and represent 10-20% of the total cases, except for HD, which is always inherited. In these familial or hereditary forms, mutations favor the aggregation process through one or more mechanisms summarized in **Figure 1.2**. This universal link between pathogenic mutation and aggregation provides clear genetic evidence that protein aggregation is a primary event in the pathogenesis of the corresponding diseases, rather than a secondary effect (Chiti and Dobson, 2017; Sperling *et al.*, 2020).
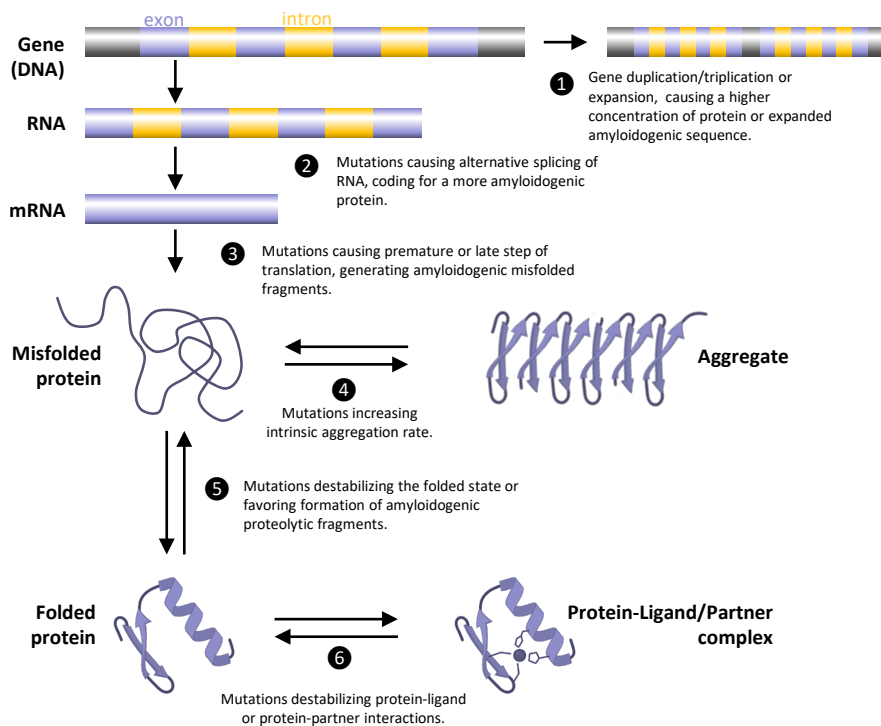
Figure 1.2. Mechanisms by which mutations associated with hereditary amyloid diseases can cause protein aggregation. Adapted from Chiti and Dobson, 2017.

1.2. PROTEIN MISFOLDING AND AGGREGATION

Proteins are synthesized on ribosomes as linear chains of amino acids. Although a fraction of mammalian proteins (15-30%) lack ordered structure partially or entirely, most newly synthesized proteins must fold into a defined three-dimensional structure to function (**Figure 1.3**). Folding of newly translated proteins can occur spontaneously or require the assistance of other proteins such as molecular chaperones. During folding there is a cooperation of many weak, noncovalent interactions between amino acids that can be close or far apart in the sequence. To perform such contacts, proteins need to cross substantial kinetic energy barriers and consequently, populate folding intermediates towards the thermodynamically favorable native state. Subtle changes due to stress conditions can destabilize the native state, leading to a partial (misfolded) or complete (unfolded) loss of ordered structures.

Partially folded proteins typically expose hydrophobic residues and regions of unstructured polypeptide backbone to the solvent, features that can give rise to non-native intermolecular interactions that lead to aggregation (Balchin, Hayer-Hartl and Hartl, 2016). Aggregation is a heterogeneous process that can generate a multiplicity of protein aggregates. Even though most aggregates are amorphous, some proteins known as amyloidogenic proteins can assemble into well-defined and organized fibrillar aggregates called amyloids. Morphologically, amyloids are unbranched and threadlike structures composed of several protofilaments that wrap around each other, forming assemblies with just a few nanometers in diameter and up to several microns long. Amyloid fibrils are characterized by an extended β-sheet secondary structure in which individual β-strands are arranged in an orientation perpendicular to the fiber axis. Such a structure is known as cross-β structure and makes amyloids thermodynamically the most stable aggregates (**Figure 1.3**).
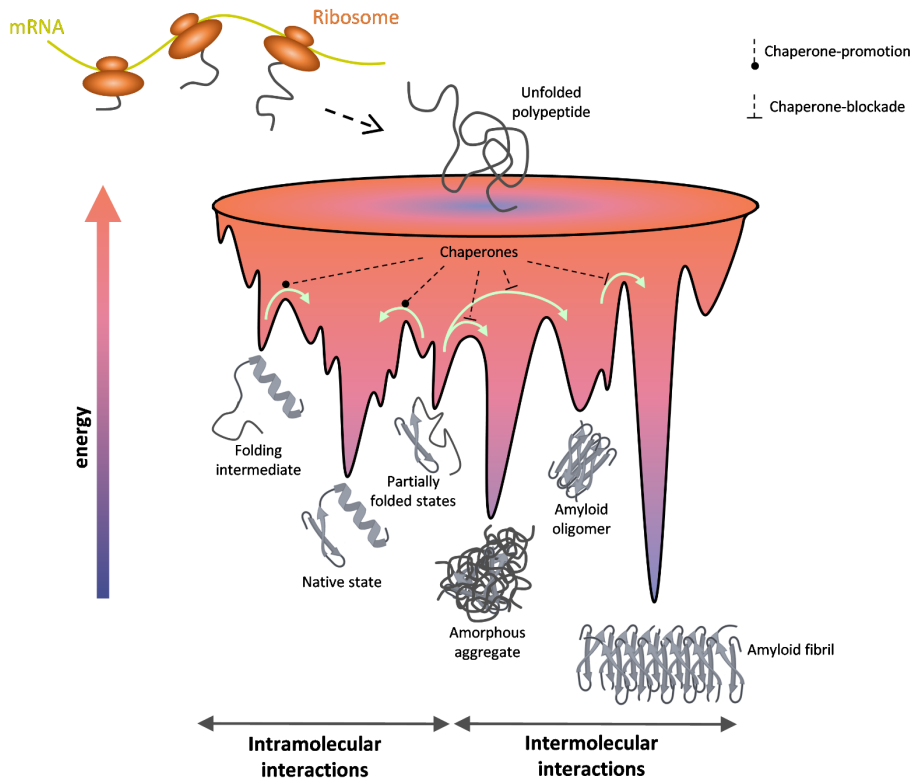
Figure 1.3. Energy landscape scheme of protein folding/aggregation. After protein synthesis, unfolded polypeptides start folding toward the thermodynamically favorable native state through intramolecular interactions, funneling down the energy landscape and populating low-energy intermediate folding states. Molecular chaperones provide assistance to folding by lowering free-energy barriers and preventing aberrant intermolecular interactions, which can lead to various forms of aggregates (amorphous, oligomeric, fibrillar). Adapted from Balchin, Hayer-Hartl and Hartl, 2016.

Regardless the type of aggregate, at early aggregation stages soluble species (oligomers) are formed, which can evolve to bigger and insoluble aggregates that tend to accumulate either intracellular or extracellularly. Protein misfolding and its deposition into proteinaceous aggregate inclusions have a two-faced pathomechanism: a loss of physiological function and a gain of toxic function

(Winklhofer and Haass, 2008). Misfolding and aggregation of proteins imply the loss of their native structure, and therefore, their physiological function. This may include loss of catalytic activity or loss of interactions with partner proteins or ligands. Additionally, the generation and accumulation of misfolded protein species also involves a gain of toxic function. These aggregate-prone species have a heightened tendency to engage in inappropriate interactions with other cellular components. Through both mechanisms, aggregates alter fundamental cellular processes, leading to cell death.

1.2.1. Amyloid assembly mechanism

The amyloid aggregation pathway is conserved among most amyloidogenic proteins (**Figure 1.4**). The process begins when a protein misfolds and starts clustering. The species formed at this initial stage are composed of a relatively small number of molecules and normally retain the structure of the native protein, thus giving rise to highly disordered oligomers if they originate from natively unfolded proteins such as α-syn or tau. Only relatively weak intermolecular interactions are involved within these early aggregates hence they are typically unstable. However, such aggregates can undergo an internal reorganization to form more stable species having β-sheet secondary structure, a conversion step often accompanied by an increase in compactness and size in a global process called nucleation (Cremades *et al.*, 2012; Iljina *et al.*, 2016; Michaels *et al.*, 2020). These β-structured aggregation nuclei (also known as seeds) can grow further by self-association or through monomer addition (elongation or polymerization). After a final reorganization of their structure, fibrils with a highly regular in-register parallel cross-β structure are formed (Chiti and Dobson, 2017).

Apart from primary nucleation, elongation and self-association, it has become evident that other secondary processes are significant in amyloid assembly (Knowles *et al.*, 2009; Cohen *et al.*, 2013; Buell *et al.*, 2014; Meisl *et al.*, 2014;

Gaspar *et al.*, 2017). Of particular interest are secondary nucleation reactions, in which the surfaces of existing fibrils catalyze the formation of new clusters of monomers, and fibril fragmentation into smaller pieces. Both secondary processes seem crucial in the formation of additional aggregation nuclei, exacerbating aggregation.
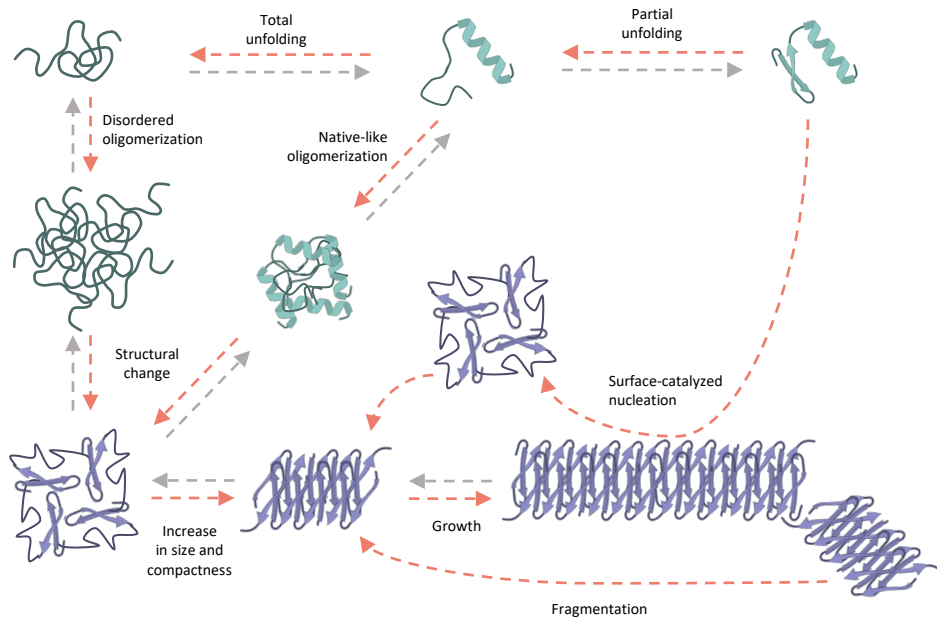
Figure 1.4. Formation of amyloid aggregates. The assembly of amyloidogenic proteins into fibrils starts with the loss of their native state. Partially or totally unfolded proteins oligomerize forming unstable early aggregate species that can evolve into more stable oligomers with β-sheet secondary structure. Further reorganization involving an increase of compactness and size creates aggregation nuclei, which can grow to form mature amyloid fibrils. Once formed, amyloids can feedback aggregation by forming new aggregate nuclei through secondary processes such as fragmentation or surface-catalyzed nucleation.

1.2.2. Structural determinants of amyloid toxicity

The gain of toxic function of amyloids primarily arises from the intermediate oligomeric species that populate the aggregation process. The transient nature and

low population levels of aggregation intermediates have hampered their identification and detailed structural characterization. Amyloid formation can take place through several pathways, generating a high heterogeneity of oligomeric species, which further complicates their characterization. Even so, several protocols to isolate aggregation intermediates have been developed for a wide variety of amyloidogenic proteins. Characterization of such aggregates has unveiled the features that confer aggregate intermediates the ability to engage in aberrant and toxic interactions with multiple key cellular factors. These include β-sheet secondary structure, solvent-exposed hydrophobic regions and size (Cremades, Chen and Dobson, 2017).

1.2.2.1. *β-sheet secondary structure*

Early amyloid oligomers are enriched in disordered structures hence they are rather unstable. Acquirement of the β-sheet structure increases their stability and thus, their half-life time, which translates into more time to participate in abnormal interactions (Cremades *et al.*, 2012; Chen *et al.*, 2015; Iljina *et al.*, 2016). In addition, this structural rearrangement causes a rigid architecture promoting the exposure of hydrophobic patches on the aggregate surface that would not be accessible otherwise (Fusco *et al.*, 2017; Captini et al., 2018; Vivoli Vega *et al.*, 2019).

1.2.2.2. *Solvent-exposed hydrophobic regions*

Hydrophobicity is a major contributing factor to protein structure and function. For most water-soluble proteins, hydrophobicity is the main force driving folding as apolar groups are forced together by water molecules, generating a strongly hydrophobic core from which the protein structure is built up. On the native protein, the surface is mainly constituted by polar residues, avoiding the energetic cost of exposing apolar groups to the polar solvent. Yet, proteins tend to present biologically relevant hydrophobic patches that are involved in the recognition and

binding of ligands and other proteins. When a protein misfolds, large hydrophobic clusters on their surface are exposed to the solvent. Such exposure seems to be a prime determinant of amyloid toxicity, favoring abnormal interactions with cellular components (Bolognesi *et al.*, 2010; Olzscha *et al.*, 2011). For a range of amyloidogenic peptides and proteins, aggregates with increased toxicities have been shown to present a higher solvent-exposed hydrophobicity: tau (Lasagna-Reeves *et al.*, 2010), $A\beta_{42}$ (Bolognesi *et al.*, 2010; Ladiwala *et al.*, 2012), α-syn (Cremades *et al.*, 2012; Chen *et al.*, 2015), the NM region of Sup35p (Krishnan *et al.*, 2012), lysozyme and the SH3 domain of PI3 kinase (Bolognesi *et al.*, 2010) and HypF-N (Campioni *et al.*, 2010). For the latter, the toxicity of different oligomer species was found to correlate strongly and inversely with their size and directly with their surface hydrophobicity (Mannini *et al.*, 2014).

1.2.2.3. Aggregate size

A wide spectrum of assembly sizes is formed along the amyloid formation process. Depending on the aggregate size, different toxicity mechanisms have been described, jointly contributing to pathogenesis.

The major toxic effect of amyloid arises from the small-sized aggregate intermediates that populate the assembly process. Their large surface/volume ratios, which increase the active surface per protein molecule, and their high diffusion coefficient, allow them to form aberrant interactions more readily (Mannini *et al.*, 2012). Particularly, they can disrupt cell membranes, induce oxidative stress, dysregulate calcium homeostasis, cause mitochondria dysfunction or impair the proteasome system (Cremades, Chen and Dobson, 2017). Analysis of the results reported on exogenously added $A\beta_{40}$ and $A\beta_{42}$ aggregates clearly showed the importance of aggregate size (Chiti and Dobson, 2017; De *et al.*, 2019). Monomers, dimers, and trimers (4–14 kDa) of Aβ displayed minimal toxicity. Small oligomers with sizes ranging 18-90 kDa exhibited the maximum toxicity, which then

gradually decreased with increasing oligomer size (100-670 kDa) and ended up being residual for mature fibrillar structures. This was corroborated for α-syn, as a comparison of two types of oligomers of this protein with the same degree of β-sheet structure and solvent-exposed hydrophobicity indicated that the smaller species were more toxic (Lorenzen *et al.*, 2014).

As the final product of the aggregation process, mature fibrils are the largest assemblies, which tend to cluster and form deposits. Their highly packed structure, low surface/volume ratio and low diffusion coefficient reduce inappropriate interactions with cellular components. Nonetheless, they are far from harmless and contribute to toxicity through indirect mechanisms. For instance, it has been shown that key components of the protein homeostasis network that attempt to clear amyloid deposit can be sequestered, reducing the cell power to cope with aggregation (Olzscha *et al.*, 2011; Park *et al.*, 2013; Hipp, Park and Hartl, 2014; Yu *et al.*, 2014; Labbadia and Morimoto, 2015; Choe *et al.*, 2016; Guo *et al.*, 2018). Additionally, mature fibrils serve as a reservoir of aggregate intermediates. Although the amyloid structure is energetically highly favorable (Baldwin *et al.*, 2011), amyloid fibrils are not static entities but exist in equilibrium with monomer and oligomeric species (Carulla *et al.*, 2005). Spontaneous fragmentation and secondary nucleation are well-established mechanisms by which mature fibrils can generate new intermediate species (Knowles *et al.*, 2009; Cohen *et al.*, 2013; Buell *et al.*, 2014; Meisl *et al.*, 2014). Indeed, such processes seem to play a key role in the spreading of the disease within an organism, as these small-sized aggregates are the ones that are transmitted between cells and within organs.

1.2.3. Prion-like propagation of amyloids

Prion diseases, such as Creutzfeldt-Jakob disease in humans, bovine spongiform encephalopathy in cattle, and scrapie in sheep, are a class of fatal neurodegenerative diseases. Although most cases of prion diseases have sporadic

or genetic causes, some are acquired due to the ability of prions to transmit between individuals of the same or different species. The 'protein-only' hypothesis (Prusiner, 1982) states that the transmissible prion agent comprises solely the PrP protein (PrP^c), which converts into an abnormal conformer (PrP^{Sc}) that aggregates into amyloid fibrils with cross-β sheet architecture that accumulate in neurons (McKinley, Bolton and Prusiner, 1983; DeArmond *et al.*, 1985; Liberski *et al.*, 1991; Aguzzi, Nuvolone and Zhu, 2013). Small soluble oligomeric species of PrP^{Sc} exert higher cytotoxicity than mature fibrils (Simoneau *et al.*, 2007) and have been shown to be the most efficient mediators of prion infectivity (Silveira *et al.*, 2005). These small intermediate amyloid species are able to propagate through several mechanisms (summarized in **Figure 1.5**) to other cells, where they transmit the toxic conformation to the local protein pool, inducing its aggregation.

In recent years, other disease-associated amyloidogenic proteins such as Aβ, tau or α-syn, have been shown to have a 'prion-like' spreading and self-propagation, transmitting the histopathological traits of their associated disease within an organism (Brundin, Melki and Kopito, 2010; Jucker and Walker, 2013; Prusiner, 2013; Brettschneider, Tredici and Lee, 2015; Walker and Jucker, 2015; Aguzzi and Lakkaraju, 2016; Kara, Marks and Aguzzi, 2018; Scheckel and Aguzzi, 2018). This phenomenon begins in a specific location, through primary nucleation or acquirement of exogenous aggregation nuclei. Transmission of such seeds from cell to cell within the same tissue, and even across interconnected regions of different organs, causes the spreading of the toxic conformation. In this new location, amyloid aggregates self-propagate through a process called seeding, catalyzing the conversion of monomers from their native state to a pathological, aggregation-prone conformation. These 'daughter' aggregation nuclei can further propagate themselves, preserving the structural features of the 'paternal' seeds.
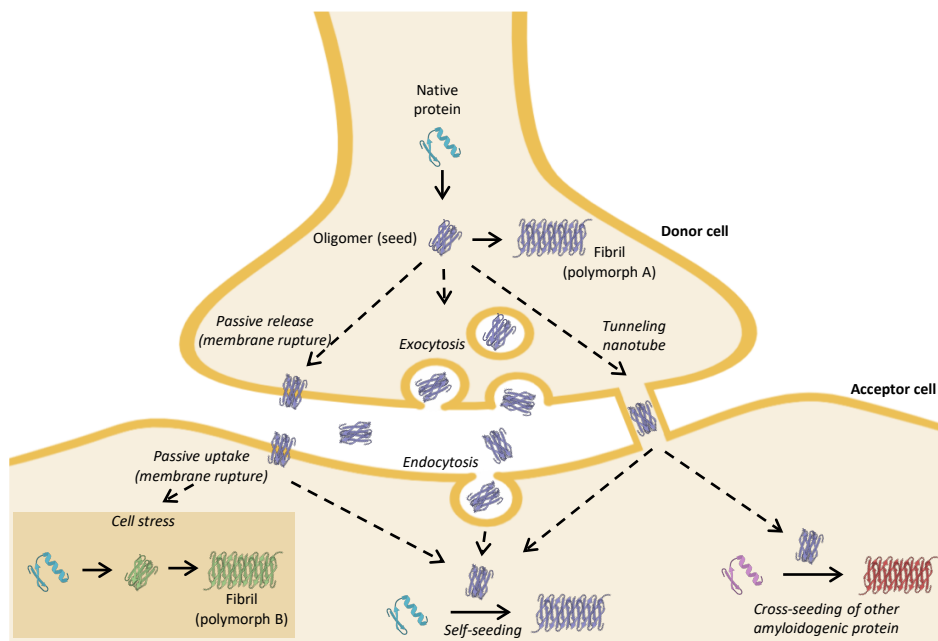
Figure 1.5. Prion-like propagation of amyloids. The aggregation process starts in the donor cell, where an amyloidogenic protein in its native state misfolds and aggregates, generating seeds through primary nucleation. These seeds can grow to form mature fibrils with a characteristic conformation (polymorph A) or can propagate to other cells via exocytosis and endocytosis, tunneling nanotubes or passive release, disrupting the cell membrane in their wake in this last case. In the acceptor cell, seeds can induce the aggregation of the same (self-seeding) or other (cross-seeding) amyloidogenic protein. Through self-seeding, aggregation occurs as a templating process, maintaining the fibril conformation. When the entry of seeds into the cell causes stress, aggregation may be indirectly induced, giving rise to a different fibril conformation (polymorph B).

It is increasingly evident that the same polypeptide sequence can adopt several pathological conformations, known as amyloid polymorphs (Rossi, Baiardi and Parchi, 2019). Polymorphs can differ in their propagation rates or the cell types they affect, which may translate into different molecular and clinical phenotypes. In those cases, polymorphs are referred to as strains and are believed to be the reason why proteins like tau or α-syn are involved in a spectrum of neurodegenerative diseases (Scheckel and Aguzzi, 2018). Although intrinsic

mechanisms of aggregate multiplication, such as elongation, fragmentation, or secondary nucleation can explain the ability of an aggregate to trigger spreading, indirect mechanisms can contribute to it. For instance, aggregate binding to or entering a cell could generate a stress response, indirectly inducing the formation of more aggregates which not necessarily share a common structure with the original seed (Meisl, Knowles and Klenerman, 2020).

Amyloid propagation is not always sequence-specific (self-seeding), as it has been observed between different isoforms, post-translationally modified variants or point-mutants of the same protein/peptide. Heterologous seeding, also known as cross-seeding, has also been observed between different amyloidogenic proteins, including PrP, Aβ, tau, α-syn, TDP-43 or Islet Amyloid Polypeptide (IAPP, a protein that forms amyloid aggregates in the pancreas) (Morales, Moreno-Gonzalez and Soto, 2013; Chaudhuri *et al.*, 2019). These cross-talked molecular interactions can be unidirectional or work in both directions for the proteins involved. The coexistence of multiple heterologous proteins in the same aggregate deposit or even within the same amyloid aggregate shows the relevance of cross-seeding processes *in vivo*. Such processes provide a mechanistic explanation for various observations in distinct diseases: the simultaneous presence of different misfolded proteins in one disease; the exacerbation of clinical features when various misfolded protein aggregates accumulate simultaneously; the epidemiological observation that one ND may be a risk factor for the development of a second one; and the coexistence of more than one ND in the same individual.

Prion infection between individuals occurs by ingestion or iatrogenic transmission of preformed PrP aggregates, which results from organ transplants or treatment with biological derivatives extracted from contaminated organisms. Although there is no evidence that amyloidogenic proteins involved in AD, PD or ALS are transmitted between individuals, considering the increasing prevalence of

these diseases and given that these proteins exhibit a similar behavior to prions, they should be treated with caution and their potential infectivity should continue being a subject of investigation (Kara, Marks and Aguzzi, 2018).

1.3. α-SYNUCLEIN

1.3.1. α-synuclein function and disease

The synucleins are a family of proteins consisting of three members: α-, β-, and γ-synuclein (Surguchov, 2015; Surguchev and Surguchov, 2017). Since their discovery, α-syn has been the focus of intensive research for its association with neurodegeneration. α-syn is very abundant in neurons, being primarily located at the presynaptic termini (Iwai *et al.*, 1995). Although it represents 1% of the cytosolic proteins, up to a third of the total α-syn can be found bound to synaptic membranes (Visanji *et al.*, 2011). It is also believed to play a major role in the regulation of synaptic trafficking, homeostasis, and neurotransmitter release by interacting with both synaptic vesicles and synaptic proteins such as phospholipase D2, members of the RAB small GTPases family and SNARE complexes (**Figure 1.6 a**). Other cellular processes in which α-syn is involved include signal transduction, mitochondria functioning and oxidative stress regulation (Cremades, Chen and Dobson, 2017).

Aggregation of α-syn into amyloid fibrils and their subsequent accumulation into intracellular inclusions is a hallmark of many neurodegenerative disorders collectively known as synucleinopathies. Within this group, dementia with Lewy bodies (DLB), multiple system atrophy (MSA) and PD are the most common. In PD and DLB, inclusions are preferentially found inside neurons and are called Lewy bodies (LBs) and Lewy neurites (LNs), while in MSA these inclusions localized in glial cells as poorly organized bundles of fibrils and are referred to as glial cytoplasmatic inclusions (Cremades, Chen and Dobson, 2017). Although the general belief was that α-syn was the major component of these intracellular inclusions, recent

studies have revealed that their composition is highly heterogeneous, containing cytoskeletal elements, membrane fragments, vesicles, lysosomes, mitochondria and other misshapen organelles (Shahmoradian *et al.*, 2019; Trinkaus *et al.*, 2020). Aggregation of α-syn plays a key role in their formation by constituting a scaffold of fibrillated protein that sequesters all these cellular components (Mahul-Mellier, 2020). Thus, the formation of LB-like inclusions has been suggested to be the major driver of neurodegeneration by disrupting cellular functions such as organellar trafficking and inducing mitochondria damage and deficits, all contributing to synaptic dysfunctions (Shahmoradian *et al.*, 2019; Mahul-Mellier, 2020).

1.3.2. Structural basis of α-synuclein aggregation

The *SNCA* gene encodes a 140 residues long protein that can be divided into three regions (**Figure 1.6 b**): the amphipathic N-terminal region which comprises residues 1-60; the non-amyloid β component (NAC) region (residues 61-95) characterized by the presence of hydrophobic residues; and the C-terminal region, which consist of residues 96-140 and is enriched in acidic residues, being responsible for the protein´s overall negative charge. Although most cases of synucleopathies are sporadic and have a late age of onset, several mutations in the *SNCA* gene have been identified in familial cases of PD, including gene duplications/triplications and several single-point mutations (A30P, E46K, A53T, A53E, A53V, H50Q, G51D). These mutations are normally linked to an early onset of the disease as most of them promote aggregation.

In the cytosol, α-syn is primarily monomeric and intrinsically disordered. Upon binding to lipid membranes, the N-terminal region and most of the NAC segment, which together contain seven imperfect repeats of 11 residues, fold into an amphipathic α-helical structure (**Figure 1.6 c**). The NAC domain is also a critical element in fibril formation, switching from a random coil state to a highly hydrophobic and easily aggregating β-sheet state (Li *et al.*, 2002). Early structural

studies on α-syn fibrils produced *in vitro* (Vilar *et al.*, 2008; Rodriguez *et al.*, 2015; Tuttle *et al.*, 2016) stated that residues 30-110 in a Greek-key topology formed the fibril core, which was flanked by the N- and C-terminal residues that remain unstructured (**Figure 1.6 d**).
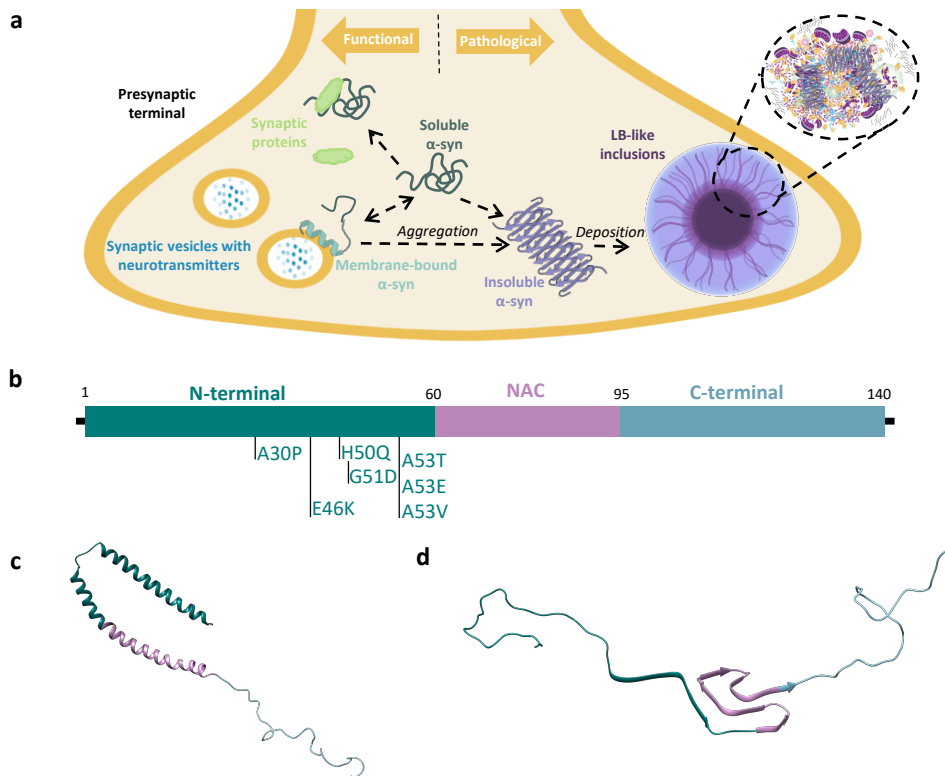
Figure 1.6. Structural basis of α-syn function and aggregation. (a) Under non-pathological circumstances, soluble and membrane-bound α-syn interact with different synaptic partners to perform its functions. Upon misfolding and aggregation, these functions are lost and insoluble α-syn starts depositing and sequestering different cellular components, giving rise to LB-like inclusions. Cartoon of the internal composition of LB was adapted from Shahmoradian et al., 2019. (b) Schematic domain organization of α-syn. PD familial mutations in the N-terminal domain are marked. (c) Structure of a micelle-bound α-syn monomer (PDB: 1XQ8). (d) Structural model of an α-syn fibril determined by solid-state nuclear magnetic resonance (PDB: 2N0A). The three domains in (c) and (d) are color-coded according to (b).

In recent years, technological advances in the cryo-electron microscopy (cryo-EM) field have made it possible to solve the structure of amyloid fibrils at high resolution. Different structures have been reported for α-syn$_{WT}$, revealing that *in vitro* aggregation might generate several possible polymorphs depending on the aggregation conditions (Guerrero-Ferreira *et al.*, 2020). In most atomic structures known to date, fibrils with a diameter of ~10 nm are composed of two identical protofilaments. The main differences between polymorphs are the number of β-strands and the residues involved in their formation (**Figure 1.7**), as well as the residues that participate in the interface between protofilaments (from 2 to 12 residues) (Li, Ge, *et al.*, 2018; Guerrero-Ferreira *et al.*, 2019). Interestingly, residues E46, H50, G51 and A53 are normally located at this interface, highlighting the relevance on fibril formation and growth of point-mutations at these sites. In fact, the structures of fibrils carrying the E46K, H50Q and A53T mutations have revealed that these mutations change the protofibril interface and can promote a different fibril fold, as is the case of E46K (Boyer *et al.*, 2019; Guerrero-Ferreira *et al.*, 2019; Zhao, Li, *et al.*, 2020).

A recent study showed that the structure of fibrils obtained from MSA patients differs from those assembled from recombinant proteins (Schweighauser et al., 2020). MSA-derived fibrils are formed by the asymmetrical packing of two pairs of different protofilaments, with a protofilament interface spanning more than 25 residues from each non-identical protofilament. In addition, they suggest that different conformers of assembled α-syn exist in DLB. This put forward that fibrils obtained *in vitro* may not fully represent the pathological aggregation occurred in some synucleopathies. Nevertheless, they are useful to describe their potential toxicity and the ability of the cellular machineries to process them.
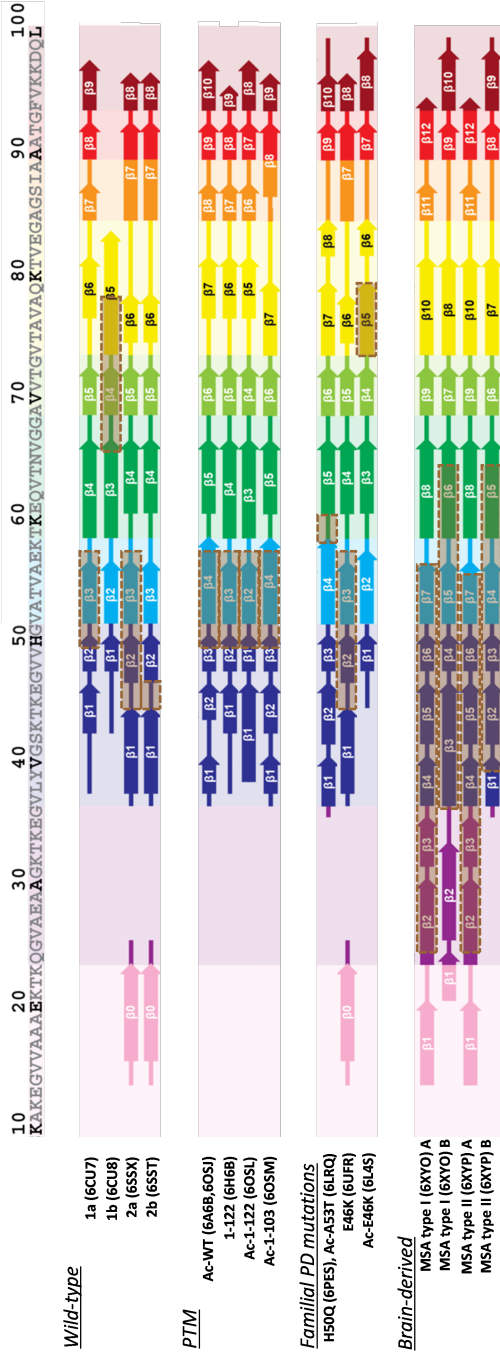
Figure 1.7. Structures of α-syn protofilament cores.

Schematic depicting of amino acids 10-100 of human α-syn, comparing secondary structure elements in protofilament cores of the different structures resolved by cryo-EM. Wild-type, PTM and Familial PD mutations groups of structures were obtained from recombinantly expressed α-syn. In these cases, fibrils are composed of two identical protofilaments and the interface between them is highlighted in brown. For the WT protein sequence, four polymorphs have been found with 3 different arrangements of β-sheets. Polymorphs 2a and 2b have the same β-sheet arrangement but differ in the protofilament interface. Regarding PTMs, both N-terminal acetylation and C-terminal truncation seem to have little effect on fibril's secondary structure, with a comparable β-sheet arrangement to polymorph 1a. Similarly, neither H50Q nor A53T have significant disturbance on the fold of 1a, instead, they change the paring geometry of the protofilaments. In the case of the E46K mutation, two structures have been published, one similar to the 2a polymorph and another one, with an N-terminal acetylated protein that has a different and more stable fold. Structures of two distinct fibrils (type I and II) derived from brains of deceased MSA patients differ from those obtained *in vitro*. In these cases fibrils are composed of two different protofilaments (A and B) that interact with each other with different residues and the interfaces are much more extended. Adapted from Schweighauser et al. 2020.

1.3.3. *In vitro* aggregation of α-synuclein

Monomeric α-syn is remarkably stable in solution at physiological concentration (50 μM) under quiescent conditions at neutral pH. *In vitro* aggregation of the protein is induced by the introduction of specific interfaces including, air/water (increased by mechanical agitation) (Campioni *et al.*, 2014), detergent/water (Giehm *et al.*, 2010), lipid/water (Galvagnion *et al.*, 2015, 2016; Grey *et al.*, 2015) or polystyrene/water (Grey *et al.*, 2011; Vácha, Linse and Lund, 2014; Gaspar *et al.*, 2017). At such interfaces, there is a surface-induced nucleation which generates aggregate-competent nuclei that can grow to finally form well-defined fibrils.

Compared to α-syn fibrils, obtaining aggregation intermediates is complicated given their transient nature. A variety of procedures have been used to trap or isolate some of these oligomeric forms. These include the involvement of a change in physicochemical conditions or the addition of chemical compounds (Cremades, Chen and Dobson, 2017). One of the most commonly employed methods to promote the formation of oligomers involves the use of lyophilization, which increases intermolecular interactions and the access of protein molecules to solvent/air interfaces. Oligomers formed by lyophilization are remarkably stable and have been suggested to be kinetically trapped, as do not elongate readily to form fibrils (Chen *et al.*, 2015). These oligomers contain largely antiparallel β-sheet structures and exist as a heterogeneous population of species with an average size of approximately 30 monomers (10-90 mer) (Chen *et al.*, 2015). More importantly, they can disrupt cellular membranes and, consequently, induce neuronal toxicity (Chen *et al.*, 2015; Fusco *et al.*, 2017). Interestingly, the fluorescence resonance energy transfer (FRET) signature and biological properties of these oligomers closely match those previously identified for toxic (type B) α-syn oligomers during *in vitro* fibril formation (Cremades *et al.*, 2012), highlighting their relevance as a model aggregate.

1.3.4. Post-translational modifications of α-synuclein

α-syn is subjected to extensive post-translational modifications (PTMs) (Barrett and Timothy Greenamyre, 2015; González *et al.*, 2019; Zhang, Li and Li, 2019; Schaffert and Carter, 2020). Of all the PTMs associated with α-syn, phosphorylation is the most studied. The majority of the reported phosphorylation sites are located at the C-terminal domain. Serine 129 is of special interest, as most of α-syn is phosphorylated at this residue in the brains of patients that suffered from synucleinopathies (González *et al.*, 2019). While the exact function of this modification is still unclear, it appears to regulate its structure, membrane binding, aggregation, neurotoxicity and subcellular distribution. Acetylation is also commonly studied for α-syn as this protein seems to be ubiquitously acetylated at the N-terminus, a modification that increases its membrane binding. N-terminal acetylation does not alter the conformational and topological properties of the fibrillar (**Figure 1.7**) or of the membrane-bound states (Li, Zhao, *et al.*, 2018; Runfola *et al.*, 2020), although it has been shown to slower fibrillation (González *et al.*, 2019; Schaffert and Carter, 2020). Such deceleration has also been reported for other modifications like SUMOlyation, nitration or O-GlcNAcylation, which interestingly favors oligomer formation by reducing their transition to fibrils (Schaffert and Carter, 2020).

Truncation is one of the predominant PTMs of α-syn. Both N- and C-terminally truncated α-syn species have been found in the brains of healthy and diseased individuals (Li *et al.*, 2005; Muntané and Ferrer, 2012; Kellie *et al.*, 2014; Bhattacharjee *et al.*, 2019). Levels of truncated variants can account for up to 15-25% of the total α-syn, being enriched in Lewy-Body insoluble fractions from cases of synucleinopathy (Baba *et al.*, 1998; Li *et al.*, 2005; Anderson *et al.*, 2006; Kellie *et al.*, 2014). Several reports show that truncation strongly influences α-syn aggregation and prion-like pathogenicity (Liu *et al.*, 2005; Terada *et al.*, 2018;

Gallardo, Escalona-Noguero and Sot, 2020). Particularly, α-syn C-terminal truncation enhances aggregation and neurodegeneration *in vivo* (Michell *et al.*, 2007; Periquet *et al.*, 2007; Ulusoy *et al.*, 2010). This relates to the increased *in vitro* aggregation propensity found for truncated mutants (Sot *et al.*, 2017; Ma *et al.*, 2018; Sorrentino *et al.*, 2018; Terada *et al.*, 2018). Certainly, it has been suggested a protective role for the charges at the C-terminus via long-range intramolecular interactions, which are disrupted upon truncation thus favoring aggregation (Murray *et al.*, 2003; Hoyer *et al.*, 2004; Izawa *et al.*, 2012; Levitan *et al.*, 2012; Gallardo, Escalona-Noguero and Sot, 2020). In terms of fibrils structure, C-terminal truncated variants present a similar fold to the full-length protein (**Figure 1.7**), but they have an increased helical twist, generating a more packed core (Ni *et al.*, 2019). Additionally, C-terminal charges have an important role to avoid interfibrillar interaction through electrostatic repulsion. Due to C-terminal deletion, these long-range repulsive interactions are lost and fibrils associate laterally, favoring their packing into higher-organized suprafibrillar aggregates that are essential for LB-like formation (Semerdzhiev *et al.*, 2014; Iyer *et al.*, 2017; Mahul-Mellier *et al.*, 2018; van der Wateren *et al.*, 2018).

1.4. TAU

1.4.1. Tau function and disease

Microtubule-associated proteins (MAPs) are a family of proteins that play a central role in microtubule (MT) dynamics by regulating their assembly, dynamic behavior, and spatial organization (Bodakuntla *et al.*, 2019). Tau constitutes over 80% of neuronal MAPs and it is mainly found in axons, where it binds, stabilizes, and bundles microtubules (Conde and Cáceres, 2009). Furthermore, tau induces the self-assembly of tubulin *in vitro*, suggesting a role as a MT inducer (Barbier *et al.*, 2019). Under pathological circumstances, tau detaches from the MTs (**Figure 1.8 a**).

PTMs such as hyperphosphorylation or mutations in the tau gene identified in frontotemporal dementia with Parkinsonism linked to chromosome 17 (FTDP-17), impair tau's binding to MTs and its stabilizing effect (Barbier *et al.*, 2019). Tau then accumulates in the cytosol, where it misfolds and starts assembling into abnormal filamentous aggregates, which gather into intracellular deposits known as neurofibrillary tangles. NDs with abundant filamentous tau inclusions are referred to as tauopathies and include AD, corticobasal degeneration (CBD), Pick´s disease (PiD) or chronic traumatic encephalopathy (CTE). These diseases present diverse clinical syndromes with substantial variability in phenotype. Traditional syndrome-based classification of tauopathies is nowadays being complemented with a molecular-pathological classification that considers the tau isoform involved (pure 3R or 4R and mixed 3R/4R tauopathies), inclusion morphology, and cell types and brain regions affected (Höglinger, Respondek and Kovacs, 2018; Götz, Halliday and Nisbet, 2019).

1.4.2. Structural basis of tau aggregation

Tau is encoded by the *MAPT* gene located at chromosome 17. Upon alternative mRNA splicing of the *MAPT* gene, six tau isoforms of different lengths (352–441 amino acids) are produced (Goedert *et al.*, 1989). Tau proteins are broadly organized into two domains, the projection and the microtubule-binding domains (**Figure 1.8 b**). The projection domain protrudes from the microtubule surface and it is composed of a highly negatively charged region, the inserts N1 and N2, and two proline-rich regions (P1 and P2). The microtubule-binding domain (MTBD) is enriched in positively charged residues, assisting its interaction with the negatively charged surfaces of MTs. This domain accommodates four imperfect repeat regions of 31/32 amino acids (R1, R2, R3, R4) flanked by the second proline-rich region and a pseudo-repeat (R´). The isoforms differ by the absence or presence of inserts N1 or N2 and the repeat region R2 (**Figure 1.8 b**).
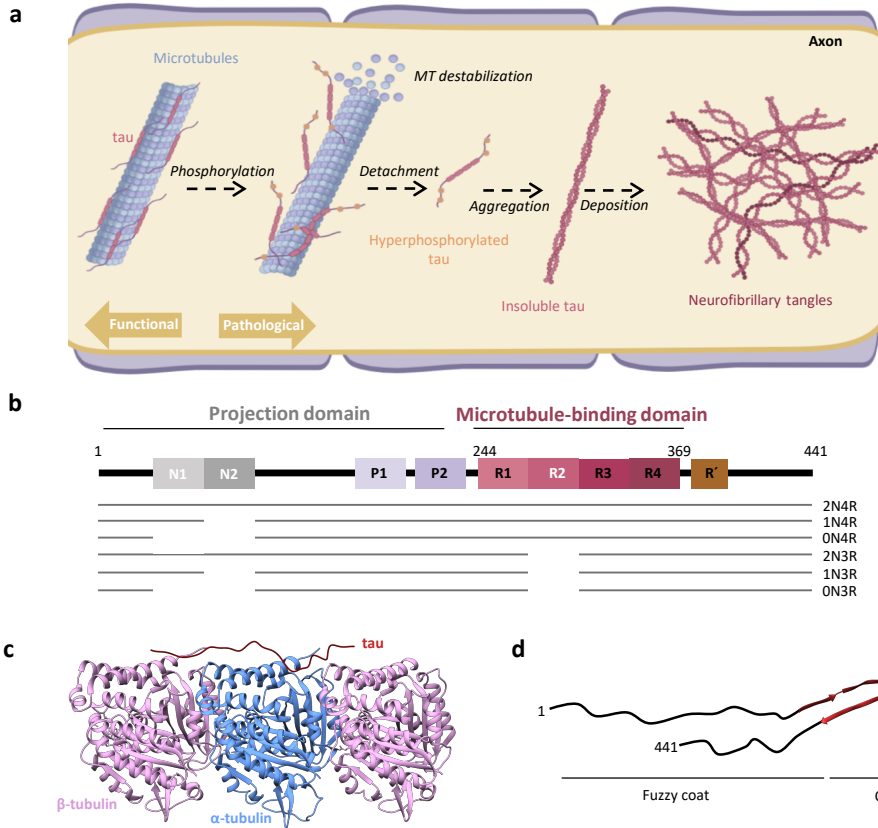
Figure 1.8. Structural basis of tau function and aggregation. (a) The functional role of tau is MT stabilization. Upon phosphorylation, tau detaches from the MTs and starts aggregating in the cytosol, giving rise to amyloid deposits. (b) Schematic domain organization of the different tau isoforms. (c) cryo-EM reconstruction of synthetic R2x4 tau on MTs (PDB: 6CVN) (d) Structural model of AD-derived tau fibrils determined by cryo-EM (PDB: 5O3T).

Due to the high amount of polar amino acids, tau is a highly soluble protein with little secondary structure, even when bound to MTs (Kellogg *et al.*, 2018) (**Figure 1.8 c**). However, two motifs within the MTBD termed PHF6* ($_{275}$VQIINK$_{280}$) and PHF6 ($_{306}$VQIVYK$_{311}$) have a high β-sheet-forming propensity and promote aggregation (von Bergen *et al.*, 2000, 2001). Recent structural studies on amyloid fibrils derived from post-mortem diseased-brains have identified differently folded forms of tau (Fitzpatrick *et al.*, 2017; Falcon *et al.*, 2018, 2019; Zhang *et al.*, 2020).

In all cases, fibrils are formed by two identical protofilaments, each presenting a fibril core flanked by the amino- and carboxy-terminal regions of tau that remain disordered and project away, forming a fuzzy coat (Fitzpatrick *et al.*, 2017) (**Figure 1.8 d**). Within the fibril core, PHF6 forms a β-strand common in tau filaments from four human tauopathies, and together with other partially conserved β-strands within residues 254-380, form fixed building blocks for fibril formation (Fitzpatrick *et al.*, 2017; Falcon *et al.*, 2018; Zhang *et al.*, 2020). Loops and turns between these strands provide flexibility, explaining the diversity between conformers (**Figure 1.9**). These results have led to the hypothesis that each tauopathy may be characterized by its unique amyloid fibril structural signature (Fitzpatrick and Saibil, 2019).

1.4.3. *In vitro* aggregation of tau

Aggregation of full-length tau *in vitro* is generally slow because of the charged, highly soluble nature of the protein. *In vitro* aggregation studies have therefore tended to focus on constructs formed from the aggregation-prone repeat region of the MTBD (K18 and K19), which lack the flanking N- and C-terminal tails and aggregate faster (Gustke *et al.*, 1994). Additionally, polyanion cofactors accelerate aggregation by interacting with tau and compensating the positive charges of the protein, which reduces the electrostatic repulsion between tau molecules (Goedert *et al.*, 1996; Kampers *et al.*, 1996; Jeganathan *et al.*, 2008). Heparin is one of the most commonly used polyanions for *in vitro* tau aggregation (Ramachandran and Udgaonkar, 2011). Although the overall fold of heparin-induced filaments is different from the folds found in tauopathies (Zhang *et al.*, 2018), there are also similarities between them (**Figure 1.9**). Heparin-induced tau filaments are also made of identical rungs of tau molecules that form cross-β structures by parallel stacking of identical β-strands along the helical axis. Perpendicular to the helical axis, the β-strands are interspersed with short loop flexible regions that allow

packing otherwise similar β-strands against each other in different cross-β arrangements. These similarities allow the use of heparin-induced filaments as an *in vitro* model, although caution must be taken when comparing with *in vivo* systems.

1.4.4. Post-translational modifications of tau

Tau protein undergoes a wide range of PTMs such as phosphorylation, glycation, nitration, O-GlcNAcylation, acetylation, oxidation, ubiquitination, sumoylation, methylation, and truncation (Kontaxi, Piccardo and Gill, 2017; Park *et al.*, 2018). Since most tauopathies show pathological inclusions of hyperphosphorylated tau, numerous studies have focused on exploring tau phosphorylation. Phosphorylation reduces tau affinity for microtubules, resulting in microtubule destabilization and facilitating tau self-fibrillization (Park *et al.*, 2018). A total of 85 phosphorylatable residues (45 serine, 35 threonine, and 5 tyrosine) are present in tau and about 50% of them have been detected as phosphorylated, most of them located outside the MTBD. Interestingly, phosphorylation of tau concurrently occurs with other modifications especially at lysine residues which could suggest a crosstalk among tau PTMs.

Acetylation of KXGS motifs (K259, K290, K312, and K353) has been reported to prevent tau phosphorylation at these same motifs and decrease aggregation of recombinant tau *in vitro* (Cohen *et al.*, 2011; Cook *et al.*, 2014). Most lysine residues that are putative sites of acetylation are distributed in the MTBD. Acetylation neutralizes the positive charge of lysine residues in the MTBD thereby disabling tau binding to negative charges on the microtubule surface (Cohen *et al.*, 2011; Trzeciakiewicz *et al.*, 2017). Charge neutralization of lysines via acetylation makes parallel, in-register stacking of β-strands more favorable because of the lower charge repulsion between positively charged sidechains (Arakhamia *et al.*, 2020).
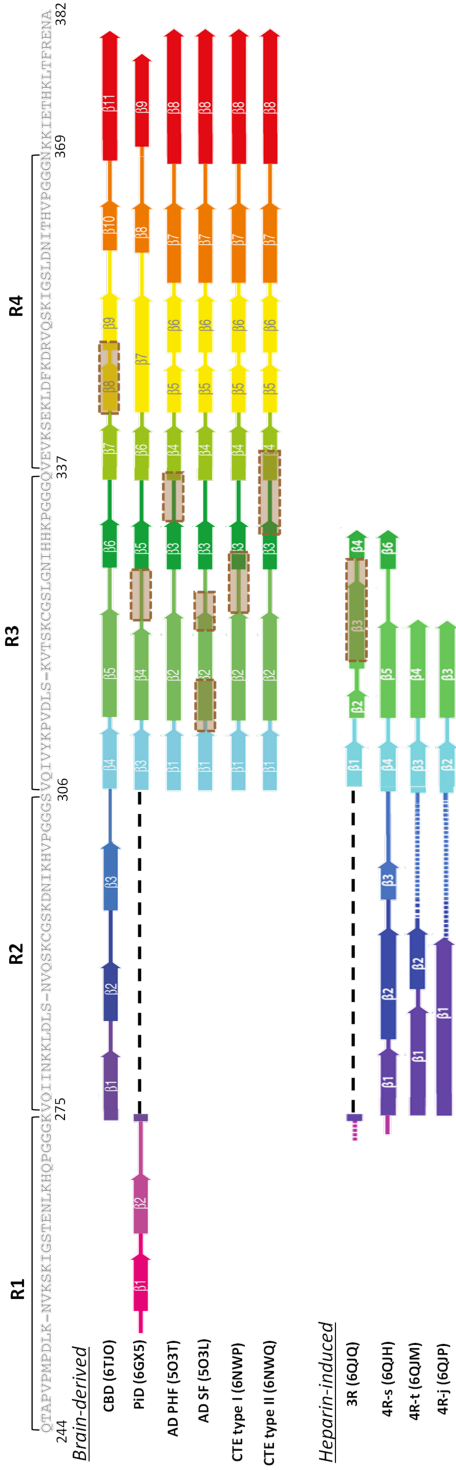
Figure 1.9. Structures of tau protofilament cores.

Schematic depicting of amino acids 244-382 of human tau, comparing secondary structure elements in protofilament cores of the different structures resolved by cryoEM. Filaments from PiD and the heparin-induced fibril called 3R are formed with an isoform lacking the R2 repeat. Two types of filaments have been reported for AD (PHF, paired helical filaments; and SF, single filaments) as well as for CTE (types I and II). The four conformers share the same β-sheet building blocks but differ in the protofilament interface (highlighted in brown). This interface is symmetric among protofilaments, except for AD SF, in which each protofilament interact with each other with different amino acids. In the case of CBD, 3 additional β-sheets are present within repeat R2. Similarly, filaments from PiD have two additional β-sheets in the repeat R1. Filaments produced *in vitro* using heparin as an inducer differ from those derived from brains. In these cases, β-sheets are formed within repeats R2 and R3. Furthermore, fibrils are composed of a single protofilament, except for the 3R fibrils, which present two protofilaments that interact with each other symmetrically. Adapted from Zhang et al. 2018 and 2020.

Furthermore, acetylation has been implicated in dysregulation of tau homeostasis due to the prevention of degradation mediated by the ubiquitin-proteasome system, preventing ubiquitination of lysine (Min *et al.*, 2010). Intriguingly, the role of tau ubiquitination in its degradation is rather controversial (Kontaxi, Piccardo and Gill, 2017; Park *et al.*, 2018). A combination of cryo-EM and MS-based proteomics of tau in sarkosyl-insoluble fractions from CBD and AD postmortem tissue shows that ubiquitination may help stabilize inter-protofilament packing by providing additional contacts between tau molecules in each protofilament (Arakhamia *et al.*, 2020). Therefore, it was proposed that PTMs, which show different profiles among tauopathies, could also be implicated in fibril´s final structure and thus, explain the structural diversity of tauopathy strains.

1.5. PROTEOSTASIS NETWORK

Cells have evolved a sophisticated protein homeostasis (proteostasis) network that coordinates protein synthesis, folding, disaggregation and degradation (Labbadia and Morimoto, 2015). The proteostasis network (PN) is composed of the translational machinery, molecular chaperones and cochaperones, the ubiquitin-proteasome system (UPS), and the autophagy-lysosome pathways (ALPs). The PN serves to ensure that correctly folded proteins are generated in the required amounts and at the right time and cellular location. Beyond regulation of protein synthesis and folding, the PN also prevents proteins from misfolding and aggregation and when this is not possible, it ensures that misfolded and aggregated protein species are removed. Together, these mechanisms avoid the existence of protein aggregates and thus, their potential toxic effect.

1.5.1. Molecular chaperones

We define a molecular chaperone as any protein that interacts with, stabilizes, or helps another protein to acquire its functionally active conformation, without being

present in its final structure. Molecular chaperones are key effectors of the PN guiding proteins along productive folding pathways, avoiding and sometimes reversing misfolding and aggregation and cooperating with the degradation machinery. There are several evolutionary conserved families of molecular chaperones and their members are often referred to as stress proteins or heat shock proteins (Hsps) because they are up-regulated in conditions of conformational stress. The major chaperone families are classified by their molecular weight, including the ATP-independent small heat shock (sHsps) and Hsp40 proteins and several ATP-dependent chaperone families (Hsp60, Hsp70, Hsp90, Hsp100).

sHsps function in holding denatured or non-native protein conformations to prevent their misfolding and aggregation and also mediate sequestration of misfolded proteins into less toxic aggregates (Treweek *et al.*, 2015). Among the ATP-dependent chaperone families, the Hsp70 family is the most ubiquitous and is essential for protein synthesis, folding, disaggregation, and degradation of a wide range of client proteins. Hsp70 disaggregation activity involves their co-chaperones, in particular J-domain proteins (Hsp40s, subdivided into classes A, B, and C) (Kampinga and Craig, 2010) and nucleotide exchange factors (NEFs) such as members of the Hsp110 family (Bracher and Verghese, 2015). In bacteria, fungi and plants, AAA+ ATPase complexes of the Hsp100 family cooperate with the Hsp70 system in disaggregation (Mogk, Kummer and Bukau, 2015). The Hsp70 chaperone system also interacts with Hsp90, which is another ATP-dependent chaperone. Together with its co-chaperones, Hsp90 aids in the folding of a wide array of clients including kinases, phosphatases, transcription factors and other signaling molecules (Morán Luengo, Mayer and Rüdiger, 2019). The chaperonins of the Hsp60 family, GroEL in bacteria and TRiC/CCT in eukaryotes, exist as multimeric assemblies that form a cage in which substrates are allowed to fold into their native state through an ATP-driven functional cycle. This machinery is critical to fold large

filamentous proteins such as actin and tubulin (Gestaut *et al.*, 2019).

All these chaperone systems differ fundamentally in their modes of substrate binding, the conformational states of the substrates they recognize, and the changes they impose on them. Such a variety allows the modulation of native/aggregate states through several mechanisms including *de novo* folding, prevention of aggregation, neutralization of aggregates, disaggregation, or protein degradation (**Figure 1.10**). Although some chaperones may be specialized in using a singular mechanism, the inherent promiscuity of several chaperones to interact with multiple conformational species of distinct substrates makes them able to interfere in various stages of the aggregation process.

1.5.1.1. Protein synthesis and folding

While the folding process was originally thought to occur spontaneously, many proteins, especially those with complex structures and/or containing multiple domains, require molecular chaperones to fold efficiently and at a biologically relevant timescale. Molecular chaperones that participate in the folding of newly synthesized proteins (*de novo* folding) recognize hydrophobic amino acid residues exposed by non-native proteins and promote their folding through ATP-regulated cycles of protein binding and release. In this mechanism of kinetic partitioning, the release of hydrophobic elements allows folding to proceed, whereas (re)binding of non-native protein blocks aggregation and may reverse misfolded states (Hipp, Kasturi and Hartl, 2019).

Chaperones can act in *de novo* folding during or after translation of the nascent polypeptide by the ribosome. Cotranslational folding is especially important for large proteins delaying chain compaction and preventing misfolding until sufficient structural elements are available for folding to be productive. Ribosome-binding chaperones interact first with the nascent polypeptide, followed

by chaperones that have no direct affinity for the ribosome, including the Hsp70 system. Completion of folding may either be accomplished by Hsp70 or require transfer to the chaperonins or Hsp90 systems. The different chaperone systems interact directly or use specific adaptor proteins to facilitate client transfer. In this way, the folding protein is constantly protected from aberrant interactions and aggregation (Balchin, Hayer-Hartl and Hartl, 2016).
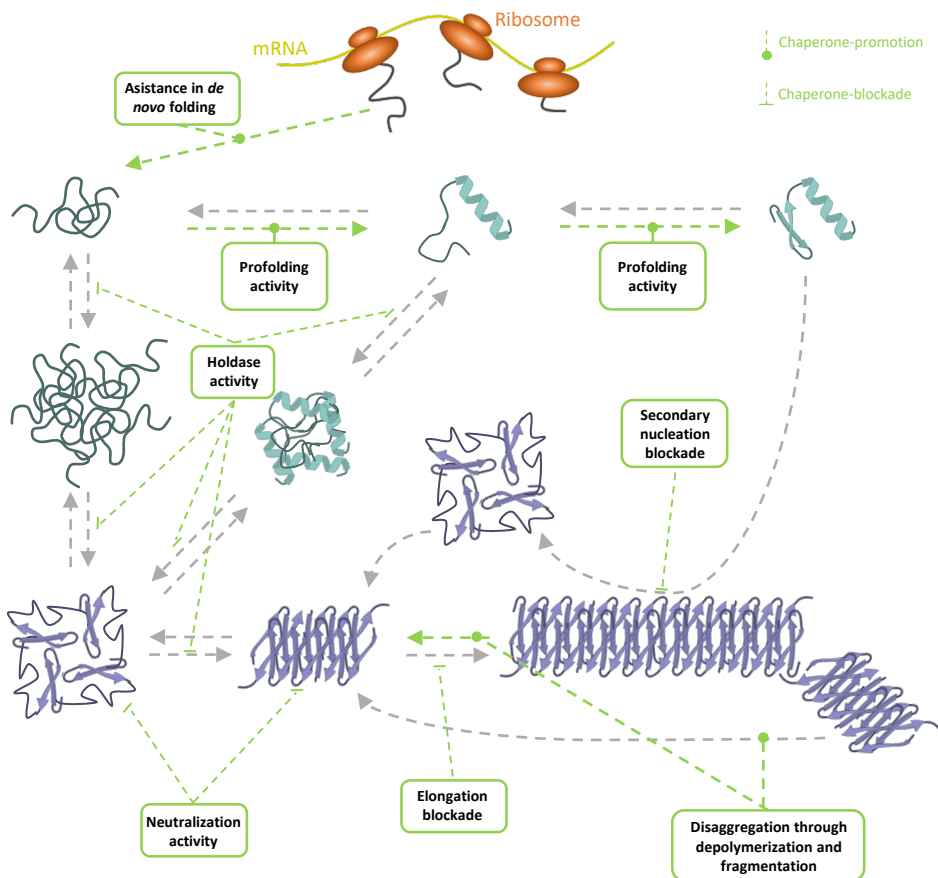
Figure 1.10. Mechanisms by which molecular chaperones modulate the different amyloid states along the aggregation process.

1.5.1.2. Prevention of protein aggregation

In most cases, the folded structures of proteins are only marginally stable, meaning that a substantial proportion of protein species may populate (partially) unfolded states. Under additional destabilizing factors, such as stress conditions or mutations, folding intermediates and misfolded states tend to aggregate, reducing the pool of functionally active molecules. To counteract aggregation, chaperones employ various molecular strategies, interacting with the different species that populate the aggregation process (Wentink, Nussbaum-krammer and Bukau, 2019).

Preservation of native protein folds is a classical strategy used by chaperones to prevent aggregation. Through folding and refolding activities, chaperones rescue destabilized or misfolded protein species back to their native state (Wentink, Nussbaum-krammer and Bukau, 2019). When the aggregation-prone protein is intrinsically disordered, which is the case of most amyloidogenic proteins, stabilization of the native state through chaperone 'profolding' activities is more challenging (Chiti and Dobson, 2017). In these cases, some chaperones can interfere with the primary nucleation step of the aggregation process. Transient interactions with aggregation-prone regions on the monomeric substrate sterically impairs the initial oligomerization step of aggregation. This strategy corresponds to the classical 'holding' activity of sHsps and canonical J-domain proteins and has also been observed for other Hsps, including Hsp70 and Hsp110 (Wentink, Nussbaum-krammer and Bukau, 2019). Primary nucleation can be also suppressed through interaction with prefibrillar oligomers rather than monomers, stabilizing intermediate non-seeding-competent states before their conversion into aggregation seeds. This particular mechanism is used by the non-canonical J-domain protein DnaJB6 to suppress the aggregation of various members of the polyQ expanded protein family and Aβ_{42} (Månsson *et al.*, 2014; Arosio *et al.*, 2016;

Kakkar *et al.*, 2016; Månsson, Van Cruchten, *et al.*, 2018) and also, by Hsp70 to inhibit IAPP aggregation (Chilukoti *et al.*, 2020).

Once nucleation occurs, aggregation seeds can rapidly elongate through the templated incorporation of monomers. Chaperones can compete with this process through the depletion of the available monomer pool (Wacker *et al.*, 2004; Luheshi *et al.*, 2010). Additionally, through a capping-like interaction localized at the ends of fibrils, chaperones prevent elongation by blocking further monomer addition and potentially, self-association of oligomers. Hsp70 has been described to act in this way, preventing the further elongation of the yeast prion Ure2p (Arosio *et al.*, 2016) and α-syn (Dedmon, Christodoulou, Wilson, *et al.*, 2005; Huang *et al.*, 2006; Aprile *et al.*, 2017). Interaction of the sHsp αB-crystallin (HspB5) with seed-component species also inhibits aggregation of Aβ, α-syn, lysozyme and β_2-microglobulin amyloid fibrils (Raman *et al.*, 2005; Waudby *et al.*, 2010; Shammas *et al.*, 2011; Mainz *et al.*, 2015). Yet, as binding αB-crystallin to fibrils occurs along the entire length of the fibril, this sHsp has been reported to interfere with secondary nucleation events catalyzed at the fibril surface as it has been described for BRICHOS domain-containing proteins (Arosio *et al.*, 2016). BRICHOS domains do not prevent the initial formation of $A\beta_{42}$ fibrils but reduce aggregate amplification by coating the aggregate surface and inhibiting secondary nucleation (Willander *et al.*, 2012; Cohen *et al.*, 2015; Arosio *et al.*, 2016).

1.5.1.3. Neutralization of protein aggregates

The β-sheet structure, exposure of hydrophobic patches to the solvent and small size of aggregation intermediates determine their cytotoxicity. Chaperone interaction with such species promotes shielding of the reactive surfaces preventing unspecific interactions with other cellular components. This neutralization mechanism is used by the sHsp HspB1 (Hsp27) and extracellular chaperones such as clusterin, α_2-macroglobulin, and haptoglobin to reduce the

toxicity of several oligomeric amyloidogenic proteins including α-syn, Aβ₄₂, IAPP, and HypF-N (Ojha *et al.*, 2011; Mannini *et al.*, 2012; Whiten *et al.*, 2018). The chaperonin TriC/CCT has also been shown to interact transiently with oligomeric and fibrillar species of Htt and α-syn, preventing aggregation and neutralizing their toxicity (Behrends *et al.*, 2006; Tam *et al.*, 2006; Shahmoradian *et al.*, 2013; Pavel *et al.*, 2016; Sot *et al.*, 2017). In some of these cases, neutralization is accompanied by the assembly into larger species upon chaperone interaction (Behrends *et al.*, 2006; Ojha *et al.*, 2011; Mannini *et al.*, 2012), consequently decreasing their diffusional mobility. A similar 'sequestrase' or 'aggregase' activity has been reported for yeast sHsp Hsp42, mediating the rapid concentration of misfolded proteins into small cytosolic aggregate foci (Specht *et al.*, 2011; Malinovska *et al.*, 2012; Escusa-Toret, Vonk and Frydman, 2014; Miller *et al.*, 2015). Interestingly, mammalian cells concentrate aggregated proteins in so-called aggresomes at the microtubule-organizing center in an ATP-dependent and microtubule-dependent process. This has been proposed to lower the level of small diffusible oligomers and thereby reduce the reactive surface and the number of bound chaperones, and also facilitate clearance by autophagy (Kopito, 2000).

1.5.1.4. Chaperone-driven disaggregation

Chaperone machineries known as protein disaggregases extract proteins from aggregates that can either be targeted to degradation or reactivated, sparing the energetic burden of novel biosynthesis. Bacteria, protists, plants, and fungi possess a powerful bi-chaperone disaggregase composed of the ring-shaped AAA+ chaperone Hsp100 (ClpB in bacteria, Hsp104 in yeast, and Hsp101 in plants) and the Hsp70 system. Hsp100 cooperates with the Hsp70 system to thread trapped polypeptides in an ATP-dependent manner through its central pore (Gates *et al.*, 2017; Avellaneda *et al.*, 2020), thereby resolving protein aggregates. Metazoan

lacks Hsp100 orthologs and thus, the disaggregation activity is chiefly provided by the Hsp70 system.

In collaboration with a specific subset of J-domain proteins (JDPs or Hsp40s) and NEFs, Hsp70 constitutes the so-called human disaggregase, which is capable of solubilizing a wide range of aggregated proteins (Shorter, 2011; Rampelt *et al.*, 2012; Gao *et al.*, 2015; Nillegoda *et al.*, 2015, 2017; Kirstein *et al.*, 2017). The functional cycle of Hsp70 is linked to ATP-hydrolysis (**Figure 1.11 a**). Protein disaggregation is initiated by JDPs, recognizing and binding to protein aggregate surfaces. JDPs then recruit Hsp70 to the aggregate, concomitantly interacting with both substrate and Hsp70, which results in stimulated ATP hydrolysis at the Hsp70 nucleotide-binding domain (NBD). ATP hydrolysis is coupled to a conformational cycle defined by large-scale movements of an alpha-helical lid domain that closes over the β-sandwich substrate binding pocket in the ADP state (**Figure 1.11 b**), resulting in substrate capture by the substrate-binding domain (SBD) of Hsp70. The ATP-bound state of Hsp70 (**Figure 1.11 c**) displays a low affinity for substrates due to high substrate off-rates. Upon ATP hydrolysis, the ADP-bound state acquires a high affinity for substrates due to the conformational change at the SBD, which lowers the substrate dissociation rate. The timely release of substrates is mediated by NEFs, which stimulate ADP exchange by ATP and reset Hsp70 for the next cycle of substrate binding. Rebinding of ATP and simultaneous opening of the substrate-binding pocket dissociates substrates from Hsp70, promoting localized polypeptide unfolding–refolding events.

The process whereby the Hsp70 chaperone converts the energy derived from ATP hydrolysis into pulling forces required for protein aggregate dissolution remains poorly understood (Wentink, Nussbaum-krammer and Bukau, 2019). It has been proposed a mechanism based on the entropic penalty associated with Hsp70 and co-chaperone binding to exposed sites on the aggregate surface (Wentink *et*

al., 2020). Such binding reduces the conformational space accessible to the large chaperone machinery due to an excluded volume effect caused by the physical barrier formed by the aggregate. In an attempt to restore conformational freedom, and the associated increase in entropic energy, Hsp70 applies a pulling force away from the aggregate surface, releasing trapped polypeptides. The initial entropic energy barrier associated with chaperone binding in this region is overcome by J-protein-stimulated ATP hydrolysis, which increases the affinity of Hsp70 for substrates by an order of magnitude through the inherent slower dissociation kinetics of the ADP state. This entropic pulling mechanism has also been used to explain Hsp70-mediated clathrin uncoating and protein translocation (Rios *et al.*, 2006; Sousa *et al.*, 2016).
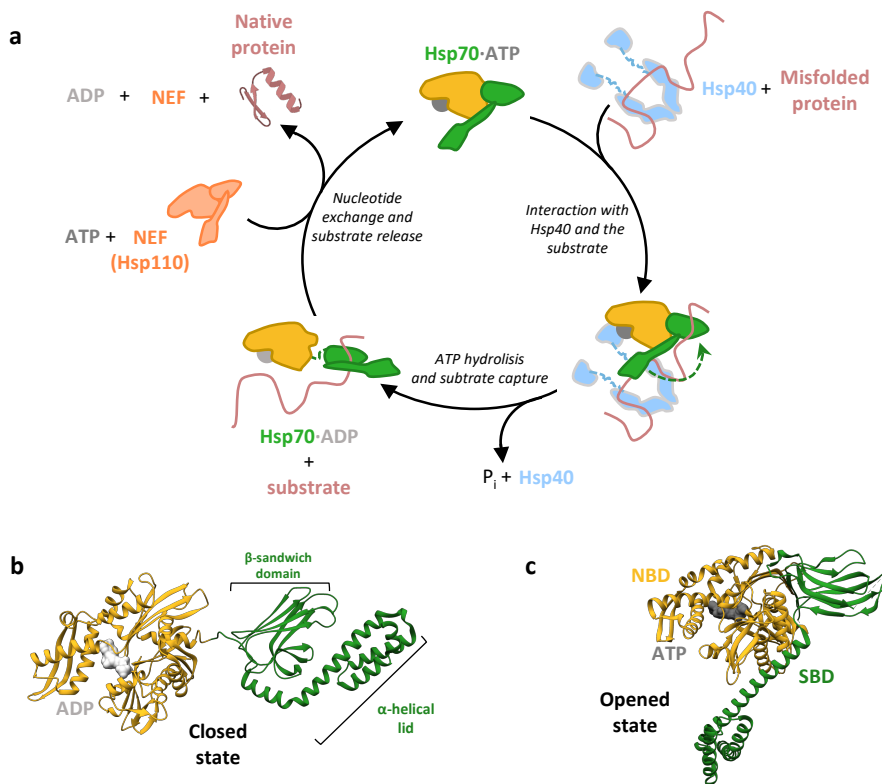
Figure 1.11. Functional cycle and structure of the Hsp70 chaperone. (a) Schematic representation of the Hsp70 ATPase cycle that mediates client protein (re)folding. (b) Closed

state of *Escherichia coli* DnaK bound to ADP (PDB: 2KHO). (c) Opened state illustrated by the crystal structure of yeast Sse1 bound to ATP (PDB: 2QXL).

The human disaggregase have been reported to revert amyloid fibrils of α-syn (Duennwald, Echeverria and Shorter, 2012; Gao *et al.*, 2015; Wentink *et al.*, 2020), Htt (Scior *et al.*, 2018) and tau (Ferrari *et al.*, 2018; Nachman *et al.*, 2019). This activity relies on the constitutive Hsp70 (HSPA8/Hsc70) in collaboration with the canonical class B J-domain protein DnaJB1 and the NEF of the Hsp110 family Apg2. In the case of α-syn, further addition of the sHsp αB-crystallin, potentiated fibril disassembly by Hsc70, DnaJB1 and Apg2 (Duennwald, Echeverria and Shorter, 2012). From a mechanistic point of view, two models have been proposed for the disaggregation of α-syn fibrils by the Hsp70 chaperone system (Duennwald, Echeverria and Shorter, 2012; Gao *et al.*, 2015). Both models state that the human disaggregase can depolymerize fibrils, extracting monomers from fibril ends. Additionally, one of the models establishes that chaperones can also extract monomers from the center of the fibrils, therefore breaking them into smaller fragments (Gao *et al.*, 2015). Fragmentation of amyloids has also been attributed to yeast Hsp104 (Winkler *et al.*, 2012). This member of the AAA+ ATPase family is composed of six protomers, forming an offset hexameric barrel. In the case of amorphous aggregates, Hsp104 hydrolyzes ATP in a probabilistic mode upon aggregate binding, being a single subunit within a hexamer enough to drive protein disaggregation. Conversely, the highly ordered structure of amyloids requires a global cooperative mechanism of ATP hydrolysis and substrate binding from the six subunits to generate force enough to extract monomer (Desantis *et al.*, 2012). Hsp104 mediated fragmentation is essential for the maintenance of prions in yeast, producing smaller seeds that are more efficiently transmitted to daughter cells (Chernoff *et al.*, 1995; Davis and Sindi, 2016). Recent studies show that human chaperones may also be implicated in the prion-like propagation of amyloidogenic

proteins through a similar fragmentation mechanism (Nachman *et al.*, 2019; Tittelmeier *et al.*, 2020).

1.5.1.5. *Chaperones in protein degradation*

Cells display an inherent bias towards refolding over degradation, salvaging misfolded proteins. Nonetheless, terminally damaged/misfolded proteins extracted from aggregates are likely to be targeted for degradation by the UPS or the autophagy machinery. Chaperones play an essential role in substrate selection and facilitation of the degradation process. Different sets of chaperones have been reported to be responsible for targeting substrates toward proteasomal degradation. Binding of CHIP and Bag1 to Hsp70 slows down the protein-refolding process, which is necessary for the switch from refolding to degradation. CHIP is an E3 ubiquitin ligase that inhibits ATP hydrolysis and ubiquitinates Hsp70/Bag1 and the bound substrate. Then, the substrate is released to the proteasome thanks to the NEF activity of Bag1, which decreases the affinity of Hsp70 for the substrate (Kästle and Grune, 2012). Furthermore, polyubiquitinated proteins that have been extracted from an aggregate by the action of Hsp70 and Hsp110 are recognized by ubiquilin 2 (UBQLN2) and shuttled to the 26S proteasome (Hjerpe *et al.*, 2016). Protein aggregates resisting disassembly are cleared by selective autophagy and lysosomal degradation. Hsp70 recognizes cargo proteins and delivers them to the different autophagy-lysosomal path-pathways (Wentink, Nussbaum-krammer and Bukau, 2019).

1.5.2. Ubiquitin-proteasome system

The UPS is a key player for the degradation of short-lived, misfolded and damaged proteins. This system performs intracellular proteolysis in a highly selective and tightly controlled manner due to the specific ubiquitin labeling of appropriate substrates and the complex architecture of the proteasome. A network of ubiquitin

ligases and conjugating enzymes are responsible for covalently attaching ubiquitin modifications to lysine side chains (Komander and Rape, 2012). The E1 ubiquitin-activating enzyme activates the ubiquitin, which is transferred to E2 ubiquitin-conjugating enzyme. Subsequently, the ubiquitin-charged E2 binds to the E3 ubiquitin-ligase enzyme, which carries the substrate and transfers the ubiquitin to it. Multiple cycles of this process result in the poly-ubiquitination of the substrate protein, targeting it to the proteasome.

The proteasome holoenzyme is the major protease in eukaryotic cells (Huang *et al.*, 2016; Bedford *et al.*, 2018; Dong *et al.*, 2019). Its proteolytic active sites reside within the chamber of the barrel-shaped 20S core particle (CP) and are accessible only through narrow axial pores, which exclude folded and even large unfolded polypeptides. Gating of these pores is controlled by the 19S regulatory particle (RP), which caps one (26S proteasome) or both (30S proteasome) ends of the 20S core peptidase. The RP is divided into two subcomplexes the base and the lid, which are bridged through one ubiquitin-receptor subunit called Rpn10 (nomenclature for yeast). The base subcomplex is composed of the structural subunit Rpn2, the ubiquitin-binding subunits Rpn1 and Rpn13, and six ATPase subunits (Rpt1–Rpt6), whose AAA+ domains form the ring-shaped heterohexameric motor of the proteasome. Meanwhile, the lid subcomplex is divided into the structural subunits Rpn3, Rpn5, Rpn6, Rpn7, Rpn8, Rpn9, Rpn12 and Sem1, and the deubiquitinase Rpn11. Processing of polyubiquitinated substrates starts with the recognition by the ubiquitin-binding subunits. After substrate engagement, Rpn11 or associated deubiquitinases remove ubiquitin chains from substrates before they enter the AAA+ ATPase. These motor subunits apply mechanical pulling forces coupled to ATP hydrolysis, disrupting higher-order structures of substrates that allow translocation of the unfolded polypeptides through the pore into the associated 20S core, where proteolytic cleavage is performed (Dong *et al.*, 2019).
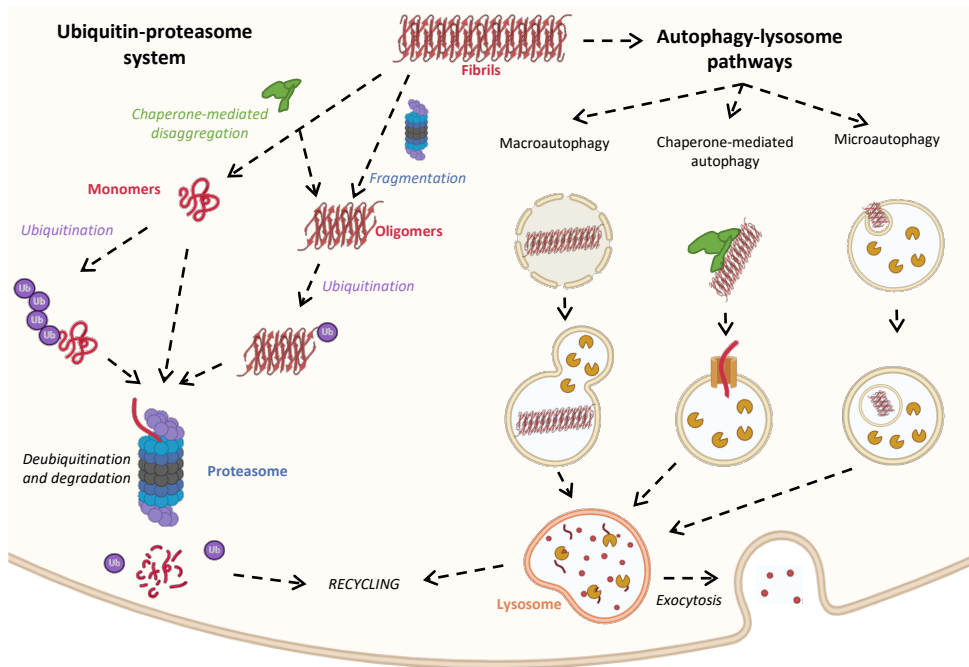
Figure 1.12. Protein degradation pathways. Protein aggregates are cleared by two main degradation pathways, the ubiquitin-proteasome system (UPS) and the autophagy-lysosome pathways (ALPs). The UPS targets for degradation of monomeric (ubiquitinated or not) and ubiquitinated oligomeric species of amyloidogenic proteins. Also, the UPS can fragment amyloid fibrils into shorter aggregates. The ALPs can be divided into three groups: macroautophagy, chaperone-mediated autophagy, and microautophagy. In all three cases, the cargo is delivered to the lysosome. Degradation products of both UPS and ALPs are either recycled or eliminated via exocytosis.

Alternatively, the 20S proteasome has been suggested to promote the degradation of unfolded and oxidized proteins in an ATP-independent manner without the requirement of poly-ubiquitination of target proteins or 19S-mediated protein unfolding (Davies, 2001). Similarly, monomers of the amyloidogenic, intrinsically disordered proteins tau and α-synuclein are degraded by the 26S proteasome holoenzyme in a ubiquitin- and ATP-independent manner (Cliffe *et al.*, 2019). Although larger aggregates of these proteins are believed to be cleared by

39

lysosomes, the proteasome holoenzyme possessed an ATP-dependent fibril-fragmenting activity, which does not require ubiquitin tag or proteolytic activity (Cliffe *et al.*, 2019). Through this mechanism, the proteasome reduces the size of large tau and α-syn fibrils into smaller entities. Interestingly, N-terminal Ub modification on tau and α-syn enables proteasomes to target and remove oligomers assembled from these modified proteins, independently of its peptidase activity (Ye, Klenerman and Finley, 2019).

1.5.3. Autophagy-lysosome pathways

Autophagy or autophagocytosis is a basic catabolic mechanism/degradation pathway that involves the delivery of cytoplasmic cargo to the lysosome. Based on the particular physiological role of the process, the mode of cargo delivery and the pathway, autophagy is typically categorized into three groups: macroautophagy, chaperone-mediated autophagy, and microautophagy. Macroautophagy is the major intracellular pathway in which intracellular cargo is enveloped within an autophagosome for delivery to the lysosome through membrane fusion. In chaperone-mediated autophagy, molecular chaperones deliver proteins to the lysosome for degradation. Otherwise, in microautophagy the lysosomal membrane forms invaginations, which contain the cytoplasmic material, and pinch off to form vesicles in the lysosomal lumen. In all these pathways, Hsp70 plays a key role in targeting specific proteins (Wentink, Nussbaum-krammer and Bukau, 2019).

The ALPs were initially described for long-lived cytoplasmic proteins and damaged organelles but recent studies show that they are also major degradation pathways for many amyloidogenic proteins (Finkbeiner, 2019). These degradation pathways seem to be important in the clearance of multimeric assemblies (i.e. oligomers and larger aggregates) as a whole, that cannot be resolved by other means. Mutations in genes with established or apparent roles in autophagy result in neurodegeneration, underscoring the conclusion that ALP dysfunction is

sufficient to cause such disorders and suggest a common thread that may even extend to the more common idiopathic forms of adult-onset NDs (Finkbeiner, 2019).

1.5.4. Failure of the proteostasis network

The PN at full capacity copes with the load of misfolded proteins by refolding, disaggregating and/or degrading aberrant proteins. Several factors promote aggregation owing to their ability to generate misfolded protein species: environmental stress, certain aspects of lifestyle (such as obesity), sustained increase in protein concentration, ingestion or iatrogenic transmission of preformed aggregates, the existence of mutant proteins with a high propensity to aggregate or aberrant proteolytic cleavage (Chiti and Dobson, 2017). Due to these factors, the PN is progressively overwhelmed leading to aberrant interactions and aggregate deposition. Aggregate deposition is also a cause of the PN decline, seeding further aggregation and sequestering PN components, which interferes with standard housekeeping functions and additionally favors aggregation. As a result, the PN drives into a vicious cycle that ultimately leads to its collapse (Labbadia and Morimoto, 2015; Balchin, Hayer-Hartl and Hartl, 2016).

Aging is undoubtedly the major risk factor for aggregate-related diseases. Accumulating evidence suggests that a progressive decline of the PN with aging may be the cause. Chaperone expression appears to be downregulated with aging (Brehme *et al.*, 2014). An age-related decline of UPS activity has also been observed and attributed to a variety of factors, including a decrease in the number of proteasome complexes, transcriptional downregulation, or defective chaperone-mediated recruitment (Mckinnon and Tabrizi, 2014). In addition, the ALPs decrease their efficiency as a result of the transcriptional downregulation of autophagy-related proteins and decreased levels of lysosomal membrane receptors (Martinez-lopez, Athonvarangkul and Singh, 2015). The age-related increase of oxidative

stress and a decrease in mitochondrial function and ATP production further reduce the efficiency of the PN. All these factors make protein aggregation control more challenging as we grow old.

CHAPTER

2

OBJECTIVES

The general objective of this doctoral thesis was to deepen in the mechanism used by chaperones to disaggregate amyloids of the proteins α-synuclein and tau, implicated in prevailing neurodegenerative diseases such as Parkinson´s and Alzheimer´s disease, respectively. To pursue this goal, the following specific objective were established:

1. Determination of the activity of the human disaggregase on the different aggregate species that populate the amyloid formation process and the disassembly mechanism used by chaperones to disaggregate them.

2. Characterization of the effect of α-synuclein truncation, a common post-translational modification of the protein, on the activity of the human disaggregase.

3. Investigation of the impact of amyloid polymorphism in the disaggregation activity of the human Hsp70-based machinery.

CHAPTER

3

MATERIALS AND METHODS

3.1. CELL CULTURES

3.1.1. *Escherichia coli* strains, growth and selection

Plasmid DNA and recombinant proteins were purified using different *E. coli* strains summarized in **Table 3.1.**

Table 3.1. *E. coli* strains used in this Thesis.

STRAIN	GENOTYPE	APPLICATION
DH5α	F⁻ *endA1 glnV44 thi-1 recA1 relA1 gyrA96 deoR nupG purB20* φ80d*lacZ*ΔM15 Δ(*lacZYA-argF*)U169, hsdR17($r_K^- m_K^+$), λ⁻	Plasmid conservation and propagation
XL1-Blue	*recA1 endA1 gyrA96 thi-1 hsdR17 supE44 relA1 lac* [F′ *proAB lacI*ᑫ*Z*ΔM15 Tn*10* (Tetʳ)]	Plasmid conservation and propagation
BL21 (DE3)	*E. coli* B F⁻ *ompT gal dcm lon hsdS_B*($r_B^- m_B^-$) λ(DE3 [*lacI lacUV5-T7p07 ind1 sam7 nin5*]) [*malB*⁺]_{K-12}(λˢ)	Expression of α-syn and tau K18
BL21 CodonPlus(DE3) RP	*E. coli* B F⁻ *ompT hsdS*(r_B^- m_B^-) *dcm*⁺ Tetʳ *gal* λ(DE3) *endA* Hte [*argU proL* Camʳ]	Expression of tau 2N4R
BL21 CodonPlus(DE3) RILP	*E. coli* B F⁻*ompT hsdS(*$r_B^- m_B^-$*) dcm*⁺ Tetʳ *gal* λ(DE3) *endA* Hte [*argU proL* Camʳ] [*argU ileY leuW* Strep/Specʳ]	Expression of Hsp70 and Hsp40
Rosetta(DE3)pLysS	*E. coli* B F⁻ *ompT gal dcm lon hsdS_B*($r_B^- m_B^-$) λ(DE3) [*malB*⁺]_{K-12}(λˢ) pLysSRARE[*T7p20 ileX argU thrU tyrU glyT thrT argW metT leuW proL ori*_{p15A} Camʳ]	Expression of Hsp110

Competent cells of the corresponding strain were transformed by electroporation or chemical transformation and inoculated on selection plates containing LB broth (Lennox) (10 g tryptone, 5 g yeast extract and 5 g NaCl per liter) with 1.5% (w/v) agar. Selective media was obtained by adding ampicillin at 100 µg/mL. When the BL21 CodonPlus(DE3) or Rosetta strains were cultured, 35 µg/mL chloramphenicol was also added to the media. After 16h of growth at 37 °C, single colonies were amplified in liquid LB broth with the corresponding antibiotics at 37 °C and 200 rpm shaking.

3.1.2. SH-S5Y5 cell line culture

Human neuroblastoma SH-SY5Y cells were cultured in Dulbecco's modified Eagle's medium (DMEM) low glucose with 1 g/L L-glutamine supplemented with 10% heat-inactivated Fetal Bovine Serum (FBS), penicillin and streptomycin (50 U/mL and 50 µg/mL, respectively) and MycoZap™ Prophylactic (Lonza, 1/1000 dilution). Cell cultures were maintained in a 5% CO_2 humidified atmosphere at 37 °C and regularly passaged at subconfluency. In each passage, media was removed and cells were detached by adding a Trypsin-EDTA (0.05%) phenol red solution. After 5 min incubation at 37 °C, trypsin was inactivated by adding FBS-containing medium and cells were centrifuged at 1,200 g for 5 min at room temperature. Then, cells were resuspended in fresh growth medium, quantified using a TC20™ Automated Cell Counter (Bio-Rad) and the desired amount of cells were seeded in new recipients. For long term cell-preservation, pelleted cells were resuspended in 90% FBS and 10% DMSO and aliquots were frozen and stored at -80 °C.

3.2. PLASMID VECTORS

3.2.1. Plasmids used in this work

Recombinant protein expression was done by using engineered plasmid vectors in which the target gene was cloned downstream of the T7 bacteriophage RNA polymerase promoter (**Table 3.2**). These constructs allow controlled and high-efficiency protein expression by using *E. coli* strains that contain the T7 bacteriophage RNA polymerase under the control of the lac operon, which is triggered by Isopropyl β-D-1-thiogalactopyranoside (IPTG), a molecular mimic of allolactose. To ensure the retention of plasmid DNA in bacterial populations, an antibiotic resistance gene is also present in the plasmid.

Table 3.2. Plasmids used in this Thesis.

PLASMID	CLONED GENE	PHENOTYPE	SOURCE
pT7-7 α-syn$_{WT}$	*SNCA*	Amp^r	Prof. J.M. Valpuesta[1]
pT7-7 α-syn$_{A53T}$	*SNCA* (A53T)	Amp^r	Prof. J.M. Valpuesta[1]
pT7-7 α-syn$_{Q24C}$	*SNCA* (Q24C)	Amp^r	Prof. Nunilo Cremades[1]
pRK-T42	*MAPT* (isoform 2N4R)	Amp^r	Prof. J.M. Valpuesta[1]
pNG2 K18 C291A C322A	*MAPT* (residues 244-372)	Amp^r	Prof. David Klenerman[1]
pE-SUMO	*HSPA8, HSPA4, DNAJB1, DNAJA1, DNAJA2*	Amp^r	Previously cloned in the laboratory

[1] The kind gift from these authors is gratefully acknowledged.

3.2.2. PCR-based mutation

Mutants of the different proteins used in this thesis were obtained using various Polymerase Chain Reaction (PCR)-based methods. The primers and restriction enzymes used for their production are described in **Table 3.3**.

Deletion mutants α-syn$_{30-140}$, α-syn$_{1-122}$ and α-syn$_{1-133}$ were obtained through a PCR amplification and cloning method. The plasmid containing the α-syn$_{WT}$ sequence (1-10 ng) was used as a template to amplify the desired sequence. Final reaction concentrations were 0.5 µM of each primer, 100 µM of each dNTP and 2.5 U *PfuTurbo* DNA polymerase (Agilent) in its reaction buffer. Amplification was carried out in a Mastercycler Gradient Thermocycler (Eppendorf) and consisted of an initial denaturation cycle (3 min at 94 °C), followed by 30 cycles of a denaturation step at 94 °C for 30s, a hybridization step at 58 °C for 30s and an elongation step at 72°C for 5 min, and a final cycle of 10 min at 72 °C. Purified PCR products were digested with *NdeI* and *HindIII* restriction enzymes (1 µL per 1 µg of DNA). After a DNA agarose electrophoresis, digested products were gel-purified using the *Gel and PCR Clean-up Kit* (Macherey-Nagel). The pT7-7 plasmid containing α-syn$_{WT}$ was digested with the same restriction enzymes and the band corresponding to the empty plasmid was purified. Ligation between insert and empty vector was done at 16°C for 16h with T4 DNA Ligase (New England Biolabs) and the ligation product was used to transform *E. coli* DH5α competent cells.

Point-mutations E46K for α-syn and P301L and ΔK280 for tau K18$_{C291A, C322A}$ (henceforth referred to as tau K18) were introduced by mutagenesis using the QuikChange II XL Site-Directed Mutagenesis Kit (Agilent) following manufacturer´s indications. 50 ng of the plasmid to be mutated were amplify using a pair of primers (125 ng each) containing the desired mutation in the middle of their sequence. Amplification consisted of an initial denaturation cycle (1 min at 95 °C), followed by 18 cycles of a denaturation step at 95 °C for 30s, a hybridization step at 55 °C for 1 min and an elongation step at 68°C for 4.5 min (for α-syn) or 6.5 min (for tau K18). After amplification, samples were digested with *DpnI* to eliminate the parental methylated template. The nicked vector DNA containing the desired mutation was then transformed into *E. coli* XL1-Blue supercompetent cells. Deletion mutant α-syn$_{1-110}$ was obtain following the same protocol but with some modifications in the

PCR, which consisted on 30 cycles of a denaturation step at 95 °C for 30s, a hybridization step at 57.2 °C for 1 min and an elongation step at 68°C for 6 min, with a final cycle of 10 min at 72 °C.

Table 3.3. Primers used to introduce mutations.

Mutant	PCR Primers (5' to 3')	Restriction enzyme
α-syn$_{30-140}$	F: *GGGCATATGGCAGGAAAGACAAAAGAGG*	5' *NdeI*
	R: *GGGAAGCTTTTAGGCTTCAGGTTCGTAG*	3' *HindIII*
α-syn$_{1-122}$	F: *GGGCATATGGATGTATTCATGAAAGGACTTTC*	5' *NdeI*
	R: *GGGAAGCTTTTAATTGTCAGGATCCACAGGC*	3' *HindIII*
α-syn$_{1-133}$	F: *GGGCATATGGATGTATTCATGAAAGGACTTTC*	5' *NdeI*
	R: *GGGAAGCTTTTAATACCCTTCCTCAGAAGGC*	3' *HindIII*
tau K18$_{P301L}$	A: CACACTGCCGCCTCCCAGGACGTGTTTAATATT	*DpnI*
	B: AATATTAAACACGTCCTGGGAGGCGGCAGTGTG	
tau K18$_{ΔK280}$	A: GCTAAGATCCAGCTTATTAATTATCTGCACCTTCCCGCC	*DpnI*
	B: GGCGGGAAGGTGCAGATAATTAATAAGCTGGATCTTAGC	
α-syn$_{E46K}$	A: CATGCACCACTCCCTTCTTGGTTTTGGAGCC	*DpnI*
	B: GGCTCCAAAACCAAGAAGGGAGTGGTGCATG	
α-syn$_{1-110}$	A: GGAGCAAAGATATTTCTTATTCCTGTGGGGCTCCTTCT	*DpnI*
	B: AGAAGGAGCCCCACAGGAATAAGAAATATCTTTGCTCC	

3.3. PROTEIN EXPRESSION AND PURIFICATION

3.3.1. Proteins used in this work

The proteins listed in **Table 3.4** have been recombinantly expressed and purified in the laboratory using the protocols described in the following sections. Other proteins used in this thesis were bought or provided by other laboratories (**Table 3.5**).

Table 3.4. Proteins purified in the laboratory.

PROTEIN	No. AMINO ACIDS	MW (Da)	pI
α-synuclein	140	14,460	4.67
α-synuclein$_{A53T}$	140	14,490	4.67
α-synuclein$_{E46K}$	140	14,459	4.81
α-synuclein$_{Q24C}$	140	14,435	4.67
α-synuclein$_{30-140}$	111	11,615	4.45
α-synuclein$_{1-133}$	133	13,627	4.87
α-synuclein$_{1-122}$	122	12,341	5.46
α-synuclein$_{1-110}$	110	11,045	8.83
tau 2N4R	441	45,850	8.24
tau K18$_{C291A,\ C322A}$	130	13,750	9.87
tau K18$_{C291A,\ C322A,\ P301L}$	130	13,766	9.87
tau K18$_{C291A,\ C322A,\ \Delta K280}$	129	13,621	9.82
Hsc70	646	70,898	5.37
Apg2	843	94,486	5.10
DnaJB1	340	38,044	8.74
DnaJA1	397	44,868	6.65
DnaJA2	412	45,746	6.06

Table 3.5. Proteins purchased/given away.

PROTEIN	MW (kDa)	ORGANISM	SOURCE	OBTAINED FROM
Pyruvate kinase	237	*O. cuniculus*	Rabbit muscle	Roche
Glucose-6-phosphate dehydrogenase	54.4	*L. mesenteroides*	*L. mesenteroides*	Worthington
Luciferase	62	*P. pyralis*	Expressed in *E. coli*	Sigma-Aldrich
Proteinase K	40.3	*E. album*	Expressed in *P. pastoris*	Roche
Calpain-1	108	*S. scrofa*	Porcine Erythrocytes	Merk
Proteasome	2,500	*H. sapiens*	Expressed in HEK293T	Prof. Yu Ye

3.3.2. Purification of α-synuclein

α-syn was expressed in BL21 (DE3) cells and purified from periplasm as previously described (Huang *et al.*, 2005). Overnight-grown culture was diluted 20 times in LB media containing ampicillin (6 flasks of 750 mL) and cells were grown at 37 °C to an OD_{600nm} of 0.6-0.8. Overexpression was induced with 1 mM IPTG at 37 °C for 4 h and afterwards, the cells were harvested by centrifugation at 6,000 g. Cell pellet was resuspended in 500 mL of 30 mM Tris-HCl, 40% sucrose, and 2 mM EDTA, adjusted to pH 7.2, and incubated for 10 min at room temperature. The pellet collected by centrifugation at 22,000 g for 20 min was resuspended with 200 mL ice-cold buffer containing 25 mM Tris-HCl pH 8 and 2.5 mM $MgCl_2$, and kept on ice for 10 min. The

supernatant containing periplasm proteins was collected by centrifugation at 22,000 rpm for 20 min and was heated at 95 °C for 15 min. Aggregated proteins were removed by centrifugation at 22,000 rpm for 20 min and the sample was stored on ice until the next day. Prior to loading onto a HiLoad Q Sepharose 26/60 column, the sample was subjected to 5 sonication cycles of 20 ON; 30 OFF and was passed through a 0.45 μm filter. Protein was eluted in 25 mM Tris-HCl pH 8 buffer with a 0-0.6 M NaCl gradient. Fractions containing the monomeric protein were pooled together, dialyzed overnight against 25 mM Tris pH 7.5, concentrated using 3K centrifugal filters, filtered through 0.22 μm sterile filters and stored at -20°C.

To purify α-syn mutants, some modifications were made in the protocol. α-syn_{1-133}, α-syn_{A53T}, syn_{E46K} and α-syn_{Q24C} were purified following the same protocol, adding 2 mM DTT to all buffers in the case of the cysteine-containing mutant. After anion exchange, α-syn_{1-122} was further purified by gel filtration using the Superdex 200 column equilibrated in 25 mM Tris-HCl pH 7.5 buffer. α-syn_{1-110} was expressed as for α-syn_{WT}, and after the heating/centrifugation step, the sample was dialyzed overnight against 20 mM MES-NaOH pH 6.8. Dialyzed sample was loaded onto a HiTrap SP HP cation exchange column equilibrated in 20 mM MES-NaOH pH 6.8 and elution was performed with a 0-0.6 mM NaCl gradient.

Protein purity was analyzed by SDS-PAGE, and protein concentrations were determined spectrophotometrically using the extinction coefficients of 5,960 $M^{-1}cm^{-1}$ for α-syn_{WT}, α-syn_{A53T}, syn_{E46K}, α-syn_{Q24C} and α-syn_{30-140}, 4,470 $M^{-1}cm^{-1}$ for α-syn_{1-133}, and 1,490 $M^{-1}cm^{-1}$ for α-syn_{1-122} and α-syn_{1-110}.

3.3.3. Purification of tau

Tau isoform 2N4R (or htau40) was expressed in BL21 CodonPlus(DE3) RP cells transformed with the pRK-T42 plasmid. Overnight-grown culture was diluted 20 times in LB media containing ampicillin and chloramphenicol (8 flasks of 800 mL)

and cells were grown at 37 °C to an OD_{600nm} of 0.6-0.8. Overexpression was induced with 1 mM IPTG at 37 °C for 4 h, and afterwards the cells were harvested by centrifugation at 6,000 g. Cell pellet was resuspended in 20 mM MES-NaOH pH 6.8 supplemented with 1 mM PMSF and stored at -80 °C until use. Cells were thawed and lysed by sonication (6 cycles of 20 ON; 30 OFF in an MSE Soniprep 150) in 20 mM MES-NaOH pH 6.8, 1 mM EDTA, 0.2 mM $MgCl_2$, 5 mM DTT, 1 mM EDTA and Complete EDTA free (Roche) protease inhibitor cocktail (1 table per 50 mL). The soluble fraction obtained by ultracentrifugation at 147,500 g (30 min at 4 °C) was passed through a 0.45 μm filter and loaded onto a HiTrap SP HP cation exchange column equilibrated in 20 mM MES-NaOH pH 6.8, 1 mM EDTA, 1 mM $MgCl_2$, 2 mM DTT, 1 mM EDTA, 0.1 mM PMSF with 50 mM NaCl (buffer A). The same buffer with 1 M NaCl (buffer B) was used to elute the protein using an initial washing step of 5 column volumes at 17% buffer B to elute degradation products. The full-length protein was eluted in a gradient from 17-60% of buffer B. Fractions containing the monomeric protein were pooled together, dialyzed overnight against 25 mM Tris pH 7.5, 150 mM NaCl and 2 mM DTT, concentrated using 3K centrifugal filters, filtered through 0.22 μm sterile filters and stored at -80°C.

The truncated tau version K18 (residues 244–372) with the two natural cysteine residues at positions 291 and 322 mutated to alanine and the point mutants of this construct, P301L and ΔK280, were expressed in BL21(DE3). Overexpression, cell harvesting and lysis was done as for tau 2N4R. 500 mM NaCl was added to the soluble fraction after ultracentrifugation and the sample was incubated for 20 min at 95 °C. Aggregates were removed by ultracentrifugation at 147,500 g for 30 min at 4 °C. Sample was dialyzed twice against buffer A at 4 °C, with a first change of 3h and another overnight change. Sample was passed through a 0.45 μm filter and loaded onto a HiTrap SP HP cation exchange column and protein was eluted with a 0-0.6 M NaCl gradient. Pooled fractions were dialyzed against 25 mM Tris-HCl pH 7.5 and degradation products were removed by gel

filtration using a Superdex 75 26/60 column. Fractions containing the monomeric protein were pooled together, dialyzed overnight against 25 mM Tris pH 7.5, concentrated using 3K centrifugal filters, filtered through 0.22 µm sterile filters and stored at -20°C.

Due to the low content of aromatic and arginine residues in the tau sequence, quantification of protein concentration by conventional methods such as absorbance at 280 nm or Bradford/BCA methods results in an underestimation. Thus, protein concentration was determined by quantitative amino acid analysis. Quantified samples were used to determine the extinction coefficient at 235 nm, being 1.1 and 1.6 $mL·mg^{-1}·cm^{-1}$ for tau 2N4R and tau K18, respectively, which was used to quantified subsequent protein stocks.

3.3.4. Purification of molecular chaperones

Molecular chaperones were purified using protocols previously developed in the laboratory (Cabrera *et al.*, 2019). Briefly, the coding sequence of each chaperone cloned into the pE-SUMO plasmid (Life Sensors) was expressed in BL21 CodonPlus(DE3) RILP cells, except for Hsp110 which was expressed in Rosetta (DE3) pLysS. This vector expresses the protein of interest fused to a His-tagged ubiquitin-like modifier (yeast SUMO Smt3) at its N-terminus, enhancing expression and promoting solubility and correct folding of the protein, and allowing affinity purification. After protein expression, cells were harvested, disrupted by sonication and the soluble fraction was collected by ultracentrifugation. Debris-free supernatant was loaded onto a column with a nickel-charged affinity resin. After elution, the His-tagged SUMO protein was removed using the SUMO protease 1 (Ulp1) and the sample was loaded again into a nickel-charged affinity chromatography. The unbound fraction contained the pure protein without tags. For Hsc70, an additional polishing step with a hydroxyapatite column was performed. Protein concentration was determined by the Bradford method and

spectrophotometrically using the extinction coefficients of 33,350, 56,270 and 18,910 $M^{-1}cm^{-1}$ at 280 nm for Hsc70, Apg2 and DnaJB1 respectively. The activity of each protein stock was checked by an ATPase assay and the refolding activity of the model substrates glucose-6-phosphate dehydrogenase (G6PDH) and luciferase.

3.4. FLUORESCENT PROTEIN LABELING

The development of different fluorescent dyes that can be chemically attached to a specific region or functional group on a target molecule has represented a great advance to study biologically relevant samples. In particular, Alexa Fluor dyes are a series of fluorescent probes that have strong absorptivity, high fluorescence quantum yield and high photostability. In this thesis, Alexa Fluor 488 has been used to label different proteins using the following protocols.

3.4.1. Labeling of α-synuclein Q24C

α-syn with a single cysteine located at residue 24 was labeled with Alexa Fluor™ 488 C_5 Maleimide. A solution of the protein at 100-200 μM in 25 mM Tris, 150 mM NaCl, 2 mM TCEP, pH 7.5 was mixed with the fluorophore at a 1:5 protein:probe molar ratio. Labeling was done with an overnight incubation at 4 °C in a vertical rotating mixer. Reaction was quenched by adding 2 mM DTT and the sample was centrifuged for 10 min at 16,000 g and 4 °C to remove possible aggregates. The supernatant was loaded on a PD10 gel filtration column (GE Healthcare) equilibrated in 50 mM Tris, 100 mM NaCl and 0.05% NaN_3, pH 7.4 to remove the probe excess. Eluted fractions (200-300 μL) were analyzed by SDS-PAGE and visualized in a VersaDoc™ MP 4000 system (Bio-Rad) to discard fractions containing free probe. Labeling efficiency (85-100 %) was measured spectrophotometrically, using absorption at 280 nm for protein concentration and at 494 nm for Alexa Fluor 488 (ε_{494} = 72,000 $M^{-1}cm^{-1}$) concentration. Due to the absorption of the probe at

280 nm, a correction factor (CF) of 0.11 must be used, subtracting the 11 % of the absorption at 494 nm to the absorption at 280 nm.

3.4.2. Labeling of G6PDH and tau K18

Labeling of G6PDH was done using Alexa Fluor 488 NHS Ester (Succinimidyl Ester) in 50 mM potassium phosphate buffer, pH 6.4 and 30 mM NaCl. At this pH the acylation of α-amino groups from primary amines is favored over that of ε-groups (Fernandez-Fernandez, Veprintsev and Fersht, 2005). Protein concentration was 2 mg/mL and an equimolar concentration of the fluorophore was used. After 1 h incubation at room temperature in a vertical rotating mixer, the sample was loaded on a PD10 gel filtration column (GE Healthcare) equilibrated in 40 mM Hepes-KOH pH7.6, 50 mM KCl, 5 mM $MgCl_2$ to remove the excess of the probe. Labeling efficiency (10-15%) was determined spectrophotometrically using absorption at 280 nm for protein (ε_{280}= 62.56 mM^{-1} cm^{-1}) concentration (with a CF of 0.11) and absorption at 494 nm for Alexa Fluor 488 (ε_{494} = 73,000 M^{-1}cm^{-1}) concentration. Tau K18 protein constructs were labeled following the same protocol, eluting the labeled protein in 25 mM Tris-HCl pH 7.5, 50 mM NaCl and yielding a labeling efficiency of 20-50%.

3.5. PROTEIN ELECTROPHORESIS AND IMMUNOBLOTTING

3.5.1. SDS-PAGE

SDS-PAGE (sodium dodecyl sulfate-polyacrylamide gel electrophoresis) is an analytical method used to separate components of a protein mixture. In the presence of SDS, all of the proteins present the same charge-to-mass ratio and lose their ternary structure, which allows a separation primarily based on differences in their molecular weight. Samples were prepared in loading buffer containing 50 mM Tris-HCl pH 6.8, 5 % (w/v) glycerol, 4 % (w/v) SDS, 0.02 % (w/v) bromophenol blue

and 100 mM DTT. Electrophoresis was carried out in a mini-PROTEAN Tetra Cell (Bio-Rad) using a buffer containing 25 mM Tris-HCl pH 8.3, 200 mM glycine and 1 % SDS (w/v) and freshly-made polycrilamide gels. Alternatively, samples were run in NuPAGE™ 4 to 12%, Bis-Tris gels (Invitrogen) using a XCell™ SureLock™ Mini-Cell (Invitrogen) and a buffer containing 50 mM MES, 50 mM Tris, 0.1 % SDS (w/v), 1 mM EDTA, pH 7.3.

3.5.2. Native-PAGE

Native-PAGE analyze proteins in their native folded state (under non-denaturing conditions) and thus, electrophoretic mobility depends not only on the charge-to-mass ratio, but also on the physical shape and size of the protein. This technique allows analyzing both the oligomeric state of proteins and the formation of complexes between different proteins. Samples were prepared in loading buffer containing 50 mM Bis-Tris, 6 N HCl, 50 mM NaCl, 10% (w/v) glycerol, 0.001% Ponceau S, pH 7.2 and loaded in NativePAGE™ 4 to 16%, Bis-Tris gels (Invitrogen). Electrophoresis was carried out in a cold room (4°C) with a XCell™ SureLock™ Mini-Cell (Invitrogen) using 50 mM Bis-Tris, 50 mM Tricine, pH 6.8 (Invitrogen) as a running buffer. Voltage was kept constant at 150 V for 1 h and raised to 250 V for another 45 min.

3.5.3. Western Blot

Western Blot (WB) is a common method to detect and analyze proteins separated by gel electrophoresis. Separated proteins are transferred (or blotted) onto a matrix (generally nitrocellulose or PVDF membrane), where the target protein is stained with specific antibodies that are ultimately detected by colorimetric, chemiluminescence or fluorescence methods.

PAGE-separated proteins were transferred to a nitrocellulose membrane in wet conditions using a Mini Trans-Blot® Electrophoretic Transfer Cell (Bio-Rad). When SDS gels were blotted, transfer was carried out for 2 h at 500 mAmp in a buffer containing 50 mM Tris-HCl, 0.1 % (w/v) SDS, 386 mM glycine, 20 % (v/v) methanol, pH 8,3. When Native gels were blotted, they were first incubated for 1.5 h at room temperature in a buffer containing 375 mM Tris-HCl pH 7.5, 1 % SDS (w/v) and then, for another 30 min in a buffer containing 30 mM Tris, 240 mM glycine, 20 % (v/v) methanol, pH 8.4, which was also used to carry out the transfer for 14-16 h at 150 mAmp. In all cases, transfer was done in a cold room (4°C) and with a cooling unit inside the tank to avoid overheating. After protein transfer, membranes were stained with specific antibodies. Unless otherwise stated, the following steps were done under mild-agitation at room temperature. Membranes were blocked for 1 h with 5 % (w/v) skimmed milk in TBS-T (10 mM Tris-HCl pH 7.5, 150 mM NaCl, 0.05 % (w/v) Tween-20). Then, membranes were incubated overnight at 4 °C with the primary antibody (see **Table 3.6** for antibody dilutions), washed three times (10 min each) with TBS-T and incubated for 1 h with a secondary antibody conjugated to horseradish peroxidase. After three additional washing steps, visualization was done by chemiluminescence using the SuperSignal®West Pico Chemiluminescent Substrate and myECL™ Imager (Thermo Fisher Scientific).

3.6. AGGREGATE PREPARATION

In this thesis, different type of aggregates have been produced following several protocols below described. Due to the great stability of amyloids, aggregate preparations of α-syn and tau proteins are stable within 3-5 days after purification as long as they are stored at room temperature (Ikenoue *et al.*, 2014). Even so, aggregate preparations were used as soon as possible to reduce experimental variability. In the case of G6PDH, aggregates were always used immediately after their production.

Table 3.6. List of antibodies used in this thesis.

COMPANY (REFF.)	TARGET	CLONALITY (EPITOPE)	SOURCE	DILUTION[1]	SECONDARY Ab DILUTION[2]
Abcam (ab1338501)	α-syn	Monoclonal (aa 118-123)	Rabbit	1:5,000	1:2,000
Santa Cruz (sc-514908)	α-syn	Monoclonal (aa 2-24)	Mouse	1:400	1:400
Invitrogen (PA5-85343)	α-syn	Polyclonal	Rabbit	1:2,000	1:1,000
Dako (A0024)	tau	Polyclonal	Rabbit	1:50,000	1:5,000
Abcam (ab51052)	Hsc70	Monoclonal (600-646)	Rabbit	1:5,000	1:2,000
Abcam (ab185962)	Apg2	Monoclonal (700-800)	Rabbit	1:5,000	1:2,000
Enzo (ADI-SPA-450)	DnaJB1	Monoclonal	Mouse	1:2,000	1:2,000

[1] All antibodies were diluted in 5 % (w/v) skimmed milk in TBS-T.
[2] Anti-rabbit (Invitrogen) and anti-mouse (Cell Signaling Technology) IgG HRP-linked secondary antibodies were used.

3.6.1. α-synunclein fibrils

α-syn fibrils were prepared by incubating 200-500 μL solution of 100 μM α-syn in 1.5 mL tubes at 37 °C under orbital agitation (1000 rpm) in an Eppendorf Thermomixer for 7 days in 50 mM Tris, 100 mM NaCl and 0.05% NaN_3, pH 7.4. Afterwards, fibrils were purified by centrifugation for 30 min at 16,000 g and 4 °C. Pelleted fibrils were resuspended, unless otherwise stated, in Disaggregation Buffer (40 mM Hepes-KaOH pH 7.6, 50 mM KCl, 5 mM $MgCl_2$ and 2 mM DTT). The final protein concentration (monomer equivalents) was determined by disassembling an

aliquot of the preparation into monomers in 4 M GdnHCl and measuring its absorption at 280 nm.

3.6.2. α-synunclein sonicated fibrils

Sonicated fibrils were obtained using a Branson 450 Digital Sonifier equipped with a tapered microtip of 3 mm diameter at 10% power. For a proper submersion of the probe, a minimum volume of 200 µL was used. **Figure 3.1** indicates the correct set up to avoid foaming or bad sample circulation. Bursting was carried out in cycles of 1 s ON; 1 s OFF with the sample set on ice-cold water to avoid overheating. Unless otherwise stated, preparation of sonicated fibril samples was done in Disaggregation Buffer with a total of 90 sonication cycles (3 min).
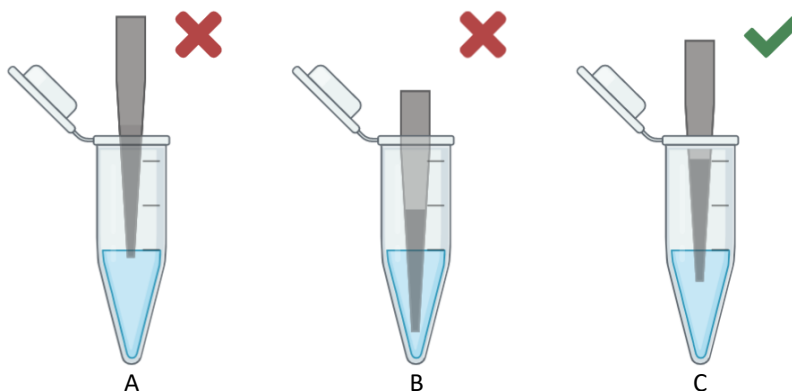
Figure 3.1. Tip depth for a correct sonication. When the tip is not submerged enough as illustrated in panel A, the sample will foam or bubble. On the opposite side, when the tip is too deep (panel B), liquid will not circulate the sample effectively. Panel C shows the correct set up to achieve good and reproducible results.

To obtain fibrils of different sizes, α-syn fibrils formed after 1-week incubation were subjected to varying sonication cycles. Soluble and insoluble fractions of samples (400 µL) sonicated for 15 or 30 cycles were separated by centrifugation (30 min at 16,000 g and 4 °C). Pellets were resuspended in 50 µL

Disaggregation Buffer. Supernatants were passed through 100 K Amicon®Ultra-0.5 mL centrifugal filters to remove any possible monomer released during sonication. This procedure consisted in 7 washing steps (4 min at 10,000 g and 20 °C) with 400 µL of Disaggregation Buffer. To collect the sample, up to 200 µL of Disaggregation Buffer was added to the filter device which was turned upside down in a clean tube and spun for 5 min at 2,000 g and 20 °C. A final 10 min centrifugation step at 16,000 g and 4 °C was done to remove any big aggregates formed during the washing process.

3.6.3. α-synunclein self-seeded fibrils

To obtain α-syn fibril preparations in a short period of time, 200-500 µL solutions of 100 µM α-syn were incubated in 1.5 mL tubes at 37 °C under quiescent conditions in an Eppendorf Thermomixer for 1-4 days in 50 mM Tris, 100 mM NaCl and 0.05% NaN$_3$, pH 7.4 in the presence of 5 % (mol/mol) seeds. When Alexa488-labeled fibrils were prepared, 15-30 % of the monomeric α-syn solution was α-syn$_{Q24C}$-488. Under these conditions, the final aggregate labeling efficiency was 10-25 %.

For seed preparation, 500 µL of α-syn fibrils, obtained as described in section 3.6.1. without the purification step, were subjected to 90 sonication cycles (1 s ON; 1 s OFF). Seeds were aliquoted, flash-frozen in liquid N$_2$ and stored at -20 °C until use.

3.6.4. α-synunclein cross-seeded fibrils

For cross-seeding experiments of α-syn$_{WT}$ and α-syn$_{1-110}$, samples were first passed through 100 K Amicon®Ultra-0.5 mL centrifugal filters to remove any pre-existing aggregation nuclei. Then, the flow-through was diluted to 100 µM in 50 mM Tris, 100 mM NaCl and 0.05% NaN$_3$, pH 7.4. Aggregation was seeded with 5% (mol/mol)

unsonicated fibrils of both variants. Samples were incubated at 37 °C under quiescent conditions for 3 days.

3.6.5. α-synunclein type B oligomers

α-syn type B oligomers were prepared by lyophilization as previously described (Chen et al., 2015). 6 mg of α-syn in 1.5-3 mL (140-280 µM final protein concentration) was dialyzed against 5 L MilliQ water overnight at 4 °C. Samples were placed into 15 mL falcon tubes, flash freeze in liquid nitrogen, and lyophilized for 48 h. Lyophilized protein was stored at -20 °C until use.

Lyophile was resuspended in 500 µL of PBS (10 mM phosphate buffer, 2.7 mM KCl, 137 mM NaCl, pH 7.4) to obtain a final protein concentration of ca. 800 µM. Protein solution was filtered through a 0.22 µm syringe filter and incubate it in 1.5 mL tubes at 37 °C under quiescent conditions for 20-24 h. In order to remove excess monomeric protein as well as the low levels of very small oligomers supernatant was placed in 100 K Amicon®Ultra-0.5 mL centrifugal filters and centrifuged at 10,000 g and 20 °C for 2 min. 400 µL of PBS was added to the filter and centrifuged again. This step was repeated 6 times to ensure that the flow-through was clean of monomeric protein. To collect the sample, up to 250 µL of PBS was added to the filter device which was turned upside down in a clean tube and spun for 2 min at 2,000 g and 20 °C. The resultant protein solution was centrifuged for 10 min at 17,000 g to remove any fibrillar species that may have formed during the process. Protein concentration was determined spectrophotometrically (280 nm) as oligomer sample produces no significant light scattering neither changes its molar extinction coefficient compared to monomers.

Preparation of Alexa488-labeled type B oligomers was done using the same procedure. Starting with 1.5 mg of α-syn$_{Q24C}$-488 and 4.5 mg of α-syn$_{WT}$, the final labeling efficiency was of ca. 10 %.

3.6.6. α-synunclein polymorphs

Several α-syn polymorphs have been studied in this thesis using α-syn$_{WT}$ and different aggregation conditions. For ribbon formation (Bousset *et al.*, 2013), α-syn was dialyzed overnight against 5 mM Tris-HCl pH 7.5 at 4 °C, diluted to 100 µM in the same buffer supplemented with 0.05% sodium azide and incubated at 37 °C for 1 week under continuous shaking in an Eppendorf Thermomixer set at 1000 rpm. The polymorphs obtained in the presence of 5% trifluoroethanol or 150 g/L dextran were produced in Prof. Nunilo Cremades´ lab as previously described (Camino *et al.*, 2020). To obtain alexa488 labeled polymorphs, aggregation was done in the same conditions but in the presence of 15-30 % monomeric α-syn$_{Q24C}$-488.

3.6.7. Calpain-1 digested α-synunclein fibrils

Calpain-1 (µ-calpain) cleavage of α-syn was carried out using previously described methods with some modifications (Mishizen-eberz *et al.*, 2003). Briefly, different amounts of calpain-1 (stated in each experiment) were added to a solution of 50 µM α-syn in buffer 40 mM Hepes pH 7.6 and 5 mM DTT. Reactions were initiated by the addition of CaCl$_2$ (1 mM final concentration) and incubated at 37 °C for 10 min. Reactions were stopped by adding SDS-PAGE loading buffer and boiling for 10 min. To determine the effect of calpain cleavage on the secondary structure of fibrils, unsonicated fibrils were digested with 13.5 ng/µL of calpain-1 and after 10 min incubation at 37°C, they were centrifuged (30 min at 17,000 g and 4°C) and resuspended in PBS buffer. For TEM experiments, after digestion (13.5 ng/µL of calpain-1) of unsonicated and sonicated fibrils, samples were incubated overnight with 12.5 µM of the Calpain inhibitor VI (SJA 6017) (Santa Cruz Biotechnology). When sonicated fibrils were digested and used in disaggregation experiments, they were incubated for 2h with 12.5 µM Calpain inhibitor VI prior to their addition to the chaperone mixture.

3.6.8. Tau fibrils

Tau K18 fibrils were prepared by incubating 200-500 µL solution of 40 µM K18 in the presence of 40 µM of heparin (sodium salt from porcine, MW 3,000, MPBio) in 25 mM Tris pH 7.5, 50 mM NaCl and 1 mM DTT. Incubation took place in 1.5 mL tubes at 37 °C under quiescent conditions in an Eppendorf Thermomixer for 1-3 days. After incubation ended, fibrils were purified, quantified and stored as described in section 3.6.1.

Tau 2N4R fibrils were prepared by incubating 200-800 µL solution of 40 µM tau 2N4R in the presence of 40 µM of heparin (sodium salt from porcine, MW 3,000, MPBio) in 25 mM Tris pH 7.5, 50 mM NaCl and 2 mM DTT supplemented with 1 mM PMSF, 1 mM EDTA, 1 mM EGTA, 1 µg/mL leupeptin, 1 µg/mL aprotinin, 1 µg/mL pepstatin to avoid protein degradation and 0.05% NaN_3 to avoid bacterial growth. Samples in 1.5 mL tubes were incubated at 37 °C under quiescent conditions in an Eppendorf Thermomixer for 7 days, refreshing the DTT every day to maintain reducing conditions. After incubation, fibrils were purified, quantified and used. Alternatively, the preparation was directly subjected to 30 sonication cycles (1 s ON; 1 s OFF), aliquoted, flash-frozen in liquid N_2 and stored at -20 °C for its use as seeds. Seeded aggregation of tau 2N4R was performed in the conditions above described with 5% (mol/mol) seeds, reducing incubation time to 1-3 days and avoiding the use of protease and bacterial growth inhibitors. Sonicated fibrils used in disaggregation experiments were obtained by 15 sonication cycles (1 s ON; 1 s OFF), ultracentrifugation for 40 min at 186,000 g and 4 °C and resuspension in Disaggregation Buffer.

3.7. AGGREGATE CHARACTERIZATION

3.7.1. Dynamic Light Scattering

Dynamic Light Scattering (DLS) is a technique that measures the size of micrometric entities subjected to Brownian motion. In this thesis, DLS has been used to estimate the size of different protein/lipid samples. Size volume distribution profiles of the different samples at 25°C were obtained using a Zetasizer Nano ZS (Malvern Instruments) at a back-scattering angle of 173°. Monomeric (100 μM) and oligomeric or fibrillar (10 μM) α-syn and tau species were measured in Refolding Buffer. Liposomes with encapsulated calcein (10 μM) were measured in Calcein Leakage Buffer (section 3.11.1).

3.7.2. Transmission Electron Microscopy

The different aggregates prepared in this thesis were visualized by negative staining and Transmission Electron Microscopy (TEM). Protein concentration was kept 0.25-2 mg/mL. 3 μL samples were applied onto glow-discharged Formvar/carbon-coated 200-mesh copper grids and incubated for 1 min. Grids were negatively stained with 1% (w/v) uranyl acetate (2 staining steps of 10 s) and air-dried for 5 min. Samples were visualized in a JEOL JEM 1400 Plus electron microscope.

3.7.3. Atomic Force microscopy

Tau K18 fibrils were imaged by atomic force microscopy (AFM) in a NanoWizard II AFM (JPK Instruments) operating in contact mode. 100 μL of aggregated samples (40 μM tau) were applied onto freshly cleaved mica and allow to deposit for 10 min. The mica surface was then rinsed extensively with tau K18 aggregation buffer (9 washing steps with 150 μL).

3.7.4. Circular Dichroism spectroscopy

Circular Dichroism (CD) spectroscopy measures the difference in absorbance of right- and left-circularly polarized light by optically active chiral molecules. This technique is typically used to study protein structure as the far-UV (ultraviolet) CD spectrum of proteins can reveal important characteristics of their secondary structure: α-helix conformation have negative bands at 222 and 208 nm and a positive band at 193 nm; β-sheet conformation have a negative band at 218 nm and positive band at 195 nm; and disordered proteins have a negative band near 195 nm. For this reason, CD spectroscopy is widely used to study the transition of monomeric intrinsically disordered amyloidogenic proteins such as α-syn and tau, to their β-sheet rich amyloid form.

Samples were prepared at 10 μM in PBS for α-syn and at 20 μM in 20 mM K_2H/KH_2PO_4 pH 7.5, 50 mM NaF for tau K18. Far-UV CD spectra were acquired at 20 °C in a Jasco J-810 circular dichroism spectropolarimeter using rectangular quartz cuvettes with 1 mm path length. Each spectrum represents the average of 15-20 scans, collected from 200-260 nm, with a spectral bandwidth of 1 nm and a response time of 1 s.

3.7.5. Fourier Transform Infrared spectroscopy

Fourier Transform Infrared (FT-IR) spectroscopy has been extensively used to follow amyloid formation and characterize aggregate structure as it allows a detailed analysis of the secondary structure of the samples. For FT-IR spectra, aggregates were prepared as described in section 3.6, changing to deuterated buffers in the aggregate purification steps. Protein concentration was kept 1-10 mg/mL to meet quality spectra criteria. Samples were applied on a 25 μm carved calcium fluoride window and placed in a Peltier cell (TempCon, Bio Tools). Measurements were performed in a Nicolet Nexus 5700 spectrometer equipped with a MCT detector.

Each spectrum with a nominal resolution of 2 cm^{-1} was obtained by the collection of 102 interferograms at 20 °C and then referred to a background. Quantitative information on the amide I, located between 1700 and 1600 cm^{-1} and mainly composed (~80%) by the C=O stretching vibration of the peptide bond, was obtained as previously described (Arrondo *et al.*, 1993). The spectra were digitally subtracted using a spectrum of deuterated buffer as a reference. With the aim of minimizing the differences in protein concentration among recorded samples, the region of the amide I band area was normalized in all spectra.

3.7.6. Proteinase K digestion

Proteinase K is a broad-spectrum serine endoprotease that was originally isolated from the fungus *Engyodontium album* (formerly called *Tritirachium album*). This protease is widely used to study the structural properties of amyloids, being able to distinguish different aggregates by their digestion resistance or pattern (Bousset *et al.*, 2013; Chen *et al.*, 2015). Monomeric or fibrillar α-syn (0.6 mg/mL) in 40 mM Hepes-KaOH pH 7.6, 50 mM KCl, 5 mM MgCl$_2$ and 2 mM DTT were incubated at 37 °C with 5 µg/mL of proteinase K in a final volume of 130 µL. Aliquots (16.7 µL) were removed at different time intervals and the reaction was stopped by adding 3.4 µL of 6x SDS-containing loading buffer and boiling the mixture for 10 min. Samples were analyzed by SDS-PAGE in 18% polyacrylamide gels.

3.7.7. Fluorophore binding assays

Fluorescent probes thioflavin T (ThT) and 1-anilino-8-naphthalene sulfonate (ANS) are widely used to study amyloids. ThT is a benzothiazole dye that increases its fluorescence upon binding to stacked β-sheets, a common fold of amyloid fibrils. ANS dye has low fluorescence quantum yield in polar environments, such as aqueous solutions, but in apolar environments, there is an increase in fluorescence intensity and a blue shift in the emission maximum wavelength. This property

makes it a sensitive indicator of hydrophobic patches in native proteins and protein aggregates.

Binding of ThT and ANS to different α-syn aggregates was done in Disaggregation Buffer by mixing 30 μL of 10 μM aggregated α-syn and 70 μL of ThT or ANS (final concentration of 50 μM and 100 μM, respectively). After a 30 min incubation at room temperature, emission spectra (450-600 nm) of the different samples were measured at 25 °C in a FluoroMax-3 (Jobin-Ybon) fluorimeter. Excitation wavelength and ex/em slits were 440 nm and 3x3 nm, respectively, for ThT and, 370 nm and 5x5 nm, for ANS.

3.7.8. Guanidine hydrochloride fibril denaturation.

Guanidine hydrochloride (GdnHCl), a strong chaotropic agent, was used to compare the chemical stability of different α-syn aggregates. α-syn fibrils were diluted to 40 μM in Disaggregation buffer containing increasing GdnHCl concentrations and placed in a 96-well plate. Samples (100 μL) were incubated 16-20 h at room temperature. After incubation, a 10 μL aliquot was taken and added to 50 μL of a 50 μM ThT solution placed in 96-Well Half Area Black plates (Non-binding surface; Corning®). Fluorescence was measured in a Synergy HTX plate reader (Biotek), from the top, using a gain of 90 and excitation and emission filters of 400/30 and 485/20 nm, respectively.

3.8. AGGREGATION KINETICS

3.8.1. Off-line aggregation kinetics

Long aggregation kinetics (7 days) of α-syn$_{WT}$ and tau 2N4R under the conditions stated in sections 3.6.1 and 3.6.8 were measured off-line using ThT and ANS to determine the time needed to reach saturation. At different time points, 10 μL aliquots were taken and added to 140 μL 20 μM ThT or 100 μM ANS solutions. After

a 40 min incubation at room temperature, samples were measured as described in section 3.7.7. Normalized intensity to the fluorescence maximum was plotted against time.

3.8.2. On-line aggregation kinetics

Short aggregation kinetics (1-3 days) of α-syn and tau under the conditions stated in sections 3.6.3., 3.6.4. and 3.6.8., were measured on-line in Synergy HTX plate reader. Samples (200 μL) were placed in 96-well transparent plates and sealed with HD clear Duck tape. Aggregation at 37 °C was followed by light scattering at different wavelengths (350, 450 and 500 nm), taking measurement every 5 min.

3.9. CHAPERONE BINDING TO AGGREGATES

3.9.1. Aggregation prevention by chaperones

Binding of chaperones to preformed α-syn fibrils (i.e. seeds) was monitored by following the inhibition of fibrillation with a ThT fluorescence assay. α-syn was incubated at 50 μM with 5% (mol/mol) seeds (sonicated fibrils) at 37°C under quiescent conditions in 50 mM Tris, 100 mM NaCl and 0.05% NaN$_3$, pH 7.4. Chaperones were added individually at 1:10 (chap:syn) molar ratio. The ThT fluorescence of the samples placed in 96-Well Half Area Black plates (Non-binding surface; Corning®) was measured on-line in a Synergy HTX plate reader using a gain of 60 and excitation and emission filters of 400/30 nm and 485/20 nm, respectively. Readings were taken from the top, every 5 min for a period of up to 80 h.

3.9.2. Co-sedimentation assay

Interaction of chaperones with α-syn unsonicated fibrils was done following a co-sedimentation assay previously described (Acebrón *et al.*, 2008; Cabrera *et al.*, 2019). α-syn fibrils were diluted to 2 μM in Disaggregation Buffer containing Hsc70

(2 µM), DnaJB1 (1 µM) and Apg2 (0.2 µM). After adding 2 mM ATP, samples (100 µL) were incubated for 10 min and subsequently centrifuged at 16,000 g and 4 °C for 30 min. Supernatants were discarded and pellets, containing mainly fibril-associated chaperones, were resuspended in 15 µL of loading buffer were analyzed and quantified by SDS-PAGE and densitometry. Normalized intensity of Hsc70 bound to the aggregate was obtained by subtracting the intensity of the Hsc70 band in each chaperone combination in the absence of aggregate and then, the intensity of the ternary chaperone combination was considered 1.

3.10. CHAPERONE-MEDIATED DISAGGREGATION

Several methods have been used to follow the chaperone-mediated disaggregation of protein aggregates. In all cases, experiments were done at 30 °C in Disaggregation Buffer (40 mM Hepes-KaOH pH 7.6, 50 mM KCl, 5 mM $MgCl_2$ and 2 mM DTT) and in the presence of 2 mM ATP and an ATP-regeneration system - 8 mM phosphoenolpyruvate (PEP) and 20 ng/µL pyruvate kinase -. Unless otherwise stated, the molar ratio of the three chaperones that compose the human disaggregase was 1:0.5:0.1 (Hsc70:DnaJB1:Apg2).

3.10.1. PAGE-based disaggregation assays

Disaggregation of amyloid aggregates was followed by three different PAGE-based methods: sedimentation assay, showing the amount of protein solubilized by chaperones; Native-PAGE assay, which distinguishes soluble species (monomeric and oligomeric); and sucrose gradient centrifugation, able to separate particles according to their density allowing the characterization of both soluble and insoluble material.

α-syn disaggregation was carried out at final protein concentrations of 2 µM α-syn, 10 µM Hsc70, 5 µM DnaJB1 and 1 µM Apg2 in a total volume of 50 µL. 20 µL

of unsonicated fibrils were mixed with 25 µL of a chaperone mixture and reaction was initiated with the addition of 5 µL of a mixture of ATP and ATP-regeneration system. After 2 h incubation at 30 °C, samples were either directly analyzed by Native-PAGE and immunoblotting, or centrifuged for 30 min at 16,000 g and 4 °C to perform a sedimentation assay. Supernatants were carefully collected, mixed with SDS-containing loading buffer, boiled for 10 min and analyzed by SDS-PAGE and immunoblotting. In the sucrose gradient centrifugation experiments, α-syn concentration was raised to 10 µM. After incubation (2.5 h at 30 °C), 400 µL of the reaction mixture was applied to 3.2 ml of a 5-40 % sucrose gradient. In the case of α-syn oligomers, sample and gradient volumes were halved to save protein. Samples were centrifuged at 162,000 g for 2h at 4°C and 400 µL fractions (200 µL for oligomers) were manually removed and subjected to SDS-PAGE and immunoblotting.

Tau 2N4R disaggregation was followed by a sedimentation assay similar to the above described for α-syn. Final protein concentrations were 1 µM tau, 10 µM Hsc70, 5 µM DnaJB1 and 1 µM Apg2 in a total volume of 50 µL. 20 µL of fibrils were mixed with 25 µL of a chaperone mixture and reaction was initiated with the addition of 5 µL of a mixture of ATP and ATP-regeneration system. After 2 h incubation at 30 °C, samples were ultracentrifuged for 40 min at 186,000 g and 4 °C. Supernatants were carefully collected, mixed with SDS-containing loading buffer, boiled for 10 min and analyzed by SDS-PAGE and immunoblotting.

3.10.2. Disaggregation followed by fluoresce-dequenching

Disaggregation kinetics of different substrates were followed as a fluorescence dequenching process in a Synergy HTX plate reader (Biotek). For that purpose, aggregates labeled with Alexa488 were obtained as described in section 3.6. Disaggregation was carried out in a final volume of 50 µL using 96-Well Half Area Black plates (Non-binding surface; Corning®) at a final aggregate concentration of

2 µM. 20 µL of aggregates were mixed with 25 µL of varying chaperone concentrations. No disaggregation and total disaggregation controls were done with the aggregates alone or in the presence of GdnHCl (4 M), respectively. Before starting the reaction, samples were incubated for 30 min at 30 °C in the plate reader to stabilize the sample. Reaction was initiated with the addition of 5 µL of a mixture of ATP and ATP-regeneration system, and immediately, plates were sealed with HD Clear Duck tape and introduced back in the plate reader for measuring. Fluorescence readings were done every 3 min from the top, using excitation and emission filters of 485/20 and 528/20 nm and a gain of 60-75. At the end of the kinetics, samples were analyzed by Native-PAGE as described in section 3.5.2. Gel inputs were prepared from concentrated aggregate stocks, dissolving an aliquot in 4 M GdnHCl to monomerize the sample, which was then used to prepare a 2 µM solution in Disaggregation Buffer. In this way, we avoid artifacts due to the loading of a high concentration of GdnHCl in native gels. In the case of G6PDH aggregates, gel inputs were made with the labeled native protein.

Disaggregation kinetics were analyzed with SigmaPlot 13.0 using the following pseudo-first order model:

$$F_m(t) = y_{max} \cdot \left(1 - e^{-k \cdot t}\right)$$

where F_m is the fraction of monomer, y_{max} is the maximum disaggregation and k is the disaggregation rate constant.

3.10.3. Disaggregation followed by high-speed AFM

Visualization of the chaperone-mediated disaggregation of α-syn fibrils was done by high-speed AFM using a NanoRazer AFM (Bruker). Sonicated fibrils (30 µM) were deposited on a freshly cleaved, poly-L-ornithine treated mica surface (10 µL drop). After 15 min of incubation, the fibrils were gently rinsed with Disaggregation buffer 3 times with 10 µL volume. 800 µL of Disaggregation buffer were added to imaging

chamber and after a good spot was identified and several stable images were acquired, the mixture of chaperones were added to the chamber. After 5 min, a mixture of ATP and ATP regeneration system were also added to the chamber resulting into a final volume of 900 μL. Final chaperone concentrations were 10 μM Hsc70, 5 μM DnaJB1 and 1 μM Apg2. Scans were done during the whole process, using tapping mode, a NanoWorld USC-F1.2-k0.15 probe (k~0.25N/m) and the following setting: working amplitude (3-6 nm), scan size (1x1 μm) and scan rate (100-300 lines/s).

3.10.4. Disaggregation of proteasome-fragmented α-syn fibrils

To test the collaboration of the human disaggregase and the proteasome in the disassembly of α-syn amyloids, unsonicated and sonicated fibrils (20% labeled) were first incubated with the 26S proteasome holoenzyme as previously described (Cliffe *et al.*, 2019). Briefly, 500 nM of α-syn fibrils were incubated with 50 nM of proteasome for 22h at 25 °C in 50 mM Tris-HCl pH 7.5, 5 mM $MgCl_2$ supplemented with 5 mM ATP, 8 mM PEP and 20 ng/μL pyruvate kinase. After the incubation, 50 μL of the sample were mixed with 75 μL of a 2x chaperone mixture (4 μM Hsc70, 2 μM DnaJB1 and 0.4 μM Apg2), 15 μL of a 10x fresh solution of ATP and ATP regeneration system (20 mM ATP, 80 mM PEP and 200 ng/μL pyruvate kinase) and disaggregation buffer to make up 150 μL final reaction volume. Samples were incubated for 16h at 30 °C and analyzed by Native-PAGE.

3.10.5. Glucose-6-phosphate dehydrogenase reactivation

G6PDH is a homodimeric protein that catalyzes the oxidation of glucose-6-phosphate (G6P) to 6-phosphogluconate, using NAD^+/$NADP^+$ as a coenzyme that is reduced to NADH/NADPH. G6PDH is commonly used as an amorphous aggregate model substrate in chaperone-mediated refolding experiments (Acebrón *et al.*, 2009; Villar-Pique *et al.*, 2012; Mattoo *et al.*, 2013; Fernández-Higuero *et al.*, 2018;

Cabrera *et al.*, 2019; Fernández-Higuero, Muga and Vilar, 2020). G6PDH (5 µM) was heat-denatured and aggregated at 50 °C for 30 min in Disaggregation Buffer. Subsequently, aggregates were stabilized at 30 °C for 30 min. 40 µL of the aggregate was mixed with 50 µL of a chaperone mixture and upon addition of 10 µL of a mixture of ATP and ATP-regeneration system, the reaction was initiated. Reactivation of aggregated G6PDH to its native and catalytically active state was monitored off-line following the formation of NADPH by measuring the absorbance increase at 340 nm. At each time point, a 5 µL aliquot was added to 250 µL of 2.5 mM G6P and 1 mM NADP$^+$ in buffer 50 mM Tris-HCl pH 7.5, 50 mM KCl, 20 mM MgCl$_2$, 2 mM DTT. Measurements were done for 5 min in transparent 96-well plates using a Synergy HTX plate reader (Biotek). Reactivation percentages were calculated considering the slope of NADPH formation of aggregated and native (in the presence of chaperones) G6PDH as 0% and 100% activity, respectively.

3.11. AGGREGATE TOXICITY DETERMINATION

3.11.1. Liposome leakage assay

The membrane-permeabilization activity of the different α-syn species was monitored by following the leakage of the fluorophore calcein entrapped within the lipid vesicles into the bulk solution. This assay is based on calcein self-quenching at high concentrations and its small permeability coefficient across a lipid bilayer, as long as the vesicles are intact. Consequently, calcein is trapped into liposomes at a concentration above the self-quenching threshold and when the membrane is disrupted due to the addition of an external agent, calcein is leaked to the solution where is diluted to a smaller concentration, producing a dequenching and generating an increase in fluorescence intensity (**Figure 3.2**).

To prepare liposomes with encapsulated calcein, 4 mg of POPS, dissolved in chloroform:methanol (2:1) at 25 mg/mL, were placed in a glass tube. To remove

the solvent, the sample was subjected to a N_2 stream until dryness and placed under vacuum for 2 h. Then, lipids were swollen in Encapsulation Buffer (10 mM Hepes-KOH, 50 mM NaCl and 50 mM calcein, pH 7.4) with two cycles of heating to 50 °C and vortexing, to obtain multilamellar vesicles (MLVs). Large unilamellar vesicles (LUV) were produced by previously described methods (Mayer, Hope and Cullis, 1986), subjecting the MLV to 10 freeze/thaw cycles, and extruding the samples in a LIPEX Liposome Extrusion System, using 0.1 μm pore size Nuclepore filters (Whatman). To remove calcein outside liposomes, these were loaded on a PD10 gel filtration column (GE Healthcare) equilibrated in Calcein Leakage Buffer (10 mM Hepes-KOH, ca. 130 mM NaCl, pH 7.4) which presented the same osmolarity to the Encapsulation Buffer. Liposome concentration was determined by phosphate analysis (Böttcher CJF, Van gent CM, 1961) and vesicle size (≈100 nm) was checked by DLS as described in section 3.7.1.

● Self-quenched calcein
● Fluorescent calcein
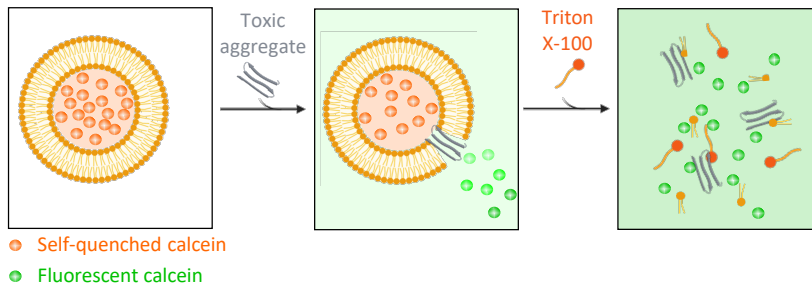
Figure 3.2. Liposome leakage assay. Calcein is encapsulated in liposomes at high concentrations, which produces the self-quenching of the fluorophore. Upon membrane disruption due to an exogenous agent, calcein is released to the medium where it is diluted and dequenched, increasing its fluorescence. Maximum fluorescence control is achieved by adding triton X-100, which fully disrupts liposomes.

Liposome leakage was performed in Calcein Leakage Buffer. 110 μL liposomes at 11 μM were mixed with 10 μL of 10 μM α-syn. Alternatively, 0 and 100 % controls were done by mixing the same liposome volume with 10 μL of Calcein

Leakage Buffer or Triton X-100 10 % (v/v), respectively. Samples were incubated for 2 h at 25 °C and 350 rpm in an Eppendorf Thermomixer. Fluorescence was measured at 25 °C in a FluoroMax-3 (Jobin-Ybon) fluorimeter (Ex. 440 nm; Em. 520).

3.11.2. Cell proliferation assay

Cytotoxicity was determined using the CellTiter 96® AQ$_{ueous}$ One Solution Cell Proliferation Assay (Promega). This colorimetric method contains a tetrazolium compound [3-(4,5-dimethylthiazol-2-yl)-5-(3-carboxymethoxyphenyl)-2-(4-sulfophenyl)-2H-tetrazolium, inner salt; MTS] and an electron coupling reagent (phenazine ethosulfate; PES). The combination of PES and MTS forms a stable solution, which is bioreduced by cells into a colored formazan product that is soluble in the culture medium. This conversion is accomplished by NADPH or NADH produced by dehydrogenase enzymes in metabolically active cells. Thus, the quantity of formazan product is directly proportional to the number of living cells in culture.

SH-SY5Y cells were seeded at 20.000 cells/well in 96-well plates and incubated overnight in DMEM supplemented with 10% FBS. The next day, the medium was replaced by 100 µL of fresh medium containing 0.15 or 0.3 µM of α-syn and cells were incubated for 24 h. Freshly prepared MTS/PES mixture was directly added (20 µL) to culture wells and incubated for 1-4 hours. Formazan amount was measured by recording the absorbance at 490 nm in a Synergy HTX plate reader (Biotek). Control values of cells without α-syn and culture medium without cells were taken as 100 and 0 % of cell viability.

3.12. STATISTICAL ANALYSIS

Statistical analyses of the experimental data shown in various figures as indicated in the main text are shown in the APPENDIX. P values were calculated in SigmaPlot 13 using one-way analysis of variance (ANOVA).

CHAPTER

4

THE HUMAN DISAGGREGASE TARGETS TOXIC AGGREGATION INTERMEDIATES OF AMYLOIDS

4.1. INTRODUCTION

To counteract the toxic effect of protein aggregates, cells have evolved a sophisticated protein homeostasis network that coordinates protein synthesis, folding, disaggregation and degradation (Labbadia and Morimoto, 2015). This network is composed of the translational machinery, molecular chaperones and cochaperones, the ubiquitin-proteasome system, and the autophagy machinery. How this network deals with amyloid aggregates remains poorly understood. It has been previously reported that the constitutive human Hsp70 (Hsc70) in collaboration with its Hsp40 cochaperone (Hdj1 or DnaJB1) slowly disassembles preformed α-syn fibrils (Duennwald, Echeverria and Shorter, 2012). This activity was further stimulated by adding the NEF Hsp110 (Apg2). HspB5, a small heat shock protein also known as αB-crystallin, potentiated α-syn fibril disassembly by the ternary chaperone mixture. Although this chaperone combination was able to disaggregate fibrils, they did it in a timescale of weeks through a depolymerization process. Only when Hsp104, a yeast representative of the Hsp100 family able of fragmenting fibrils, was added to the mixture, disassembly occurred within hours. The lack of Hsp104 homologs in metazoans questioned whether this activity was physiologically relevant in humans. A later study revealed that a chaperone complex composed solely of members of the Hsp70, Hsp40 and Hsp110 families, was able to efficiently reverse α-syn amyloid fibrils through both fragmentation and

depolymerization, generating smaller fibrils, oligomers, and ultimately, monomers (Gao *et al.*, 2015). Recently, this exact chaperone mixture has been also reported to disaggregate tau and Htt fibrils (Ferrari *et al.*, 2018; Scior *et al.*, 2018; Nachman *et al.*, 2019), pointing to this Hsp70-based machinery as a potential human disaggregase of amyloids.

In this chapter, we aimed to shed light on the mechanism used by the human disaggregase to disassemble amyloids. For that purpose, we investigated the ability of this chaperone mixture to target different aggregation states that populate the amyloid formation process, including toxic oligomers and fibrils of different sizes.

4.2. RESULTS

4.2.1. Human Hsp70 disaggregase solubilizes α-syn fibrils

Disassembly of α-syn fibrils by the human Hsp70 machinery has been reported by two groups, with some disagreements in the chaperone mixture needed, the efficiency and time-scale of the process and the mechanism of disaggregation (Duennwald, Echeverria and Shorter, 2012; Gao *et al.*, 2015). In this regard, we first looked for the conditions that best worked in our hands. Aggregation of α-syn was followed by ThT and ANS fluorescence (**Figure 4.1 a**) and after 1 week, amyloid fibril morphology was confirmed by negative-stain EM (**Figure 4.1 b**). 2 µM of α-syn fibrils were incubated with 10 µM of Hsc70, 5 µM of the class B JDP DnaJB1 and, considering that substoichiometric NEF levels relative to Hsc70 seem critical for a good performance (Gao *et al.*, 2015), we titrated Apg2. After 2h incubation at 30°C in the presence of 2 mM ATP and an ATP regeneration system (8 mM PEP, 20 ng/µL PK), disaggregation reactions were subjected to centrifugation and the amount of soluble α-syn was analyzed by SDS-PAGE and immunoblotting. Hsc70 and DnaJB1 solubilized only a small fraction –around 10%- of the fibrils (**Figure 4.1 c**). However, when Apg2 was added to the mixture, solubilization increased substantially, up to

30%, reaching its maximum at a molar ratio of 1:0.5:0.1 (Hsc70:DnaJB1:Apg2), in agreement with previous data (Gao *et al.*, 2015). Therefore, this chaperone mixture has been used throughout this study.
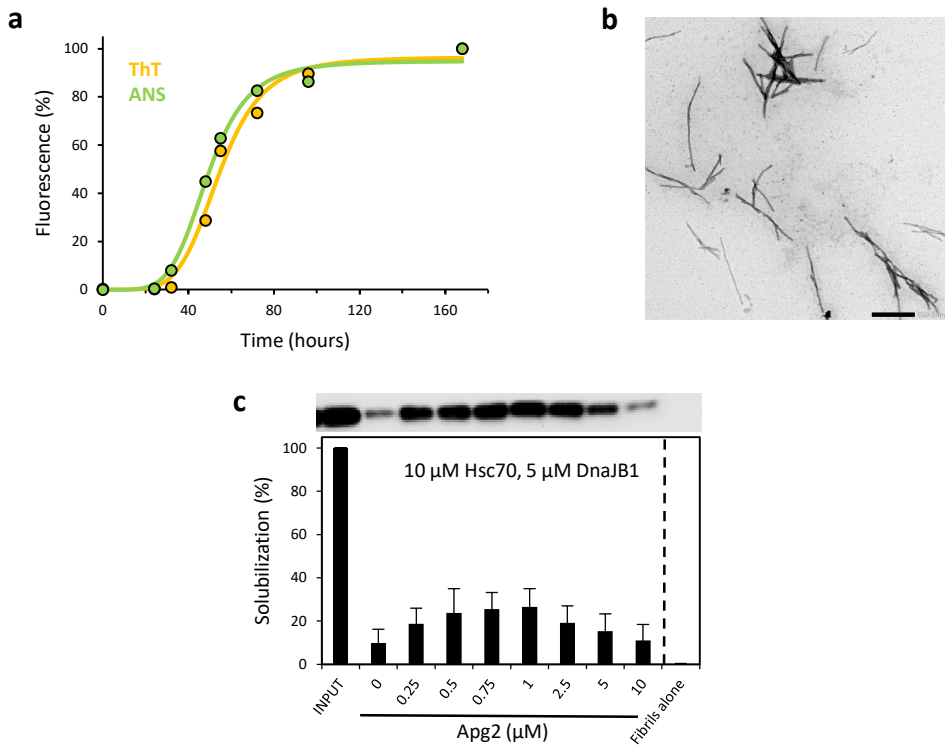
Figure 4.1. α-synuclein fibril formation and solubilization by the human disaggregase. (a) Aggregation kinetics of a 100 µM solution of α-syn followed by ThT and ANS fluorescence. At each time point, an aliquot from the reaction was mixed with the dyes and the fluorescence of the sample was measured. (b) After 1-week incubation, fibrillar morphology of the aggregates was confirmed by negative-stain EM (scale bar, 500 nm). (c) Solubilization of α-syn fibrils (2 µM) by different chaperone mixtures were analyzed by a sedimentation assay. After 2h incubation at 30°C in the presence of ATP, samples were centrifuged and solubilized α-syn was detected in the supernatant by immunoblotting. Fibrils without chaperones were used as a control. INPUT was made with a 2 µM solution of monomeric α-syn.

4.2.2. Human chaperones disaggregate toxic oligomers of α-synuclein

Oligomeric aggregates formed during the early events of the amyloid self-assembly process accumulate in the brains and tissues of patients suffering from neurodegenerative disorders. These soluble oligomers are believed to be the primary origin of the toxicity in amyloid diseases (Cremades, Chen and Dobson, 2017). In this context, we wanted to explore the ability of the human disaggregase to process such toxic species. To this aim, we produced α-syn oligomers kinetically trapped during the self-assembly process, previously designated as type B oligomers (Cremades *et al.*, 2012; Chen *et al.*, 2015; Fusco *et al.*, 2017). The FRET signatures of these oligomers match those found for the transient oligomeric and toxic forms generated during aggregation (Cremades *et al.*, 2012). Thus, they allow us to explore whether chaperones can perform their disaggregation activity at this initial stage of the amyloid formation process. Endorsing previous studies, these oligomers had a cylinder-like morphology and a size in the range of 10-40 nm as seen by EM (**Figure 4.2 a**) and DLS (**Figure 4.2 b**) (Chen *et al.*, 2015; Fusco *et al.*, 2017). In terms of secondary structure, type B oligomers were enriched in β-sheet structure as seen by CD (**Figure 4.2 c**), a conformation that favors the exposure of the N-terminal region of α-syn, which binds lipid bilayers and causes membrane disruption and cytotoxicity (Fusco *et al.*, 2017).

The presence of the Hsp40 component is essential for the disaggregase activity of the Hsp70 chaperone system. J-domain proteins form the largest chaperone family and guide Hsp70 to specific functions, therefore being responsible for the functional diversification of the central Hsp70 component (Cyr and Ramos, 2015). A recent report put forward a size-specific aggregate targeting for J-proteins: large aggregates were targeted by class B J-proteins whereas class A J-proteins aimed for small ones (Nillegoda *et al.*, 2015). Being type B oligomers small α-syn aggregates, we decided to test whether this specific targeting was also

observed. To this aim, three different J-proteins were assayed together with the Hsc70 and Apg2 components of the disaggregase: DnaJB1, the class B J-protein used above, and two class A J-proteins, DnaJA1 (Hdj2) and DnaJA2. 2 µM type B oligomers of α-syn were incubated with a 5-fold excess of Hsc70 and the cochaperone ratio described in the previous section. As type B oligomers are soluble, disaggregation reactions were directly run on a 4-16% Native-PAGE and analyzed by immunoblotting. The Hsc70-Agp2 combination showed disaggregase activity only with DnaJB1, and not with either of the class A JDP used (**Figure 4.2 d**). This activity was ATP-dependent and resulted in the oligomer to monomer conversion of α-syn, with barely any intermediate species. These data indicate that Hsc70, working in concert with Apg2 and the same class B J-protein that disassembles fibrils, can target toxic oligomeric species formed at the early stages of the aggregation process.
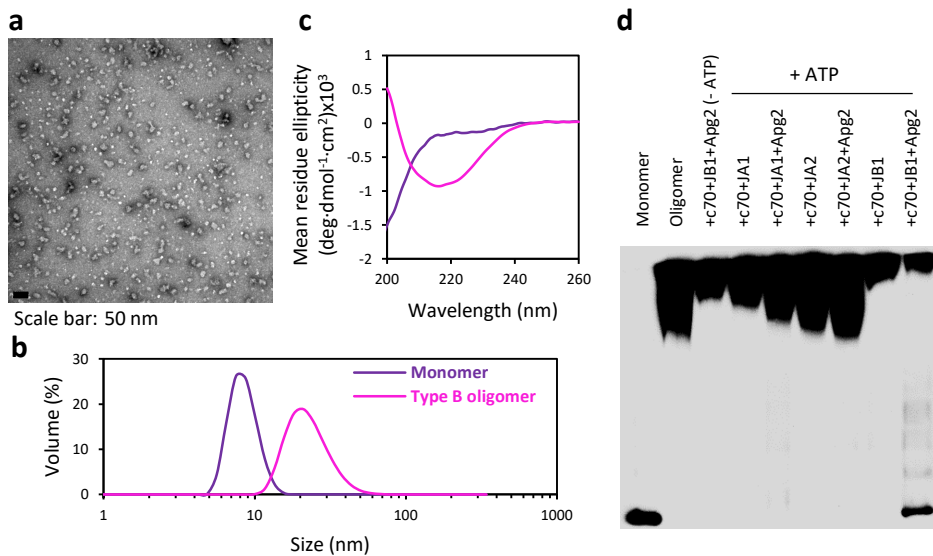
Figure 4.2. Disaggregation of type B α-syn oligomers by human chaperones. Type B oligomer morphology, size and secondary structure were confirmed by EM (a), DLS (b) and Far-UV CD (c). (d) Oligomer disaggregation reactions after 2h incubation at 30 °C with different chaperone mixtures were analyzed by Native-PAGE and immunoblotting. Monomeric and oligomeric solutions in the absence of chaperone were used as controls.

4.2.3. Fragmented fibrils generated by sonication are better disaggregated by chaperones

The overall aggregation process of α-syn, and other amyloidogenic polypeptides, was initially defined as a nucleation-polymerization process in which a primary nucleation step determines that monomeric protein goes through an oligomerization event whose products can grow to ultimately give rise to mature fibrils (Jarrett and Lansbury, 1992). It has become evident that other secondary processes, such as nucleation catalyzed on aggregate surfaces and fibril fragmentation, exist and may be crucial in the formation of short fibrillar and toxic aggregation intermediates (Knowles *et al.*, 2009; Cohen *et al.*, 2013; Buell *et al.*, 2014). In this regard, we also wanted to explore the effect of fibril fragmentation on the disassembly activity of the human disaggregase.

Mechanical fragmentation of fibrils by agitation or sonication produces a time-dependent decrease in size, accompanied by an increase in aggregate toxicity (Xue *et al.*, 2009; Mirbaha *et al.*, 2015, 2018; Abdelmotilib *et al.*, 2017; Ghag *et al.*, 2018). Thus, we subjected α-syn fibrils to 15 or 30 sonication cycles and separated the soluble and insoluble fractions by centrifugation to obtain more homogeneous fibril populations (**Figure 4.3 a**). EM (**Figure 4.3 b**) and DLS (**Figure 4.3 c**) of the samples confirmed that increasing sonication time reduced fibril size. Importantly, as previously seen for other amyloids (Xue *et al.*, 2009), sonication did not alter the conformation or chemical properties of α-syn fibrils. Neither interaction with ThT nor binding of the solvent-sensitive dye ANS, were importantly altered upon (**Figure 4.3 d**), indicating that β-sheet-rich regions and exposure of hydrophobic surfaces to the solvent were similar for fibrils of different sizes. FT-IR spectroscopy analysis of the samples confirmed these results, as unsonicated and sonicated fibrils showed similar spectra with absorption maxima at 1628 cm^{-1} (**Figure 4.3 e**), characteristic of proteins with a high β-sheet content (Arrondo *et al.*, 1993).
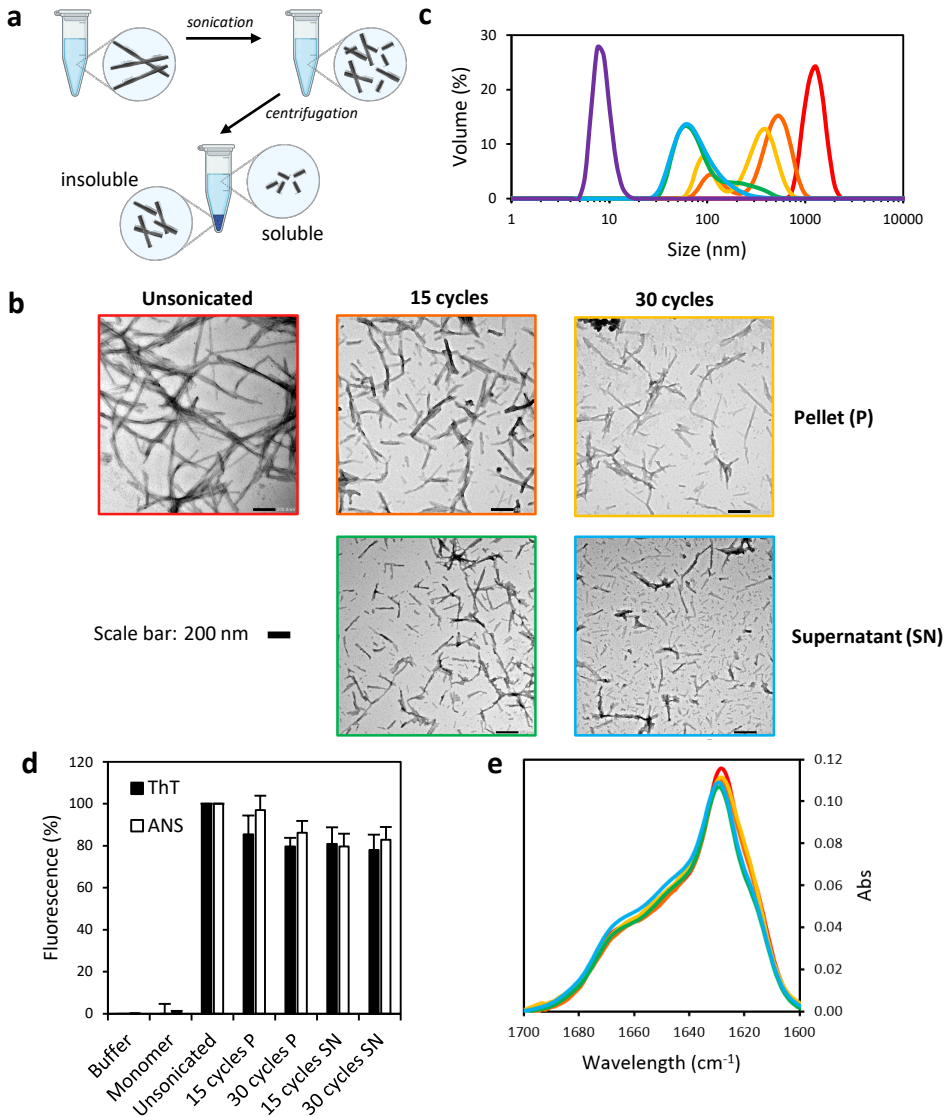
Figure 4.3. Fibril fragmentation by sonication changes fibril size without altering its structure. (a) Schematic representation of the procedure used to obtain fibril populations of different sizes. Fibrils were either not sonicated (unsonicated) or sonicated by 15 or 30 cycles. After sonication, samples were centrifuged at 16,000 g for 30 min and soluble (SN) and insoluble (P) fractions were separated. Fibril size was analyzed by TEM (b) and DLS (c). To confirm that sonication did not perturb the chemical or structural properties of fibrils, the different samples obtained were analyzed by ThT and ANS binding (d) and by FT-IR spectroscopy (e). Each sample is color-coded as shown in panel (b).

The different sized fibril preparations were then incubated with chaperones to compare their disaggregation susceptibility. As for type B oligomers, native electrophoresis allowed us to compare both initially soluble and insoluble material as well as to distinguish the disassembly of fibrils into monomeric or oligomeric species. Regardless the size of the fibrils, the human disaggregase mainly generated α-syn monomers (**Figure 4.4 a**) and its disassembly activity inversely correlated with fibril size (**Figure 4.4b**), disaggregating more efficiently shorter fibrils. This observation, together with the fact that chaperones can disassemble α-syn oligomers, suggests a preferential targeting of smaller amyloid aggregates by the human disaggregase.
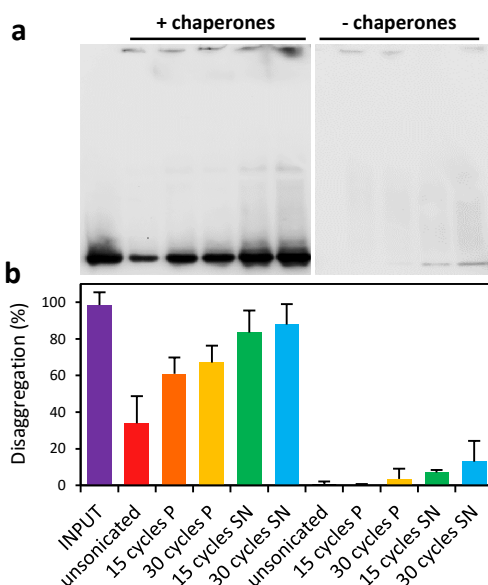
Figure 4.4. Disaggregation of different sized fibrils by the human disaggregase.

2 µM of α-syn fibrils of different lengths were incubated with a 5-fold excess of Hsc70 in the presence of its cochaperones and ATP. Disaggregation reactions after 2h incubation at 30 °C were analyzed by Native-PAGE and immunoblotting (a). Monomeric (INPUT) and fibril solutions in the absence of chaperones were used as controls. Disaggregation (%) was calculated as the relative amount of monomeric α-syn with respect to the INPUT (b).

4.2.4. α-syn aggregates that are better disassembled by chaperones are the most toxic

We then sought to determine if there was a correlation between aggregate toxicity and chaperone targeting. One of the toxicity mechanisms described for α-syn is

cellular membrane disruption (Fusco *et al.*, 2017), which can be mimicked in assays monitoring content release from liposomes. The addition of monomeric α-syn to liposomes produced negligible leakage of encapsulated calcein (**Figure 4.5 a**). Meanwhile, unsonicated fibrils provoked low leakage –around 10% - and their fragmentation into shorter species increased their membrane-disrupting activity in a size-dependent manner, reaching 45% leakage for the shortest ones, similarly to type B oligomers. This membrane disruption activity strongly correlated with the decrease in the viability of human neuroblastoma SH-SY5Y cells (**Figure 4.5 b**). At 0.3 µM α-syn, neither monomers nor unsonicated fibrils affected cell viability, but doubling protein concentration reduced it around 13% for both samples. Nonetheless, we observed an aggregate size-dependent reduction in cell viability upon addition of sonicated fibrils or type B oligomers. The viability values obtained for the shortest fibrils and type B oligomers lowered to 75 and 66% at 0.3 and 0.6 µM α-syn, respectively, in agreement with previous reports (Fusco *et al.*, 2017). Altogether, we show that chaperones disaggregate more efficiently the most toxic aggregation intermediates of α-syn.
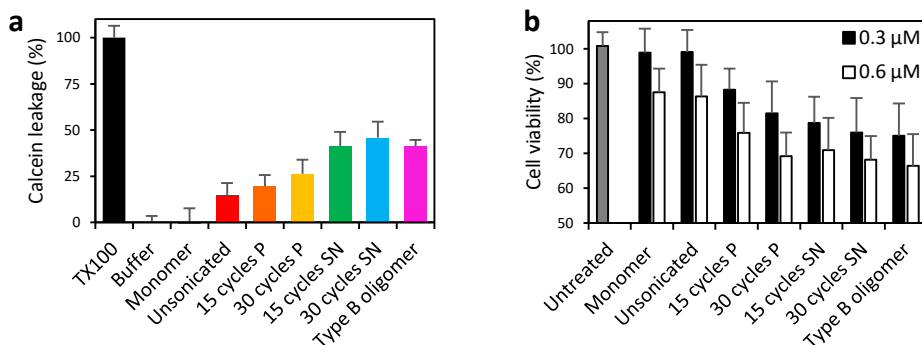
Figure 4.5. Toxicity of the different α-syn aggregates. (a) Liposomes with encapsulated calcein were incubated with different α-syn species (0.8 µM). Calcein release was measured with respect to the total fluorescence signal obtained after complete disruption of LUVs using Triton X-100. (b) The different α-syn species (0.3 or 0.6 µM) were added to a culture of human neuroblastoma SH-SY5Y cells. After 24h incubation, cell viability was measured monitoring mitochondrial activity by the reduction of MTS. Control cells in the absence of α-syn (untreated) are shown in grey.

4.2.5. Disassembly kinetics of α-syn aggregates suggests a one-step mechanism favored by the amyloid structure

To get further insights into the mechanism used by chaperones to disaggregate α-syn amyloids, we monitored the disaggregation kinetics of fibrils and type B oligomers as a fluorescence dequenching process (Cremades *et al.*, 2012; Gao *et al.*, 2015). AlexaFluor488 labeled fibrils (unsonicated and sonicated) and type B oligomers at 2 μM were mixed with different concentrations of the human disaggregase up to 1:2 (α-syn:Hsc70 molar ratio). As we had previously seen, only low disaggregation was obtained for unsonicated fibrils at high chaperone concentrations (**Figure 4.6 a**). In stark contrast, sonicated fibrils (**Figure 4.6 c**) and type B oligomers (**Figure 4.6 e**) were efficiently disaggregated in a dose-dependent manner, reaching maximum disassembly (85-100%) at 1:0.5 α-syn:Hsc70 molar ratio (**Figure 4.6 g**). Native-PAGE analysis of the disaggregation product of the three aggregate species showed that chaperone-mediated disassembly resulted in a major band corresponding to the monomeric protein (**Figure 4.6 b, d, f**). Although some faint bands compatible with low molecular weight oligomers were observed, the absence of larger intermediate species, especially under low disaggregation conditions (i.e. unsonicated fibrils at all chaperone concentration assayed or sonicated fibrils/type B oligomers at low chaperone concentrations) suggested a one-step disassembly mechanism in which monomers are individually extracted from the aggregate (seen on the top of the gels). Indeed, fitting of the disaggregation kinetics of sonicated fibrils and type B oligomers was consistent with a pseudo-first order kinetic model, which allowed us to calculate the disaggregation rate constant (k) at each chaperone concentration. The disaggregation rate for type B oligomers was 3-4 times lower than for sonicated fibrils below 2 μM Hsc70, and only above this concentration, oligomers disassembled faster than fibrils (**Figure 4.6 h**).
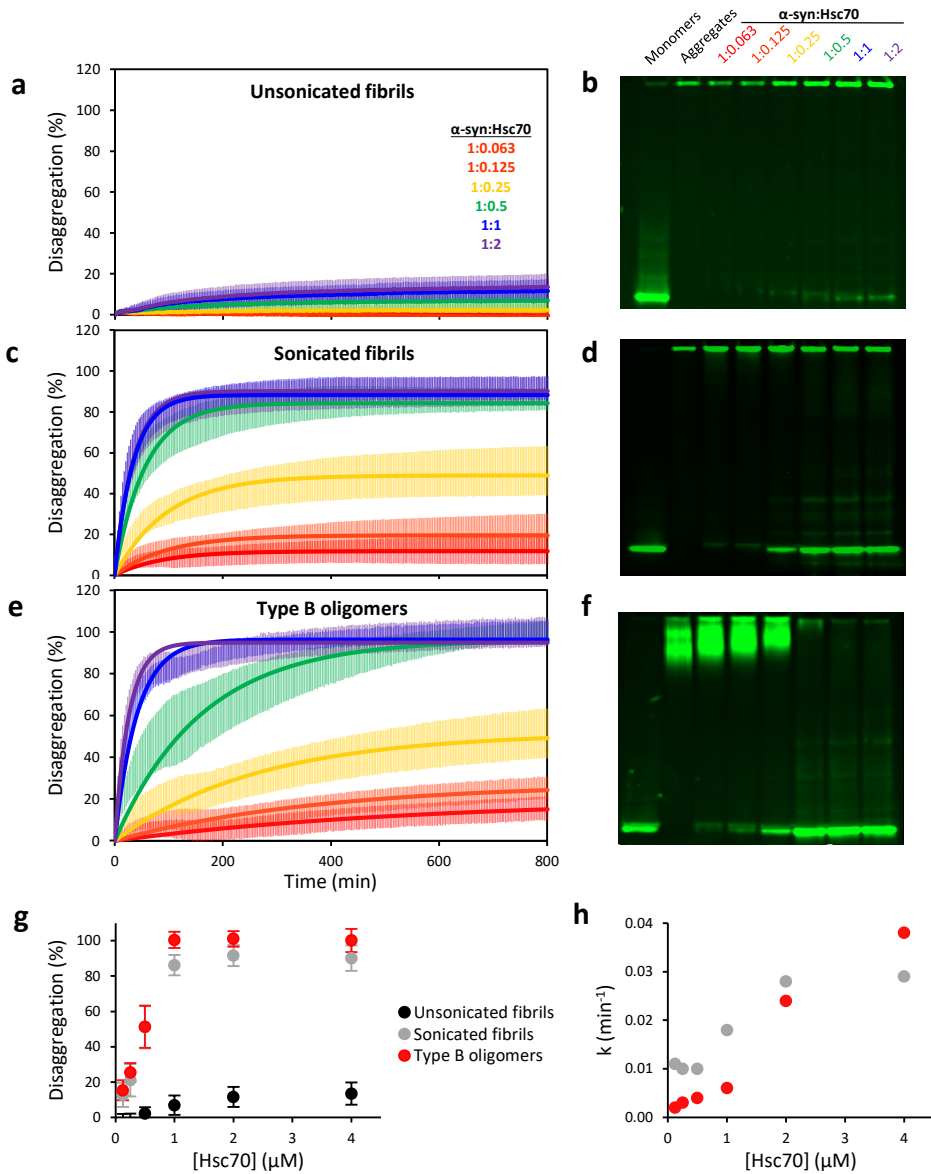
Figure 4.6. Disaggregation kinetics of α-synuclein aggregates. α-syn (2 µM) unsonicated fibrils (a, b), sonicated fibrils (c, d) and type B oligomers (e, f) labeled with alexaFluor488 were disaggregated at different chaperone concentrations with a molar ratio of Hsc70:DnaJB1:Apg2 constant at 1:0.5:0.1. Disaggregation was followed as a fluorescence dequenching process (a, c, e) and at the end of the kinetics, samples were analyzed by Native-PAGE (b, d, f). The final disaggregation percentage was plotted as a function of Hsc70 concentration (g). Disassembly kinetics in (c and e) were fitted to a pseudo-first order function (solid lines) and disaggregation rate constants at each chaperone concentration were calculated (h).

The fact that type B oligomers, which are smaller than sonicated fibrils, showed a slower disaggregation rate at low chaperone concentration seemed to contrast the increased chaperone activity observed as fibril size shortened. Nevertheless, we hypothesized that the higher-ordered organization (i.e. β-sheet content and structural topology) of fibrils in comparison to type B oligomers (Chen *et al.*, 2015), could favor a faster disaggregation rate. To prove this hypothesis, we followed the disaggregation kinetics of amorphous aggregates of G6PDH, a model protein whose chaperone-mediated reactivation has been modeled for the bacterial system composed of the DnaK system (DnaK, DnaJ and GrpE) and the disaggregase ClpB (Fernández-Higuero, Muga and Vilar, 2020).

Fluorescently labeled G6PDH aggregates (2 µM) were titrated with the human disaggregase up to 1:5 (G6PDH:Hsc70) molar ratio (**Figure 4.7 a**). Disaggregation only started to be significant (around 85%) at G6PDH:Hsc70 molar ratio 1:2, at which disaggregation showed a lag phase of approx. 90 min. Further increase in the chaperone concentration resulted in the same final disaggregation percentage with a significant reduction in the lag phase. At the end of the kinetics, samples were analyzed by Native-PAGE visualizing the in-gel fluorescence (**Figure 4.7 b**). As expected, disaggregation efficiency values correlated with the amount of dimeric protein present in the gel. Furthermore, the fact that aggregate reactivation (**Figure 4.7 c, d**) paralleled very well the kinetics of fluorescence dequenching, indicated that the dimeric protein was the active, native conformation. Comparison of these results with those obtained for α-syn, clearly evidenced that the amyloid structure favors chaperone-mediated disaggregation, requiring less chaperone concentration and bypassing the lag phase observed for amorphous aggregates.
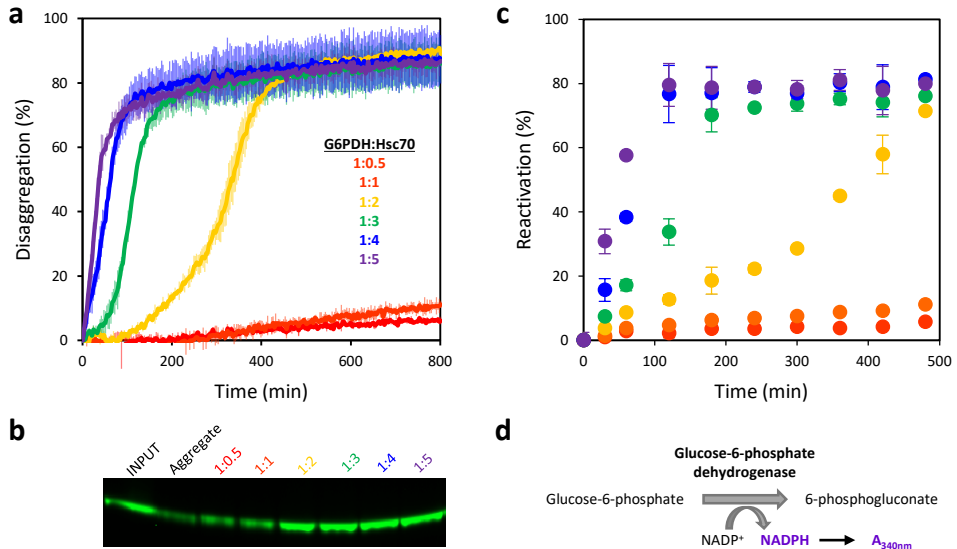
Figure 4.7. Disaggregation kinetics of glucose-6-phosphate dehydrogenase aggregates. Thermally aggregated (50 °C) G6PDH (2 µM) was disaggregated at different concentrations of the ternary chaperone mixture with molar ratios of Hsc70:DnaJB1:Apg2 constant at 1:0.5:0.1. In panel (a), disaggregation was followed as a dequenching process using G6PDH labeled with AlexaFluor488 and at the end of the kinetics, samples were analyzed by Native-PAGE (b). In panel (c), aggregate reactivation kinetics was followed by taking an aliquot at different time points and following the reaction catalyzed by the enzyme (d), monitoring the reduction of NADP$^+$, which produces an absorbance increase at 340 nm.

4.2.6. Chaperone-mediated disaggregation of α-syn fibrils occurs through depolymerization from the fibrils ends

The low disaggregation efficiency of unsonicated fibrils, together with the fact that disaggregation kinetics of type B oligomers and sonicated fibrils fit a one-step mechanism and being monomers the main disassembly product, lead us to the only possible explanation that chaperone-mediated disaggregation primarily entails depolymerization from the aggregate ends. To prove this, we followed the chaperone-mediated disaggregation of α-syn fibrils using high-speed AFM. For that, we placed sonicated fibrils on poly-L-ornithine coated mica and washed the sample

with disaggregation buffer. After an initial visualization time to ensure the stability of the sample, chaperones, ATP and an ATP-regeneration system were added to the chamber (**Figure 4.8 a**). Immediately after chaperone and nucleotide addition, fibrils disaggregation events started to happen, with a total of 42 disaggregation events observed within the first 50 min (**Figure 4.8 d**). No additional disassembly reactions were observed at longer incubation times (80 min) (**Figure 4.8 b**), although a second injection of the same chaperones and ATP concentrations promoted 10 more disaggregation events within 20 min (**Figure 4.8 c, d**).

Analysis of individual disaggregation events revealed that disassembly began at one fibril end and once started, propagated rapidly towards the opposite end, resulting in the complete fibril disaggregation within 4 minutes. Two representative disaggregation events are shown in **Figure 4.8 e** and **f**, recorded during the first and second chaperone injection, respectively. Interestingly, we observed that depolymerization started with an initial unwinding of the fibrils, which peeled and curled as they were disassembled, resulting in a depolymerization process similar to the one described for MTs (Bollinger and Stevens, 2018). We observed that chaperones could destabilize both fibril ends simultaneously, which indicates that fibril depolymerization could start at any of the two fibril ends. Yet, the fast propagation of the disassembly process favors unidirectional disaggregation in most of the cases.

Summing up, we show that the human disaggregase disassembles amyloids through a depolymerization process that starts at the fibril tips. Consequently, chaperone-mediated disassembly relies on the available number of fibril ends, which is reduced in large fibrils (i.e. unsonicated) and increases upon fragmentation. This mechanism explains the low disaggregation efficiencies observed for larger fibrils and the chaperone targeting towards shorter and more toxic aggregate species.
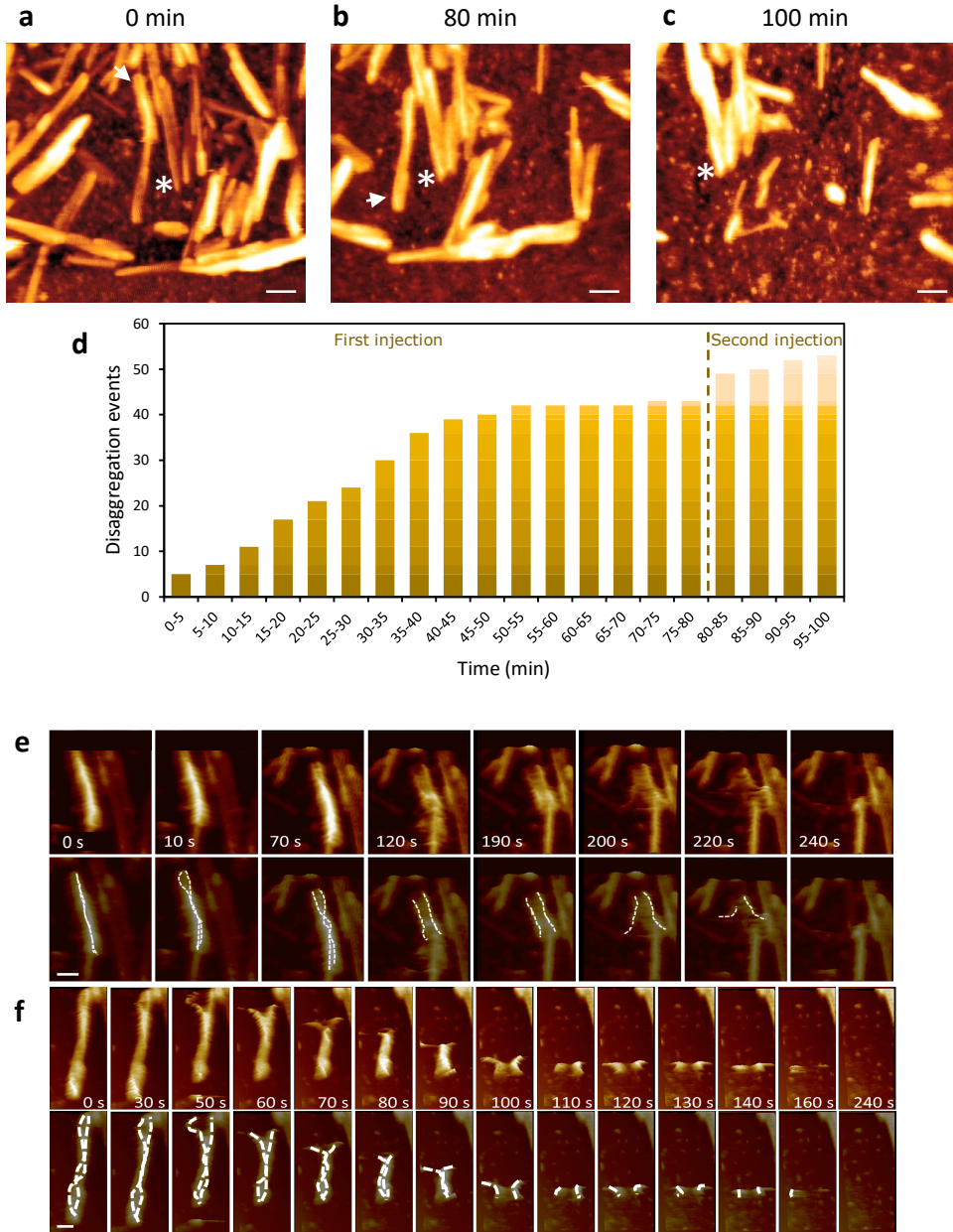
Figure 4.8. Chaperone mediated-disaggregation of α-syn fibrils followed by high-speed AFM. High-speed AFM movie frames of the chaperone-mediated disaggregation of α-syn sonicated fibrils immediately after chaperones, ATP and an ATP-regeneration system were added to the chamber – time 0 – (a) and after 80 min incubation (b). At 80 min, more chaperones were added to the chamber, further scanning until 100 min (c). White asterisk in panels a-c represent the same scan location, which drifted during the measurement. (d) Cumulative disaggregation events were plotted as a function of time (min). Time-resolved

disassembly of fibrils marked with white arrows in panel a (e) and panel b (f), respectively. Scale bar in panels a-c and e-f represents 100 and 40 nm, respectively.

4.2.7. The human disaggregase collaborates with the proteasome in the clearance of α-syn fibrils

A human disaggregase that shows a predominant depolymerization activity suggests that clearance of large amyloid assemblies by this machinery may not be efficient in the cell. Although mature fibrils tend to cluster and form deposits, which reduces inappropriate interactions with cellular components, they can still contribute to toxicity, feeding back aggregation. In yeast, Hsp70 and Hsp40 efficiently disaggregate both amorphous aggregates and amyloids in collaboration with Hsp104 (Desantis *et al.*, 2012; Davis and Sindi, 2016). This member of the AAA+ ATPase family is able to fragment amyloids (Winkler *et al.*, 2012) but metazoan lack of Hsp100 disaggregases. A recent report evidenced that the 26S proteasome was able to fragment α-syn and tau fibrils into toxic oligomeric species (Cliffe *et al.*, 2019). Therefore, we hypothesized that the proteasome and the human disaggregase could collaborate in the clearance of large amyloid assemblies.

To test this hypothesis, we incubated fluorescently labeled unsonicated and sonicated α-syn fibrils with the 26S proteasome holoenzyme (**Figure 4.9 a**). After 22h incubation, chaperones were added to each mixture and after an additional incubation of 16h, they were analyzed by Native-PAGE (**Figure 4.9 b**). Unsonicated fibrils, which were poorly disaggregated by the chaperones alone, increased their disaggregation to 16% after proteasome treatment (**Figure 4.9 c**), confirming that the fragmentation ability of this machinery favors chaperone-mediated disassembly of α-syn fibrils. In addition, proteasome pretreatment of sonicated fibrils also increased chaperone activity (from 39 to 54% of disaggregation) (**Figure 4.9 c**), which could indicate that proteasomes are able to further fragment sonicated fibrils into shorter aggregate spices that are more susceptible to

disaggregation. Importantly, the proteasome action alone on unsonicated or sonicated fibrils did not generate monomeric protein (**Figure 4.9 b**). Although further investigation is needed, this is a promising finding and suggests that the proteasome could compensate for the lack of an Hsp100 homolog in metazoan, fragmenting amyloids and thus, preparing large aggregates for their subsequent disassembly by the human Hsp70-based disaggregase.
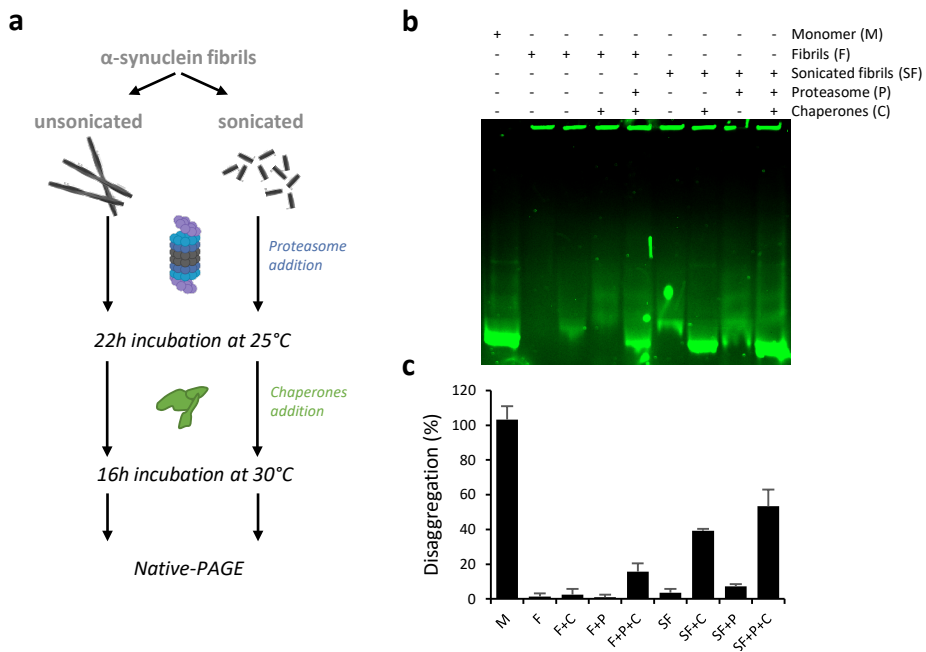
Figure 4.9. Proteasome-pretreatment of α-syn fibrils favors chaperone-mediated disaggregation. (a) Schematic representation of the experimental approach used to test the collaboration between the proteasome and the human disaggregase. Disaggregation was analyzed by Native-PAGE (b) and quantified by the in-gel fluorescence of the band corresponding to the monomeric protein (c).

4.2.8. The aggregate-size dependence activity of the human disaggregase is conserved for tau fibrils

Finally, we wanted to test whether the aggregate-size dependence activity of chaperones observed for α-syn also occurred with other amyloidogenic proteins. We assembled tau fibrils from the recombinant full-length isoform 2N4R (**Figure**

4.10 a, b). After aggregation, two tau fibril populations were produced, unsonicated and sonicated, which showed the expected fibril fragmentation upon sonication as seen by DLS (**Figure 4.10 c**). Then, the human disaggregase was added to each sample and solubilization was analyzed by a sedimentation assay. Chaperones solubilized poorly –around 6%- unsonicated tau fibrils, while disaggregation increased substantially –up to 40%- for the sonicated sample (**Figure 4.10 d**). These preliminary results suggest that the human disaggregase targeting of amyloid intermediates might be conserved among amyloidogenic proteins. Furthermore, considering that the proteasome can fragment tau fibrils (Cliffe *et al.*, 2019), chaperones could also coordinate with this machinery to disassemble tau fibrils.
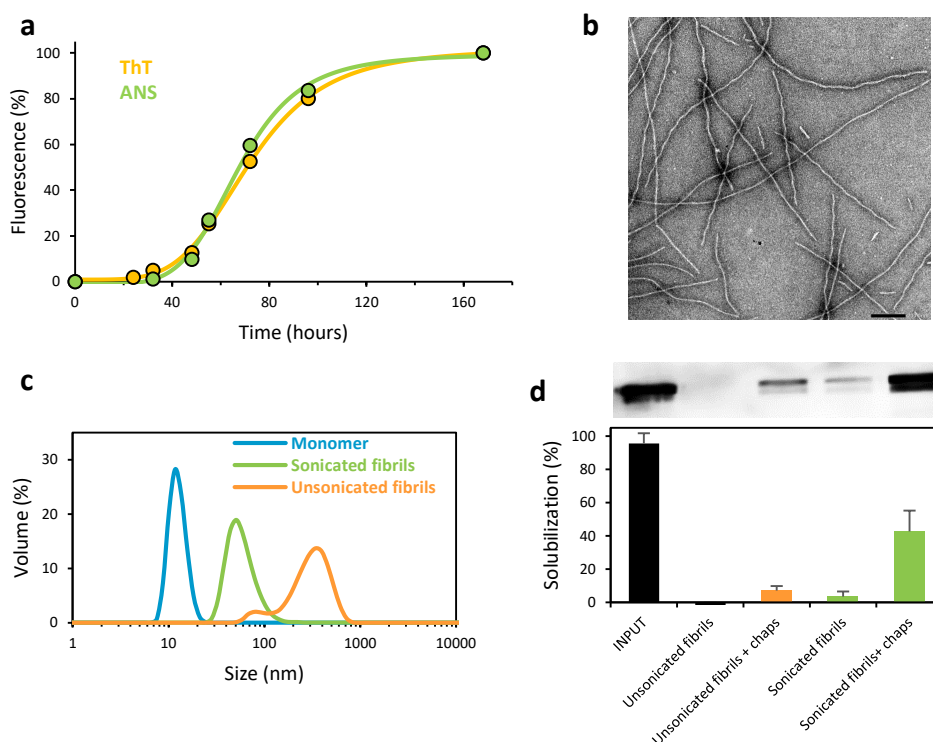
Figure 4.10. The human disaggregase disassembles more efficiently fragmented tau fibrils. (a) Aggregation kinetics of a 40 µM solution of tau 2N4R followed by ThT and ANS fluorescence. At each time point, an aliquot was taken from the reaction, mixed with the fluorophores and the fluorescence of the sample was measured. (b) After 1-week incubation, fibrillar morphology of the aggregates was confirmed by negative-stain EM

(scale bar, 200 nm). (c) DLS-derived size distribution of monomeric and fibrillar (unsonicated and sonicated) tau solutions. (d) Solubilization of tau fibrils (1 µM) by the human disaggregase was analyzed by a sedimentation assay. After 2h incubation at 30°C in the presence of ATP, reaction mixtures were ultracentrifuged and solubilized tau was detected in the supernatant by immunoblotting. Fibrils without chaperones were used as a control. INPUT was made with a 1 µM solution of monomeric tau.

4.3. DISCUSSION

The Hsp70-based chaperone system has been shown to revert α-syn fibrils, although the exact disaggregation mechanism remains unclear, with two proposed models to date (Duennwald, Echeverria and Shorter, 2012; Gao *et al.*, 2015). Both models state that the human disaggregase can depolymerize fibrils, extracting monomers from fibrils ends, whereas one proposes that chaperones can also extract monomers from the center of the fibrils, therefore breaking them into smaller fragments (Gao *et al.*, 2015). Our data supports a model in which fibril disassembly occurs through depolymerization (Duennwald, Echeverria and Shorter, 2012). We show that α-syn fibrils are poorly disassembled by chaperones unless they are mechanically fragmented through sonication, which increases the number of fibril ends. Disassembly of sonicated fibrils yields monomeric α-syn with a very minor population of small oligomers. Indeed, we show that this Hsp70-based machinery can also efficiently disaggregate small toxic oligomeric species of α-syn with the same class B J-protein, DnaJB1. Kinetics analysis of the disassembly of sonicated fibrils and type B oligomers of α-syn could be reasonably explained by a one-step disassembly mechanism, in agreement with a recent study (Schneider *et al.*, 2020), which have also put forward that this chaperone system disaggregates α-syn fibrils through the removal of monomers form fibril ends without intermediate fragmentation steps. Comparison of the disaggregation kinetics of both types of α-syn amyloid intermediates and amorphous aggregates showed that the highly organized structure of amyloids favored chaperone-mediated

disaggregation, requiring less amount of chaperones and bypassing the lag phase seen for amorphous aggregates, which results in the generation of monomer immediately after addition of the chaperones.

Since the amyloid structure can be considered the most stable aggregate state from a thermodynamic point of view, the fact that such architecture could favor chaperone-mediated disaggregation seemed contradictory. Yet, the fibrillar structure of amyloids allows Hsc70 to interact throughout the whole aggregate surface (Gao *et al.*, 2015), binding up to every other protomer in the case of α-syn fibrils (Wentink *et al.*, 2020). This α-syn to Hsc70 stoichiometry is consistent with our disaggregation experiments, which saturates at α-syn:Hsc70 molar ratio of 1:0.5. The DnaJB1-induced ultra-affinity for the amyloid substrate provides the energy required to load Hsc70 in this dense arrangement (Wentink *et al.*, 2020). Crowding of Hsc70 at the fibril surface provokes steric clashes between neighboring Hsc70 molecules, making this conformation energetically unfavorable and thus, exerting entropic pulling forces on Hsc70-bound α-syn molecules (Wentink *et al.*, 2020). Furthermore, the high molecular mass of Apg2 impedes the shuffling of crowded Hsc70 molecules, biasing NEF activity to those that are not densely packed on the fibrils (Wentink *et al.*, 2020). Therefore, we rationalize that Apg2 starts disassembly at the fibril ends, where the excluded volume effect of Hsc70 molecules is the lowest. Time-resolved AFM clearly shows that depolymerization starts at the fibril tips and propagates fast through the fibril longitudinal axis. The images captured during the solubilization process display a "ram's horns" motif that resemble those described for depolymerization of microtubules (Bollinger and Stevens, 2018). Microtubule depolymerization requires uncapping of the plus end filament aided by a conformational change of tubulin, which leads to a catastrophically fast process (Bollinger and Stevens, 2018). Similarly, our data suggest that after destabilization of any of the fibril ends by the action of the human disaggregase, the depolymerization process rapidly propagates towards the

opposite end. Such a fast propagation could be due to the unfavorable dense packing of Hsc70 molecules along the fibril longitudinal axis, which would be rapidly released in a concatenated way by the action of Apg2 at the fibril ends. The "ram´s horns" motif observed during depolymerization suggest unzipping of the twisted filaments that build the fibril, which could further help in monomer extraction.

Fibril fragmentation increases the number of ends and thus, the likelihood of starting a depolymerization process. Within α-syn fibrils, each monomer establishes intra- and inter-protofilament interactions with neighboring monomers (Guerrero-Ferreira *et al.*, 2018, 2019; Li, Ge, *et al.*, 2018; Li, Zhao, *et al.*, 2018; Boyer *et al.*, 2019, 2020; Ni *et al.*, 2019; Schweighauser et al., 2020; Sun *et al.*, 2020). Monomers located at the end of the fibril lack half of these interactions and thus, their extraction is energetically less demanding. This, together with the fact that Apg2 is sterically excluded from the fibril center due to Hsc70 crowding (Wentink *et al.*, 2020), lead us to the conclusion that fibril fragmentation by chaperones may not be favorable. Nonetheless, a previous report showed that within a few minutes after chaperone addition, there was a fibril shortening that was attributed to fragmentation (Gao *et al.*, 2015). Our results show that this observation is compatible with a fast depolimerization-only mechanism, whose propagation may be interrupted eventually when fibrils are too long (i.e. unsonicated), for which the probability of kinks, interfibril contacts or other defects increases, rendering monomers and shorter fibrils without altering the number of fibrils ends. Endorsing this hypothesis, no fragmentation was observed when the same chaperone complex disaggregated tau fibrils (Nachman *et al.*, 2020), which was further corroborated with our results showing that chaperone activity was only significant after mechanical fragmentation of tau fibrils. Fragmentation of amyloids has classically been attributed to yeast Hsp104 (Winkler *et al.*, 2012), a member of the AAA+ ATPase Hsp100 disaggregases with no homologs in metazoan. A recent report showed that large fibrils assembled from α-syn and tau are substrates of the 26S

proteasome holoenzyme, which fragments them into small aggregates (Cliffe *et al.*, 2019). We show that pretreatment of α-syn fibrils with the proteasome enhances chaperone disassembly activity, suggesting that clearance of amyloids could potentially be accomplished with the coordinated collaboration of both proteostasis machineries.

An important aspect to decipher the consequences of the Hsp70-based amyloid disassembly activity in neurodegeneration is to consider the toxicity of the disaggregation products. The initial *in vitro* observations indicated that α-syn disaggregation could be beneficial and cytoprotective since fibrillar α-syn was eventually dissolved into non-toxic monomers (Gao *et al.*, 2015). Furthermore, altering the human disaggregase activity can have beneficial effects on α-syn aggregation in cell culture and animal models (Taguchi *et al.*, 2019; Tittelmeier *et al.*, 2020). Our data also demonstrate that this beneficial effect is expected as the human disaggregase efficiently solubilizes toxic α-syn oligomers into monomers. Nevertheless, it has also been reported that the chaperone-mediated disaggregation process could also generate spreading-competent oligomeric species that may serve as a template for further aggregation (Nachman *et al.*, 2020; Tittelmeier *et al.*, 2020). We show herein that a Hsp70 machinery only able of depolymerizing could be crucial to avoid the formation of new aggregation intermediates, which are the most cytotoxic species. As pointed out by Tittelmeier et al. (Tittelmeier *et al.*, 2020), the final outcome could depend on the state of the protein quality control network, which declines with aging and disease. The high proteostasis capacity characteristic of healthy or young organisms could ensure fast disaggregation of toxic amyloids, including oligomers and small fibrils, reducing their lifetime and thus, their negative effect in the cell. In contrast, in sick or old individuals the proteostasis capacity gets progressively impaired due to a reduction in the chaperones available to process toxic aggregates, which transiently

accumulate, inducing cell-death and spreading from cell to cell (Tittelmeier *et al.*, 2020).

CHAPTER

5

PHYSIOLOGICAL C-TERMINAL TRUNCATION OF α-SYNUCLEIN BLOCKS DISAGGREGATION BY THE HSP70-BASED CHAPERONE MACHINERY

5.1. INTRODUCTION

A plethora of PTMs, including phosphorylation, ubiquitination, nitration, O-GlcNAcylation and truncation, seem to play a key role in α-syn pathogenesis (Zhang, Li and Li, 2019). Truncation is one of the predominant modifications of α-syn. Both N-terminally and C-terminally truncated α-syn species have been found in the brain of healthy and diseased individuals (Li *et al.*, 2005; Muntané and Ferrer, 2012; Kellie *et al.*, 2014; Bhattacharjee *et al.*, 2019). By epitope mapping and/or mass spectroscopy (MS), confirmed truncated forms of α-syn include those starting at residues 5, 10, 18, 19, and 68 (N-truncations) and those cleaved after residues 103, 110, 113, 114, 115, 119, 122, 124, 125, 133, and 135 (C-truncations) (Sorrentino and Giasson, 2020). Interestingly, many of these truncations are enriched within the insoluble fraction of diseased brain lysates compared to healthy controls, pointing to an important role of truncation in disease pathogenesis (Baba *et al.*, 1998; Li *et al.*, 2005; Anderson *et al.*, 2006; Kellie *et al.*, 2014).

Intracellular protein degradation relies on two major pathways: the autophagy-lysosomal pathways and the ubiquitin-proteasome system. Through both pathways, proteins confront proteases that aim for partial or full degradation

of substrates. Depending on the protease and the assembly state of α-syn (monomeric, oligomeric or fibrillar), several truncated forms are produced. Among lysosomal proteases, cathepsin D (CstD) is able to C-truncate both monomeric and fibrillar α-syn; cathepsin B (CtsB) degrades monomers but only truncate fibrils; while cathepsin L (CtsL) can fully degrade all forms of α-syn (Sorrentino and Giasson, 2020). The cytosolic protease calpain-1 cleaves monomeric α-syn at its N-terminus and NAC region and fibrillized α-syn predominantly at the C-terminus (Mishizen-eberz *et al.*, 2003). Monomeric α-syn is also processed by the 20S proteasome and caspase I, both cleaving at the protein´s C-terminus (Liu *et al.*, 2005; Wang *et al.*, 2016; Ma *et al.*, 2018). Other proteases that contribute to α-syn truncation include the lysosomal protease asparagine endopeptidase (AEP) and extracellular proteases such as neurosin/kallikrein-6, matrix metalloproteases 1 and 3 (MMP1 and MMP3) and plasmin (Sorrentino and Giasson, 2020). The combined action of these proteases results in the formation of numerous truncated forms at different stages of the aggregation process.

Although it has been shown that truncation strongly influences α-syn aggregation and prion-like pathogenicity (Liu *et al.*, 2005; Terada *et al.*, 2018; Gallardo, Escalona-Noguero and Sot, 2020), very little is known about the effect of this PTM on aggregate clearance. Fibrils of a truncated mutant of α-syn lacking the N- and C-terminus (α-syn$_{30\text{-}110}$) are not disassembled by the Hsc70/DnaJB1/Apg2 machinery (Gao *et al.*, 2015). This behavior was explained assuming that the N-and/or C-terminal parts of the α-syn molecule might provide a specific binding platform for the functional formation of the composite Hsc70/DnaJB1/Apg2 machinery. In this chapter, we sought to deepen the effect of α-syn truncation on chaperone-mediated disaggregation, which could have implications in aggregate clearance and thus, in pathogenesis.

5.2. RESULTS

5.2.1. Effect of α-syn N- and C-terminal truncation on chaperone activity

Recent studies have determined the cryo-EM structure of recombinantly produced α-syn fibrils (Guerrero-Ferreira *et al.*, 2018; Li, Ge, *et al.*, 2018; Li, Zhao, *et al.*, 2018; Ni *et al.*, 2019). In these 3D reconstructions, both N- and C-terminal ends are not visible, indicating a high degree of flexibility due to their predicted intrinsically disordered structure (**Figure 5.1 a**). NMR data and limited proteolysis proved these terminal residues to be solvent-exposed and unprotected in nature (Vilar *et al.*, 2008). The structural model of a full-length α-syn fibril based on NMR data shows that these disordered terminal tails surround the structured core of the fibril (Tuttle et al. 2016; **Figure 6.1 b**).

To understand the importance of these unstructured regions in chaperone-mediated fibril disaggregation, we generated two mutants, lacking either the first 29 N-terminal residues (α-syn$_{30-140}$) or the last 30 C-terminal amino acids (α-syn$_{1-110}$). After one week of aggregation, amyloid fibrils of WT and both mutants were subjected to sonication as fibril fragmentation facilitates an efficient chaperone-mediated disaggregation (**Chapter 4**). Sonicated fibrils were then incubated with the human disaggregase, a chaperone mixture composed of Hsc70 and its cochaperones DnaJB1 and Apg2, in the presence of ATP and an ATP-regeneration system. Reaction products were fractionated in a density-gradient centrifugation and analyzed by immunoblotting (**Figure 5.1 c**). As expected, sonicated fibrils were detected in fractions of higher density in the absence of chaperones. After incubation with chaperones, α-syn$_{WT}$ and α-syn$_{30-140}$ were also detected in fractions 1-3, confirming their disassembly into soluble monomers. Conversely, α-syn$_{1-110}$ was mainly detected in fraction 9, indicating that this truncation mutant was not susceptible to disaggregation.
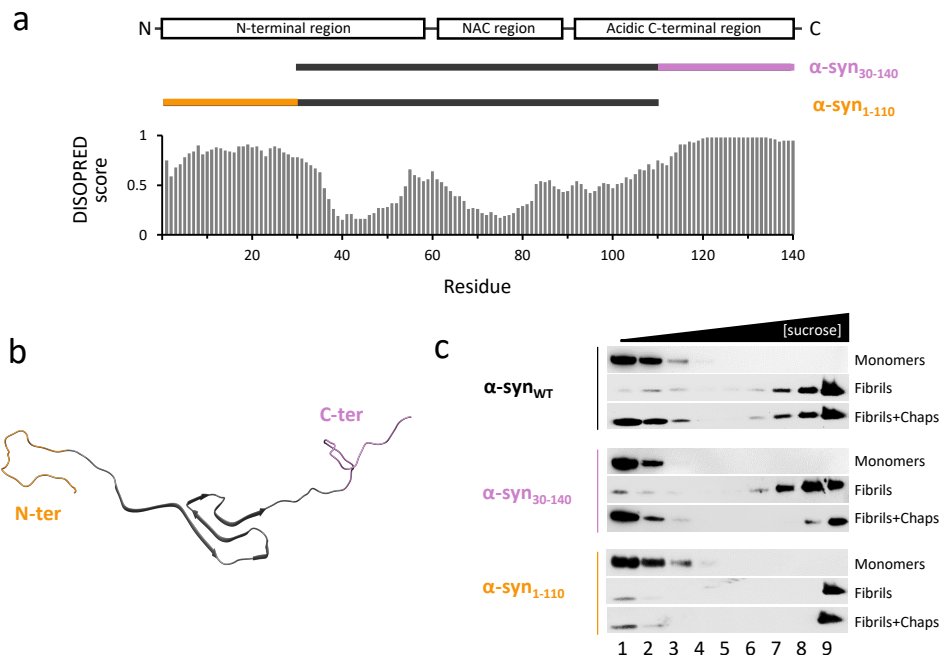
Figure 5.1. Truncation of the last 30 residues of α-syn blocks fibril disaggregation by chaperones. (a) Full-length α-syn and truncation mutants sequence scheme laid out on a disorder prediction obtained with DISOPRED3 software (0=ordered, 1= disordered). (b) Structural model of an α-syn monomer within a fibril determined by solid-state nuclear magnetic resonance (PDB: 2N0A). N- (orange) and C- (violet) truncated terminal residues are colored in the structure. (c) Fibrils disaggregation of full-length and truncated mutants of α-syn analyzed by sucrose-gradient fractionation. Reactions of 10 μM α-syn monomers, sonicated fibrils, or sonicated fibrils incubated with 10 μM Hsc70, 5 μM DnaJB1 and 1 μM Apg2 for 2.5 h, were loaded on a 5-40% sucrose-gradient and ultracentrifuged. Fractions were analyzed by SDS-PAGE and immunoblotting.

Disaggregation of fibrils requires binding of the three chaperone components to the fibrils (Gao *et al.*, 2015). Both N- and C-terminal residues have been proven important for the interaction of different heat shock proteins with monomeric α-syn (Burmann *et al.*, 2019; Jia *et al.*, 2019). Hsc70 binds α-syn preferentially through its N-terminus (Burmann *et al.*, 2019) while DnaJB1 binds to its C-terminal domain (Jia *et al.*, 2019). As DnaJB1 is the first chaperone that binds to fibrils, coating the

surface and recruiting Hsc70 to the aggregate, we first thought that binding of DnaJB1 to α-syn$_{1-110}$ could be impaired. Chaperone-substrate interaction is commonly assayed by testing the chaperone´s ability to prevent aggregation of the substrate. Hsp70 prevents aggregate formation by interacting with prefibrillar aggregates (i.e. seeds) blocking elongation, rather than interacting with monomers (Dedmon, Christodoulou, Wilsonʈ, *et al.*, 2005; Huang *et al.*, 2006; Arosio *et al.*, 2016; Aprile *et al.*, 2017). This mechanism seems to be extended to members of the Hsp40 family (Månsson *et al.*, 2014; Arosio *et al.*, 2016; Kakkar *et al.*, 2016; Månsson, van Cruchten, *et al.*, 2018). Therefore, we followed the increase in ThT fluorescence of self-seeded α-syn in the absence and presence of each of the three components of the human disaggregase system at 10:1 (α-syn/chaperone) molar ratio. Although aggregation of both truncation mutants and the full-length protein occurred in different time-scales, it was delayed for the three variants in the presence of any of the chaperones (**Figure 5.2 a**). Interestingly, DnaJB1 inhibited aggregation of α-syn$_{1-110}$, discarding binding impairment when the C-terminus is lacking.

We then sought to determine whether the DnaJB1-mediated recruitment of Hsc70 to α-syn$_{1-110}$ fibrils was compromised. Through a co-sedimentation assay, we saw that Hsc70 bound poorly to WT fibrils in the absence of DnaJB1 and that cochaperone addition increased 12-fold the amount of fibril-bound chaperone (**Figure 5.2 b and c**). Further addition of Apg2 slightly improved Hsc70 binding, following a comparable association pattern seen for amorphous aggregates (Cabrera *et al.*, 2019). A similar Hsc70 recruitment in the absence and presence of cochaperones was observed for the α-syn variants lacking either of the terminal regions. Altogether, these data indicate that disaggregation of α-syn$_{1-110}$ fibrils by chaperones is blocked, even though chaperone interaction with the aggregated substrate is not deficient.
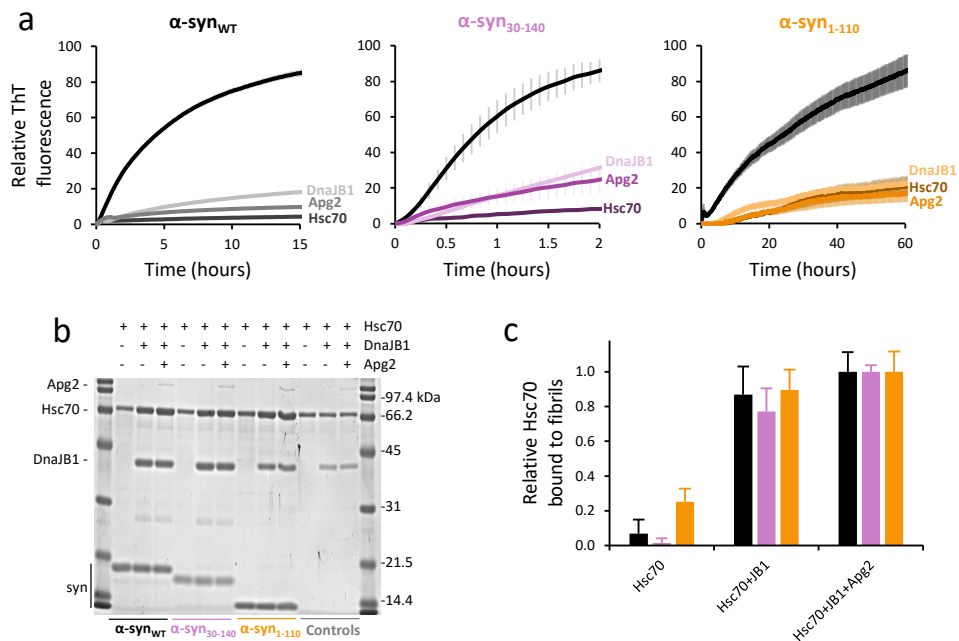
Figure 5.2. Chaperones interact similarly with WT and N- or C-terminally truncated α-syn fibrils. (a) Aggregation of self-seeded α-syn (full-length or truncation mutants) followed by the increase in ThT fluorescence in the absence and presence of each of the three components of the human disaggregase system at 10:1 (α-syn:chaperone) molar ratio. (b) Co-sedimentation of 2 μM α-syn fibrils (full-length or truncation mutants) and Hsc70 (2 μM) in the presence of DnaJB1 (1 μM) alone or in combination of Apg2 (0.2 μM). As controls, the same chaperone mixtures were analyzed in the absence of fibrils. (c) The relative amount of Hsc70 bound to fibrils in the absence and presence of cochaperones was quantified by densitometry.

5.2.2. α-syn fibrils lacking the C-terminal residues render more stable structures due to lateral association

The formation of a different aggregate structure due to C-terminal truncation could explain the difficulty of chaperones to disaggregate α-syn$_{1-110}$ fibrils. Indeed, it has been recently described that a C-terminal truncated mutant of α-syn (α-syn$_{1-108}$) forms amyloid fibrils with a distinct structure and morphology (Iyer *et al.*, 2017). In this deletion mutant, the canonical circular dichroism spectrum of amyloid fibrils with a broad minimum at 218 nm and a positive maximum at 200 nm were red-

shifted, a behavior we replicate with the α-syn$_{1-110}$ mutant and not with α-syn$_{30-140}$ (**Figure 5.3 a**). This red-shift has been associated with strongly twisted β-sheets (Iyer *et al.*, 2017), in good agreement with recent cryo-EM structural data indicating that fibril helical twist increased upon removal of C-terminal residues (Ni *et al.*, 2019). In this report, deletion of C-terminal residues correlated with an increased stability as seen by limited proteolysis experiments with proteinase K. In our case, α-syn$_{WT}$ and α-syn$_{30-140}$ show a similar proteinase K digestion pattern, with most of the full-length protein degraded within 30 min (**Figure 5.3 b**). In contrast, the α-syn$_{1-110}$ band persisted even after 2h, highlighting its increased stability against proteolysis. We further checked the resistance of the three variant fibrils to GdnHCl denaturation by ThT fluorescence (**Figure 5.3 c**). Fibrils of α-syn$_{30-140}$ showed a significantly lower resistance to chemical denaturation compared to α-syn$_{WT}$ and α-syn$_{1-110}$ fibrils. Between these two variants, α-syn$_{1-110}$ fibrils showed an increased resistance compared to α-syn$_{WT}$, with EC$_{50}$ values of 0.75 M and 0.61 M respectively. This minor increase suggests a more compact structure for fibrils of the deletion variant which could explain, at least partially, the observed differences in disaggregation.

One consequence of the increased stability of α-syn$_{1-110}$ fibrils could be the reduction of fibril fragmentation upon sonication, which in turn would diminish the chaperone-mediated disaggregation. To test this possibility, we analyzed the effect of sonication on fibrils of the three protein species by DLS (**Figure 5.3 d**). Sonication of both α-syn$_{WT}$ and α-syn$_{30-140}$ fibrils reduced fibril length from microns to hundreds of nanometers, whereas barely diminished the size of α-syn$_{1-110}$ fibrils. Electron microscopy analysis of these samples showed that unlike syn$_{WT}$ and α-syn$_{30-140}$ fibrils which were shown as disperse/individual fibrils with rod-like morphologies, α-syn$_{1-110}$ fibrils seemed to associate laterally and clump together into suprafibrillar morphologies (**Figure 5.3 e**), a behavior previously described for fibrils of the α-syn$_{1-108}$ mutant (Semerdzhiev *et al.*, 2014; Iyer *et al.*, 2017). After sonication, the three
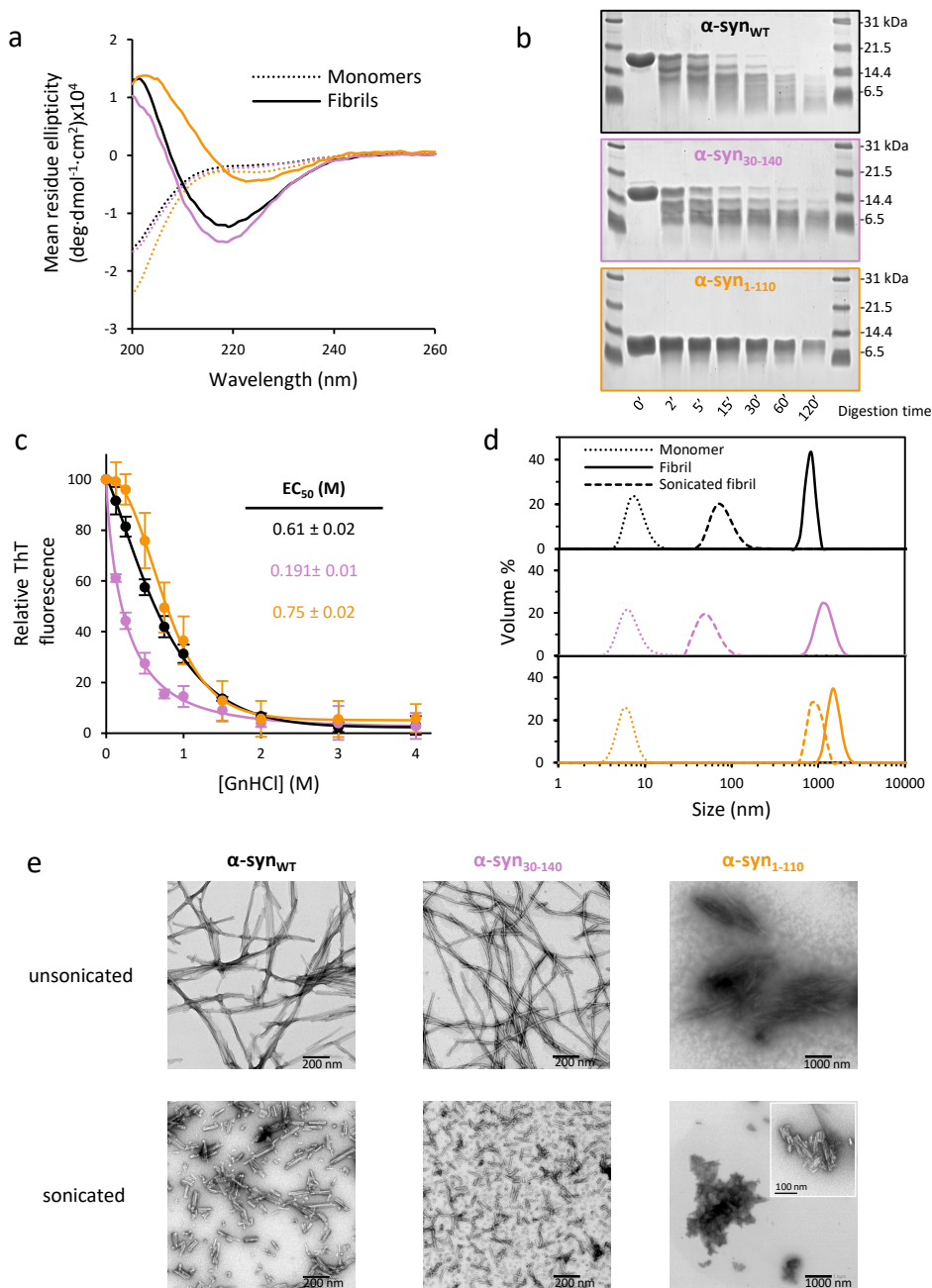
Figure 5.3. Truncation of the last 30 residues of α-syn increases fibril stability and lateral association. The secondary structure of monomeric and fibrillar species of α-syn$_{WT}$ and truncated mutants was compared by Far-UV CD (a). The stability of the fibrils obtained with each variant was analyzed by Proteinase-K digestion (b), GdnHCl chemical denaturation (c), and fragmentation susceptibility upon sonication as seen by DLS (d) and EM (e).

variants showed fragmentation into shorter fibrils but in the case of α-syn$_{1-110}$ mutant, fragments clumped together into large structures. This behavior suggests that disaggregation failure could be due to the assembly of these stable structures driven by the lateral association.

To understand the structural basis of the stability of α-syn$_{1-110}$ fibrils and the formation of suprafibrillar assemblies, we performed cross-seeding experiments with α-syn$_{WT}$ and α-syn$_{1-110}$. We aggregated monomeric α-syn$_{WT}$ with α-syn$_{WT}$ or α-syn$_{1-110}$ seeds (mWTsWT and mWTs1-110, respectively) and monomeric α-syn$_{1-110}$ with α-syn$_{WT}$ or α-syn$_{1-110}$ seeds (m1-110sWT and m1-110s1-110, respectively). The resulting fibrils were analyzed by FT-IR spectroscopy (**Figure 5.4 a**). Self-seeded samples showed spectra similar to those obtained for non-seeded α-syn$_{WT}$ and α-syn$_{1-108}$, with a broader low-frequency amide-I peak for 1-110s1-110 (Iyer *et al.*, 2017). Comparison with the spectra of cross-seeded samples revealed that seeds imposed their structural characteristics, a behavior widely established (Goedert, Masuda-Suzukake and Falcon, 2017). Then, we explored the behavior of cross-seeded samples upon sonication by DLS (**Figure 5.4 b**). Self-seeded samples behaved as the unseeded ones (**Figure 5.3 d**). Intriguingly, size distribution of sonicated cross-seeded fibrils did not correlate with the structural data shown above. mWTs1-110 fibrils, which resemble α-syn$_{1-110}$ in terms of secondary structure, showed a reduction in size after sonication whereas m1-110sWT, with a WT-like secondary structure, did not. Electron microscopy of both samples, before and after sonication, confirmed DLS data and showed that mWTs1-110 fibrils appeared dispersed in contrast to m1-110sWT, which formed suprafibrillar structures even after fragmentation (**Figure 5.4 c**), similarly to pure α-syn$_{1-110}$ fibrils. Sonicated cross-seeded fibrils were then incubated with chaperones to test their susceptibility to disaggregation (**Figure 5.4 d**). mWTs1-110 fibrils were disaggregated, yielding soluble monomeric α-syn at the top of the density gradient, while m1-110sWT fibrils were not susceptible to disaggregation. Altogether, our

data indicate that the lateral association of fibrils is not determined by their secondary structure but depends on the absence of the C-terminus. In addition, the formation of such assemblies correlates with a reduced chaperone disaggregase activity.
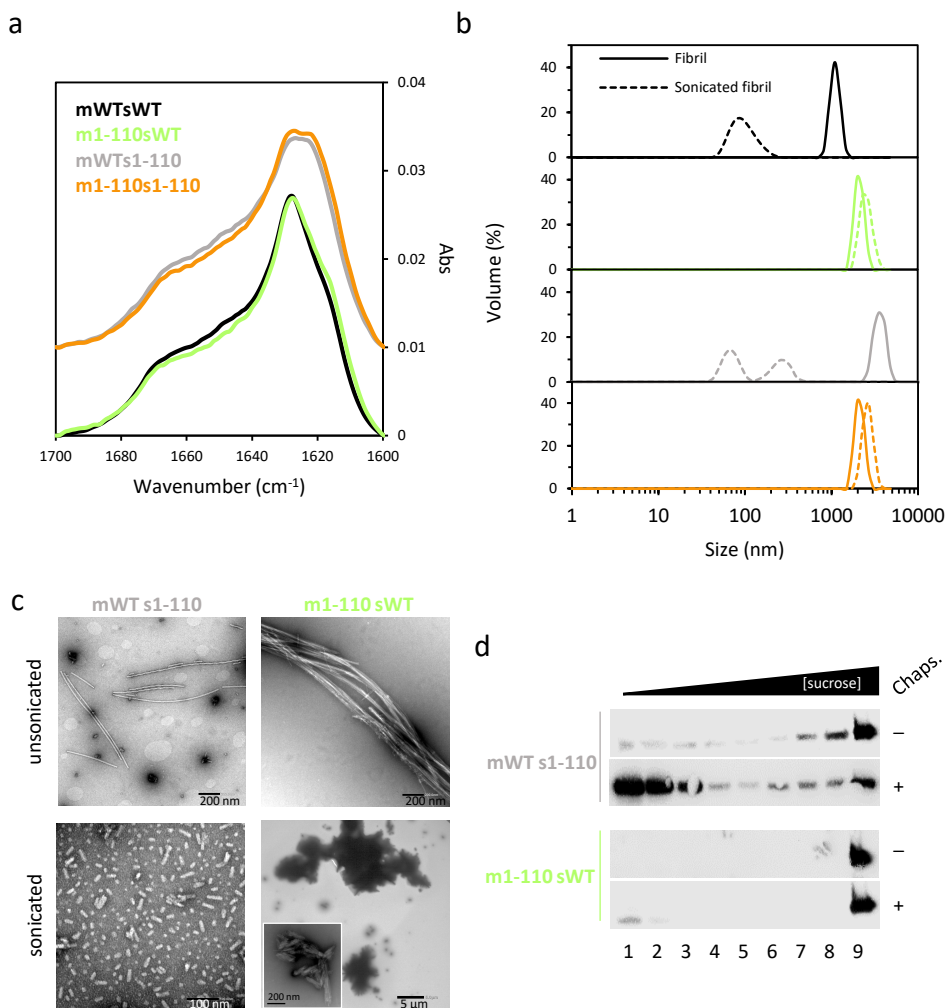
Figure 5.4. The absence of the C-terminal domain induces the formation of stable suprafibrilar assemblies with low disaggregation susceptibility. (a) Fibrils produced with monomeric α-syn$_{WT}$ with α-syn$_{WT}$ (mWTsWT) or α-syn$_{1-110}$ (mWT s1-110) seeds, and monomeric α-syn$_{1-110}$ with α-syn$_{1-110}$ (m1-110s1-110) or α-syn$_{WT}$ (m1-110sWT) seeds were analyzed by FT-IR spectroscopy. Unsonicated and sonicated samples were then analyzed by

DLS (b) and EM (c). Sonicated cross-seeded fibrils were mixed with the human disaggregase and their disassembly susceptibility was analyzed by a sucrose-gradient separation (d).

5.2.3. The disaggregase activity of chaperones decreases with the length of the region deleted at C-terminus of α-syn

The C-terminal domain of α-syn is a highly acidic region (**Figure 5.5 a**), which under physiological conditions can be cleaved at different positions by several proteases (**Figure 5.5 b**). In this context, we sought to determine the region of this domain that could be deleted without affecting the solubilizing activity of chaperones. To this aim, we compared the conformational properties and chaperone-mediated disaggregation of α-syn$_{WT}$ and α-syn$_{1-110}$ with those of other two physiologically relevant truncation mutants, α-syn$_{1-122}$ and α-syn$_{1-133}$. The differential FT-IR spectra (**Figure 5.5 c, bottom panel**) obtained after subtracting the IR spectrum of each truncated mutant from that of the WT protein (**Figure 5.5 c, upper panel**) showed a progressive structural conversion from the α-syn$_{WT}$ to the α-syn$_{1-110}$ conformation as the length of the region deleted increased. The first conformation change occurred upon deletion of the last 7 residues (α-syn$_{1-133}$), and was evidenced by a slight broadening of the main amide I band component, which was better seen as a positive band at 1620 cm^{-1} in the difference spectrum. Further deletion of 18 and 30 residues induced a second conformational transition that was characterized by a stronger broadening of the β-sheet spectral region, which in the difference spectra resulted in an increase in the intensity of the 1620 cm^{-1} band, and the appearance of the following differential features: a positive band at around 1635 cm^{-1} and two negative bands at 1650 and 1674 cm^{-1}. These spectral features have been assigned to different types of β-structures (1620 and 1625 cm^{-1}) and to α-helix (1650 cm^{-1}) and turns (1674 cm^{-1}) (Arrondo *et al.*, 1993). Therefore, these data suggest that the main structural rearrangement of α-syn starts upon deletion of the last 18 residues at its C-terminal region, and is compatible with an increase in the heterogeneity of its β-structure, with the concomitant decrease in turns and helical

conformations. EM images of unsonicated α-syn$_{1-133}$ and α-syn$_{1-122}$ fibrils showed that both truncation mutants displayed increased lateral association compared to α-syn$_{WT}$ (**Figure 5.5 d**). Upon sonication, fibrils of both mutants were fragmented but tended to cluster together, forming clumps of fragmented fibrils similar to those seen for α-syn$_{1-110}$. Sonicated fibrils of these two mutants were then incubated with chaperones and disaggregation was followed by a sucrose-gradient fractionation (**Figure 5.5 e**). Monomeric α-syn appeared at the top of the gradient, showing that fibrils of both mutants were susceptible to disaggregation. These data indicate that although the lateral association is increased for fibrils of these two partially truncated mutants, the interfibrillar interactions may not be strong enough to block chaperone activity and further C-terminal cleavage is needed to fully abolish it.

The qualitative analysis of the disaggregase activity of the chaperone mixture by WB precluded a straight comparison of the different α-syn deletion variants. Therefore, we resorted to fluorescence dequenching measurements to compare the chaperone-induced disaggregation kinetics of these samples. To generate fluorescently labeled fibrils, monomers of each C-terminal truncation mutant were aggregated in the presence of AlexaFluor488 labeled α-syn$_{Q24C}$ monomers and seeds of α-syn$_{WT}$. The resulting hybrid fibrils contained 85:10:5 (molar percentage) of truncated mutant:α-syn$_{Q24C-488}$:α-syn$_{WT}$ seeds (**Figure 5.6 a**). Immediately after sonication (day 0), the different fibril preparations were mixed with the human disaggregase and their disassembly was followed as a fluorescence dequenching process. Compared to α-syn$_{WT}$, we saw a gradual reduction of the final disaggregation efficiency as more of the C-terminal domain was truncated (**Figure 5.6 b**). Intriguingly, hybrid fibrils formed with the α-syn$_{1-110}$ mutant showed a final disaggregation as high as 70%, contrasting with the results obtained for fibrils entirely composed of this mutant (**Figure 5.1 c**). This may be explained by the presence of the whole C-terminal domain in 15% of the molecules that form hybrid
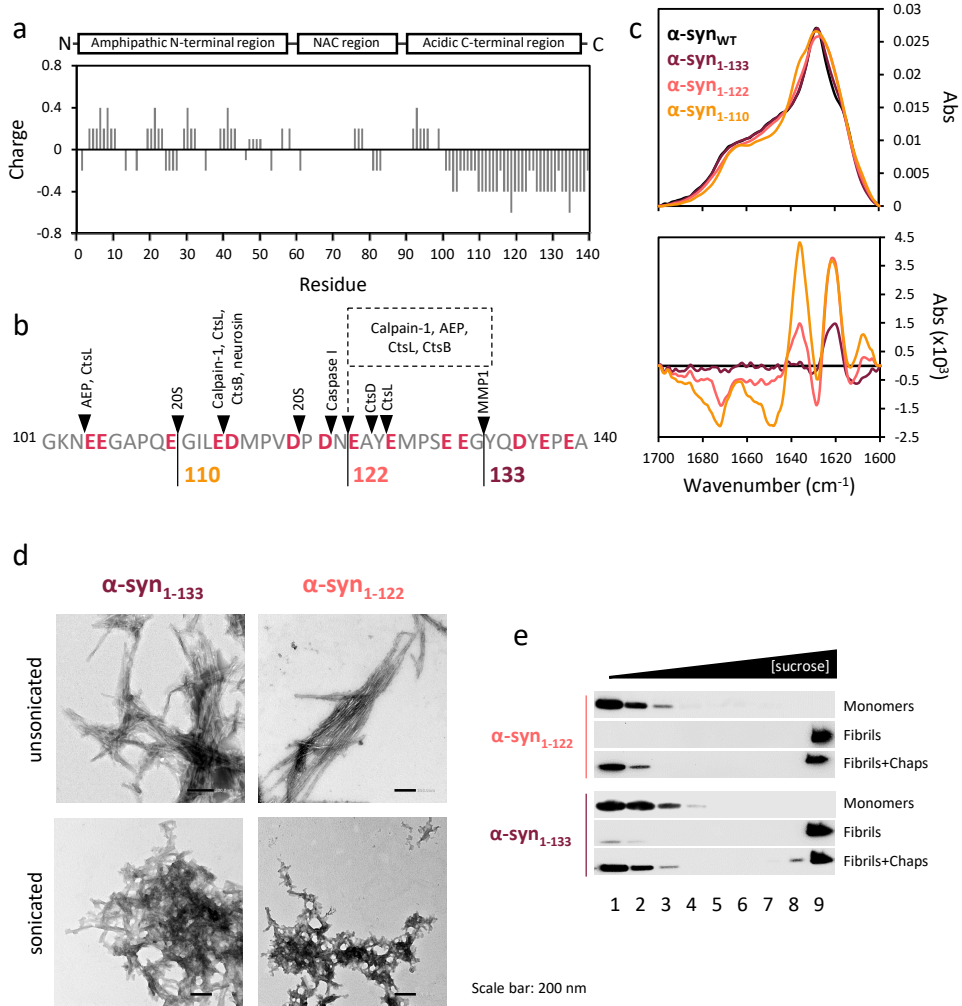
Figure 5.5. Effect of physiologically relevant C-terminal truncations on fibril organization and chaperone-mediated disaggregation. (a) Charge distribution of α-syn showing a concentration of negatively charged amino acids at its C-terminus. (b) Cleavage sites described for different proteases at the C-terminal region are marked with black arrows and negatively charged residues are highlighted in red. The three terminal truncation mutants analyzed in this work are marked and color-coded as in the next panels. (c) Original (upper panel) and differential (bottom panel) FT-IR spectra of α-syn variants. The differential ones were obtained after subtracting the spectrum of each variant from that of α-syn$_{WT}$. (d) Unsonicated and sonicated α-syn$_{1-122}$ and α-syn$_{1-133}$ fibrils were analyzed by EM. (e) Sonicated samples were mixed with the human disaggregase to check their disassembly susceptibility. Disaggregation reactions were analyzed by sucrose-gradient fractionation followed by SDS-PAGE and immunoblotting of the fractions.

fibrils, which maybe enough to reduce interfibril associations through electrostatic repulsion. Interestingly, the difference in disaggregation between α-syn$_{WT}$ and truncated mutants increased with the incubation time of the sonicated fibrils at room temperature (**Figure 5.6 b)**. Four days after sonication, the efficiency of the human disaggregase to solubilize hybrid fibrils formed with α-syn$_{1-133}$ showed a small (around 13%) reduction, as also found for α-syn$_{WT}$, whereas the decrease observed for fibrils made of α-syn$_{1-122}$ and α-syn$_{1-110}$ mutants was significantly stronger, being disaggregation almost abolished for the latter after 1-day incubation (**Figure 5.6 b and c**). We hypothesize that unlike α-syn$_{1-110}$ pure fibrils, which rapidly cluster together after sonication, the presence of a minor population (15%) of α-syn molecules with an intact C-terminal domain in the hybrid fibrils, could slow down the fibril rearrangement that modulate chaperone-mediated disaggregation. Summing up, we show that progressive deletion of the C-terminus results in a gradual decrease in the ability of chaperones to disaggregate α-syn fibrils. This behavior is explained due to the reduction in the number of negative charges present in the C-terminus, which in turn promotes fibril lateral association as previously reported (Semerdzhiev *et al.*, 2014; Mahul-Mellier *et al.*, 2018; van der Wateren *et al.*, 2018).

5.2.4. Disaggregation of calpain-cleaved α-syn fibrils

Physiological C-terminal truncation of α-syn renders heterogeneous aggregate populations, with varying amounts of uncleaved and cleaved protomers at different sites. In this context, we decided to cleave α-syn$_{WT}$ fibrils *in vitro* with calpain-1. This cytosolic protease hydrolyzes monomeric α-syn at different sites located in the N-terminal and NAC regions, but primarily cleaves fibrillized α-syn at the C-terminal domain (Mishizen-eberz *et al.*, 2003). We confirmed these results (**Figure 5.7 a**), obtaining two main fragments after digestion of α-syn fibrils, previously identified as α-syn$_{1-122}$ and α-syn$_{1-114}$ (Mishizen-eberz *et al.*, 2003). Increasing concentrations
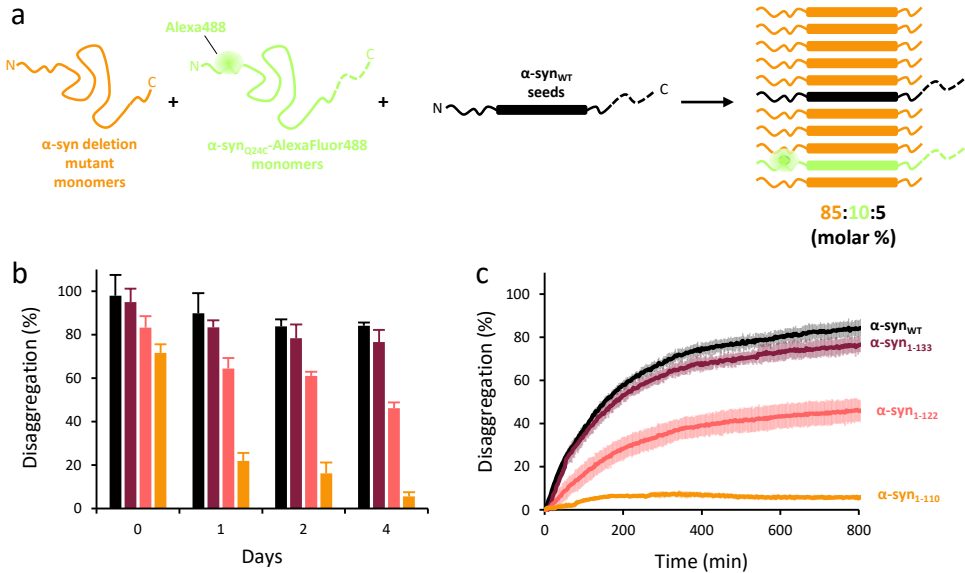
Figure 5.6. Chaperone-mediated disaggregation is gradually reduced as truncation of α-syn C-terminal domain increases. (a) Hybrid fibrils preparation scheme. (b) Disaggregation percentage of the different hybrid fibril preparations (2 μM) after 800 min incubation with chaperones at a α-syn:Hsc70 1:1 molar ratio. Chaperones were added the same day of fibril purification and sonication (day 0) or after incubating the fibrils at room temperature 1, 2 and 4 days. (c) Disaggregation kinetics of hybrid fibrils incubated for 4 days after sonication.

of calpain-1 resulted in an augmented generation of the low molecular mass forms. Interestingly, fibril digestion with the highest calpain-1 concentration (13.50 ng/μL) did not change the secondary structure of the sample as seen by Far-UV CD (**Figure 5.7 b**), showing that the structural integrity of the sample was maintained. However, calpain-digested fibrils did not show the size particle reduction upon sonication (**Figure 5.7 c**) previously seen for α-syn$_{WT}$ (**Figure 5.3 d**). TEM of digested fibrils confirmed an increased lateral association of the sample, with more bunches of fibrils instead of dispersed ones seen for undigested fibrils (**Figure 5.3 e**). Then, we wondered whether calpain-digestion could also trigger lateral association on sonicated fibrils. For that, we first sonicated α-syn$_{WT}$ fibrils and subsequently, cleaved them with calpain-1. DLS measurement of the sample showed an increase in particle size after cleavage from nanometers to microns (**Figure 5.7 c**). TEM of

the sample showed that proteolysis triggered the clumping of sonicated fibrils into larger particles, instead of the dispersed fibril fragments previously seen with the undigested sample (**Figure 5.3 d**).
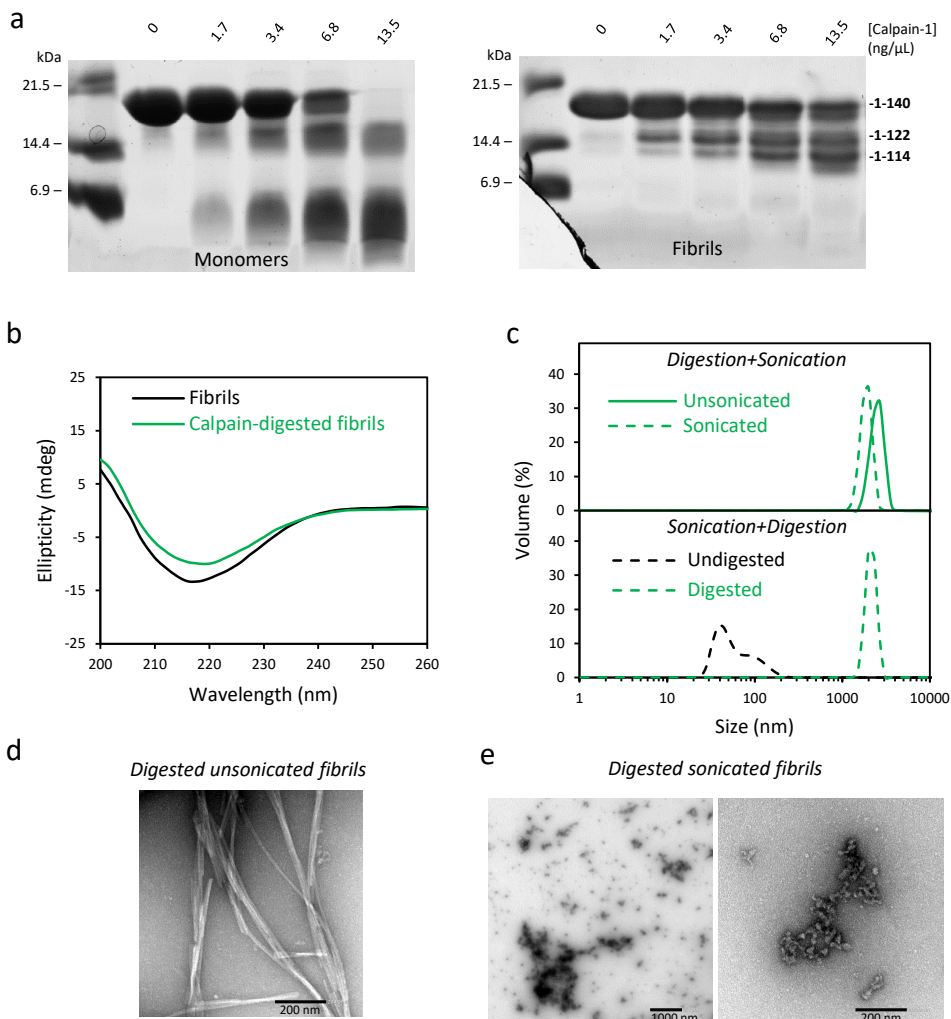
Figure 5.7. Cleavage of α-synWT fibrils with calpain-1 induces their lateral association. (a) Monomeric (left panel) or fibrillar (right panel) α-syn was incubated at 37°C for 10 min in the absence or presence of different calpain-1 concentrations and the samples were analyzed by SDS-PAGE. (b) FarUV CD spectra of undigested and calpain-digested α-syn fibrils. (c) Size distribution measured by DLS of unsonicated and sonicated calpain-1 digested fibrils (upper panel) or undigested and digested sonicated fibrils (lower panel). (d,e) TEM images of calpain-digested unsonicated (d) and sonicated (e) fibrils. In panels b, c, d and e protease concentration was 13.50 ng/μL.

Next, we checked the effect of calpain-1 cleavage on chaperone-mediated disaggregation. For that purpose, fluorescently labeled α-syn fibrils were sonicated and incubated with increasing amounts of calpain-1, rendering samples with a different proportion of full-length and truncated bands (**Figure 5.8 a**). Importantly, in-gel fluorescence visualization showed that the two main fragments contained the AlexaFluor488 fluorophore, located in the N-terminal domain, confirming that cleavage occurred at the C-terminus. Chaperone-mediated disaggregation kinetics
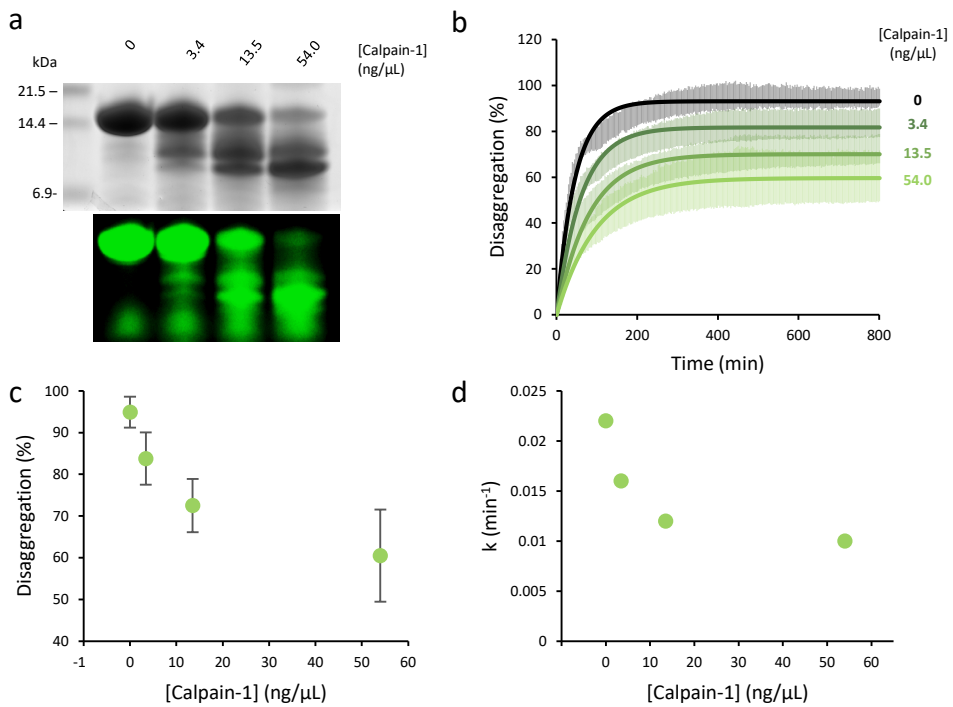
Figure 5.8. Calpain-cleavage of α-synuclein fibrils reduces chaperone-mediated disaggregation. (a) Sonicated α-syn fibrils were incubated at 37°C for 10 min in the absence or presence of different calpain-1 concentrations. Then, after 2h incubation with a calpain-1 inhibitor (SJA6017), samples were analyzed by SDS-PAGE. Gel was visualized by coomassie blue staining (upper panel) or in-gel fluorescence of AlexaFluor488 in a VersadocMP. (b) Alternatively, samples (2 μM final concentration) were mixed with chaperones (1:0.5 α-syn:Hsc70 molar ratio) and their disaggregation kinetics were followed by means of fluorescence dequenching. Solid lines represent the fitting of the process with a pseudo-first order model, which was used to determine the final disaggregation efficiency (c) and disaggregation rate constant (d) as a function of calpain-1 concentration.

of the different samples was followed as a fluorescence dequenching process (**Figure 5.8 b**). As the relative proportion of the C-terminal truncation fragments increased with calpain-1 concentration, the disassembly activity of the human disaggregase was reduced (**Figure 5.8 c**), which correlated with a reduction of the disaggregation rate constant (**Figure 5.8 d**). Such a reduction confirmed the results obtained with the recombinantly produced truncation mutants and points towards physiological C-terminal truncation of α-syn as a key pathological event that could impair aggregate clearance.

5.2.5. C-terminal truncation impairs disaggregation of α-syn oligomers

It is now widely accepted that the most toxic species of α-syn are soluble oligomers generated during the early steps of the self-assembly process. In this context, we also wanted to know if the C-terminal truncation of such species could also hamper the disaggregase activity of chaperones. To this aim, type B oligomers of the three C-terminal truncated mutants were obtained by lyophilization and their size and conformational characteristics were studied. The CD spectra of oligomers of the C-terminal truncated mutants showed the characteristic β-sheet minimum at 218 nm, with a loss of ellipticity that became especially evident upon deletion of the last 18 residues (**Figure 5.9 a**). This behavior was similar to that described for fibrils (**Figure 5.3 a**) and indicates that type B oligomers of the shorter truncated mutants adopt a different secondary structure compared to WT. Upon C-terminal truncation, type B oligomers showed a gradual increase in the particle size as seen by DLS (**Figure 5.9 b**), suggesting an increased tendency to laterally associate. TEM confirmed DLS measurements and showed that as the C-terminus shortens, more cylinder-like particles are able to associate (**Figure 5.9 c**).

Chaperone-mediated disaggregation of type B oligomers of the four different protein variants was studied by a sucrose-gradient fractionation. As expected, in the absence of chaperones they appeared in intermediate fractions of the gradient

(**Figure 5.9 d**). Upon chaperone addition, α-syn$_{WT}$ was fully disaggregated and moved as monomers to the top of the gradient. In the case of the truncated variants, the disaggregase activity was progressively reduced as the length of the deleted fragment increased. Interestingly, this reduction was accompanied by an increase in the amount of protein at the bottom of the gradient, which may indicate an increase in size upon chaperone binding. This was confirmed by comparing the fraction-distribution of chaperones in disaggregation mixtures of α-syn$_{WT}$ and α-syn$_{1-122}$, which showed an increased proportion of DnaJB1 and Hsc70 in the heaviest fractions for the truncated mutant (**Figure 5.9 e**). Therefore, we conclude that the C-truncation of α-syn also hampers chaperone-disassembly activity towards toxic oligomeric α-syn species by favoring lateral association. Albeit this, chaperones are still able to bind C-truncated oligomers and generate larger species. This behavior could potentially neutralize hydrophobic patches on oligomers surfaces and reduce their diffusional mobility, counteracting their toxic effect.

5.3. DISCUSSION

The Hsp70-based chaperone machinery constitutes a powerful ATP-dependent amyloid disaggregase, which efficiently disassembles α-syn fibrils (Duennwald, Echeverria and Shorter, 2012; Gao *et al.*, 2015). α-syn fibrils lacking the flexible and protruding N- and C-terminal regions are not disassembled by this chaperone machinery (Gao *et al.*, 2015). This behavior was explained considering that both terminal ends of the α-syn molecule provide a specific binding platform for the formation of the functional Hsc70/DnaJB1/Apg2 complex. Our results indicate that deletion of neither the N-terminus nor the C-terminus affects sequential chaperone binding to fibrils, in agreement with recently published data (Wentink *et al.*, 2020). This observation was staggering, as N- and C-terminal residues have been proven important in complex stabilization of monomeric α-syn with Hsc70 and DnaJB1, respectively (Burmann *et al.*, 2019; Jia *et al.*, 2019; Wentink *et al.*, 2020). Neverthe-
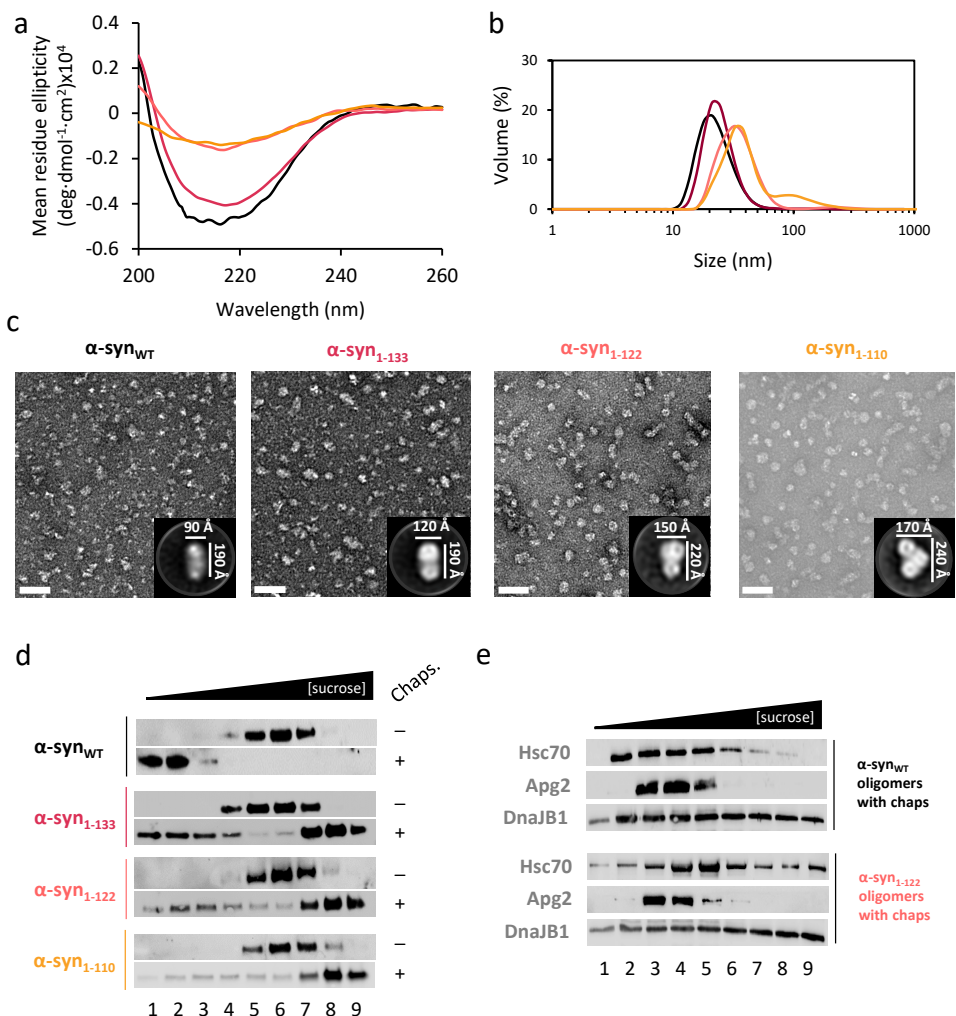
Figure 5.9. Effect of α-syn C-terminal truncation on the structure and chaperone-induced disaggregation of type B oligomers. Far-UV CD spectra (a) and DLS-derived size distribution (b) of type B oligomers of WT and C-terminal deletion mutants of α-syn. (c) Particle morphology and interoligomer associations were determined by TEM, scale bar 500 nm. (d) Type B oligomers of the different variants were mixed with the human disaggregase and their disassembly was analyzed by a sucrose-gradient fractionation (d). In the case of α-syn$_{WT}$ and α-syn$_{1-122}$, the same reactions were also analyzed with antibodies against each chaperone component of the human disaggregase (e).

less, this result may indicate that chaperones might rely on different mechanisms to bind distinct assemblies of α-syn. Regarding disaggregation, fibrils lacking the N-

terminal region were efficiently processed by the chaperone machinery while deletion at the C-terminal drastically impaired the activity of the disaggregase complex, in agreement with a recent work (Wentink *et al.*, 2020).

α-syn C-terminal truncation enhances aggregation and neurodegeneration *in vivo* (Michell *et al.*, 2007; Periquet *et al.*, 2007; Ulusoy *et al.*, 2010). Levels of truncated variants of α-syn can account for up to 15-25% of the total α-syn, being enriched in Lewy-Body insoluble fractions from cases of α-synucleinopathy (Li *et al.*, 2005). Insolubility of these variants increases as more of the C-terminal region is truncated (Li *et al.*, 2005) and correlates with their enhanced aggregation propensity found *in vitro* (Sot *et al.*, 2017; Ma *et al.*, 2018; Sorrentino *et al.*, 2018; Terada *et al.*, 2018). It has been suggested a protective role of the charges at the C-terminus via long-range intramolecular interactions, which are disrupted upon truncation favoring aggregation (Murray *et al.*, 2003; Hoyer *et al.*, 2004; Izawa *et al.*, 2012; Levitan *et al.*, 2012; Gallardo, Escalona-Noguero and Sot, 2020). C-terminal charges also seem to play an important role after fibril formation, generating an interfibrillar electrostatic repulsion. Deletion of the C-terminal region abrogates these long-range repulsive interactions promoting lateral interfibrillar associations into higher-organized suprafibrillar aggregates (Semerdzhiev *et al.*, 2014; Iyer *et al.*, 2017; Mahul-Mellier *et al.*, 2018; van der Wateren *et al.*, 2018). We show herein that such aggregates pose a challenge for chaperones. The high efficiency of the human disaggregase to disassemble fibrils relies on the rapid concatenated extraction of monomers from fibrils ends (**Chapter 4**). We rationalize that the enhanced tendency to laterally associate observed in fibrils lacking the C-terminus could slow down or even block the disassembly process. This is evidenced by the gradual reduction in fibril disaggregation as the length of the C-terminus decreases, which correlates with an increased lateral association of fibrils. Additionally, our results with oligomeric α-syn species of truncated mutants suggest that C-terminal cleavage at early stages of the amyloid formation may also contribute to pathogenesis, reducing the disassembly activity of chaperones.

Similar to fibrils, C-truncated oligomers display a structural rearrangement and associate laterally, which inhibits their chaperone-mediated disassembly. Interestingly, chaperone binding to C-truncated oligomers results in the formation of larger species. This mechanism has been observed for other chaperones (Behrends *et al.*, 2006; Ojha *et al.*, 2011; Mannini *et al.*, 2012) and might be a way of neutralizing the toxic effect of these oligomers when disaggregation is hampered.

The loss of chaperone activity to disassemble C-truncated species may be linked to their enhanced propensity to deposit *in vivo*. Several reports point towards C-terminal truncation as a master regulator of α-syn inclusion formation (Mahul-Mellier *et al.*, 2018, 2020). Different forms of α-syn in nigral LBs and LNs show an onion skin-like architecture, with a structured framework of α-syn phosphorylated at Ser129 and neurofilaments, encapsulating a core of C-terminally truncated α-syn (Prasad *et al.*, 2012; Moors *et al.*, 2018). Within this core, α-syn species with a larger deletion at the C-terminus tend to be located more in the center (Moors *et al.*, 2018). α-syn inclusions have the ability to recruit α-syn monomers through a prion-like process termed conformational templating (Goedert, Masuda-Suzukake and Falcon, 2017). In this regard, C-terminal truncated aggregates have been shown to seed aggregation of α-syn$_{WT}$, increasing pathogenesis (Li *et al.*, 2005; Sorrentino *et al.*, 2018, 2020; Terada *et al.*, 2018). We show that although α-syn$_{1-110}$ can seed aggregation of α-syn$_{WT}$ transferring its secondary structure, chaperones are able to disaggregate these cross-seeded fibrils. Ongoing research establishes that post-fibrillization C-terminal truncation mediated by calpains 1 and 2 plays critical roles in regulating α-syn seeding, fibrillization and orchestrates many of the events associated with LB formation and maturation (Mahul-Mellier *et al.*, 2018; Mahul-Mellier, 2020). We show that cleavage of α-syn$_{WT}$ fibrils with calpain-1 results in an increase of lateral association

accompanied by a reduction of the chaperone activity. Thus, a deficient chaperone activity could be implicated in the formation of inclusions.

Summing up, we suggest that in the cell, clearance of C-terminally truncated α-syn aggregates through pathways that require monomer extraction by chaperones such as the ubiquitin-proteasome system (Hjerpe *et al.*, 2016) may be impaired. We show that binding of chaperones to C-terminally truncated aggregates is unaffected, making it possible to clear them through ALPs, which are able to handle multimeric assemblies through chaperone delivering (Schneider and Cuervo, 2013) or macroautophagy (Maday, 2016; Kulkarni and Maday, 2018). Yet, aggregate abundance could be excessive for only one type of clearance pathway, leading to deposition, which could feedback aggregation by seeding and/or sequestration of components of the protein homeostasis network (Olzscha *et al.*, 2011).

CHAPTER

6

IMPACT OF AMYLOID POLYMORPHISM ON CHAPERONE-MEDIATED DISAGGREGATION

6.1. INTRODUCTION

Most NDs are characterized by variations in the time course, clinical presentation and neuropathology among patients with the same disorder. This behavior has been attributed to the intrinsic property of amyloids referred to as polymorphism, which occurs when a single amyloidogenic peptide/protein assembles into multiple molecular structures (Tycko, 2015). Recent near-atomic characterization of amyloid filaments from patient-derived material strongly supports this theory and suggests that each ND has its own unique amyloid fibril structural signature that could potentially be linked to the clinical phenotype (Fitzpatrick and Saibil, 2019). These findings explain why proteins like α-syn and tau are related to different NDs, collectively known as synucleinopathies and tauopathies, respectively. Different tau polymorphs have been associated with Alzheimer´s disease, Pick´s disease, corticobasal degeneration and chronic traumatic encephalopathy (Fitzpatrick *et al.*, 2017; Falcon *et al.*, 2018, 2019; Zhang *et al.*, 2020). Similarly, distinct structures of α-syn have been found in patients with multiple system atrophy or dementia with Lewy bodies (Schweighauser et al., 2020). This behavior is not exclusive of these two proteins, indeed it had been previously described for other amyloidogenic proteins like PrP (Rossi, Baiardi and Parchi, 2019) or amyloid-β (Paravastu *et al.*, 2008; Lu *et al.*, 2013; Qiang *et al.*, 2017), and highlights the complexity of the pathogenesis derived from amyloids.

Different amyloid polymorphs can differ in the cell types they affect and their cytotoxicity, which may translate into different molecular and clinical phenotypes (Scheckel and Aguzzi, 2018). In addition, their propagation might be different, with distinct rates of spontaneous nucleation, elongation, fragmentation, and secondary nucleation (Tycko, 2015). In terms of structure, the number of protofilaments forming amyloid fibrils, as well as their organization (protofilament interface and orientation, twist-degree between protofilaments), are major determinants of polymorph formation (Adamcik and Mezzenga, 2018). Within each protofilament, variability comes from the number of β-strands and the identities of the residues that compose them, the type of β-sheets (parallel versus antiparallel intermolecular alignment), the nature of the interactions between β-sheet layers or the conformations of non-β strand segments (Tycko, 2015). In the case of tau, some β-strands seem to be conserved and constitute the building blocks of different disease-associated polymorphs (Zhang *et al.*, 2020).

Molecular structures within amyloid fibrils formed *in vitro* are determined by the amino acid sequence of the amyloid-forming peptide/protein and the growth conditions. α-syn is a clear example of this relationship, as aggregation under different conditions, including different ionic strengths and pHs or in the presence of lipid vesicles, can give rise to a variety of fibrils polymorphs (Bousset *et al.*, 2013; Gath *et al.*, 2014; Makky *et al.*, 2016; Roeters *et al.*, 2017; Li, Ge, *et al.*, 2018; Guerrero-Ferreira *et al.*, 2019; Meade, Williams and Mason, 2020). Other factors that contribute to α-syn fibril structure variety include point-mutations identified in families with a history of PD [E46K (Guerrero-Ferreira *et al.*, 2019; Boyer *et al.*, 2020; Zhao, Li, *et al.*, 2020), H50Q (Boyer *et al.*, 2019), A53T (Sun *et al.*, 2020)] and PTMs such as N-terminal acetylation (Guerrero-Ferreira *et al.*, 2019; Ni *et al.*, 2019), phosphorylation at S129 (Guerrero-Ferreira *et al.*, 2019) or T39 (Zhao, Lim, *et al.*, 2020) or C-terminal truncation (Ni *et al.*, 2019). This structural fibril diversity due to PTMs has also been found *in vivo* for tau and has been proposed as a major

contributor to the variety of tauopathy strains found in human brain tissue (Arakhamia *et al.*, 2020).

In this chapter, we aim to challenge the human disaggregase with different polymorphs of α-syn obtained under different aggregation conditions. Furthermore, we want to determine the effect of the structural change on α-syn and tau fibrils induced by point-mutations associated with NDs in the human disaggregase activity.

6.2. RESULTS

6.2.1. Chaperone-mediated disaggregation of α-synuclein ribbons

One of the most studied α-syn fibril polymorphs is that obtained in the absence of salt, commonly referred to as ribbons (Bousset *et al.*, 2013; Roeters *et al.*, 2017). Comparison of fibrils and ribbons have shown that both polymorphs have different structures, levels of toxicity, and *in vitro* and *in vivo* seeding and propagation properties (Bousset *et al.*, 2013). In this context, we wanted to explore the ability of the human disaggregase to disassemble this type of α-syn aggregate. For that, we aggregated α-syn in the absence of salt, obtaining dispersed and long rod-like structures as seen by EM (**Figure 6.1 a**). Far-UV CD showed that ribbons had a comparable β-sheet content to fibrils (**Figure 6.1 b**), in agreement with previous studies (Bousset *et al.*, 2013). One of the main characteristics of ribbons is their increased susceptibility to limited proteolysis by proteinase K. We confirmed this behavior in our ribbon sample, being most of the band of full-length α-syn degraded within the first 5 min and enduring up to 30 min in the case of fibrils (**Figure 6.1 c**).

Considering that chaperones disaggregate more efficiently fragmented fibrils (**Chapter 4**), we sonicated the sample and confirmed that ribbons were susceptible to fragmentation, observing a decrease from microns to hundreds of nanometers
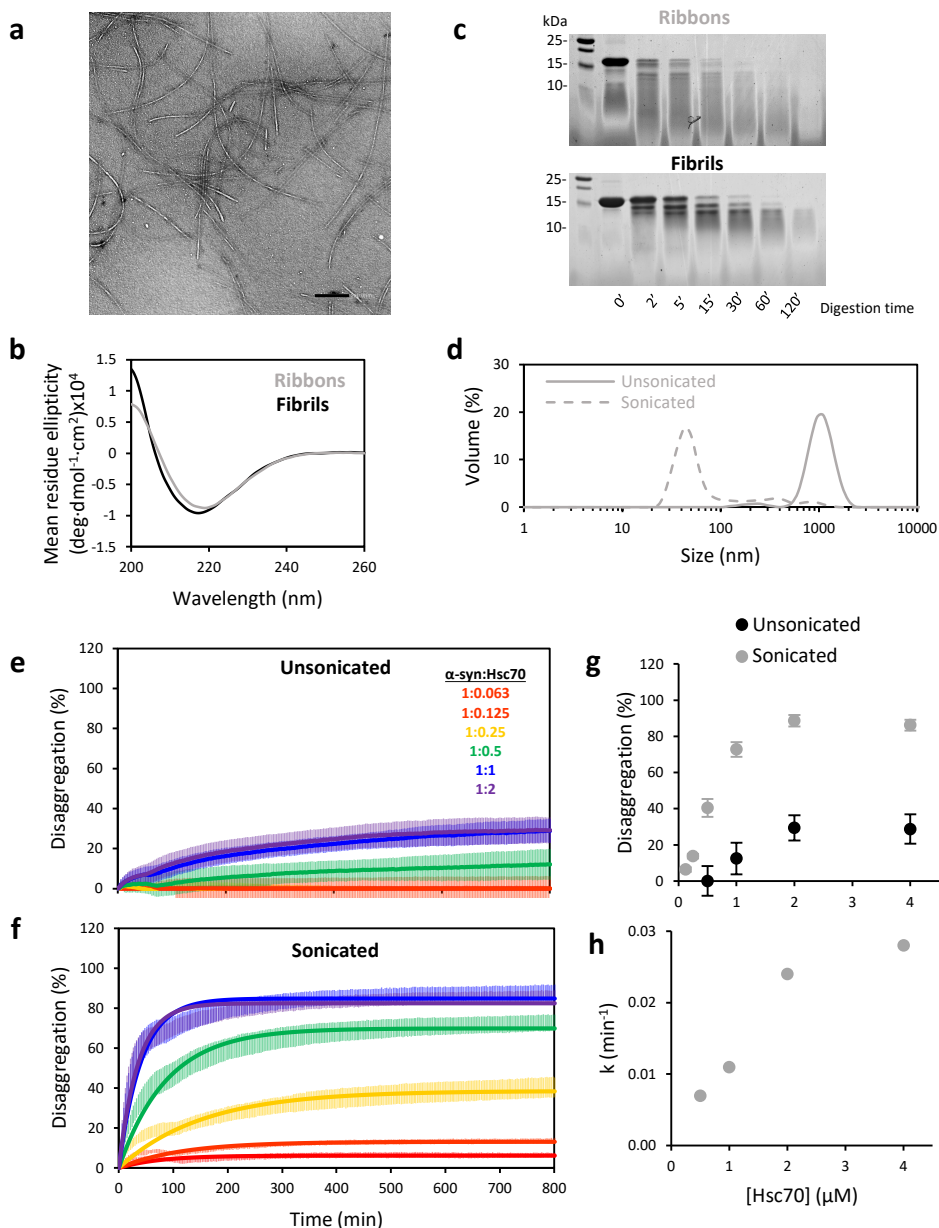
Figure 6.1. Structural characterization and chaperone-induced disaggregation of α-syn ribbons. α-syn ribbons were visualized by TEM (a). Ribbon and fibril samples were compared by means of Far-UV CD (b) and Proteinase-K digestion (c). Fragmentation of ribbons upon sonication was analyzed by DLS (d). Disaggregation kinetics of unsonicated (e) and sonicated (g) α-syn ribbons (2 μM) labeled with alexaFluor488 was followed at different chaperone concentrations keeping the molar ratio of Hsc70:DnaJB1:Apg2 constant at 1:0.5:0.1. The final disaggregation percentage was plotted as a function of Hsc70

concentration (g). Disaggregation kinetics in (f) were fitted to a pseudo-first order function (solid lines) and disaggregation rate constants at each chaperone concentration were calculated (h).

by DLS (**Figure 6.1 d**). Both unsonicated (**Figure 6.1 e**) and sonicated (**Figure 6.1 f**) fluorescently labeled ribbons were mixed with different chaperone concentrations and their disaggregation kinetics were followed by fluorescence dequenching. Unsonicated ribbons were poorly disassembled by the human disaggregase and after sonication, most of the sample was disaggregated at α-syn:Hsc70 molar ratios higher than 1:0.5 (**Figure 6.1 g**), which was similar to the results obtained for sonicated fibrils (**Figure 4.6**). This similarity extended to the disaggregation rate, which increased with the chaperone concentration and stabilized at 2 μM Hsc70 (**Figure 6.1 h**). Altogether these data indicate the structural differences that arise from aggregating α-syn at low ionic strengths do not affect the chaperone-mediated disassembly.

6.2.2. Disaggregation of α-synuclein polymorphs obtained in the presence of different chemical compounds

Recently published work by Prof. Nunilo Cremades showed that aggregation of α-syn in the presence of different co-solvents or additives that limit hydration conditions resulted in the formation of different fibril polymorphs (Camino *et al.*, 2020). In particular, we tested the human disaggregase activity with aggregates formed in the presence of the molecular crowder dextran 70 and the fluorinated alcohol 2,2,2-trifuoroethanol (TFE) (**Table 6.1**).

Mild concentrations (150 g/L) of dextran accelerated aggregation of α-syn and resulted in the formation of fibrillar aggregates with similar FT-IR spectra to those obtained in the absence of dextran, with a slight reduction in the β-sheet content from 54 ± 4% to 42 ± 4% (Camino *et al.*, 2020). Interestingly, fibrils obtained

in the presence of dextran (henceforth named dextran fibrils), were significantly shorter, with 6.4 ± 0.8 nm in height and 206 ± 117 nm in length, according to AFM analysis. Disaggregation of Alexa488 labeled dextran fibrils showed a dependence with chaperone concentration similar to that observed for fibrils and ribbons, with a saturation of the process at a 1:0.5 α-syn:Hsc70 molar ratio (**Figure 6.2 a**), above which disaggregation was around 80% (**Figure 6.2 e**). The high disassembly efficiency of unsonicated dextran fibrils clearly evidenced the size-dependent activity of the chaperones shown in **Chapter 4**, and suggests that polymorphs obtained under conditions that favors the formation of shorter fibrils are better disassembled by chaperones. Upon sonication, dextran fibrils fragmented into small globular-like species with a height of 5.3 ± 0.9 nm and a diameter of 83 ± 14 nm, whose disaggregation rendered similar efficiencies to the unsonicated sample (**Figure 6.2 b and e**). Comparison of the disaggregation rate constants obtained for unsonicated and sonicated dextran fibrils showed a slower process for the latter (**Figure 6.2 f**). This reduction in the disaggregation rate could be explained by the change from a fibrillar to a globular morphology, unfavoring depolymerization propagation as seen for type B oligomers (**Chapter 4**).

Table 6.1. Characteristics of α-syn fibril polymorphs obtained in the presence of dextran and TFE. β-sheet content (%) of polymorphs was taken from (Camino *et al.*, 2020) and size measurements were done by AFM analysis.

Compound	β-sheet content (%)	Size (nm)	
		Unsonicated	*Sonicated*
Dextran (150 g/L)	42±4	Height 6.4±0.8 Length 206±117	Height 5.3 ± 0.9 Diameter 83±14
TFE (5%)	49±3	Height 10±1 Length 600±300	Height 5±1 Length 114±33
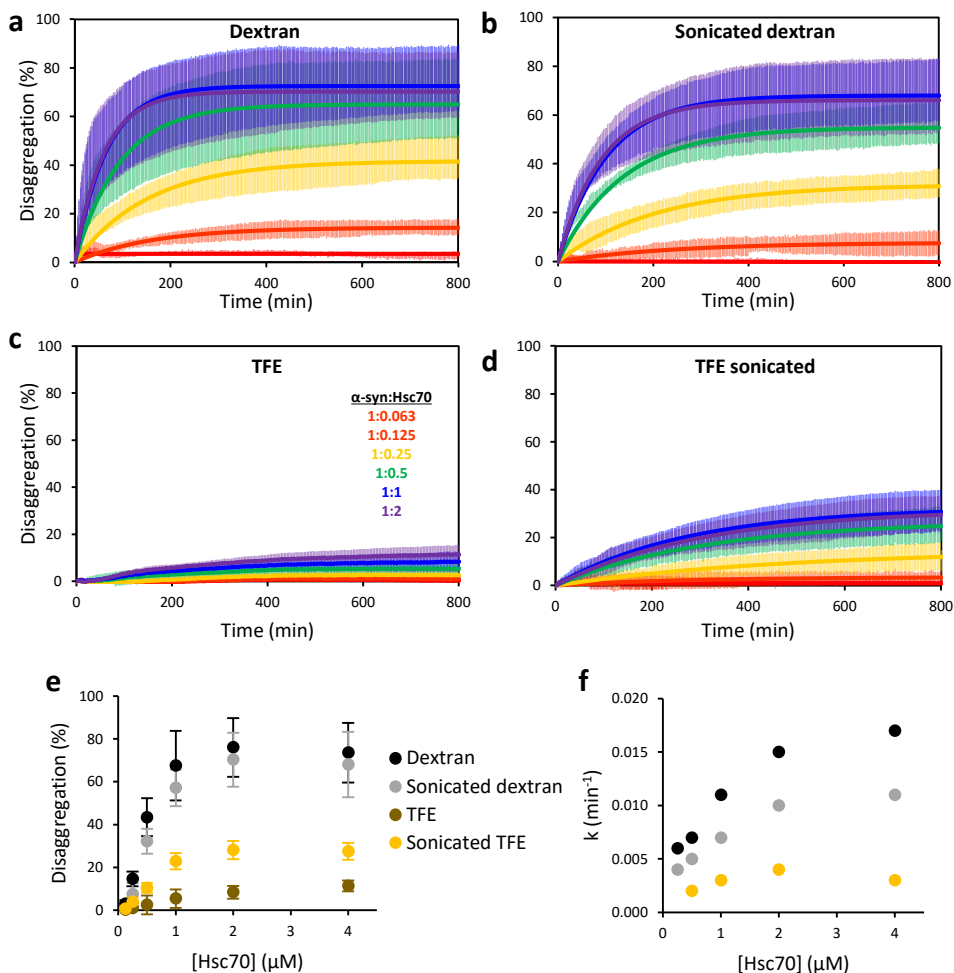
Figure 6.2. Disaggregation kinetics of α-synuclein polymorphs obtained in the presence of different compounds. α-syn (2 μM) polymorphs produced in the presence of dextran - unsonicated (a) and sonicated (b) - or TFE - unsonicated (c) and sonicated (d) - were disaggregated at different concentrations of the ternary chaperone mixture keeping the molar ratio of Hsc70:DnaJB1:Apg2 constant at 1:0.5:0.1. Final disaggregation percentage was plotted as a function of Hsc70 concentration (e) and disaggregation kinetics in (a, b and d) were fitted to a pseudo-first order function (solid lines), calculating the disaggregation rate constants at each chaperone concentration (f).

Similarly to dextran, low concentrations of TFE significantly increased the rate of α-syn aggregation and resulted in fibrils (henceforth named TFE fibrils) with similar FT-IR spectra (β-sheet content of 49 ± 3%) to those obtained in the absence

of TFE, and with an average 10 ± 1 nm height, 600 ± 300 nm length and a twisting periodic pitch of 61 ± 2 nm (Camino *et al.*, 2020). Unsonicated fluorescently labeled TFE fibrils disaggregated poorly - less than 10% - even at the highest chaperone concentration (4 µM Hsc70) (**Figure 6.2 c and e**). Upon sonication, TFE fibrils fragmented with an average 5 ± 1 nm height and 114 ± 33 nm length. Even though we observed a 3-fold increase in disaggregation efficiency upon sonication of TFE fibrils, the maximum efficiency of the process was only 30% (**Figure 6.2 d and e**). This low solubilization efficiency correlated with small values in the disaggregation rate constant (**Figure 6.2 f**). Such a slow chaperone-mediated disassembly of TFE fibrils, even when fragmented, suggests a more stable fibril structure that impairs chaperone activity.

6.2.3. Disaggregation of α-synuclein polymorphs produced by point-mutations associated with PD

Individuals with mutations in the gene encoding α-syn have been reported to be more prone to develop Parkinson's disease and often with an earlier age of onset (Klein and Westenberger, 2012). Indeed, several missense mutations in the *SNCA* gene have been found in heterozygosis in familial cases of Parkinson's disease. Such mutations have been shown to affect the kinetics of the protein aggregation *in vitro* and alter significantly the nature of the fibrillar structures, which could be associated with differences in the clinical phenotypes of familial Parkinson's disease (Ruggeri *et al.*, 2020). We decided to challenge the human disaggregase with fibrils composed of two point-mutants found in patients with PD: A53T and E46K.

The A53T mutation was first reported in an Italian kindred and in three unrelated Greek families with autosomal dominant inheritance for PD (Polymeropoulos *et al.*, 1997), while the E46K mutation was reported in a family from the Basque Country with autosomal dominant parkinsonism (Zarranz *et al.*, 2003). After aggregation, both point mutants and the WT protein showed

comparable, long thread-like structures (**Figure 6.3 a**). The secondary structure of fibrils of the three variants was compared by Far-UV CD (**Figure 6.3 b**), showing the characteristic ellipticity minimum at 218 nm. While WT and A53T showed overlapped spectra, E46K had a loss of ellipticity. Further structural characterization by FT-IR spectroscopy of the three proteins evidenced changes in the amide I band that can be better distinguish in the differential spectra (**Figure 6.3 c**). They showed that compared to WT, A53T had a negative band at 1627 cm^{-1} and a positive band 1620 cm^{-1}, while E46K had two negative bands at 1626 and 1614 cm^{-1} and a positive band at 1660 cm^{-1}. These changes can be associated with a rearrangement of the β-sheet strands and confirmed that both mutants adopted fibril structures different to their WT counterpart. Then, we checked the susceptibility of the three variants to fragmentation upon sonication, showing that in all cases, sonication decreased fibril size from microns to hundreds of nanometers (**Figure 6.3 d**).

To evaluate the disaggregation kinetics of the fibril structures induced by the two point-mutations, monomers of each mutant were self-seeded in the presence of 15% AlexaFluor488 labeled monomeric Q24C, which rendered hybrid fibrils with ca. 11% of labeled protomers (**Figure 6.4 a**). The fact that fibrils of the point mutants showed different ThT binding efficiencies compared to WT (**Figure 6.4 b**) - A53T bound 2-times more while E46K 3-times less ThT -, allowed us to confirm that the characteristic polymorph structure of each protein species was maintained in the hybrid fibrils (**Figure 6.4 b**). Then, disaggregation of sonicated hybrid fibrils of each mutant was followed as a dequenching process, keeping α-syn concentration at 2 μM and titrating the human disaggregase up to 1:4 α-syn:Hsc70 molar ratio (**Figure 6.4 c**). A53T showed a disaggregation kinetics comparable to that previously seen for WT fibrils both in terms of final disaggregation percentage (**Figure 6.4 d**) and disaggregation rate (**Figure 6.4 e**). Meanwhile, E46K showed 2-8 times lower disaggregation efficiencies at α-syn:Hsc70 molar ratio under 1:1, and did not reach similar yields to WT and A53T until the α-syn:Hsc70 ratio was 1:4 (**Figure 6.4 d**). Sur-
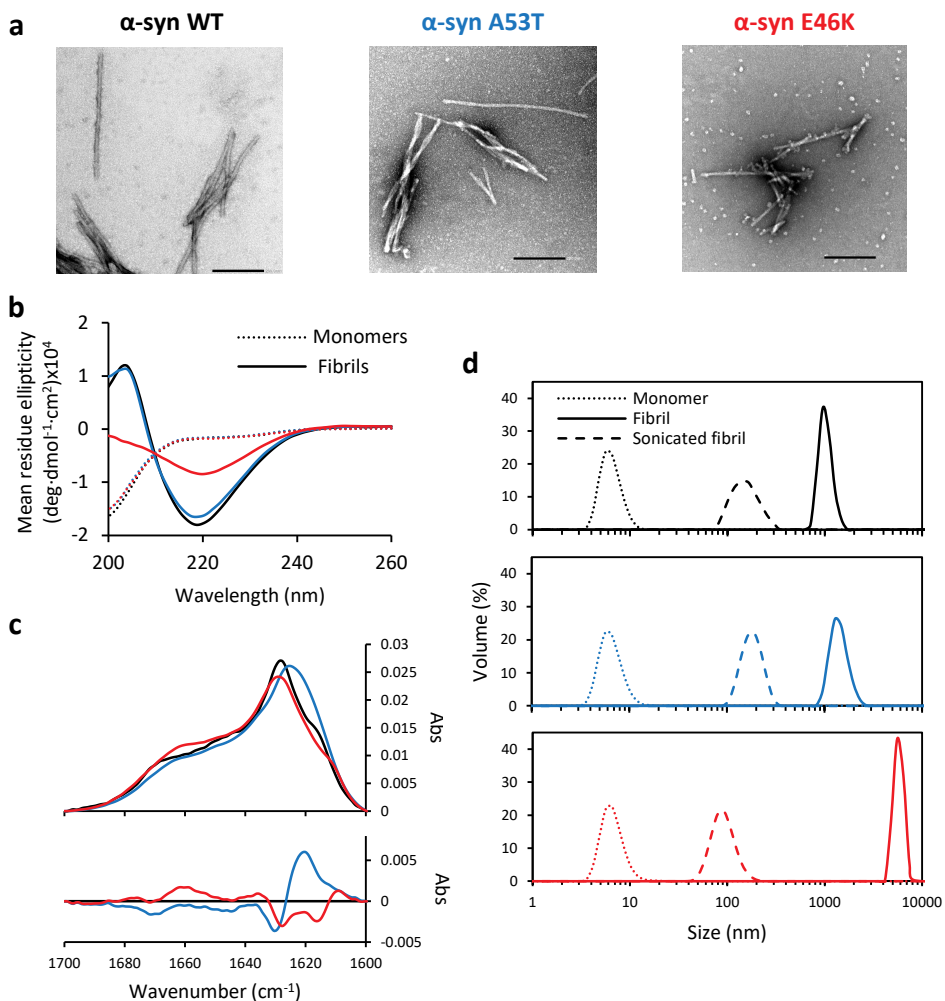
Figure 6.3. Characterization of polymorphs of α-syn point-mutants associated with PD. (a) Negative-stain TEM images of α-syn WT, A53T and E46K fibrils. (b) The secondary structure of monomeric and fibrillar species of the three variants was compared by Far-UV CD. (c) FT-IR spectra of fibrils of each of these variants (upper panel) and differential spectra of the two point-mutants with respect to the WT protein (lower panel). The differential spectra were obtained after subtracting the spectrum of the variant form that of the WT protein. (d) Fragmentation susceptibility upon sonication of fibrils of the three protein species measured by DLS.

prisingly, E46K showed a faster disaggregation rate that remained comparable at the different chaperone concentrations (**Figure 6.4 e**). This could indicate that the

E46K substitution induces a more stable fibril structure requiring a higher chaperone concentration to induce the initial destabilization of fibrils but once chaperones have triggered it, depolymerization along the fibril axis occurs at a faster rate than that observed for WT α-syn. The heterogeneity of the fibril sample might explain the lower disaggregation yield observed for this mutant, as disassembly efficiency might be related to the fibril population that can be destabilized at a given chaperone concentration.

6.2.4. Disaggregation of tau K18 polymorphs produced by point mutations associated with FTDP-17

Similar to α-syn, several point-mutations have been described in the *MAPT* gene in patients with frontotemporal dementia and parkinsonism linked to chromosome 17. Of particular interest are mutations located at the MTB domain of tau, as this is the protein region responsible for its aggregation. These mutations tend to reduce the ability of tau to interact with MTs and promote fibril formation (Goedert and Spillantini, 2000). We chose two of these mutations, P301L, firstly identified in families from the USA and the Netherlands (Hutton et al., 1998), and ΔK280, originally identified in a Dutch individual (Rizzu *et al.*, 1999), and introduced them into the tau K18 construct. After aggregation, both point mutants and the WT protein showed comparable, long thread-like structures as seen by AFM (**Figure 6.5 a**). The secondary structure of fibrils of the three variants was compared by Far-UV CD (**Figure 6.5 b**). K18 WT and P301L showed a single ellipticity minimum at 220 and 218 nm, respectively, with P301L displaying an increased ellipticity compared to WT. The spectrum of ΔK280 fibrils was also shifted towards lower wavelengths, suggesting a higher content of disordered structure for this polymorph. Further structural characterization by FT-IR spectroscopy (**Figure 6.5 c**) showed differences in the amide I band of the three protein species that can be better analyzed in the
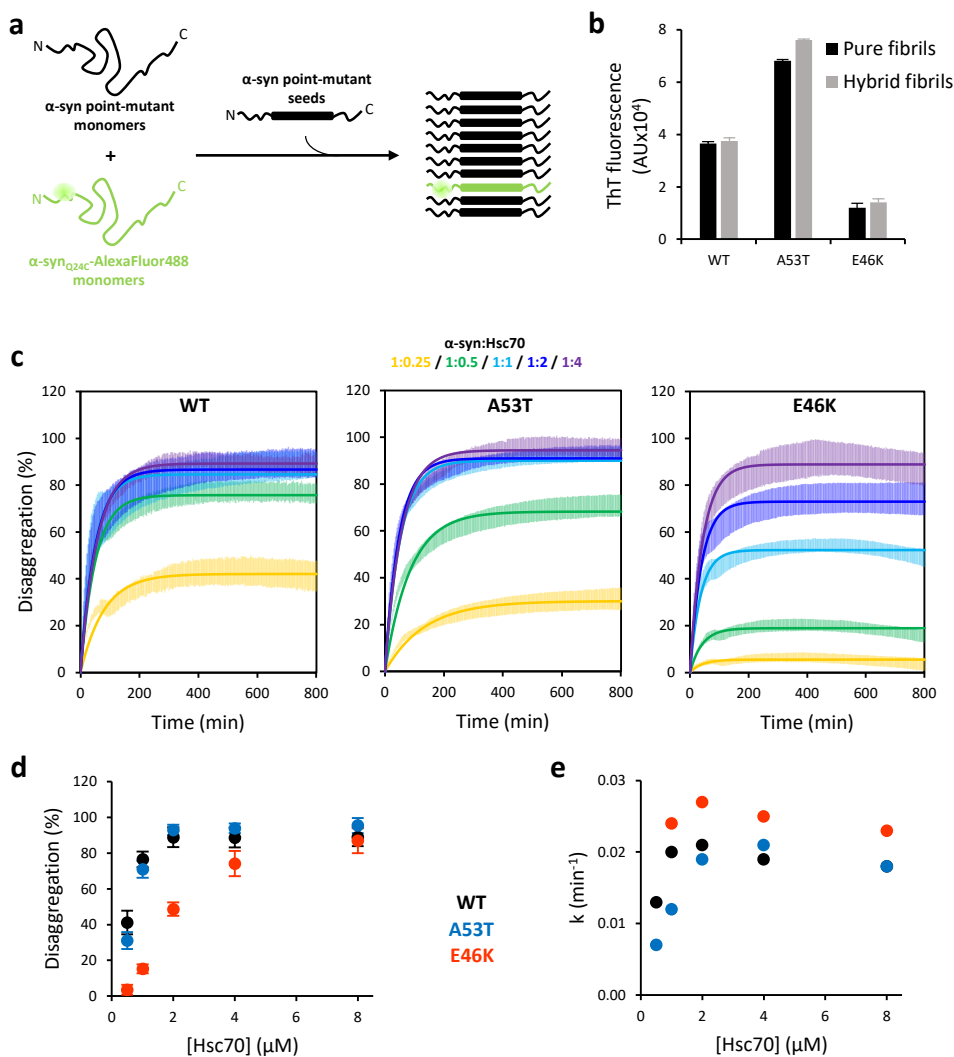
Figure 6.4. Disaggregation kinetics of polymorphs of α-syn point-mutants associated with PD. (a) Scheme of the experimental procedure used to generate labeled fibrils of α-syn point-mutants. (b) ThT binding of fibrils obtained in the absence (pure fibrils) or presence (hybrid fibrils) of 15% unlabeled monomers of the Q24C mutant. (c) Sonicated fibrils of the three α-syn (2 μM) species were disaggregated at different concentrations of the ternary chaperone mixture maintaining the molar ratio of Hsc70:DnaJB1:Apg2 constant at 1:0.5:0.1. Final disaggregation percentage was plotted as a function of Hsc70 concentration (d). Disaggregation kinetics in (c) were fitted to a pseudo-first order function (solid lines) to estimate the disaggregation rate constants at each chaperone concentration (e).

differential spectra. As compared with WT, P301L had a positive band at around 1630 cm^{-1} and two negative bands at 1616 and 1647 cm^{-1}, pointing towards a different β-sheet organization. The differential spectrum of ΔK280 fibrils displayed a positive broad band at around 1656 cm^{-1} and a negative band at 1616 cm^{-1}, compatible with the CD data, as they can be interpreted as a consequence of an increase in disordered structure at the expenses of the β-structure. Then, we checked the susceptibility of the three variant to fragmentation upon sonication, showing that in all cases the fibril size decreased from microns to hundreds of nanometers, thus confirming their fragmentation (**Figure 6.5 d**).

To obtain the chaperone-mediated disaggregation kinetics of each tau K18 variant, the corresponding monomers were labeled with AlexaFluor488 (NHS ester; labeling efficiency of 20-50%) and aggregated in the presence of heparin. Then, disaggregation of sonicated labeled fibrils of each mutant was followed as a dequenching process, keeping tau concentration at 2 μM and titrating the human disaggregase up to 1:4 tau:Hsc70 molar ratio (**Figure 6.6 a**). As seen for α-syn, disaggregation kinetics of tau K18 followed a chaperone-concentration dependence, although without a clear saturation of the process even at the highest chaperone concentration that gave a disaggregation yield of 55%. This is in good agreement with the results obtained with sonicated fibrils of tau 2N4R (**Figure 4.10**), which only disaggregated around 40% at a 1:10 tau:Hsc70 molar ratio, and may indicate that fibrils composed of tau proteins render more stable structures that need more chaperone concentrations, similar to what we saw with α-syn$_{E46K}$. Regarding disaggregation of fibrils composed of the two point-mutants associated with FTDP-17, we saw that while the P301L behaved similarly to the WT protein in terms of final disaggregation percentage (**Figure 6.6 b**), it showed a faster disaggregation rate regardless of chaperone concentration. Disaggregation rates of ΔK280 fibrils, however, were similar to WT but with lower disaggregation yields, which saturated at around 30% at the 1:1 tau:Hsc70 molar ratio. Taken together,

these data suggest that the fibrillar structure induced by the P301L substitution may accelerate the extraction of monomers by the chaperones, while the structural change provoked by the deletion of K280 may result in fibrils with increased resistance to chaperone-induced destabilization.
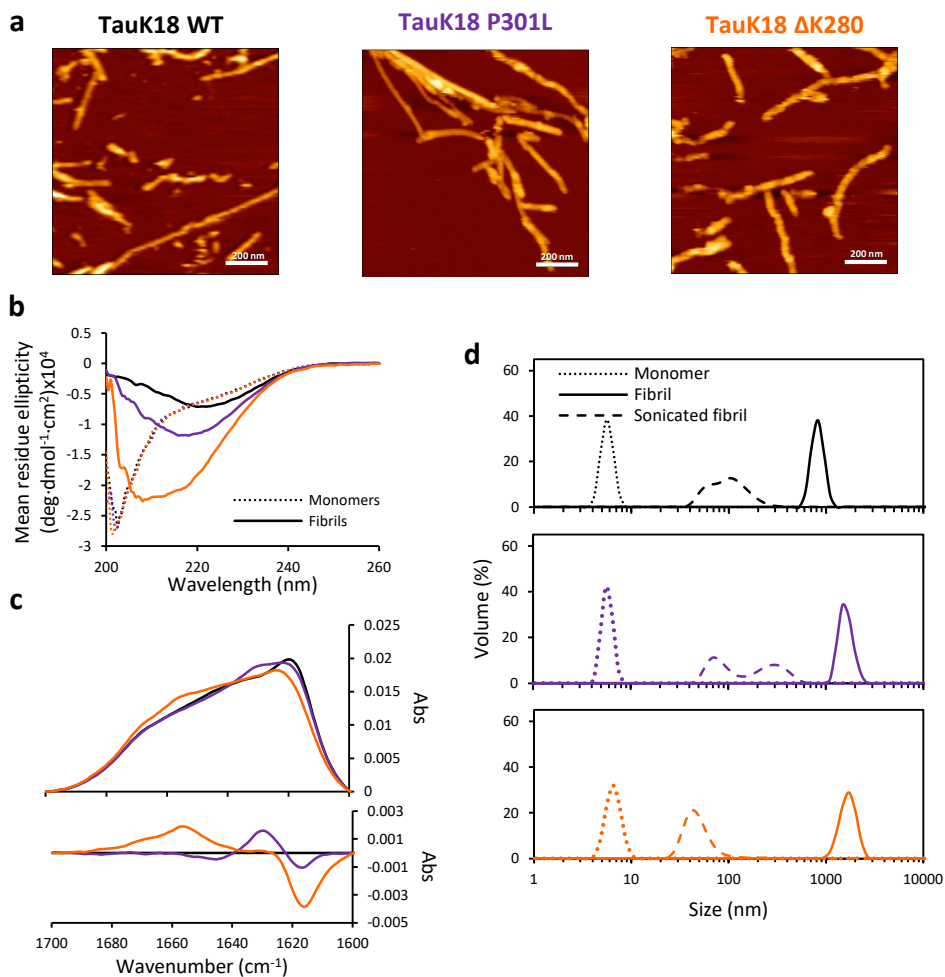
Figure 6.5. Characterization of tau K18 polymorphs produced by pathogenic point-mutations. (a) AFM images of tau K18 WT, P301L and ΔK280 fibrils. (b) Structure of monomeric and fibrillar species of the three variants as seen by Far-UV CD. (c) FT-IR spectra of fibrils of each protein species (upper panel) and differential spectra of the two tau K18 point-mutants relative to that of the WT protein (lower panel). (d) Fragmentation susceptibility of fibrils of the three proteins upon sonication measured by DLS.
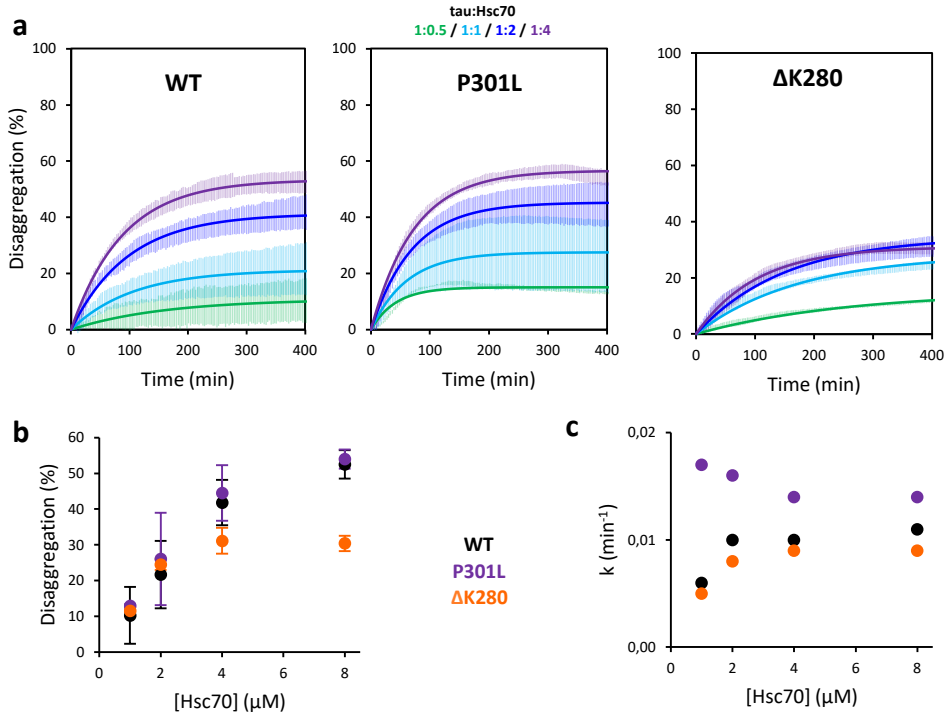
Figure 6.6. Disaggregation kinetics of tau K18 polymorphs produced by pathogenic point-mutations. (a) Sonicated fibrils of tau K18 WT, P301L and ΔK280 (2 µM) were disaggregated at different concentrations of the ternary chaperone mixture maintaining the Hsc70:DnaJB1:Apg2 molar ratio constant at 1:0.5:0.1. (b) Final disaggregation percentage as a function of Hsc70 concentration. Disaggregation kinetics in (a) were fitted to a pseudo-first order function (solid lines) and disaggregation rate constants at each chaperone concentration were calculated (c).

6.3. DISCUSSION

The process of amyloid formation can take place through several pathways, generating a high diversity of fibril structures from a single peptide/protein sequence and such heterogeneity has been proposed as a possible explanation for the multiplicity of clinical presentations observed for most NDs (Tycko, 2015; Fitzpatrick and Saibil, 2019). In this chapter, we have produced various fibril polymorphs of α-syn and tau by using different aggregation conditions and point-

mutations associated with NDs and compared their disassembly by the Hsp70-based disaggregase machinery. Regardless of the structure of α-syn polymorph, long (microns of length) fibrillar aggregates yielded low disaggregation efficiencies, which increased upon mechanical fragmentation. Only fibrils obtained in the presence of dextran, which are significantly shorter (Camino *et al.*, 2020), can be efficiently disassembled without a previous sonication step. These data endorse the results obtained in **Chapter 4**, showing a preferential targeting of shorter fibrils by the human disaggregase. Comparison of disaggregation yields and rates of all the sonicated polymorphs (**Figure 6.7**) evidenced the impact of some fibril structures in chaperone activity.

Among α-syn polymorphs obtained *in vitro*, ribbons, which are generated in the absence of salt, are one of the most studied. Structural comparison of fibrils and ribbons by NMR showed that β-sheets with an in-register parallel stacking are the dominating secondary structure elements for both polymorphs, although with a divergent number of subunits and distribution (Bousset *et al.*, 2013; Gath *et al.*, 2014). In fibrils, the succession of β-strands run from residue 38 to 94, in excellent agreement with the recently solved atomic structures (Tuttle *et al.*, 2016; Guerrero-Ferreira *et al.*, 2018; Li, Ge, *et al.*, 2018; Li, Zhao, *et al.*, 2018; Ni *et al.*, 2019). Meanwhile, β-sheet elements in ribbons start at the N-terminus, distributing within residues 1 to 97. Despite these differences, chaperone-mediated disaggregation rates and efficiencies for ribbons and fibrils were similar (**Figure 6.7**). The α-syn polymorph resulting from the A53T substitution also showed comparable chaperone activity values, which is consistent with a recent report showing that this mutation does not alter the fibril fold but changes the protofilament interface (Sun *et al.*, 2020). In contrast to α-syn ribbons and A53T fibrils, polymorphs obtained with TFE or the E46K mutation displayed a significant reduction in chaperone activity (**Figure 6.7**), which suggested a more stable fibril structure in both cases. Two structures have been reported for E46K fibrils, one also seen in WT and

referred to as 2a (Guerrero-Ferreira *et al.*, 2019; Zhao *et al.*, 2019) and another one with a different, more stable and compact fold (Boyer *et al.*, 2020). The lack of a structural model for our preparations prevents us from associating a particular polymorphic structure with a determined chaperone activity, but the increased resistance to disaggregation might be related to the second fold reported (Boyer *et al.*, 2020). In fact, our results are in agreement with previously reported data obtained with the Hsp104 disaggregase, which in collaboration with the Hsp70 system efficiently disaggregated fibrils composed of WT and A53T α-syn but failed in disassembling E46K fibrils (Desantis *et al.*, 2012). From a mechanistic point of view, we hypothesize that the increased stability of some polymorphs may affect different steps of the chaperone-mediated disassembly process. We have previously shown that disaggregation starts with a destabilization of the fibril ends that is followed by a rapid propagation of the depolymerization through the fibril axis. At low chaperone concentration, E46K fibrils showed higher disaggregation rates than WT ones but yielded lower disassembly efficiencies. This may indicate an increased stability towards the initial fibril destabilization by chaperones but once depolymerization starts, the fold induced by the E46K substitution could favor disassembly propagation. Conversely, disaggregation rates of TFE fibrils are significantly low, which translates into low disaggregation yields and suggests that fibril structure induced by this alcohol (Camino *et al.*, 2020) might disfavor propagation of depolymerization by chaperones.

Similar to α-syn, we show herein that point-mutations in tau K18 associated with FTDP-17 can drastically change fibril structure, which translates into different chaperone-mediated disassembly outcomes (**Figure 6.7**). P301L, showed similar disaggregation yields to WT but with faster rates, which could indicate a favored propagation of depolymerization akin to α-syn E46K, but in this case, resulting in disaggregation yields similar to tau K18 WT in a shorter period of time. Meanwhile, the ΔK280 mutation induced a lower disaggregation efficiency with a comparable

rate, and thus propagation, to tau K18 WT, suggesting a higher resistance to the initial destabilization of fibrils.
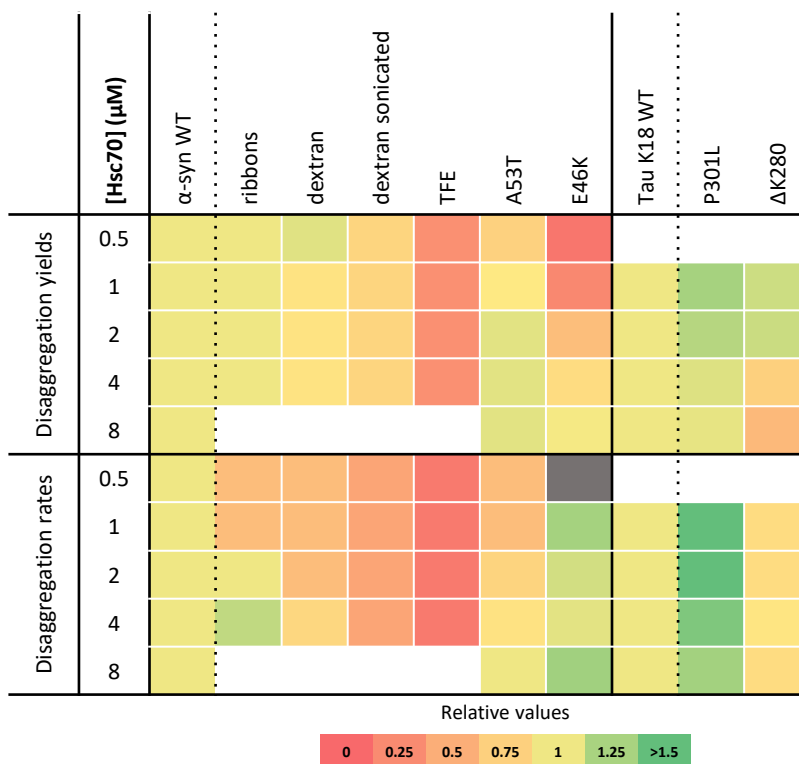
Figure 6.7. Heatmap depicting the effect of polymorphs in chaperone activity. For each chaperone concentration, disaggregation yields and rates of each polymorph were compared to α-syn WT or tau K18 WT and the values obtained were color-coded as in the legend. In all cases, compared values correspond to sonicated samples, except for α-syn dextran fibrils for which values for both unsonicated and sonicated are presented. Conditions marked with a white cell were not measured and that marked in gray could not be determined accurately due to the low disaggregation yield.

The toxicity of physiologically relevant polymorphs has normally been associated with their different abilities to induce cellular stress and death and propagate neurodegeneration (Scheckel and Aguzzi, 2018). Here we show that another important factor to determine the extent of a polymorph toxicity could be their chaperone disaggregation susceptibility. An increased resistance to

chaperone-mediated disassembly would result in a reduced clearance of these aggregates, which would translate into an increased half-life time and therefore, possibility to participate in abnormal interactions leading to cytotoxicity. Furthermore, pathogenesis of point-mutations in α-syn and tau associated with PD and FTDP-17, respectively, has been related to their increased aggregation propensity. Here we show that their toxicity may also come from the formation of a fibril fold with increased resistance to disaggregation, as is the case of mutations E46K for α-syn or ΔK280 for tau.

Recently solved structures of fibrils of α-syn and tau obtained *in vitro* or from patient-derived material, evidenced that *in vitro* models may not represent the pathological events occurring *in vivo* (Fitzpatrick *et al.*, 2017; Falcon *et al.*, 2018, 2019; Schweighauser et al., 2020; Zhang *et al.*, 2020). Working with brain-derived fibrils poses a challenge in terms of sample complexity and production yields. Tuning fibril growth conditions can result in the production of physiologically relevant polymorphs. As an example, α-syn ribbons produced *in vitro*, exhibited a polymorph appearance similar to those observed for PD and MSA patient-derived material (Van der Perren *et al.*, 2020) and caused a histopathological phenotype with PD and MSA traits (Peelaerts *et al.*, 2015). Indeed, cryo-EM structure of fibrils obtained from individuals with MSA showed a structured N-terminal arm with β-sheet elements comprising residues 14 to 94 (Schweighauser et al., 2020), a region also structured in ribbons (Bousset *et al.*, 2013; Gath *et al.*, 2014). Alternatively, the protein misfolding cyclic amplification assay (PMCA) (Saá and Cervenakova, 2015) have resulted useful to propagate *in vitro* the structural and histopathological characteristic of patient-derived polymorphs (Van der Perren *et al.*, 2020). Analyzing whether the impact of amyloid polymorphs we show herein extends to different disease-associated polymorphs is an interesting direction for future investigations.

CHAPTER

7

CONCLUSIONS

With the results presented in this doctoral thesis, the following conclusions are drawn:

❖ The human disaggregase, composed of the chaperone Hsc70, its cochaperone DnaJB1 and the nucleotide exchange factor Apg2, shows a fibril-size dependent activity, disaggregating more efficiently shorter fibrils of α-syn and tau. The same chaperone mixture can also disassemble small oligomeric species of α-syn. Importantly, aggregates towards which chaperones show more activity are the most cytotoxic. Taken together, these results suggest that chaperones preferentially target toxic amyloid intermediates.

❖ Chaperone-mediated disassembly of α-syn amyloids occurs via a depolymerization process that starts at the ends of the aggregate and propagates fast through the fibril axis. This mechanism favors the fast disaggregation of small amyloid intermediate species. Clearance of large amyloids may require the coordinated processing of both the proteasome, which first fragments fibrils into smaller species, and the human disaggregase, which afterwards depolymerize them.

❖ C-terminal truncation of α-syn induces lateral association of fibrils and oligomers, which hampers chaperone-mediated disaggregation. This behavior explains the higher propensity of C-truncated species to deposit *in vivo*.

❖ Amyloid polymorphism has an impact on chaperone activity. Some fibril structures of tau and α-syn, induced by altering the aggregation conditions or by point-mutations related to NDs, are more resistant to chaperone-mediated disaggregation. This observation could explain the increased toxicity of certain amyloid strains, adding another factor to consider when evaluating their pathogenesis.

REFERENCES

Abdelmotilib, H., Maltbie, T., Delic, V., Liu, Z., Hu, X., Fraser, K. B., Moehle, M. S., Stoyka, L., Anabtawi, N., Krendelchtchikova, V., Volpicelli-Daley, L. A., & West, A. (2017). α-Synuclein fibril-induced inclusion spread in rats and mice correlates with dopaminergic Neurodegeneration. *Neurobiology of disease*, *105*, 84–98. https://doi.org/10.1016/j.nbd.2017.05.014

Acebrón, S. P., Fernández-Sáiz, V., Taneva, S. G., Moro, F., & Muga, A. (2008). DnaJ recruits DnaK to protein aggregates. *The Journal of biological chemistry*, *283*(3), 1381–1390. https://doi.org/10.1074/jbc.M706189200

Acebrón, S. P., Martín, I., del Castillo, U., Moro, F., & Muga, A. (2009). DnaK-mediated association of ClpB to protein aggregates. A bichaperone network at the aggregate surface. *FEBS letters*, *583*(18), 2991–2996. https://doi.org/10.1016/j.febslet.2009.08.020

Adamcik, J., & Mezzenga, R. (2018). Amyloid Polymorphism in the Protein Folding and Aggregation Energy Landscape. *Angewandte Chemie (International ed. in English)*, *57*(28), 8370–8382. https://doi.org/10.1002/anie.201713416

Aguzzi, A., Nuvolone, M., & Zhu, C. (2013). The immunobiology of prion diseases. *Nature reviews. Immunology*, *13*(12), 888–902. https://doi.org/10.1038/nri3553

Aguzzi, A., & Lakkaraju, A. (2016). Cell Biology of Prions and Prionoids: A Status Report. *Trends in cell biology*, *26*(1), 40–51. https://doi.org/10.1016/j.tcb.2015.08.007

Anderson, J. P., Walker, D. E., Goldstein, J. M., de Laat, R., Banducci, K., Caccavello, R. J., Barbour, R., Huang, J., Kling, K., Lee, M., Diep, L., Keim, P. S., Shen, X., Chataway, T., Schlossmacher, M. G., Seubert, P., Schenk, D., Sinha, S., Gai, W. P., & Chilcote, T. J. (2006). Phosphorylation of Ser-129 is the dominant pathological modification of alpha-synuclein in familial and sporadic Lewy body disease. *The Journal of biological chemistry*, *281*(40), 29739–29752. https://doi.org/10.1074/jbc.M600933200

Aprile, F. A., Arosio, P., Fusco, G., Chen, S. W., Kumita, J. R., Dhulesia, A., Tortora, P., Knowles, T. P., Vendruscolo, M., Dobson, C. M., & Cremades, N. (2017). Inhibition of α-Synuclein Fibril Elongation by Hsp70 Is Governed by a Kinetic Binding Competition between α-Synuclein Species. *Biochemistry*, *56*(9), 1177–1180. https://doi.org/10.1021/acs.biochem.6b01178

Arakhamia, T., Lee, C. E., Carlomagno, Y., Duong, D. M., Kundinger, S. R., Wang, K., Williams, D., DeTure, M., Dickson, D. W., Cook, C. N., Seyfried, N. T., Petrucelli, L., & Fitzpatrick, A. (2020). Posttranslational Modifications Mediate the Structural Diversity of Tauopathy Strains. *Cell*, *180*(4), 633–644.e12. https://doi.org/10.1016/j.cell.2020.01.027

References

Arosio, P., Michaels, T. C., Linse, S., Månsson, C., Emanuelsson, C., Presto, J., Johansson, J., Vendruscolo, M., Dobson, C. M., & Knowles, T. P. (2016). Kinetic analysis reveals the diversity of microscopic mechanisms through which molecular chaperones suppress amyloid formation. *Nature communications*, *7*, 10948. https://doi.org/10.1038/ncomms10948

Arrondo, J. L., Muga, A., Castresana, J., & Goñi, F. M. (1993). Quantitative studies of the structure of proteins in solution by Fourier-transform infrared spectroscopy. *Progress in biophysics and molecular biology*, *59*(1), 23–56. https://doi.org/10.1016/0079-6107(93)90006-6

Avellaneda, M. J., Franke, K. B., Sunderlikova, V., Bukau, B., Mogk, A., & Tans, S. J. (2020). Processive extrusion of polypeptide loops by a Hsp100 disaggregase. *Nature*, *578*(7794), 317–320. https://doi.org/10.1038/s41586-020-1964-y

Baba, M., Nakajo, S., Tu, P. H., Tomita, T., Nakaya, K., Lee, V. M., Trojanowski, J. Q., & Iwatsubo, T. (1998). Aggregation of alpha-synuclein in Lewy bodies of sporadic Parkinson's disease and dementia with Lewy bodies. *The American journal of pathology*, *152*(4), 879–884. https://pubmed.ncbi.nlm.nih.gov/9546347/

Balchin, D., Hayer-Hartl, M., & Hartl, F. U. (2016). In vivo aspects of protein folding and quality control. *Science (New York, N.Y.)*, *353*(6294), aac4354. https://doi.org/10.1126/science.aac4354

Baldwin, A. J., Knowles, T. P., Tartaglia, G. G., Fitzpatrick, A. W., Devlin, G. L., Shammas, S. L., Waudby, C. A., Mossuto, M. F., Meehan, S., Gras, S. L., Christodoulou, J., Anthony-Cahill, S. J., Barker, P. D., Vendruscolo, M., & Dobson, C. M. (2011). Metastability of native proteins and the phenomenon of amyloid formation. *Journal of the American Chemical Society*, *133*(36), 14160–14163. https://doi.org/10.1021/ja2017703

Barbier, P., Zejneli, O., Martinho, M., Lasorsa, A., Belle, V., Smet-Nocca, C., Tsvetkov, P. O., Devred, F., & Landrieu, I. (2019). Role of Tau as a Microtubule-Associated Protein: Structural and Functional Aspects. *Frontiers in aging neuroscience*, *11*, 204. https://doi.org/10.3389/fnagi.2019.00204

Barrett, P. J., & Timothy Greenamyre, J. (2015). Post-translational modification of α-synuclein in Parkinson's disease. *Brain research*, *1628*(Pt B), 247–253. https://doi.org/10.1016/j.brainres.2015.06.002

Bedford, L., Paine, S., Sheppard, P. W., Mayer, R. J., & Roelofs, J. (2010). Assembly, structure, and function of the 26S proteasome. *Trends in cell biology*, *20*(7), 391–401. https://doi.org/10.1016/j.tcb.2010.03.007

Behrends, C., Langer, C. A., Boteva, R., Böttcher, U. M., Stemp, M. J., Schaffar, G., Rao, B. V., Giese, A., Kretzschmar, H., Siegers, K., & Hartl, F. U. (2006). Chaperonin TRiC promotes the assembly of polyQ expansion proteins into nontoxic oligomers. *Molecular cell*, *23*(6), 887–897. https://doi.org/10.1016/j.molcel.2006.08.017

Bhattacharjee, P., Öhrfelt, A., Lashley, T., Blennow, K., Brinkmalm, A., & Zetterberg, H. (2019). Mass Spectrometric Analysis of Lewy Body-Enriched α-Synuclein in Parkinson's Disease. *Journal of proteome research*, *18*(5), 2109–2120. https://doi.org/10.1021/acs.jproteome.8b00982

Bodakuntla, S., Jijumon, A. S., Villablanca, C., Gonzalez-Billault, C., & Janke, C. (2019). Microtubule-Associated Proteins: Structuring the Cytoskeleton. *Trends in cell biology*, *29*(10), 804–819. https://doi.org/10.1016/j.tcb.2019.07.004

Bollinger, J. A., , & Stevens, M. J., (2018). Catastrophic depolymerization of microtubules driven by subunit shape change. *Soft matter*, *14*(10), 1748–1752. https://doi.org/10.1039/c7sm02033c

Bolognesi, B., Kumita, J. R., Barros, T. P., Esbjorner, E. K., Luheshi, L. M., Crowther, D. C., Wilson, M. R., Dobson, C. M., Favrin, G., & Yerbury, J. J. (2010). ANS binding reveals common features of cytotoxic amyloid species. *ACS chemical biology*, *5*(8), 735–740. https://doi.org/10.1021/cb1001203

Böttcher CJF, Van gent CM, P. C. (1961). A rapid and sensitive sub-micro phosphorus determination. *Anal Chim Acta* 24:203–204.

Bousset, L., Pieri, L., Ruiz-Arlandis, G., Gath, J., Jensen, P. H., Habenstein, B., Madiona, K., Olieric, V., Böckmann, A., Meier, B. H., & Melki, R. (2013). Structural and functional characterization of two alpha-synuclein strains. *Nature communications*, *4*, 2575. https://doi.org/10.1038/ncomms3575

Boyer, D. R., Li, B., Sun, C., Fan, W., Sawaya, M. R., Jiang, L., & Eisenberg, D. S. (2019). Structures of fibrils formed by α-synuclein hereditary disease mutant H50Q reveal new polymorphs. *Nature structural & molecular biology*, *26*(11), 1044–1052. https://doi.org/10.1038/s41594-019-0322-y

Boyer, D. R., Li, B., Sun, C., Fan, W., Zhou, K., Hughes, M. P., Sawaya, M. R., Jiang, L., & Eisenberg, D. S. (2020). The α-synuclein hereditary mutation E46K unlocks a more stable, pathogenic fibril structure. *Proceedings of the National Academy of Sciences of the United States of America*, *117*(7), 3592–3602. https://doi.org/10.1073/pnas.1917914117

References

Bracher, A., & Verghese, J. (2015). The nucleotide exchange factors of Hsp70 molecular chaperones. *Frontiers in molecular biosciences*, *2*, 10. https://doi.org/10.3389/fmolb.2015.00010

Brehme, M., Voisine, C., Rolland, T., Wachi, S., Soper, J. H., Zhu, Y., Orton, K., Villella, A., Garza, D., Vidal, M., Ge, H., & Morimoto, R. I. (2014). A chaperome subnetwork safeguards proteostasis in aging and neurodegenerative disease. *Cell reports*, *9*(3), 1135–1150. https://doi.org/10.1016/j.celrep.2014.09.042

Brettschneider, J., Del Tredici, K., Lee, V. M., & Trojanowski, J. Q. (2015). Spreading of pathology in neurodegenerative diseases: a focus on human studies. *Nature reviews. Neuroscience*, *16*(2), 109–120. https://doi.org/10.1038/nrn3887

Brundin, P., Melki, R., & Kopito, R. (2010). Prion-like transmission of protein aggregates in neurodegenerative diseases. *Nature reviews. Molecular cell biology*, *11*(4), 301–307. https://doi.org/10.1038/nrm2873

Buell, A. K., Galvagnion, C., Gaspar, R., Sparr, E., Vendruscolo, M., Knowles, T. P., Linse, S., & Dobson, C. M. (2014). Solution conditions determine the relative importance of nucleation and growth processes in α-synuclein aggregation. *Proceedings of the National Academy of Sciences of the United States of America*, *111*(21), 7671–7676. https://doi.org/10.1073/pnas.1315346111

Burmann, B. M., Gerez, J. A., Matečko-Burmann, I., Campioni, S., Kumari, P., Ghosh, D., Mazur, A., Aspholm, E. E., Šulskis, D., Wawrzyniuk, M., Bock, T., Schmidt, A., Rüdiger, S., Riek, R., & Hiller, S. (2020). Regulation of α-synuclein by chaperones in mammalian cells. *Nature*, *577*(7788), 127–132. https://doi.org/10.1038/s41586-019-1808-9

Cabrera, Y., Dublang, L., Fernández-Higuero, J. A., Albesa-Jové, D., Lucas, M., Viguera, A. R., Guerin, M. E., Vilar, J., Muga, A., & Moro, F. (2019). Regulation of Human Hsc70 ATPase and Chaperone Activities by Apg2: Role of the Acidic Subdomain. *Journal of molecular biology*, *431*(2), 444–461. https://doi.org/10.1016/j.jmb.2018.11.026

Camino, J.D., Gracia, P., Chen, S.W., Sot, J., De la Arada, I., Sebastián, V., Arrondo, J.L.R., Goñi, F.M., Dobson, C.M., Cremades, N. (2020) The extent of protein hydration dictates the preference for heterogeneous or homogeneous nucleation generating either parallel or antiparallel β-sheet α-synuclein aggregates. *Chemical Science*, pp. 11902–11914. 10.1039/D0SC05297C

Campioni, S., Carret, G., Jordens, S., Nicoud, L., Mezzenga, R., & Riek, R. (2014). The presence of an air-water interface affects formation and elongation of α-Synuclein

fibrils. *Journal of the American Chemical Society*, *136*(7), 2866–2875. https://doi.org/10.1021/ja412105t

Campioni, S., Mannini, B., Zampagni, M., Pensalfini, A., Parrini, C., Evangelisti, E., Relini, A., Stefani, M., Dobson, C. M., Cecchi, C., & Chiti, F. (2010). A causative link between the structure of aberrant protein oligomers and their toxicity. *Nature chemical biology*, *6*(2), 140–147. https://doi.org/10.1038/nchembio.283

Capitini, C., Patel, J. R., Natalello, A., D'Andrea, C., Relini, A., Jarvis, J. A., Birolo, L., Peduzzo, A., Vendruscolo, M., Matteini, P., Dobson, C. M., De Simone, A., & Chiti, F. (2018). Structural differences between toxic and nontoxic HypF-N oligomers. *Chemical communications (Cambridge, England)*, *54*(62), 8637–8640. https://doi.org/10.1039/c8cc03446j

Carulla, N., Caddy, G. L., Hall, D. R., Zurdo, J., Gairí, M., Feliz, M., Giralt, E., Robinson, C. V., & Dobson, C. M. (2005). Molecular recycling within amyloid fibrils. *Nature*, *436*(7050), 554–558. https://doi.org/10.1038/nature03986

Chaudhuri, P., Prajapati, K. P., Anand, B. G., Dubey, K., & Kar, K. (2019). Amyloid cross-seeding raises new dimensions to understanding of amyloidogenesis mechanism. *Ageing research reviews*, *56*, 100937. https://doi.org/10.1016/j.arr.2019.100937

Chen, S. W., Drakulic, S., Deas, E., Ouberai, M., Aprile, F. A., Arranz, R., Ness, S., Roodveldt, C., Guilliams, T., De-Genst, E. J., Klenerman, D., Wood, N. W., Knowles, T. P., Alfonso, C., Rivas, G., Abramov, A. Y., Valpuesta, J. M., Dobson, C. M., & Cremades, N. (2015). Structural characterization of toxic oligomers that are kinetically trapped during α-synuclein fibril formation. *Proceedings of the National Academy of Sciences of the United States of America*, *112*(16), E1994–E2003. https://doi.org/10.1073/pnas.1421204112

Chernoff, Y. O., Lindquist, S. L., Ono, B., Inge-Vechtomov, S. G., & Liebman, S. W. (1995). Role of the chaperone protein Hsp104 in propagation of the yeast prion-like factor [psi+]. *Science (New York, N.Y.)*, *268*(5212), 880–884. https://doi.org/10.1126/science.7754373

Chilukoti, N., Sahoo, B., Deepa, S., Cherakara, S., Maddheshiya, M., Garai, K. (2020). Hsp70 inhibits aggregation of Islet amyloid polypeptide by binding to the heterogeneous prenucleation oligomers. bioRxiv https://doi.org/10.1101/2020.03.30.016881

Chiti, F., & Dobson, C. M. (2017). Protein Misfolding, Amyloid Formation, and Human Disease: A Summary of Progress Over the Last Decade. *Annual review of biochemistry*, *86*, 27–68. https://doi.org/10.1146/annurev-biochem-061516-045115

References

Choe, Y. J., Park, S. H., Hassemer, T., Körner, R., Vincenz-Donnelly, L., Hayer-Hartl, M., & Hartl, F. U. (2016). Failure of RQC machinery causes protein aggregation and proteotoxic stress. *Nature*, *531*(7593), 191–195. https://doi.org/10.1038/nature16973

Cliffe, R., Sang, J. C., Kundel, F., Finley, D., Klenerman, D., & Ye, Y. (2019). Filamentous Aggregates Are Fragmented by the Proteasome Holoenzyme. *Cell reports*, *26*(8), 2140–2149.e3. https://doi.org/10.1016/j.celrep.2019.01.096

Cohen, T. J., Guo, J. L., Hurtado, D. E., Kwong, L. K., Mills, I. P., Trojanowski, J. Q., & Lee, V. M. (2011). The acetylation of tau inhibits its function and promotes pathological tau aggregation. *Nature communications*, *2*, 252. https://doi.org/10.1038/ncomms1255

Cohen, S. I., Linse, S., Luheshi, L. M., Hellstrand, E., White, D. A., Rajah, L., Otzen, D. E., Vendruscolo, M., Dobson, C. M., & Knowles, T. P. (2013). Proliferation of amyloid-β42 aggregates occurs through a secondary nucleation mechanism. *Proceedings of the National Academy of Sciences of the United States of America*, *110*(24), 9758–9763. https://doi.org/10.1073/pnas.1218402110

Cohen, S., Arosio, P., Presto, J., Kurudenkandy, F. R., Biverstal, H., Dolfe, L., Dunning, C., Yang, X., Frohm, B., Vendruscolo, M., Johansson, J., Dobson, C. M., Fisahn, A., Knowles, T., & Linse, S. (2015). A molecular chaperone breaks the catalytic cycle that generates toxic Aβ oligomers. *Nature structural & molecular biology*, *22*(3), 207–213. https://doi.org/10.1038/nsmb.2971

Conde, C., & Cáceres, A. (2009). Microtubule assembly, organization and dynamics in axons and dendrites. *Nature reviews. Neuroscience*, *10*(5), 319–332. https://doi.org/10.1038/nrn2631

Cook, C., Carlomagno, Y., Gendron, T. F., Dunmore, J., Scheffel, K., Stetler, C., Davis, M., Dickson, D., Jarpe, M., DeTure, M., & Petrucelli, L. (2014). Acetylation of the KXGS motifs in tau is a critical determinant in modulation of tau aggregation and clearance. *Human molecular genetics*, *23*(1), 104–116. https://doi.org/10.1093/hmg/ddt402

Cremades, N., Chen, S. W., & Dobson, C. M. (2017). Structural Characteristics of α-Synuclein Oligomers. *International review of cell and molecular biology*, *329*, 79–143. https://doi.org/10.1016/bs.ircmb.2016.08.010

Cremades, N., Cohen, S. I., Deas, E., Abramov, A. Y., Chen, A. Y., Orte, A., Sandal, M., Clarke, R. W., Dunne, P., Aprile, F. A., Bertoncini, C. W., Wood, N. W., Knowles, T. P., Dobson, C. M., & Klenerman, D. (2012). Direct observation of the interconversion of normal

and toxic forms of α-synuclein. *Cell*, *149*(5), 1048–1059. https://doi.org/10.1016/j.cell.2012.03.037

Cyr, D. M., & Ramos, C. H. (2015). Specification of Hsp70 function by Type I and Type II Hsp40. *Sub-cellular biochemistry*, *78*, 91–102. https://doi.org/10.1007/978-3-319-11731-7_4

Davies K. J. (2001). Degradation of oxidized proteins by the 20S proteasome. *Biochimie*, *83*(3-4), 301–310. https://doi.org/10.1016/s0300-9084(01)01250-0

Davis, J. K., & Sindi, S. S. (2016). A mathematical model of the dynamics of prion aggregates with chaperone-mediated fragmentation. *Journal of mathematical biology*, *72*(6), 1555–1578. https://doi.org/10.1007/s00285-015-0921-0

De, S., Wirthensohn, D. C., Flagmeier, P., Hughes, C., Aprile, F. A., Ruggeri, F. S., Whiten, D. R., Emin, D., Xia, Z., Varela, J. A., Sormanni, P., Kundel, F., Knowles, T., Dobson, C. M., Bryant, C., Vendruscolo, M., & Klenerman, D. (2019). Different soluble aggregates of Aβ42 can give rise to cellular toxicity through different mechanisms. *Nature communications*, *10*(1), 1541. https://doi.org/10.1038/s41467-019-09477-3

De Los Rios, P., Ben-Zvi, A., Slutsky, O., Azem, A., & Goloubinoff, P. (2006). Hsp70 chaperones accelerate protein translocation and the unfolding of stable protein aggregates by entropic pulling. *Proceedings of the National Academy of Sciences of the United States of America*, *103*(16), 6166–6171. https://doi.org/10.1073/pnas.0510496103

DeArmond, S. J., McKinley, M. P., Barry, R. A., Braunfeld, M. B., McColloch, J. R., & Prusiner, S. B. (1985). Identification of prion amyloid filaments in scrapie-infected brain. *Cell*, *41*(1), 221–235. https://doi.org/10.1016/0092-8674(85)90076-5

Dedmon, M. M., Christodoulou, J., Wilson, M. R., & Dobson, C. M. (2005). Heat shock protein 70 inhibits alpha-synuclein fibril formation via preferential binding to prefibrillar species. *The Journal of biological chemistry*, *280*(15), 14733–14740. https://doi.org/10.1074/jbc.M413024200

Dedmon, M. M., Christodoulou, J., Wilson, M. R., & Dobson, C. M. (2005). Heat shock protein 70 inhibits alpha-synuclein fibril formation via preferential binding to prefibrillar species. *The Journal of biological chemistry*, *280*(15), 14733–14740. https://doi.org/10.1074/jbc.M413024200

DeSantis, M. E., Leung, E. H., Sweeny, E. A., Jackrel, M. E., Cushman-Nick, M., Neuhaus-Follini, A., Vashist, S., Sochor, M. A., Knight, M. N., & Shorter, J. (2012). Operational

References

plasticity enables hsp104 to disaggregate diverse amyloid and nonamyloid clients. *Cell*, *151*(4), 778–793. https://doi.org/10.1016/j.cell.2012.09.038

Dong, Y., Zhang, S., Wu, Z., Li, X., Wang, W. L., Zhu, Y., Stoilova-McPhie, S., Lu, Y., Finley, D., & Mao, Y. (2019). Cryo-EM structures and dynamics of substrate-engaged human 26S proteasome. *Nature*, *565*(7737), 49–55. https://doi.org/10.1038/s41586-018-0736-4

Duennwald, M. L., Echeverria, A., & Shorter, J. (2012). Small heat shock proteins potentiate amyloid dissolution by protein disaggregases from yeast and humans. *PLoS biology*, *10*(6), e1001346. https://doi.org/10.1371/journal.pbio.1001346

Escusa-Toret, S., Vonk, W. I., & Frydman, J. (2013). Spatial sequestration of misfolded proteins by a dynamic chaperone pathway enhances cellular fitness during stress. *Nature cell biology*, *15*(10), 1231–1243. https://doi.org/10.1038/ncb2838

Falcon, B., Zhang, W., Murzin, A. G., Murshudov, G., Garringer, H. J., Vidal, R., Crowther, R. A., Ghetti, B., Scheres, S., & Goedert, M. (2018). Structures of filaments from Pick's disease reveal a novel tau protein fold. *Nature*, *561*(7721), 137–140. https://doi.org/10.1038/s41586-018-0454-y

Falcon, B., Zhang, W., Schweighauser, M., Murzin, A. G., Vidal, R., Garringer, H. J., Ghetti, B., Scheres, S., & Goedert, M. (2018). Tau filaments from multiple cases of sporadic and inherited Alzheimer's disease adopt a common fold. *Acta neuropathologica*, *136*(5), 699–708. https://doi.org/10.1007/s00401-018-1914-z

Falcon, B., Zivanov, J., Zhang, W., Murzin, A. G., Garringer, H. J., Vidal, R., Crowther, R. A., Newell, K. L., Ghetti, B., Goedert, M., & Scheres, S. (2019). Novel tau filament fold in chronic traumatic encephalopathy encloses hydrophobic molecules. *Nature*, *568*(7752), 420–423. https://doi.org/10.1038/s41586-019-1026-5

Fernandez-Fernandez, M. R., Veprintsev, D. B., & Fersht, A. R. (2005). Proteins of the S100 family regulate the oligomerization of p53 tumor suppressor. *Proceedings of the National Academy of Sciences of the United States of America*, *102*(13), 4735–4740. https://doi.org/10.1073/pnas.0501459102

Fernández-Higuero, J. A., Aguado, A., Perales-Calvo, J., Moro, F., & Muga, A. (2018). Activation of the DnaK-ClpB Complex is Regulated by the Properties of the Bound Substrate. *Scientific reports*, *8*(1), 5796. https://doi.org/10.1038/s41598-018-24140-5

Fernández-Higuero, J. A., Muga, A., & Vilar, J. (2020). Extraction and Refolding Determinants of Chaperone-Driven Aggregated Protein Reactivation. *Journal of molecular biology*, *432*(10), 3239–3250. https://doi.org/10.1016/j.jmb.2020.03.002

Ferrari, L., Geerts, W.J.C,. van Wezel, M., Kos, R., Konstantoulea, A., van Bezouwen, L.S., Förster, F.G., Rüdiger, S.G.D. (2018) Human chaperones untangle fibrils of the Alzheimer protein Tau. bioRxiv 426650; https://doi.org/10.1101/426650

Finkbeiner S. (2020). The Autophagy Lysosomal Pathway and Neurodegeneration. *Cold Spring Harbor perspectives in biology*, *12*(3), a033993. https://doi.org/10.1101/cshperspect.a033993

Fitzpatrick, A., Falcon, B., He, S., Murzin, A. G., Murshudov, G., Garringer, H. J., Crowther, R. A., Ghetti, B., Goedert, M., & Scheres, S. (2017). Cryo-EM structures of tau filaments from Alzheimer's disease. *Nature*, *547*(7662), 185–190. https://doi.org/10.1038/nature23002

Fitzpatrick, A. W., & Saibil, H. R. (2019). Cryo-EM of amyloid fibrils and cellular aggregates. *Current opinion in structural biology*, *58*, 34–42. https://doi.org/10.1016/j.sbi.2019.05.003

Fusco, G., Chen, S. W., Williamson, P., Cascella, R., Perni, M., Jarvis, J. A., Cecchi, C., Vendruscolo, M., Chiti, F., Cremades, N., Ying, L., Dobson, C. M., & De Simone, A. (2017). Structural basis of membrane disruption and cellular toxicity by α-synuclein oligomers. *Science (New York, N.Y.)*, *358*(6369), 1440–1443. https://doi.org/10.1126/science.aan6160

Gallardo, J., Escalona-Noguero, C., & Sot, B. (2020). Role of α-Synuclein Regions in Nucleation and Elongation of Amyloid Fiber Assembly. *ACS chemical neuroscience*, *11*(6), 872–879. https://doi.org/10.1021/acschemneuro.9b00527

Galvagnion, C., Brown, J. W., Ouberai, M. M., Flagmeier, P., Vendruscolo, M., Buell, A. K., Sparr, E., & Dobson, C. M. (2016). Chemical properties of lipids strongly affect the kinetics of the membrane-induced aggregation of α-synuclein. *Proceedings of the National Academy of Sciences of the United States of America*, *113*(26), 7065–7070. https://doi.org/10.1073/pnas.1601899113

Galvagnion, C., Buell, A. K., Meisl, G., Michaels, T. C., Vendruscolo, M., Knowles, T. P., & Dobson, C. M. (2015). Lipid vesicles trigger α-synuclein aggregation by stimulating primary nucleation. *Nature chemical biology*, *11*(3), 229–234. https://doi.org/10.1038/nchembio.1750

Gao, X., Carroni, M., Nussbaum-Krammer, C., Mogk, A., Nillegoda, N. B., Szlachcic, A., Guilbride, D. L., Saibil, H. R., Mayer, M. P., & Bukau, B. (2015). Human Hsp70

References

Disaggregase Reverses Parkinson's-Linked α-Synuclein Amyloid Fibrils. *Molecular cell*, *59*(5), 781–793. https://doi.org/10.1016/j.molcel.2015.07.012

Gaspar, R., Meisl, G., Buell, A. K., Young, L., Kaminski, C. F., Knowles, T., Sparr, E., & Linse, S. (2017). Secondary nucleation of monomers on fibril surface dominates α-synuclein aggregation and provides autocatalytic amyloid amplification. *Quarterly reviews of biophysics*, *50*, e6. https://doi.org/10.1017/S0033583516000172

Gates, S. N., Yokom, A. L., Lin, J., Jackrel, M. E., Rizo, A. N., Kendsersky, N. M., Buell, C. E., Sweeny, E. A., Mack, K. L., Chuang, E., Torrente, M. P., Su, M., Shorter, J., & Southworth, D. R. (2017). Ratchet-like polypeptide translocation mechanism of the AAA+ disaggregase Hsp104. *Science (New York, N.Y.)*, *357*(6348), 273–279. https://doi.org/10.1126/science.aan1052

Gath, J., Bousset, L., Habenstein, B., Melki, R., Böckmann, A., & Meier, B. H. (2014). Unlike twins: an NMR comparison of two α-synuclein polymorphs featuring different toxicity. *PloS one*, *9*(3), e90659. https://doi.org/10.1371/journal.pone.0090659

Gestaut, D., Limatola, A., Joachimiak, L., & Frydman, J. (2019). The ATP-powered gymnastics of TRiC/CCT: an asymmetric protein folding machine with a symmetric origin story. *Current opinion in structural biology*, *55*, 50–58. https://doi.org/10.1016/j.sbi.2019.03.002

Ghag, G., Bhatt, N., Cantu, D. V., Guerrero-Munoz, M. J., Ellsworth, A., Sengupta, U., & Kayed, R. (2018). Soluble tau aggregates, not large fibrils, are the toxic species that display seeding and cross-seeding behavior. *Protein science : a publication of the Protein Society*, *27*(11), 1901–1909. https://doi.org/10.1002/pro.3499

Giehm, L., Oliveira, C. L., Christiansen, G., Pedersen, J. S., & Otzen, D. E. (2010). SDS-induced fibrillation of alpha-synuclein: an alternative fibrillation pathway. *Journal of molecular biology*, *401*(1), 115–133. https://doi.org/10.1016/j.jmb.2010.05.060

Goedert, M., & Spillantini, M. G. (2000). Tau mutations in frontotemporal dementia FTDP-17 and their relevance for Alzheimer's disease. *Biochimica et biophysica acta*, *1502*(1), 110–121. https://doi.org/10.1016/s0925-4439(00)00037-5

Goedert, M., Jakes, R., Spillantini, M. G., Hasegawa, M., Smith, M. J., & Crowther, R. A. (1996). Assembly of microtubule-associated protein tau into Alzheimer-like filaments induced by sulphated glycosaminoglycans. *Nature*, *383*(6600), 550–553. https://doi.org/10.1038/383550a0

Goedert, M., Masuda-Suzukake, M., & Falcon, B. (2017). Like prions: the propagation of aggregated tau and α-synuclein in neurodegeneration. *Brain : a journal of neurology*, *140*(2), 266–278. https://doi.org/10.1093/brain/aww230

Goedert, M., Spillantini, M. G., Jakes, R., Rutherford, D., & Crowther, R. A. (1989). Multiple isoforms of human microtubule-associated protein tau: sequences and localization in neurofibrillary tangles of Alzheimer's disease. *Neuron*, *3*(4), 519–526. https://doi.org/10.1016/0896-6273(89)90210-9

González, N., Arcos-López, T., König, A., Quintanar, L., Menacho Márquez, M., Outeiro, T. F., & Fernández, C. O. (2019). Effects of alpha-synuclein post-translational modifications on metal binding. *Journal of neurochemistry*, *150*(5), 507–521. https://doi.org/10.1111/jnc.14721

Götz, J., Halliday, G., & Nisbet, R. M. (2019). Molecular Pathogenesis of the Tauopathies. *Annual review of pathology*, *14*, 239–261. https://doi.org/10.1146/annurev-pathmechdis-012418-012936

Grey, M., Dunning, C. J., Gaspar, R., Grey, C., Brundin, P., Sparr, E., & Linse, S. (2015). Acceleration of α-synuclein aggregation by exosomes. *The Journal of biological chemistry*, *290*(5), 2969–2982. https://doi.org/10.1074/jbc.M114.585703

Grey, M., Linse, S., Nilsson, H., Brundin, P., & Sparr, E. (2011). Membrane interaction of α-synuclein in different aggregation states. *Journal of Parkinson's disease*, *1*(4), 359–371. https://doi.org/10.3233/JPD-2011-11067

Guerrero-Ferreira, R., Kovacik, L., Ni, D., & Stahlberg, H. (2020). New insights on the structure of alpha-synuclein fibrils using cryo-electron microscopy. *Current opinion in neurobiology*, *61*, 89–95. https://doi.org/10.1016/j.conb.2020.01.014

Guerrero-Ferreira, R., Taylor, N. M., Arteni, A. A., Kumari, P., Mona, D., Ringler, P., Britschgi, M., Lauer, M. E., Makky, A., Verasdonck, J., Riek, R., Melki, R., Meier, B. H., Böckmann, A., Bousset, L., & Stahlberg, H. (2019). Two new polymorphic structures of human full-length alpha-synuclein fibrils solved by cryo-electron microscopy. *eLife*, *8*, e48907. https://doi.org/10.7554/eLife.48907

Guerrero-Ferreira, R., Taylor, N. M., Mona, D., Ringler, P., Lauer, M. E., Riek, R., Britschgi, M., & Stahlberg, H. (2018). Cryo-EM structure of alpha-synuclein fibrils. *eLife*, *7*, e36402. https://doi.org/10.7554/eLife.36402

Guo, Q., Lehmer, C., Martínez-Sánchez, A., Rudack, T., Beck, F., Hartmann, H., Pérez-Berlanga, M., Frottin, F., Hipp, M. S., Hartl, F. U., Edbauer, D., Baumeister, W., & Fernández-Busnadiego, R. (2018). In Situ Structure of Neuronal C9orf72 Poly-GA

References

Aggregates Reveals Proteasome Recruitment. *Cell*, *172*(4), 696–705.e12. https://doi.org/10.1016/j.cell.2017.12.030

Gustke, N., Trinczek, B., Biernat, J., Mandelkow, E. M., & Mandelkow, E. (1994). Domains of tau protein and interactions with microtubules. *Biochemistry*, *33*(32), 9511–9522. https://doi.org/10.1021/bi00198a017

Hipp, M. S., Kasturi, P., & Hartl, F. U. (2019). The proteostasis network and its decline in ageing. *Nature reviews. Molecular cell biology*, *20*(7), 421–435. https://doi.org/10.1038/s41580-019-0101-y

Hipp, M. S., Park, S. H., & Hartl, F. U. (2014). Proteostasis impairment in protein-misfolding and -aggregation diseases. *Trends in cell biology*, *24*(9), 506–514. https://doi.org/10.1016/j.tcb.2014.05.003

Hjerpe, R., Bett, J. S., Keuss, M. J., Solovyova, A., McWilliams, T. G., Johnson, C., Sahu, I., Varghese, J., Wood, N., Wightman, M., Osborne, G., Bates, G. P., Glickman, M. H., Trost, M., Knebel, A., Marchesi, F., & Kurz, T. (2016). UBQLN2 Mediates Autophagy-Independent Protein Aggregate Clearance by the Proteasome. *Cell*, *166*(4), 935–949. https://doi.org/10.1016/j.cell.2016.07.001

Höglinger, G. U., Respondek, G., & Kovacs, G. G. (2018). New classification of tauopathies. *Revue neurologique*, *174*(9), 664–668. https://doi.org/10.1016/j.neurol.2018.07.001

Hoyer, W., Cherny, D., Subramaniam, V., & Jovin, T. M. (2004). Impact of the acidic C-terminal region comprising amino acids 109-140 on alpha-synuclein aggregation in vitro. *Biochemistry*, *43*(51), 16233–16242. https://doi.org/10.1021/bi048453u

Huang, C., Cheng, H., Hao, S., Zhou, H., Zhang, X., Gao, J., Sun, Q. H., Hu, H., & Wang, C. C. (2006). Heat shock protein 70 inhibits alpha-synuclein fibril formation via interactions with diverse intermediates. *Journal of molecular biology*, *364*(3), 323–336. https://doi.org/10.1016/j.jmb.2006.08.062

Huang, C., Ren, G., Zhou, H., & Wang, C. C. (2005). A new method for purification of recombinant human alpha-synuclein in Escherichia coli. *Protein expression and purification*, *42*(1), 173–177. https://doi.org/10.1016/j.pep.2005.02.014

Huang, X., Luan, B., Wu, J., & Shi, Y. (2016). An atomic structure of the human 26S proteasome. *Nature structural & molecular biology*, *23*(9), 778–785. https://doi.org/10.1038/nsmb.3273

Hutton, M., Lendon, C. L., Rizzu, P., Baker, M., Froelich, S., Houlden, H., Pickering-Brown, S., Chakraverty, S., Isaacs, A., Grover, A., Hackett, J., Adamson, J., Lincoln, S., Dickson,

D., Davies, P., Petersen, R. C., Stevens, M., de Graaff, E., Wauters, E., van Baren, J., … Heutink, P. (1998). Association of missense and 5'-splice-site mutations in tau with the inherited dementia FTDP-17. *Nature*, *393*(6686), 702–705. https://doi.org/10.1038/31508

Ikenoue, T., Lee, Y. H., Kardos, J., Saiki, M., Yagi, H., Kawata, Y., & Goto, Y. (2014). Cold denaturation of α-synuclein amyloid fibrils. *Angewandte Chemie (International ed. in English)*, *53*(30), 7799–7804. https://doi.org/10.1002/anie.201403815

Iljina, M., Garcia, G. A., Horrocks, M. H., Tosatto, L., Choi, M. L., Ganzinger, K. A., Abramov, A. Y., Gandhi, S., Wood, N. W., Cremades, N., Dobson, C. M., Knowles, T. P., & Klenerman, D. (2016). Kinetic model of the aggregation of alpha-synuclein provides insights into prion-like spreading. *Proceedings of the National Academy of Sciences of the United States of America*, *113*(9), E1206–E1215. https://doi.org/10.1073/pnas.1524128113

Iwai, A., Masliah, E., Yoshimoto, M., Ge, N., Flanagan, L., de Silva, H. A., Kittel, A., & Saitoh, T. (1995). The precursor protein of non-A beta component of Alzheimer's disease amyloid is a presynaptic protein of the central nervous system. *Neuron*, *14*(2), 467–475. https://doi.org/10.1016/0896-6273(95)90302-x

Iyer, A., Roeters, S. J., Kogan, V., Woutersen, S., Claessens, M., & Subramaniam, V. (2017). C-Terminal Truncated α-Synuclein Fibrils Contain Strongly Twisted β-Sheets. *Journal of the American Chemical Society*, *139*(43), 15392–15400. https://doi.org/10.1021/jacs.7b07403

Izawa, Y., Tateno, H., Kameda, H., Hirakawa, K., Hato, K., Yagi, H., Hongo, K., Mizobata, T., & Kawata, Y. (2012). Role of C-terminal negative charges and tyrosine residues in fibril formation of α-synuclein. *Brain and behavior*, *2*(5), 595–605. https://doi.org/10.1002/brb3.86

Jarrett, J. T., & Lansbury, P. T., Jr (1992). Amyloid fibril formation requires a chemically discriminating nucleation event: studies of an amyloidogenic sequence from the bacterial protein OsmB. *Biochemistry*, *31*(49), 12345–12352. https://doi.org/10.1021/bi00164a008

Jeganathan, S., von Bergen, M., Mandelkow, E. M., & Mandelkow, E. (2008). The natively unfolded character of tau and its aggregation to Alzheimer-like paired helical filaments. *Biochemistry*, *47*(40), 10526–10539. https://doi.org/10.1021/bi800783d

Jia, C., Ma, X., Liu, Z., Gu, J., Zhang, X., Li, D., & Zhang, S. (2019). Different Heat Shock Proteins Bind α-Synuclein With Distinct Mechanisms and Synergistically Prevent Its Amyloid Aggregation. *Frontiers in neuroscience*, *13*, 1124. https://doi.org/10.3389/fnins.2019.01124

References

Jucker, M., & Walker, L. C. (2013). Self-propagation of pathogenic protein aggregates in neurodegenerative diseases. *Nature*, *501*(7465), 45–51. https://doi.org/10.1038/nature12481

Kakkar, V., Månsson, C., de Mattos, E. P., Bergink, S., van der Zwaag, M., van Waarde, M., Kloosterhuis, N. J., Melki, R., van Cruchten, R., Al-Karadaghi, S., Arosio, P., Dobson, C. M., Knowles, T., Bates, G. P., van Deursen, J. M., Linse, S., van de Sluis, B., Emanuelsson, C., & Kampinga, H. H. (2016). The S/T-Rich Motif in the DNAJB6 Chaperone Delays Polyglutamine Aggregation and the Onset of Disease in a Mouse Model. *Molecular cell*, *62*(2), 272–283. https://doi.org/10.1016/j.molcel.2016.03.017

Kampers, T., Friedhoff, P., Biernat, J., Mandelkow, E. M., & Mandelkow, E. (1996). RNA stimulates aggregation of microtubule-associated protein tau into Alzheimer-like paired helical filaments. *FEBS letters*, *399*(3), 344–349. https://doi.org/10.1016/s0014-5793(96)01386-5

Kampinga, H. H., & Craig, E. A. (2010). The HSP70 chaperone machinery: J proteins as drivers of functional specificity. *Nature reviews. Molecular cell biology*, *11*(8), 579–592. https://doi.org/10.1038/nrm2941

Kara, E., Marks, J. D., & Aguzzi, A. (2018). Toxic Protein Spread in Neurodegeneration: Reality versus Fantasy. *Trends in molecular medicine*, *24*(12), 1007–1020. https://doi.org/10.1016/j.molmed.2018.09.004

Kästle, M., & Grune, T. (2012). Interactions of the proteasomal system with chaperones: protein triage and protein quality control. *Progress in molecular biology and translational science*, *109*, 113–160. https://doi.org/10.1016/B978-0-12-397863-9.00004-3

Kellie, J. F., Higgs, R. E., Ryder, J. W., Major, A., Beach, T. G., Adler, C. H., Merchant, K., & Knierman, M. D. (2014). Quantitative measurement of intact alpha-synuclein proteoforms from post-mortem control and Parkinson's disease brain tissue by intact protein mass spectrometry. *Scientific reports*, *4*, 5797. https://doi.org/10.1038/srep05797

Kellogg, E. H., Hejab, N., Poepsel, S., Downing, K. H., DiMaio, F., & Nogales, E. (2018). Near-atomic model of microtubule-tau interactions. *Science (New York, N.Y.)*, *360*(6394), 1242–1246. https://doi.org/10.1126/science.aat1780

Kirstein, J., Arnsburg, K., Scior, A., Szlachcic, A., Guilbride, D. L., Morimoto, R. I., Bukau, B., & Nillegoda, N. B. (2017). In vivo properties of the disaggregase function of J-proteins

and Hsc70 in Caenorhabditis elegans stress and aging. *Aging cell*, *16*(6), 1414–1424. https://doi.org/10.1111/acel.12686

Klein, C., & Westenberger, A. (2012). Genetics of Parkinson's disease. *Cold Spring Harbor perspectives in medicine*, *2*(1), a008888. https://doi.org/10.1101/cshperspect.a008888

Knowles, T. P., Waudby, C. A., Devlin, G. L., Cohen, S. I., Aguzzi, A., Vendruscolo, M., Terentjev, E. M., Welland, M. E., & Dobson, C. M. (2009). An analytical solution to the kinetics of breakable filament assembly. *Science (New York, N.Y.)*, *326*(5959), 1533–1537. https://doi.org/10.1126/science.1178250

Komander, D., & Rape, M. (2012). The ubiquitin code. *Annual review of biochemistry*, *81*, 203–229. https://doi.org/10.1146/annurev-biochem-060310-170328

Kontaxi, C., Piccardo, P., & Gill, A. C. (2017). Lysine-Directed Post-translational Modifications of Tau Protein in Alzheimer's Disease and Related Tauopathies. *Frontiers in molecular biosciences*, *4*, 56. https://doi.org/10.3389/fmolb.2017.00056

Kopito R. R. (2000). Aggresomes, inclusion bodies and protein aggregation. *Trends in cell biology*, *10*(12), 524–530. https://doi.org/10.1016/s0962-8924(00)01852-3

Krishnan, R., Goodman, J. L., Mukhopadhyay, S., Pacheco, C. D., Lemke, E. A., Deniz, A. A., & Lindquist, S. (2012). Conserved features of intermediates in amyloid assembly determine their benign or toxic states. *Proceedings of the National Academy of Sciences of the United States of America*, *109*(28), 11172–11177. https://doi.org/10.1073/pnas.1209527109

Kulkarni, V. V., & Maday, S. (2018). Compartment-specific dynamics and functions of autophagy in neurons. *Developmental neurobiology*, *78*(3), 298–310. https://doi.org/10.1002/dneu.22562

Labbadia, J., & Morimoto, R. I. (2015). The biology of proteostasis in aging and disease. *Annual review of biochemistry*, *84*, 435–464. https://doi.org/10.1146/annurev-biochem-060614-033955

Ladiwala, A. R., Litt, J., Kane, R. S., Aucoin, D. S., Smith, S. O., Ranjan, S., Davis, J., Van Nostrand, W. E., & Tessier, P. M. (2012). Conformational differences between two amyloid β oligomers of similar size and dissimilar toxicity. *The Journal of biological chemistry*, *287*(29), 24765–24773. https://doi.org/10.1074/jbc.M111.329763

Lasagna-Reeves, C. A., Castillo-Carranza, D. L., Guerrero-Muoz, M. J., Jackson, G. R., & Kayed, R. (2010). Preparation and characterization of neurotoxic tau oligomers. *Biochemistry*, *49*(47), 10039–10041. https://doi.org/10.1021/bi1016233

References

Levitan, K., Chereau, D., Cohen, S. I., Knowles, T. P., Dobson, C. M., Fink, A. L., Anderson, J. P., Goldstein, J. M., & Millhauser, G. L. (2011). Conserved C-terminal charge exerts a profound influence on the aggregation rate of α-synuclein. *Journal of molecular biology*, *411*(2), 329–333. https://doi.org/10.1016/j.jmb.2011.05.046

Li, B., Ge, P., Murray, K. A., Sheth, P., Zhang, M., Nair, G., Sawaya, M. R., Shin, W. S., Boyer, D. R., Ye, S., Eisenberg, D. S., Zhou, Z. H., & Jiang, L. (2018). Cryo-EM of full-length α-synuclein reveals fibril polymorphs with a common structural kernel. *Nature communications*, *9*(1), 3609. https://doi.org/10.1038/s41467-018-05971-2

Li, H. T., Du, H. N., Tang, L., Hu, J., & Hu, H. Y. (2002). Structural transformation and aggregation of human alpha-synuclein in trifluoroethanol: non-amyloid component sequence is essential and beta-sheet formation is prerequisite to aggregation. *Biopolymers*, *64*(4), 221–226. https://doi.org/10.1002/bip.10179

Li, W., West, N., Colla, E., Pletnikova, O., Troncoso, J. C., Marsh, L., Dawson, T. M., Jäkälä, P., Hartmann, T., Price, D. L., & Lee, M. K. (2005). Aggregation promoting C-terminal truncation of alpha-synuclein is a normal cellular process and is enhanced by the familial Parkinson's disease-linked mutations. *Proceedings of the National Academy of Sciences of the United States of America*, *102*(6), 2162–2167. https://doi.org/10.1073/pnas.0406976102

Li, Y., Zhao, C., Luo, F., Liu, Z., Gui, X., Luo, Z., Zhang, X., Li, D., Liu, C., & Li, X. (2018). Amyloid fibril structure of α-synuclein determined by cryo-electron microscopy. *Cell research*, *28*(9), 897–903. https://doi.org/10.1038/s41422-018-0075-x

Liberski, P. P., Brown, P., Xiao, S. Y., & Gajdusek, D. C. (1991). The ultrastructural diversity of scrapie-associated fibrils isolated from experimental scrapie and Creutzfeldt-Jakob disease. *Journal of comparative pathology*, *105*(4), 377–386. https://doi.org/10.1016/s0021-9975(08)80107-7

Liu, C. W., Giasson, B. I., Lewis, K. A., Lee, V. M., Demartino, G. N., & Thomas, P. J. (2005). A precipitating role for truncated alpha-synuclein and the proteasome in alpha-synuclein aggregation: implications for pathogenesis of Parkinson disease. *The Journal of biological chemistry*, *280*(24), 22670–22678. https://doi.org/10.1074/jbc.M501508200

Lorenzen, N., Nielsen, S. B., Buell, A. K., Kaspersen, J. D., Arosio, P., Vad, B. S., Paslawski, W., Christiansen, G., Valnickova-Hansen, Z., Andreasen, M., Enghild, J. J., Pedersen, J. S., Dobson, C. M., Knowles, T. P., & Otzen, D. E. (2014). The role of stable α-synuclein oligomers in the molecular events underlying amyloid formation. *Journal of the American Chemical Society*, *136*(10), 3859–3868. https://doi.org/10.1021/ja411577t

Lu, J. X., Qiang, W., Yau, W. M., Schwieters, C. D., Meredith, S. C., & Tycko, R. (2013). Molecular structure of β-amyloid fibrils in Alzheimer's disease brain tissue. *Cell*, *154*(6), 1257–1268. https://doi.org/10.1016/j.cell.2013.08.035

Luheshi, L. M., Hoyer, W., de Barros, T. P., van Dijk Härd, I., Brorsson, A. C., Macao, B., Persson, C., Crowther, D. C., Lomas, D. A., Ståhl, S., Dobson, C. M., & Härd, T. (2010). Sequestration of the Abeta peptide prevents toxicity and promotes degradation in vivo. *PLoS biology*, *8*(3), e1000334. https://doi.org/10.1371/journal.pbio.1000334

Ma, L., Yang, C., Zhang, X., Li, Y., Wang, S., Zheng, L., & Huang, K. (2018). C-terminal truncation exacerbates the aggregation and cytotoxicity of α-Synuclein: A vicious cycle in Parkinson's disease. *Biochimica et biophysica acta. Molecular basis of disease*, *1864*(12), 3714–3725. https://doi.org/10.1016/j.bbadis.2018.10.003

Maday S. (2016). Mechanisms of neuronal homeostasis: Autophagy in the axon. *Brain research*, *1649*(Pt B), 143–150. https://doi.org/10.1016/j.brainres.2016.03.047

Mahul-Mellier, A. L., Burtscher, J., Maharjan, N., Weerens, L., Croisier, M., Kuttler, F., Leleu, M., Knott, G. W., & Lashuel, H. A. (2020). The process of Lewy body formation, rather than simply α-synuclein fibrillization, is one of the major drivers of neurodegeneration. *Proceedings of the National Academy of Sciences of the United States of America*, *117*(9), 4971–4982. https://doi.org/10.1073/pnas.1913904117

Mahul-Mellier, A.L., Altay, M.F., Burtscher, J., Maharjan, N., Ait-Bouziad, N., Chiki,A., Vingill,S., Wade-Martins, R., Holton, J., Strand, C., Haikal,C., Li, J.Y., Hamelin, R., Croisier, M., Knott, G., Mairet-Coello, G., Weerens, L., Michel, A., Downey, P., Citron, M., Lashuel, H.A. (2018). The making of a Lewy body: the role of α-synuclein post-fibrillization modifications in regulating the formation and the maturation of pathological inclusions. bioRxiv https://doi.org/10.1101/500058

Mainz, A., Peschek, J., Stavropoulou, M., Back, K. C., Bardiaux, B., Asami, S., Prade, E., Peters, C., Weinkauf, S., Buchner, J., & Reif, B. (2015). The chaperone αB-crystallin uses different interfaces to capture an amorphous and an amyloid client. *Nature structural & molecular biology*, *22*(11), 898–905. https://doi.org/10.1038/nsmb.3108

Makky, A., Bousset, L., Polesel-Maris, J., & Melki, R. (2016). Nanomechanical properties of distinct fibrillar polymorphs of the protein α-synuclein. *Scientific reports*, *6*, 37970. https://doi.org/10.1038/srep37970

Malinovska, L., Kroschwald, S., Munder, M. C., Richter, D., & Alberti, S. (2012). Molecular chaperones and stress-inducible protein-sorting factors coordinate the spatiotemporal distribution of protein aggregates. *Molecular biology of the cell*, *23*(16), 3041–3056. https://doi.org/10.1091/mbc.E12-03-0194

References

Mannini, B., Cascella, R., Zampagni, M., van Waarde-Verhagen, M., Meehan, S., Roodveldt, C., Campioni, S., Boninsegna, M., Penco, A., Relini, A., Kampinga, H. H., Dobson, C. M., Wilson, M. R., Cecchi, C., & Chiti, F. (2012). Molecular mechanisms used by chaperones to reduce the toxicity of aberrant protein oligomers. *Proceedings of the National Academy of Sciences of the United States of America*, *109*(31), 12479–12484. https://doi.org/10.1073/pnas.1117799109

Mannini, B., Mulvihill, E., Sgromo, C., Cascella, R., Khodarahmi, R., Ramazzotti, M., Dobson, C. M., Cecchi, C., & Chiti, F. (2014). Toxicity of protein oligomers is rationalized by a function combining size and surface hydrophobicity. *ACS chemical biology*, *9*(10), 2309–2317. https://doi.org/10.1021/cb500505m

Månsson, C., Arosio, P., Hussein, R., Kampinga, H. H., Hashem, R. M., Boelens, W. C., Dobson, C. M., Knowles, T. P., Linse, S., & Emanuelsson, C. (2014). Interaction of the molecular chaperone DNAJB6 with growing amyloid-beta 42 (Aβ42) aggregates leads to sub-stoichiometric inhibition of amyloid formation. *The Journal of biological chemistry*, *289*(45), 31066–31076. https://doi.org/10.1074/jbc.M114.595124

Månsson, C., van Cruchten, R., Weininger, U., Yang, X., Cukalevski, R., Arosio, P., Dobson, C. M., Knowles, T., Akke, M., Linse, S., & Emanuelsson, C. (2018). Conserved S/T Residues of the Human Chaperone DNAJB6 Are Required for Effective Inhibition of Aβ42 Amyloid Fibril Formation. *Biochemistry*, *57*(32), 4891–4902. https://doi.org/10.1021/acs.biochem.8b00353

Månsson, C., van Cruchten, R., Weininger, U., Yang, X., Cukalevski, R., Arosio, P., Dobson, C. M., Knowles, T., Akke, M., Linse, S., & Emanuelsson, C. (2018). Conserved S/T Residues of the Human Chaperone DNAJB6 Are Required for Effective Inhibition of Aβ42 Amyloid Fibril Formation. *Biochemistry*, *57*(32), 4891–4902. https://doi.org/10.1021/acs.biochem.8b00353

Martinez-Lopez, N., Athonvarangkul, D., & Singh, R. (2015). Autophagy and aging. *Advances in experimental medicine and biology*, *847*, 73–87. https://doi.org/10.1007/978-1-4939-2404-2_3

Mattoo, R. U., Sharma, S. K., Priya, S., Finka, A., & Goloubinoff, P. (2013). Hsp110 is a bona fide chaperone using ATP to unfold stable misfolded polypeptides and reciprocally collaborate with Hsp70 to solubilize protein aggregates. *The Journal of biological chemistry*, *288*(29), 21399–21411. https://doi.org/10.1074/jbc.M113.479253

Mayer, L. D., Hope, M. J., & Cullis, P. R. (1986). Vesicles of variable sizes produced by a rapid extrusion procedure. *Biochimica et biophysica acta*, *858*(1), 161–168. https://doi.org/10.1016/0005-2736(86)90302-0

McKinley, M. P., Bolton, D. C., & Prusiner, S. B. (1983). A protease-resistant protein is a structural component of the scrapie prion. *Cell*, *35*(1), 57–62. https://doi.org/10.1016/0092-8674(83)90207-6

McKinnon, C., & Tabrizi, S. J. (2014). The ubiquitin-proteasome system in neurodegeneration. *Antioxidants & redox signaling*, *21*(17), 2302–2321. https://doi.org/10.1089/ars.2013.5802

Meade, R. M., Williams, R. J., & Mason, J. M. (2020). A series of helical α-synuclein fibril polymorphs are populated in the presence of lipid vesicles. *NPJ Parkinson's disease*, *6*, 17. https://doi.org/10.1038/s41531-020-00122-1

Meisl, G., Knowles, T. P., & Klenerman, D. (2020). The molecular processes underpinning prion-like spreading and seed amplification in protein aggregation. *Current opinion in neurobiology*, *61*, 58–64. https://doi.org/10.1016/j.conb.2020.01.010

Meisl, G., Yang, X., Hellstrand, E., Frohm, B., Kirkegaard, J. B., Cohen, S. I., Dobson, C. M., Linse, S., & Knowles, T. P. (2014). Differences in nucleation behavior underlie the contrasting aggregation kinetics of the Aβ40 and Aβ42 peptides. *Proceedings of the National Academy of Sciences of the United States of America*, *111*(26), 9384–9389. https://doi.org/10.1073/pnas.1401564111

Michaels, T., Šarić, A., Curk, S., Bernfur, K., Arosio, P., Meisl, G., Dear, A. J., Cohen, S., Dobson, C. M., Vendruscolo, M., Linse, S., & Knowles, T. (2020). Dynamics of oligomer populations formed during the aggregation of Alzheimer's Aβ42 peptide. *Nature chemistry*, *12*(5), 445–451. https://doi.org/10.1038/s41557-020-0452-1

Michell, A. W., Tofaris, G. K., Gossage, H., Tyers, P., Spillantini, M. G., & Barker, R. A. (2007). The effect of truncated human alpha-synuclein (1-120) on dopaminergic cells in a transgenic mouse model of Parkinson's disease. *Cell transplantation*, *16*(5), 461–474. https://doi.org/10.3727/000000007783464911

Miller, S. B., Ho, C. T., Winkler, J., Khokhrina, M., Neuner, A., Mohamed, M. Y., Guilbride, D. L., Richter, K., Lisby, M., Schiebel, E., Mogk, A., & Bukau, B. (2015). Compartment-specific aggregases direct distinct nuclear and cytoplasmic aggregate deposition. *The EMBO journal*, *34*(6), 778–797. https://doi.org/10.15252/embj.201489524

Min, S. W., Cho, S. H., Zhou, Y., Schroeder, S., Haroutunian, V., Seeley, W. W., Huang, E. J., Shen, Y., Masliah, E., Mukherjee, C., Meyers, D., Cole, P. A., Ott, M., & Gan, L. (2010). Acetylation of tau inhibits its degradation and contributes to tauopathy. *Neuron*, *67*(6), 953–966. https://doi.org/10.1016/j.neuron.2010.08.044

Mirbaha, H., Chen, D., Morazova, O. A., Ruff, K. M., Sharma, A. M., Liu, X., Goodarzi, M., Pappu, R. V., Colby, D. W., Mirzaei, H., Joachimiak, L. A., & Diamond, M. I. (2018).

References

Inert and seed-competent tau monomers suggest structural origins of aggregation. *eLife*, *7*, e36584. https://doi.org/10.7554/eLife.36584

Mirbaha, H., Holmes, B. B., Sanders, D. W., Bieschke, J., & Diamond, M. I. (2015). Tau Trimers Are the Minimal Propagation Unit Spontaneously Internalized to Seed Intracellular Aggregation. *The Journal of biological chemistry*, *290*(24), 14893–14903. https://doi.org/10.1074/jbc.M115.652693

Mishizen-Eberz, A. J., Guttmann, R. P., Giasson, B. I., Day, G. A., 3rd, Hodara, R., Ischiropoulos, H., Lee, V. M., Trojanowski, J. Q., & Lynch, D. R. (2003). Distinct cleavage patterns of normal and pathologic forms of alpha-synuclein by calpain I in vitro. *Journal of neurochemistry*, *86*(4), 836–847. https://doi.org/10.1046/j.1471-4159.2003.01878.x

Mogk, A., Kummer, E., & Bukau, B. (2015). Cooperation of Hsp70 and Hsp100 chaperone machines in protein disaggregation. *Frontiers in molecular biosciences*, *2*, 22. https://doi.org/10.3389/fmolb.2015.00022

Moors T.E., Maat, C.A., Niedieker, D., Mona, D., Petersen, D., Timmermans-Huisman, E., Kole, J., El-Mashtoly, S.F., Spycher, L., Zago,W., Barbour, R., Mundigl, O., Kaluza, K., Huber, S., Hug, M.N., Kremer, T., Ritter,M., Dziadek, S., Geurts, J.J.G., Gerwert, K., Britschgi, M., van de Berg, W.D.J. (2018) Subcellular orchestration of alpha-synuclein variants in Parkinson's disease brains revealed by 3D multicolor STED microscopy. bioRxiv https://doi.org/10.1101/470476

Morales, R., Moreno-Gonzalez, I., & Soto, C. (2013). Cross-seeding of misfolded proteins: implications for etiology and pathogenesis of protein misfolding diseases. *PLoS pathogens*, *9*(9), e1003537. https://doi.org/10.1371/journal.ppat.1003537

Morán Luengo, T., Mayer, M. P., & Rüdiger, S. (2019). The Hsp70-Hsp90 Chaperone Cascade in Protein Folding. *Trends in cell biology*, *29*(2), 164–177. https://doi.org/10.1016/j.tcb.2018.10.004

Muntané, G., Ferrer, I., & Martinez-Vicente, M. (2012). α-synuclein phosphorylation and truncation are normal events in the adult human brain. *Neuroscience*, *200*, 106–119. https://doi.org/10.1016/j.neuroscience.2011.10.042

Murray, I. V., Giasson, B. I., Quinn, S. M., Koppaka, V., Axelsen, P. H., Ischiropoulos, H., Trojanowski, J. Q., & Lee, V. M. (2003). Role of alpha-synuclein carboxy-terminus on fibril formation in vitro. *Biochemistry*, *42*(28), 8530–8540. https://doi.org/10.1021/bi027363r

Nachman, E., Wentink, A. S., Madiona, K., Bousset, L., Katsinelos, T., Allinson, K., Kampinga, H., McEwan, W. A., Jahn, T. R., Melki, R., Mogk, A., Bukau, B., & Nussbaum-Krammer, C. (2020). Disassembly of Tau fibrils by the human Hsp70 disaggregation machinery generates small seeding-competent species. *The Journal of biological chemistry*, *295*(28), 9676–9690. https://doi.org/10.1074/jbc.RA120.013478

Nachman, E., Wentink, A. S., Madiona, K., Bousset, L., Katsinelos, T., Allinson, K., Kampinga, H., McEwan, W. A., Jahn, T. R., Melki, R., Mogk, A., Bukau, B., & Nussbaum-Krammer, C. (2020). Disassembly of Tau fibrils by the human Hsp70 disaggregation machinery generates small seeding-competent species. *The Journal of biological chemistry*, *295*(28), 9676–9690. https://doi.org/10.1074/jbc.RA120.013478

Ni, X., McGlinchey, R. P., Jiang, J., & Lee, J. C. (2019). Structural Insights into α-Synuclein Fibril Polymorphism: Effects of Parkinson's Disease-Related C-Terminal Truncations. *Journal of molecular biology*, *431*(19), 3913–3919. https://doi.org/10.1016/j.jmb.2019.07.001

Nillegoda, N. B., Kirstein, J., Szlachcic, A., Berynskyy, M., Stank, A., Stengel, F., Arnsburg, K., Gao, X., Scior, A., Aebersold, R., Guilbride, D. L., Wade, R. C., Morimoto, R. I., Mayer, M. P., & Bukau, B. (2015). Crucial HSP70 co-chaperone complex unlocks metazoan protein disaggregation. *Nature*, *524*(7564), 247–251. https://doi.org/10.1038/nature14884

Nillegoda, N. B., Stank, A., Malinverni, D., Alberts, N., Szlachcic, A., Barducci, A., De Los Rios, P., Wade, R. C., & Bukau, B. (2017). Evolution of an intricate J-protein network driving protein disaggregation in eukaryotes. *eLife*, *6*, e24560. https://doi.org/10.7554/eLife.24560

Ojha, J., Masilamoni, G., Dunlap, D., Udoff, R. A., & Cashikar, A. G. (2011). Sequestration of toxic oligomers by HspB1 as a cytoprotective mechanism. *Molecular and cellular biology*, *31*(15), 3146–3157. https://doi.org/10.1128/MCB.01187-10

Olzscha, H., Schermann, S. M., Woerner, A. C., Pinkert, S., Hecht, M. H., Tartaglia, G. G., Vendruscolo, M., Hayer-Hartl, M., Hartl, F. U., & Vabulas, R. M. (2011). Amyloid-like aggregates sequester numerous metastable proteins with essential cellular functions. *Cell*, *144*(1), 67–78. https://doi.org/10.1016/j.cell.2010.11.050

Paravastu, A. K., Leapman, R. D., Yau, W. M., & Tycko, R. (2008). Molecular structural basis for polymorphism in Alzheimer's beta-amyloid fibrils. *Proceedings of the National Academy of Sciences of the United States of America*, *105*(47), 18349–18354. https://doi.org/10.1073/pnas.0806270105

Park, S. H., Kukushkin, Y., Gupta, R., Chen, T., Konagai, A., Hipp, M. S., Hayer-Hartl, M., & Hartl, F. U. (2013). PolyQ proteins interfere with nuclear degradation of cytosolic

proteins by sequestering the Sis1p chaperone. *Cell*, *154*(1), 134–145. https://doi.org/10.1016/j.cell.2013.06.003

Park, S., Lee, J. H., Jeon, J. H., & Lee, M. J. (2018). Degradation or aggregation: the ramifications of post-translational modifications on tau. *BMB reports*, *51*(6), 265–273. https://doi.org/10.5483/bmbrep.2018.51.6.077

Pavel, M., Imarisio, S., Menzies, F. M., Jimenez-Sanchez, M., Siddiqi, F. H., Wu, X., Renna, M., O'Kane, C. J., Crowther, D. C., & Rubinsztein, D. C. (2016). CCT complex restricts neuropathogenic protein aggregation via autophagy. *Nature communications*, *7*, 13821. https://doi.org/10.1038/ncomms13821

Peelaerts, W., Bousset, L., Van der Perren, A., Moskalyuk, A., Pulizzi, R., Giugliano, M., Van den Haute, C., Melki, R., & Baekelandt, V. (2015). α-Synuclein strains cause distinct synucleinopathies after local and systemic administration. *Nature*, *522*(7556), 340–344. https://doi.org/10.1038/nature14547

Periquet, M., Fulga, T., Myllykangas, L., Schlossmacher, M. G., & Feany, M. B. (2007). Aggregated alpha-synuclein mediates dopaminergic neurotoxicity in vivo. *The Journal of neuroscience : the official journal of the Society for Neuroscience*, *27*(12), 3338–3346. https://doi.org/10.1523/JNEUROSCI.0285-07.2007

Polymeropoulos, M. H., Lavedan, C., Leroy, E., Ide, S. E., Dehejia, A., Dutra, A., Pike, B., Root, H., Rubenstein, J., Boyer, R., Stenroos, E. S., Chandrasekharappa, S., Athanassiadou, A., Papapetropoulos, T., Johnson, W. G., Lazzarini, A. M., Duvoisin, R. C., Di Iorio, G., Golbe, L. I., & Nussbaum, R. L. (1997). Mutation in the alpha-synuclein gene identified in families with Parkinson's disease. *Science (New York, N.Y.)*, *276*(5321), 2045–2047. https://doi.org/10.1126/science.276.5321.2045

Prasad, K., Beach, T. G., Hedreen, J., & Richfield, E. K. (2012). Critical role of truncated α-synuclein and aggregates in Parkinson's disease and incidental Lewy body disease. *Brain pathology (Zurich, Switzerland)*, *22*(6), 811–825. https://doi.org/10.1111/j.1750-3639.2012.00597.x

Prusiner S. B. (1982). Novel proteinaceous infectious particles cause scrapie. *Science (New York, N.Y.)*, *216*(4542), 136–144. https://doi.org/10.1126/science.6801762

Prusiner S. B. (2013). Biology and genetics of prions causing neurodegeneration. *Annual review of genetics*, *47*, 601–623. https://doi.org/10.1146/annurev-genet-110711-155524

Qiang, W., Yau, W. M., Lu, J. X., Collinge, J., & Tycko, R. (2017). Structural variation in amyloid-β fibrils from Alzheimer's disease clinical subtypes. *Nature*, *541*(7636), 217–221. https://doi.org/10.1038/nature20814

Ramachandran, G., & Udgaonkar, J. B. (2011). Understanding the kinetic roles of the inducer heparin and of rod-like protofibrils during amyloid fibril formation by Tau protein. *The Journal of biological chemistry*, *286*(45), 38948–38959. https://doi.org/10.1074/jbc.M111.271874

Raman, B., Ban, T., Sakai, M., Pasta, S. Y., Ramakrishna, T., Naiki, H., Goto, Y., & Rao, C. (2005). AlphaB-crystallin, a small heat-shock protein, prevents the amyloid fibril growth of an amyloid beta-peptide and beta2-microglobulin. *The Biochemical journal*, *392*(Pt 3), 573–581. https://doi.org/10.1042/BJ20050339

Rampelt, H., Kirstein-Miles, J., Nillegoda, N. B., Chi, K., Scholz, S. R., Morimoto, R. I., & Bukau, B. (2012). Metazoan Hsp70 machines use Hsp110 to power protein disaggregation. *The EMBO journal*, *31*(21), 4221–4235. https://doi.org/10.1038/emboj.2012.264

Rizzu, P., Van Swieten, J. C., Joosse, M., Hasegawa, M., Stevens, M., Tibben, A., Niermeijer, M. F., Hillebrand, M., Ravid, R., Oostra, B. A., Goedert, M., van Duijn, C. M., & Heutink, P. (1999). High prevalence of mutations in the microtubule-associated protein tau in a population study of frontotemporal dementia in the Netherlands. *American journal of human genetics*, *64*(2), 414–421. https://doi.org/10.1086/302256

Rodriguez, J. A., Ivanova, M. I., Sawaya, M. R., Cascio, D., Reyes, F. E., Shi, D., Sangwan, S., Guenther, E. L., Johnson, L. M., Zhang, M., Jiang, L., Arbing, M. A., Nannenga, B. L., Hattne, J., Whitelegge, J., Brewster, A. S., Messerschmidt, M., Boutet, S., Sauter, N. K., Gonen, T., … Eisenberg, D. S. (2015). Structure of the toxic core of α-synuclein from invisible crystals. *Nature*, *525*(7570), 486–490. https://doi.org/10.1038/nature15368

Roeters, S. J., Iyer, A., Pletikapić, G., Kogan, V., Subramaniam, V., & Woutersen, S. (2017). Evidence for Intramolecular Antiparallel Beta-Sheet Structure in Alpha-Synuclein Fibrils from a Combination of Two-Dimensional Infrared Spectroscopy and Atomic Force Microscopy. *Scientific reports*, *7*, 41051. https://doi.org/10.1038/srep41051

Rossi, M., Baiardi, S., & Parchi, P. (2019). Understanding Prion Strains: Evidence from Studies of the Disease Forms Affecting Humans. *Viruses*, *11*(4), 309. https://doi.org/10.3390/v11040309

Ruggeri, F. S., Flagmeier, P., Kumita, J. R., Meisl, G., Chirgadze, D. Y., Bongiovanni, M. N., Knowles, T., & Dobson, C. M. (2020). The Influence of Pathogenic Mutations in α-

References

Synuclein on Biophysical and Structural Characteristics of Amyloid Fibrils. *ACS nano*, *14*(5), 5213–5222. https://doi.org/10.1021/acsnano.9b09676

Runfola, M., De Simone, A., Vendruscolo, M., Dobson, C. M., & Fusco, G. (2020). The N-terminal Acetylation of α-Synuclein Changes the Affinity for Lipid Membranes but not the Structural Properties of the Bound State. *Scientific reports*, *10*(1), 204. https://doi.org/10.1038/s41598-019-57023-4

Saá, P., & Cervenakova, L. (2015). Protein misfolding cyclic amplification (PMCA): Current status and future directions. Virus research, 207, 47–61. https://doi.org/10.1016/j.virusres.2014.11.007

Schaffert, L. N., & Carter, W. G. (2020). Do Post-Translational Modifications Influence Protein Aggregation in Neurodegenerative Diseases: A Systematic Review. *Brain sciences*, *10*(4), 232. https://doi.org/10.3390/brainsci10040232

Scheckel, C., & Aguzzi, A. (2018). Prions, prionoids and protein misfolding disorders. *Nature reviews. Genetics*, *19*(7), 405–418. https://doi.org/10.1038/s41576-018-0011-4

Schneider, J. L., & Cuervo, A. M. (2013). Chaperone-mediated autophagy: dedicated saviour and unfortunate victim in the neurodegeneration arena. *Biochemical Society transactions*, *41*(6), 1483–1488. https://doi.org/10.1042/BST20130126

Schneider, M.M., Gautam, S., Herling, T.W., Andrzejewska, E., Krainer, G., Miller, A.M., Peter, Q.A.E., Ruggeri, F.S., Vendruscolo, M., Bracher, A., Dobson, C.M., Ulrich-Hartl, F., Knowles, T.P.J. (2020). The Hsc70 Disaggregation Machinery Removes Monomer Units Directly from α-Synuclein Fibril Ends. *bioRxiv* https://doi.org/10.1101/2020.11.02.365825

Schweighauser, M., Shi, Y., Tarutani, A., Kametani, F., Murzin, A. G., Ghetti, B., Matsubara, T., Tomita, T., Ando, T., Hasegawa, K., Murayama, S., Yoshida, M., Hasegawa, M., Scheres, S., & Goedert, M. (2020). Structures of α-synuclein filaments from multiple system atrophy. *Nature*, *585*(7825), 464–469. https://doi.org/10.1038/s41586-020-2317-6

Scior, A., Buntru, A., Arnsburg, K., Ast, A., Iburg, M., Juenemann, K., Pigazzini, M. L., Mlody, B., Puchkov, D., Priller, J., Wanker, E. E., Prigione, A., & Kirstein, J. (2018). Complete suppression of Htt fibrilization and disaggregation of Htt fibrils by a trimeric chaperone complex. *The EMBO journal*, *37*(2), 282–299. https://doi.org/10.15252/embj.201797212

Semerdzhiev, S. A., Dekker, D. R., Subramaniam, V., & Claessens, M. M. (2014). Self-assembly of protein fibrils into suprafibrillar aggregates: bridging the nano- and mesoscale. *ACS nano*, *8*(6), 5543–5551. https://doi.org/10.1021/nn406309c

Shahmoradian, S. H., Galaz-Montoya, J. G., Schmid, M. F., Cong, Y., Ma, B., Spiess, C., Frydman, J., Ludtke, S. J., & Chiu, W. (2013). TRiC's tricks inhibit huntingtin aggregation. *eLife*, *2*, e00710. https://doi.org/10.7554/eLife.00710

Shahmoradian, S. H., Lewis, A. J., Genoud, C., Hench, J., Moors, T. E., Navarro, P. P., Castaño-Díez, D., Schweighauser, G., Graff-Meyer, A., Goldie, K. N., Sütterlin, R., Huisman, E., Ingrassia, A., Gier, Y., Rozemuller, A., Wang, J., Paepe, A., Erny, J., Staempfli, A., Hoernschemeyer, J., … Lauer, M. E. (2019). Lewy pathology in Parkinson's disease consists of crowded organelles and lipid membranes. *Nature neuroscience*, *22*(7), 1099–1109. https://doi.org/10.1038/s41593-019-0423-2

Shammas, S. L., Waudby, C. A., Wang, S., Buell, A. K., Knowles, T. P., Ecroyd, H., Welland, M. E., Carver, J. A., Dobson, C. M., & Meehan, S. (2011). Binding of the molecular chaperone αB-crystallin to Aβ amyloid fibrils inhibits fibril elongation. *Biophysical journal*, *101*(7), 1681–1689. https://doi.org/10.1016/j.bpj.2011.07.056

Shorter J. (2011). The mammalian disaggregase machinery: Hsp110 synergizes with Hsp70 and Hsp40 to catalyze protein disaggregation and reactivation in a cell-free system. *PLoS one*, *6*(10), e26319. https://doi.org/10.1371/journal.pone.0026319

Silveira, J. R., Raymond, G. J., Hughson, A. G., Race, R. E., Sim, V. L., Hayes, S. F., & Caughey, B. (2005). The most infectious prion protein particles. *Nature*, *437*(7056), 257–261. https://doi.org/10.1038/nature03989

Simoneau, S., Rezaei, H., Salès, N., Kaiser-Schulz, G., Lefebvre-Roque, M., Vidal, C., Fournier, J. G., Comte, J., Wopfner, F., Grosclaude, J., Schätzl, H., & Lasmézas, C. I. (2007). In vitro and in vivo neurotoxicity of prion protein oligomers. *PLoS pathogens*, *3*(8), e125. https://doi.org/10.1371/journal.ppat.0030125

Sorrentino, Z. A., & Giasson, B. I. (2020). The emerging role of α-synuclein truncation in aggregation and disease. *The Journal of biological chemistry*, *295*(30), 10224–10244. https://doi.org/10.1074/jbc.REV120.011743

Sorrentino, Z. A., Vijayaraghavan, N., Gorion, K. M., Riffe, C. J., Strang, K. H., Caldwell, J., & Giasson, B. I. (2018). Physiological C-terminal truncation of α-synuclein potentiates the prion-like formation of pathological inclusions. *The Journal of biological chemistry*, *293*(49), 18914–18932. https://doi.org/10.1074/jbc.RA118.005603

References

Sorrentino, Z. A., Xia, Y., Gorion, K. M., Hass, E., & Giasson, B. I. (2020). Carboxy-terminal truncations of mouse α-synuclein alter aggregation and prion-like seeding. *FEBS letters*, *594*(8), 1271–1283. https://doi.org/10.1002/1873-3468.13728

Sot, B., Rubio-Muñoz, A., Leal-Quintero, A., Martínez-Sabando, J., Marcilla, M., Roodveldt, C., & Valpuesta, J. M. (2017). The chaperonin CCT inhibits assembly of α-synuclein amyloid fibrils by a specific, conformation-dependent interaction. *Scientific reports*, *7*, 40859. https://doi.org/10.1038/srep40859

Sousa, R., Liao, H. S., Cuéllar, J., Jin, S., Valpuesta, J. M., Jin, A. J., & Lafer, E. M. (2016). Clathrin-coat disassembly illuminates the mechanisms of Hsp70 force generation. *Nature structural & molecular biology*, *23*(9), 821–829. https://doi.org/10.1038/nsmb.3272

Specht, S., Miller, S. B., Mogk, A., & Bukau, B. (2011). Hsp42 is required for sequestration of protein aggregates into deposition sites in Saccharomyces cerevisiae. *The Journal of cell biology*, *195*(4), 617–629. https://doi.org/10.1083/jcb.201106037

Sperling, R. A., Donohue, M. C., Raman, R., Sun, C. K., Yaari, R., Holdridge, K., Siemers, E., Johnson, K. A., Aisen, P. S., & A4 Study Team (2020). Association of Factors With Elevated Amyloid Burden in Clinically Normal Older Individuals. *JAMA neurology*, *77*(6), 735–745. https://doi.org/10.1001/jamaneurol.2020.0387

Sun, Y., Hou, S., Zhao, K., Long, H., Liu, Z., Gao, J., Zhang, Y., Su, X. D., Li, D., & Liu, C. (2020). Cryo-EM structure of full-length α-synuclein amyloid fibril with Parkinson's disease familial A53T mutation. *Cell research*, *30*(4), 360–362. https://doi.org/10.1038/s41422-020-0299-4

Surguchev, A. A., & Surguchov, A. (2017). Synucleins and Gene Expression: Ramblers in a Crowd or Cops Regulating Traffic?. *Frontiers in molecular neuroscience*, *10*, 224. https://doi.org/10.3389/fnmol.2017.00224

Surguchov A. (2015). Intracellular Dynamics of Synucleins: "Here, There and Everywhere". *International review of cell and molecular biology*, *320*, 103–169. https://doi.org/10.1016/bs.ircmb.2015.07.007

Taguchi, Y. V., Gorenberg, E. L., Nagy, M., Thrasher, D., Fenton, W. A., Volpicelli-Daley, L., Horwich, A. L., & Chandra, S. S. (2019). Hsp110 mitigates α-synuclein pathology in vivo. Proceedings of the National Academy of Sciences of the United States of America, 116(48), 24310–24316. https://doi.org/10.1073/pnas.1903268116

Tam, S., Geller, R., Spiess, C., & Frydman, J. (2006). The chaperonin TRiC controls polyglutamine aggregation and toxicity through subunit-specific interactions. *Nature cell biology*, *8*(10), 1155–1162. https://doi.org/10.1038/ncb1477

Terada, M., Suzuki, G., Nonaka, T., Kametani, F., Tamaoka, A., & Hasegawa, M. (2018). The effect of truncation on prion-like properties of α-synuclein. *The Journal of biological chemistry*, *293*(36), 13910–13920. https://doi.org/10.1074/jbc.RA118.001862

Tittelmeier, J., Sandhof, C. A., Ries, H. M., Druffel-Augustin, S., Mogk, A., Bukau, B., & Nussbaum-Krammer, C. (2020). The HSP110/HSP70 disaggregation system generates spreading-competent toxic α-synuclein species. The EMBO journal, 39(13), e103954. https://doi.org/10.15252/embj.2019103954

Treweek, T. M., Meehan, S., Ecroyd, H., & Carver, J. A. (2015). Small heat-shock proteins: important players in regulating cellular proteostasis. *Cellular and molecular life sciences : CMLS*, *72*(3), 429–451. https://doi.org/10.1007/s00018-014-1754-5

Trinkaus, V.A.,Riera-Tur I., Martínez-Sánchez, A., Bäuerlein F.J.B., Guo Q., Arzberger, T., Baumeister, W., Dudanova, I.,Hipp, M.S., Ulrich Hartl, F.,Fernández-Busnadiego, R. (2020). In situ architecture of neuronal α-Synuclein inclusions. bioRxiv https://doi.org/10.1101/2020.08.07.234138

Trzeciakiewicz, H., Tseng, J. H., Wander, C. M., Madden, V., Tripathy, A., Yuan, C. X., & Cohen, T. J. (2017). A Dual Pathogenic Mechanism Links Tau Acetylation to Sporadic Tauopathy. *Scientific reports*, *7*, 44102. https://doi.org/10.1038/srep44102

Tuttle, M. D., Comellas, G., Nieuwkoop, A. J., Covell, D. J., Berthold, D. A., Kloepper, K. D., Courtney, J. M., Kim, J. K., Barclay, A. M., Kendall, A., Wan, W., Stubbs, G., Schwieters, C. D., Lee, V. M., George, J. M., & Rienstra, C. M. (2016). Solid-state NMR structure of a pathogenic fibril of full-length human α-synuclein. *Nature structural & molecular biology*, *23*(5), 409–415. https://doi.org/10.1038/nsmb.3194

Tycko R. (2015). Amyloid polymorphism: structural basis and neurobiological relevance. *Neuron*, *86*(3), 632–645. https://doi.org/10.1016/j.neuron.2015.03.017

Ulusoy, A., Febbraro, F., Jensen, P. H., Kirik, D., & Romero-Ramos, M. (2010). Co-expression of C-terminal truncated alpha-synuclein enhances full-length alpha-synuclein-induced pathology. *The European journal of neuroscience*, *32*(3), 409–422. https://doi.org/10.1111/j.1460-9568.2010.07284.x

Vácha, R., Linse, S., & Lund, M. (2014). Surface effects on aggregation kinetics of amyloidogenic peptides. *Journal of the American Chemical Society*, *136*(33), 11776–11782. https://doi.org/10.1021/ja505502e

References

Van der Perren, A., Gelders, G., Fenyi, A., Bousset, L., Brito, F., Peelaerts, W., Van den Haute, C., Gentleman, S., Melki, R., & Baekelandt, V. (2020). The structural differences between patient-derived α-synuclein strains dictate characteristics of Parkinson's disease, multiple system atrophy and dementia with Lewy bodies. *Acta neuropathologica*, *139*(6), 977–1000. https://doi.org/10.1007/s00401-020-02157-3

van der Wateren, I. M., Knowles, T., Buell, A. K., Dobson, C. M., & Galvagnion, C. (2018). C-terminal truncation of α-synuclein promotes amyloid fibril amplification at physiological pH. *Chemical science*, *9*(25), 5506–5516. https://doi.org/10.1039/c8sc01109e

Vilar, M., Chou, H. T., Lührs, T., Maji, S. K., Riek-Loher, D., Verel, R., Manning, G., Stahlberg, H., & Riek, R. (2008). The fold of alpha-synuclein fibrils. *Proceedings of the National Academy of Sciences of the United States of America*, *105*(25), 8637–8642. https://doi.org/10.1073/pnas.0712179105

Villar-Pique, A., de Groot, N. S., Sabaté, R., Acebrón, S. P., Celaya, G., Fernàndez-Busquets, X., Muga, A., & Ventura, S. (2012). The effect of amyloidogenic peptides on bacterial aging correlates with their intrinsic aggregation propensity. *Journal of molecular biology*, *421*(2-3), 270–281. https://doi.org/10.1016/j.jmb.2011.12.014

Visanji, N. P., Wislet-Gendebien, S., Oschipok, L. W., Zhang, G., Aubert, I., Fraser, P. E., & Tandon, A. (2011). Effect of Ser-129 phosphorylation on interaction of α-synuclein with synaptic and cellular membranes. *The Journal of biological chemistry*, *286*(41), 35863–35873. https://doi.org/10.1074/jbc.M111.253450

Vivoli Vega, M., Cascella, R., Chen, S. W., Fusco, G., De Simone, A., Dobson, C. M., Cecchi, C., & Chiti, F. (2019). The Toxicity of Misfolded Protein Oligomers Is Independent of Their Secondary Structure. *ACS chemical biology*, *14*(7), 1593–1600. https://doi.org/10.1021/acschembio.9b00324

von Bergen, M., Barghorn, S., Li, L., Marx, A., Biernat, J., Mandelkow, E. M., & Mandelkow, E. (2001). Mutations of tau protein in frontotemporal dementia promote aggregation of paired helical filaments by enhancing local beta-structure. *The Journal of biological chemistry*, *276*(51), 48165–48174. https://doi.org/10.1074/jbc.M105196200

von Bergen, M., Friedhoff, P., Biernat, J., Heberle, J., Mandelkow, E. M., & Mandelkow, E. (2000). Assembly of tau protein into Alzheimer paired helical filaments depends on a local sequence motif ((306)VQIVYK(311)) forming beta structure. *Proceedings of the National Academy of Sciences of the United States of America*, *97*(10), 5129–5134. https://doi.org/10.1073/pnas.97.10.5129

Wacker, J. L., Zareie, M. H., Fong, H., Sarikaya, M., & Muchowski, P. J. (2004). Hsp70 and Hsp40 attenuate formation of spherical and annular polyglutamine oligomers by partitioning monomer. *Nature structural & molecular biology*, *11*(12), 1215–1222. https://doi.org/10.1038/nsmb860

Walker, L. C., & Jucker, M. (2015). Neurodegenerative diseases: expanding the prion concept. *Annual review of neuroscience*, *38*, 87–103. https://doi.org/10.1146/annurev-neuro-071714-033828

Wang, W., Nguyen, L. T., Burlak, C., Chegini, F., Guo, F., Chataway, T., Ju, S., Fisher, O. S., Miller, D. W., Datta, D., Wu, F., Wu, C. X., Landeru, A., Wells, J. A., Cookson, M. R., Boxer, M. B., Thomas, C. J., Gai, W. P., Ringe, D., Petsko, G. A., … Hoang, Q. Q. (2016). Caspase-1 causes truncation and aggregation of the Parkinson's disease-associated protein α-synuclein. *Proceedings of the National Academy of Sciences of the United States of America*, *113*(34), 9587–9592. https://doi.org/10.1073/pnas.1610099113

Waudby, C. A., Knowles, T. P., Devlin, G. L., Skepper, J. N., Ecroyd, H., Carver, J. A., Welland, M. E., Christodoulou, J., Dobson, C. M., & Meehan, S. (2010). The interaction of alphaB-crystallin with mature alpha-synuclein amyloid fibrils inhibits their elongation. *Biophysical journal*, *98*(5), 843–851. https://doi.org/10.1016/j.bpj.2009.10.056

Wentink, A., Nussbaum-Krammer, C., & Bukau, B. (2019). Modulation of Amyloid States by Molecular Chaperones. *Cold Spring Harbor perspectives in biology*, *11*(7), a033969. https://doi.org/10.1101/cshperspect.a033969

Wentink, A. S., Nillegoda, N. B., Feufel, J., Ubartaitė, G., Schneider, C. P., De Los Rios, P., Hennig, J., Barducci, A., & Bukau, B. (2020). Molecular dissection of amyloid disaggregation by human HSP70. Nature, 587(7834), 483–488. https://doi.org/10.1038/s41586-020-2904-6

Whiten, D. R., Cox, D., Horrocks, M. H., Taylor, C. G., De, S., Flagmeier, P., Tosatto, L., Kumita, J. R., Ecroyd, H., Dobson, C. M., Klenerman, D., & Wilson, M. R. (2018). Single-Molecule Characterization of the Interactions between Extracellular Chaperones and Toxic α-Synuclein Oligomers. *Cell reports*, *23*(12), 3492–3500. https://doi.org/10.1016/j.celrep.2018.05.074

Willander, H., Presto, J., Askarieh, G., Biverstål, H., Frohm, B., Knight, S. D., Johansson, J., & Linse, S. (2012). BRICHOS domains efficiently delay fibrillation of amyloid β-peptide. *The Journal of biological chemistry*, *287*(37), 31608–31617. https://doi.org/10.1074/jbc.M112.393157

References

Winkler, J., Tyedmers, J., Bukau, B., & Mogk, A. (2012). Hsp70 targets Hsp100 chaperones to substrates for protein disaggregation and prion fragmentation. *The Journal of cell biology*, *198*(3), 387–404. https://doi.org/10.1083/jcb.201201074

Winklhofer, K. F., Tatzelt, J., & Haass, C. (2008). The two faces of protein misfolding: gain- and loss-of-function in neurodegenerative diseases. *The EMBO journal*, *27*(2), 336–349. https://doi.org/10.1038/sj.emboj.7601930

Xue, W. F., Hellewell, A. L., Gosal, W. S., Homans, S. W., Hewitt, E. W., & Radford, S. E. (2009). Fibril fragmentation enhances amyloid cytotoxicity. *The Journal of biological chemistry*, *284*(49), 34272–34282. https://doi.org/10.1074/jbc.M109.049809

Ye, Y., Klenerman, D., & Finley, D. (2020). N-Terminal Ubiquitination of Amyloidogenic Proteins Triggers Removal of Their Oligomers by the Proteasome Holoenzyme. *Journal of molecular biology*, *432*(2), 585–596. https://doi.org/10.1016/j.jmb.2019.08.021

Yu, A., Shibata, Y., Shah, B., Calamini, B., Lo, D. C., & Morimoto, R. I. (2014). Protein aggregation can inhibit clathrin-mediated endocytosis by chaperone competition. *Proceedings of the National Academy of Sciences of the United States of America*, *111*(15), E1481–E1490. https://doi.org/10.1073/pnas.1321811111

Zarranz, J. J., Alegre, J., Gómez-Esteban, J. C., Lezcano, E., Ros, R., Ampuero, I., Vidal, L., Hoenicka, J., Rodriguez, O., Atarés, B., Llorens, V., Gomez Tortosa, E., del Ser, T., Muñoz, D. G., & de Yebenes, J. G. (2004). The new mutation, E46K, of alpha-synuclein causes Parkinson and Lewy body dementia. *Annals of neurology*, *55*(2), 164–173. https://doi.org/10.1002/ana.10795

Zhang, J., Li, X., & Li, J. D. (2019). The Roles of Post-translational Modifications on α-Synuclein in the Pathogenesis of Parkinson's Diseases. *Frontiers in neuroscience*, *13*, 381. https://doi.org/10.3389/fnins.2019.00381

Zhang, W., Falcon, B., Murzin, A. G., Fan, J., Crowther, R. A., Goedert, M., & Scheres, S. H. (2019). Heparin-induced tau filaments are polymorphic and differ from those in Alzheimer's and Pick's diseases. *eLife*, *8*, e43584. https://doi.org/10.7554/eLife.43584

Zhang, W., Tarutani, A., Newell, K. L., Murzin, A. G., Matsubara, T., Falcon, B., Vidal, R., Garringer, H. J., Shi, Y., Ikeuchi, T., Murayama, S., Ghetti, B., Hasegawa, M., Goedert, M., & Scheres, S. (2020). Novel tau filament fold in corticobasal degeneration. Nature, 580(7802), 283–287. https://doi.org/10.1038/s41586-020-2043-0

Zhao, K., Li, Y., Liu, Z., Long, H., Zhao, C., Luo, F., Sun, Y., Tao, Y., Su, X. D., Li, D., Li, X., & Liu, C. (2020). Parkinson's disease associated mutation E46K of α-synuclein triggers the formation of a distinct fibril structure. *Nature communications*, *11*(1), 2643. https://doi.org/10.1038/s41467-020-16386-3

Zhao, K., Lim, Y. J., Liu, Z., Long, H., Sun, Y., Hu, J. J., Zhao, C., Tao, Y., Zhang, X., Li, D., Li, Y. M., & Liu, C. (2020). Parkinson's disease-related phosphorylation at Tyr39 rearranges α-synuclein amyloid fibril structure revealed by cryo-EM. *Proceedings of the National Academy of Sciences of the United States of America*, *117*(33), 20305–20315. https://doi.org/10.1073/pnas.1922741117

Zhao, Z., & Michaely, P. (2008). The epidermal growth factor homology domain of the LDL receptor drives lipoprotein release through an allosteric mechanism involving H190, H562, and H586. *The Journal of biological chemistry*, *283*(39), 26528–26537. https://doi.org/10.1074/jbc.M804624200

VITA

Education

2011-2015
    Undergraduate Studies: Bachelors in Biotechnology
    Bachelors Thesis Project: Complejos proteicos elipsoidales NP:Octámero y su relación en el ensamblaje de nucleosomas
    Supervision: Prof. Adelina Prado
    Institution: University of the Basque Country, department of Biochemistry and Molecular Biology and Biofisika Institute (CSIC)

2015-2016
    Master Program: Molecular Biology and Biomedicine
    Master Thesis Project: Role of the C-terminal domain of nucleoplasmin in its interaction with core histones
    Supervision: Prof. Adelina Prado and Prof. Arturo Muga
    Institution: University of Cantabria and University of the Basque Country, department of Biochemistry and Molecular Biology and Biofisika Institute (CSIC)

List of publications

Fernández-Rivero N, Franco A, Velázquez-Campoy A, Alonso E, Muga A, Prado A. A Quantitative Characterization of Nucleoplasmin/Histone Complexes Reveals Chaperone Versatility. Sci Rep. 2016 Aug 25;6:32114. doi: 10.1038/srep32114.

Franco A, Fernández-Rivero N, Prado A, Muga A. Nucleoplasmin: A Versatile Histone Chaperone. eLS John Wiley & Sons 2017. doi: 10.1002/9780470015902.a0027010

Franco A, Arranz R, Fernández-Rivero N, Velázquez-Campoy A, Martín-Benito J, Segura J, Prado A, Valpuesta JM, Muga A. Structural insights into the ability of nucleoplasmin to assemble and chaperone histone octamers for DNA deposition. Sci Rep. 2019 Jul 1;9(1):9487. doi: 10.1038/s41598-019-45726-7.

APPENDIX

Fig. 4.1 c. Solubilization of α-syn fibrils. n=8	
Condition	*P value*
0 μM Apg2 vs. 0.25 μM Apg2	0.089
0 μM Apg2 vs. 0.5 μM Apg2	0.006
0 μM Apg2 vs. 0.75 μM Apg2	0.002
0 μM Apg2 vs. 1 μM Apg2	<0.001
0 μM Apg2 vs. 2.5 μM Apg2	0.09
0 μM Apg2 vs. 5 μM Apg2	0.313
0 μM Apg2 vs. 10 μM Apg2	0.757

Fig. 4.3 d. ThT and ANS binding to different sized α-syn fibrils. n≥5		
Condition	*P value*	
	ThT	ANS
Unsonicated vs. monomer	<0.001	<0.001
Unsonicated vs. 15 cyles P	<0.001	0.249
Unsonicated vs. 30 cyles P	<0.001	<0.001
Unsonicated vs. 15 cycles SN	<0.001	<0.001
Unsonicated vs. 30 cyles SN	<0.001	<0.001

Fig. 4.4 b. Disaggregation of different sized α-syn fibrils. n≥4	
Condition	*P value*
Unsonicated vs. monomer	<0.001
Unsonicated vs. 15 cyles P	<0.001
Unsonicated vs. 30 cyles P	<0.001
Unsonicated vs. 15 cycles SN	<0.001
Unsonicated vs. 30 cyles SN	<0.001

Fig. 4.5. Toxicity of the different α-syn aggregates. n≥5			
	P value		
Condition	Liposome leakage	MTS assay	
		0.3 µM α-syn	0.6 µM α-syn
monomer vs. unsonicated	<0.001	0.956	0.781
monomer vs. 15 cycles P	<0.001	0.05	0.023
monomer vs. 30 cycles P	<0.001	0.002	<0.001
monomer vs. 15 cycles SN	<0.001	<0.001	0.002
monomer vs. 30 cycles SN	<0.001	<0.001	<0.001
monomer vs. type B oligomers	<0.001	<0.001	<0.001

Fig. 4.6 c and e. Fitting of the disaggregation kinetics of α-synuclein aggregates to a pseudo first-order function n=10							
Condition		[Hsc70] (µM)					
		0.125	0.25	0.5	1	2	4
Sonicated	Fitting R^2	0.861	0.882	0.944	0.963	0.974	0.968
	k value	0.011	0.011	0.010	0.018	0.028	0.029
	k Std. Error	3.489E-4	3.486E-4	2.058E-4	2.896E-4	3.989E-4	4.461E-4
Type B	Fitting R^2	0.912	0.919	0.953	0.946	0.917	0.949
	k value	0.002	0.003	0.004	0.006	0.024	0.038
	k Std. Error	1.118E-4	1.141E-4	9.856E-5	1.359E-4	6.009E-4	0.001

Fig. 4.6 g. Disaggregation kinetics of α-synuclein aggregates n≥8						
Condition	*P value*					
	[Hsc70] (µM)					
	0.125	0.25	0.5	1	2	4
Unsonicated vs. Sonicated	<0.001	<0.001	<0.001	<0.001	<0.001	<0.001
Unsonicated vs. Type B	<0.001	<0.001	<0.001	<0.001	<0.001	<0.001

Fig. 4.7 a and c. Disaggregation of glucose-6-phosphate dehydrogenase at 500 min n=2 per method						
Condition	*P value*					
	[Hsc70] (µM)					
	1	2	4	6	8	10
Dequenching vs. Reactivation	0.265	0.01	0.113	0.414	0.659	0.695

Fig. 4.9 c. Proteasome-pretreatment of α-syn fibrils favors chaperone-mediated disaggregation.
n=3

Condition	P value
F+C vs F+P+C	0.038
SF vs SF+C	<0.001
SF+C vs SF+P+C	<0.001

Fig. 4.10 d. The human disaggregase disassemble more efficiently fragmented tau fibrils
n=4

Condition	P value
Unsonicated fibrils+chaps vs. sonicated fibrils+chaps	<0.001

Fig. 5.2 c. Relative amount of Hsc70 bound to α-syn fibrils.
n=4

Condition	P value		
	Hsc70	Hsc70+DnaJB1	Hsc70+DnaJB1+Apg2
WT vs. 30-140	0.264	0.444	1
WT vs. 1-110	0.006	0.444	1

Fig. 5.3 c. GdnHCl chemical denaturation of α-syn$_{WT}$, α-syn$_{30-140}$ and α-syn$_{1-110}$ fibrils.
n=3

Condition	[Hsc70] (µM)								
	0.13	0.25	0.5	0.75	1	1.5	2	3	4
WT vs 30-110	<0.001	<0.001	0.004	0.004	0.034	>0.5	>0.5	>0.5	>0.5
WT vs. 1-110	0.138	0.008	0.018	0.193	0.350	>0.5	>0.5	>0.5	>0.5

Fig. 5.6 b. Disaggregation percentage of the different α-syn hybrid fibril preparations
n≥3

Condition	P value			
	Day 0	Day 1	Day 2	Day 4
WT vs. 1-133	0.385	0.103	0.127	0.044
WT vs. 1-122	<0.001	<0.001	<0.001	<0.001
WT vs. 1-110	<0.001	<0.001	<0.001	<0.001

Fig. 5.8 b. Fitting of the disaggregation kinetics of calpain-cleaved α-synuclein fibrils to a pseudo first-order function
n=3

Condition	[calpain] (ng/µL)			
	0	3.4	13.5	54
Fitting R^2	0.931	0.963	0.969	0.991
k value	0.022	0.016	0.012	0.010
k Std. Error	4.488E-4	2.715E-4	1.866E-4	8.837E-5

Fig. 5.8 c. Calpain-cleavage of α-synuclein fibrils reduces chaperone-mediated disaggregation
n=3

Condition	P value
0 vs. 3.4 ng/µL calpain	0.1
0 vs. 13.5 ng/µL calpain	0.011
0 vs. 54 ng/µL calpain	<0.001

Fig. 6.1 f. Fitting of chaperone-induced disaggregation of α-syn ribbons to a pseudo first-order function
n=10

Condition		[Hsc70] (µM)					
		0.125	0.25	0.5	1	2	4
Sonicated	Fitting R^2	0.44	0.822	0.942	0.959	0.903	0.848
	k value	0.018	0.009	0.007	0.011	0.024	0.024
	k Std. Error	8.417E-4	3.016E-4	1.449E-4	1.969E-4	6.454E-4	6.454E-4

Fig. 6.1 g. Chaperone-induced disaggregation of α-syn ribbons
n=10

Condition	P value					
	[Hsc70] (µM)					
	0.125	0.25	0.5	1	2	4
Unsonicated vs. Sonicated	<0.001	<0.001	<0.001	<0.001	<0.001	<0.001

Fig. 6.2 a, b and d. Fitting of the disaggregation kinetics of α α-synuclein polymorphs obtained in the presence of different compounds to a pseudo first-order function
n≥4

Condition		[Hsc70] (µM)					
		0.125	0.25	0.5	1	2	4
Dextran	Fitting R^2	0.128	0.949	0.972	0.965	0.935	0.933
	k value	0.263	0.006	0.007	0.011	0.015	0.017
	k Std. Error	0.089	1.331E-4	1.040E-4	1.711E-4	3.218E-4	3.577E-4
Dextran sonicated	Fitting R^2	0.089	0.973	0.986	0.984	0.979	0.981
	k value	8.904E-8	0.004	0.005	0.007	0.010	0.011
	k Std. Error	0.003	8.421E-5	6.203E-5	8.598E-5	1.244E-4	1.317E-4
TFE sonicated	Fitting R^2	0.138	0.877	0.993	0.998	0.997	0.997
	k value	0.142	0.004	0.002	0.003	0.004	0.003
	k Std. Error	0.038	1.567E-4	3.706E-5	2.231E-5	2.795E-5	2.702E-5

Fig. 6.2 e. Disaggregation kinetics of α-synuclein polymorphs obtained in the presence of different compounds
n≥4

Condition	P value					
	[Hsc70] (µM)					
	0.125	0.25	0.5	1	2	4
Dextran vs. sonicated dextran	<0.001	0.054	0.056	0.253	0.43	0.316
TFE vs. sonicated TFE	0.573	0.06	0.005	<0.001	<0.001	<0.001

Fig. 6.4 b. ThT binding of fibrils obtained in the absence (pure fibrils) or presence (hybrid fibrils) of 15% unlabeled monomers of the α-syn Q24C mutant.
n=3

Condition	P value		
	Hybrid WT	Hybrid A53T	Hybrid E46K
Pure WT	0.328	<0.001	<0.001
Pure A53T	<0.001	<0.001	<0.001
Pure E46K	<0.001	<0.001	0.084

Fig. 6.4 c. Fitting of the disaggregation kinetics of α-syn point-mutants associated with PD

n≥5

Condition		[Hsc70] (µM)				
		0.5	1	2	4	8
WT	Fitting R^2	0.915	0.945	0.900	0.942	0.982
	k value	0.013	0.020	0.021	0.019	0.018
	k Std. Error	3.040E-4	3.897E-4	5.61E-4	3.977E-4	2.062E-4
A53T	Fitting R^2	0.978	0.961	0.955	0.947	0.970
	k value	0.007	0.012	0.019	0.021	0.018
	k Std. Error	1.026E-4	1.988E-4	3.477E-4	4.136E-4	2.651E-4
E46K	Fitting R^2	0.455	0.829	0.936	0.935	0.97
	k value	0.024	0.024	0.027	0.025	0.023
	k Std. Error	0.002	9.608E-4	6.132E-4	5.585E-4	3.527E-4

Fig. 6.4 d. Disaggregation kinetics of polymorphs of α-syn point-mutants associated with PD

n≥5

Condition	P value				
	[Hsc70] (µM)				
	0.5	1	2	4	8
WT vs A53T	<0.001	0.017	0.075	0.125	0.129
WT vs E46K	<0.001	<0.001	<0.001	<0.001	0.506

Fig. 6.6 a. Fitting of the disaggregation kinetics of tau K18 polymorphs produced by pathogenic point-mutations to a pseudo first-order function

n=7

Condition		[Hsc70] (µM)			
		1	2	4	8
WT	Fitting R^2	0.982	0.992	0.995	0.997
	k value	0.006	0.01	0.01	0.011
	k Std. Error	1.750E-4	1.443E-4	1.162E-4	1.028E-4
P301L	Fitting R^2	0.952	0.979	0.994	0.992
	k value	0.017	0.016	0.014	0.014
	k Std. Error	0.001	3.592E-4	1.704E-4	1.901E-4
ΔK280	Fitting R^2	0.998	0.997	0.997	0.997
	k value	0.005	0.008	0.009	0.009
	k Std. Error	5.307E-5	8.408E-5	8.366E-5	8.147E-5

Fig. 6.6 b. Disaggregation kinetics of tau K18 polymorphs produced by pathogenic point-mutations.
n=7

Condition	P value [Hsc70] (µM)			
	1	2	4	8
WT vs P301L	0.562	0.670	0.425	0.389
WT vs ΔK280	0.562	0.670	0.009	<0.001